Contribution à la modélisation des convertisseurs continu/continu dans une perspective de commande – Influence du filtre d'entrée

Muhammad Usman Iftikhar

N° D'ORDRE : 9319

THÈSE DE DOCTORAT

SPECIALITE : PHYSIQUE

Ecole Doctorale « Sciences et Technologies de l'Information des Télécommunications et des Systèmes »

Présentée par : Muhammad USMAN IFTIKHAR

Sujet :

Contribution à la modélisation des convertisseurs continu/continu dans une perspective de commande – Influence du filtre d'entrée

Soutenue le **15 décembre 2008** devant les membres du jury :

M. Paul LESAGE	*Professeur à l'université de Paris-XI*	Président
M. Seddik BACHA	*Professeur à l'université Joseph Fourier*	Rapporteur
Mme. Xuefang LIN SHI	*MC-HDR à l'INSA de Lyon*	Rapporteur
M. Mohamed GABSI	*Professeur à l'ENS Cachan*	Examinateur
M. Emmanuel GODOY	*Professeur à Supélec*	Examinateur
M. Daniel SADARNAC	*Professeur à Supélec*	Directeur de thèse
M. Bertrand LACOMBE	*Senior Expert à Hispano-Suiza*	Invité

DOCTORAL THESIS

SPECIALITY : PHYSICS

Ecole Doctorale « Sciences et Technologies de l'Information des Télécommunications et des Systèmes »

Presented by : Muhammad USMAN IFTIKHAR

Title :

Investigation of DC-DC Converter Modeling from the Perspective of Control and Input-Filter Influence

Defended on **15 December 2008** in front of the following Jury :

Mr. Paul LESAGE	*Professor at the University of Paris-XI*	President
Mr. Seddik BACHA	*Professor at University Joseph Fourier*	Reviewer
Mme. Xuefang LIN SHI	*MC-HDR at INSA Lyon*	Reviewer
Mr. Mohamed GABSI	*Professor at ENS Cachan*	Examiner
Mr. Emmanuel GODOY	*Professor at Supélec*	Examiner
Mr. Daniel SADARNAC	*Professor at Supélec*	Thesis advisor
Mr. Bertrand LACOMBE	*Senior Expert à Hispano-Suiza*	Guest

REMERCIEMENTS

Cette thèse de doctorat conclut les travaux que j'ai effectués au sein du département énergie de l'Ecole Supérieure d'Électricité (Supélec), France, depuis novembre 2005. C'est avec un très grand plaisir que je réserve cette page en signe de gratitude et de profonde reconnaissance à tous ceux qui m'ont aidé dans la réalisation de ce modeste travail.

Tout d'abord, je dois une énorme dette de gratitude à mon directeur de thèse M. Daniel Sadarnac, *chef de l'équipe électronique de puissance*, pour la confiance qu'il m'a accordé en acceptant de m'encadrer pour cette thèse. Je lui remercie très chaleureusement pour son soutien, son orientation et son encouragement au cours de ma thèse.

Je tiens à exprimer mes appréciations à M. Charif Karimi, *professeur adjoint*, et M. Pierre Lefranc, *professeur assistant*, pour leur précieuse participation à l'encadrement de ces travaux et leur disponibilité tout au long de cette thèse. Ils ont été toujours disponibles pour répondre à mes questions, m'encourager et m'aider à résoudre les problèmes rencontrés dans ce travail. Leurs conseils pertinents et leur aide étaient d'une importance capitale dans la réalisation de ce travail. En plus, je dois mes remerciements particuliers à M. Pierre Lefranc pour sa relecture volontaire de cette thèse. Ses suggestions et recommandations m'ont beaucoup aidé dans l'amélioration de la structure, d'organization et de présentation du contenu technique de ce texte.

Je tiens également à remercier M. Jean-Claude Vannier, *chef de département*, pour son aide constant et son orientation dans toutes les activités techniques ainsi que des questions administratives. Son attitude amicale et son soutien moral ont toujours été avec moi tout au long de ma thèse. Mes remerciements vont également à M. Emmanuel Godoy, *professeur au département d'automatique*, pour son aide efficace dans le domaine de l'automatique et aussi pour le temps que j'ai passé avec lui dans des discussions techniques et pour les connaissances dont il m'a fait bénéficier.

Mes sincères remerciements vont également à mon organisme, SUPARCO, pour m'avoir donné cette grande opportunité pour les études supérieures à l'étranger et me permettre de poursuivre mes ambitions de recherche en doctorat. Sans leur appui positif je ne pouvais pas avoir atteint cet objectif.

Je tiens également à remercier tous mes collègues, tous les enseignants, les doctorants et les stagiaires de mon département dont l'amitié a fourni une base pour l'accomplissement de ce travail. J'apprécie le temps magnifique que nous avons passé ensemble. Je pense également à tous les membres du personnel administratif du département énergie, en particulier Mme Christiane Lebouquin, *secrétaire*, et Si-Mohamed Benhamed, *comptable*, qui ont été très aimables avec moi et m'ont aidé à effectuer toutes les démarches administratives sans difficulté.

Je suis également très reconnaissant à mon ami M. Masood Maqbool, *doctorant à Telecom Paris*, pour son temps et son aide précieux pour les corrections et les améliorations linguistiques lors de la publication de mes travaux de recherche pendant ma thèse.

Enfin, je dédicace cette mémoire à ma famille : mon père, ma mère, mes sœurs et mes grands parents, qui m'ont moralement soutenue malgré la distance qui nous sépare. Je les remercie du fond du cœur pour l'amour qu'ils me donnent. Sans eux je ne saurais arriver là ou je suis.

Et au fond de mon cœur sont aussi des remerciements particuliers à mes amis. Les mots ne suffisent pas pour exprimer la formidable chance que j'ai. Qu'ils trouvent ici le témoignage de mon amitié : *Waqqas, Youcef, Danish, Anas, Sheraz, Yacine, Ange, Mazhar* et tous ceux qui m'ont portés beaucoup!

M. Usman Iftikhar

Octobre 2008

Paris, France

ACKNOWLEDGMENTS

This doctoral dissertation finalizes the work which I have carried out in the Department of Energy and Power Systems of Ecole Supérieure d'Electricité (Supélec), France, since November 2005. It's a big pleasure for me to reserve this page as a symbol of gratitude to all those who helped me realize this milestone.

First of all I owe an enormous debt of gratitude to my supervisor Prof. Daniel Sadarnac, *Head of the Power Electronics Team*, for the confidence that he accorded to me by accepting to supervise this thesis. I express my warm gratitude for his precious support, valuable guidance and consistent encouragement throughout the course of my PhD.

I would like to express my appreciations to Mr. Charif Karimi, *Assistant Professor*, and Mr. Pierre Lefranc, *Associate Professor*, for their valuable participation in the realization of this work and their availability throughout this thesis. They were always available to answer my questions, to encourage me and to help me solve the problems encountered in this work. Their advice and assistance are of great importance in the achievement of this research work. In addition to that, I owe my special thanks to Mr. Pierre Lefranc for his volunteer proofreading of this thesis. His valuable suggestions and recommendations helped me a lot in the improvement of structure, organisation and presentation of the technical contents of this text.

I would also like to thank Prof. Jean-Claude Vannier, *Head of Department*, for his consistent help and guidance in all technical as well as administrative matters. His friendly attitude and moral support have always been with me throughout my PhD. My acknowledgments equally go to Mr. Emmanuel Godoy, *Professor in Automatic Controls Department*, for his effective assistance in the field of automatic controls and also for the time I spent with him in technical discussions and gaining knowledge of various aspects of control theory.

My sincere acknowledgments also go to my organization, SUPARCO, for providing me this great opportunity for higher studies abroad and allowing me to pursue my research goals in PhD. Without their positive support I could not have achieved this milestone.

I would also like to thank all of my colleagues, all the teachers, the Ph.D. students and the trainees of my department whose friendship provided a base for the accomplishment of this work. I cherish the wonderful time that we spent together. I also think of all the administrative staff of the Department of Energy, especially Mme Christiane Lebouquin, *Secretary*, and Si-Mohamed Benhamed, *Accountant and Book-keeper*, who have always been very gentle with me and helped me to get things done very smoothly.

I am also greatly indebted to my friend Mr. Masood Maqbool, *PhD student at Telecom Paris*, for his time and invaluable help for proofreading, linguistic improvements and troubleshooting during the publications of my research papers throughout the course of my PhD.

Finally, I dedicate this thesis to my family: my dear father, my mother, my sisters and my grandparents who supported me morally despite the distance that separates us. I thank them from the bottom of my heart for the love they always give me. Without them I could never have reached where I am today.

And deep in my heart are special thanks to my friends. Words are simply not enough to express the tremendous goodluck that I have, just to name a few of them: *Waqqas, Youcef, Danish, Anas, Sheraz, Yacine, Ange, Mazhar* and all others who bring to me a lot!

M. Usman Iftikhar

October 2008

Paris, France

RÉSUMÉ

La modélisation et la commande des convertisseurs de type continu/continu occupent une place de plus en plus importante dans le domaine de l'électronique de puissance. La « modélisation moyenne » est la plus courante. C'est un outil efficace permettant d'analyser le comportement dynamique global d'un convertisseur et de dégager les principaux phénomènes physiques intervenant sur ce comportement. Les modèles moyennés en espace d'état sont largement acceptées dans la pratique, principalement de par leur simplicité, leur généralité et leur utilité pratique qui n'est plus à démontrer. Divers modèles moyennés ont été présentés dans la littérature spécialisée. Il subsiste cependant quelques questions fondamentales en ce qui concerne les méthodologies moyennes qui n'apportent pas toujours une réponse satisfaisante. Ces problèmes non résolus de modélisation touchent essentiellement à la validation pratique, à l'intégration des parasites du circuit électrique réel et à l'application à la conception de la boucle de commande. L'une des principales préoccupations de cette thèse est d'étudier et d'évaluer les performances de la modélisation moyenne des convertisseurs dc/dc en vue de leur commande. En particulier, l'accent est mis sur l'étude théorique et expérimentale des modèles moyennés en mode de conduction discontinu (DCM). Divers modèles moyens analytiques de différents ordres, présentés dans la littérature, sont reformulés en incluant les parasites. Leur validité relative est examinée expérimentalement par rapport à un prototype physique.

En ce qui concerne la commande, la stabilité est d'une importance capitale dans tout système de régulation de tension. Toutefois, assurer la stabilité en boucle fermée n'est pas évident en présence d'un filtre en entrée du convertisseur. L'origine de ce problème réside dans l'interaction du filtre avec le comportement du convertisseur dc/dc de type « résistance dynamique négative ». La littérature fournit une solution pour résoudre ce problème et propose une solution « passive » pour amortir les oscillations liées au filtre d'entrée. La valeur de la résistance d'amortissement nécessaire peut être déterminée en utilisant un modèle de convertisseur idéal. Toutefois, cette valeur n'est pas systématiquement confirmée par l'expérience. Dans cette thèse, des fonctions de transfert en régime de petits signaux sont utilisés pour formuler systématiquement des règles de dimensionnement pour éviter l'instabilité. Les régions de la stabilité sont déterminées en fonction des paramètres du circuit d'amortissement. Cette approche est étendue au cas de convertisseurs en cascade. Tout au long de cette étude, la modélisation moyenne en petit-signal est utilisée pour l'analyse de la stabilité.

Bien que l'ajout d'une résistance suffisante assure la stabilité, l'amortissement passif est critiquable à cause de pertes énergétiques indésirables dans les résistances utilisées. Afin d'en étudier les retombées sur le rendement du convertisseur, les pertes dues à l'amortissement sont quantifiées d'une manière plus systématique dans cette thèse. Une analyse théorique de ces pertes est présentée dans diverses conditions de fonctionnement. La validation expérimentale est toujours présente. Les résultats obtenus sont généralisés à toutes les topologies fondamentales de convertisseurs.

L'un des principaux thèmes de cette thèse touche au développement d'une commande assurant la stabilité du convertisseur dc/dc avec son filtre d'entrée sans utiliser d'amortisseur dissipatif.

Afin d'atteindre cet objectif, une solution avec commande par retour d'état et placement des pôles est proposée. Un modèle moyen d'ordre élevé est mis en place pour concevoir un correcteur qui combine le retour d'état avec une boucle PI. L'efficacité de l'algorithme de commande proposé est démontrée par des résultats de simulation. Il apparaît que des performances dynamiques intéressantes peuvent être atteintes en présence de grandes perturbations en utilisant un retour d'état avec gains variables. En outre, cette stratégie de commande assure la stabilité du système sans composant passif additionnel dans le filtre d'entrée et sans pertes supplémentaires. Ensuite, dans un deuxième temps, une commande par mode-glissement basée sur l'approche de la fonction de Lyapunov est discutée, laquelle est présentée dans la litérature pour l'ensemble abaisseur-filtre. Nous discutons les performances de la commande par retour d'état, proposée dans cette thèse, comparées à celles d'un contrôleur mode-glissant.

Mots clés: *Modélisation moyenne, convertisseurs continu/continu, interactions filtre d'entrée, stabilité de régulation, circuits d'amortissement, commande par retour d'état.*

ABSTRACT

Modeling and control of switched-mode dc-dc converters has occupied a center stage in the field of modern power electronics due to their widespread military and industrial applications. Averaged modeling is most commonly applied as an effective tool to analyze dynamic behavior of a converter and to get physical insights into various dynamical phenomena. State-space averaged models are widely accepted in practice mainly because of their simplicity, generality and demonstrated practical utility. Various averaged models have been presented in literature; however, some fundamental questions regarding averaging methodologies still lack satisfactory answers. These unresolved modeling issues are primarily related to their practical validation, inclusion of circuit parasitics and their application to the control-loop design. One of the primary concerns of this thesis is to study and evaluate the performance of averaged modeling of dc-dc converters from control perspective. In particular, the main emphasis is placed on the theoretical and experimental investigation of averaged modeling in discontinuous conduction mode (DCM). Various analytical averaged models of different orders, presented in literature, are reformulated in this thesis by including all appropriate parasitics. Parasitics are introduced to take into account those phenomena which can possibly induce instability. Then, the validities of these averaged models are experimentally examined by comparing analytical results with experimental results measured from a hardware prototype.

As far as control is concerned, stability is of prime importance in any dc voltage regulation system. However, closed-loop stability is not guaranteed if a low-pass filter is present at converter-input. The origin of this problem lies in the filter interactions with the negative dynamic resistance behavior of the dc-dc converter input port. Literature provides a gateway to solve this issue and proposes a "passive" solution to damp the input-filter oscillations. Although exact values of the required damping resistance can be determined using an ideal converter model, this value is not systematically confirmed through experiments. In this thesis small-signal control-to-output transfer functions are used to systematically formulate some design rules to avoid instability. Safe operating regions are identified in terms of damping-circuit parameters and this approach is subsequently extended to the case of cascade converters. Throughout this study the small-signal averaged modeling is used for the stability analysis.

Although adding adequate resistance to the filter can solve instability problem, one drawback for which passive damping is commonly criticized is the undesirable power dissipation in the damping resistors. To properly investigate its adverse impact on conversion efficiency, these damping losses are quantified in this thesis. A detailed theoretical power-loss analysis is presented under varying operating conditions followed by its experimental verification. Obtained results are generalized for all fundamental topologies.

One of the main themes of this dissertation is the development of a control solution for the stability of dc-dc converter in presence of input filter, hence avoiding the use of dissipative

damping. To achieve this objective, this thesis suggests the use of full state-feedback control with pole-placement technique. An augmented state-space averaged model is used to design the controller which combines state-feedback with PI-control loop. First of all a theoretical approach is presented. Then the effectiveness of the proposed control algorithm is demonstrated with simulation studies. It appears that an adequate level of dynamic performance under large perturbations can be achieved by using a varying gain state-feedback. A pseudo large-signal stability analysis is also performed with the help of this technique. Importantly, this control strategy assures stability of the system without using any passive components in the filter circuit and thus avoiding undesirable losses. An alternate control scheme, chosen from the literature, is also discussed for filter-converter system stability. This scheme is based upon sliding-mode control and Lyapunov function approach. Its dynamic performance is compared with that of the full state-feedback controller proposed in this thesis while explaining pros and cons of both control strategies.

Key words: *State-space averaged modeling, dc-dc converter, input-filter interactions, closed-loop stability, damping network, state-feedback control.*

CONTENTS

LIST OF PUBLICATIONS

The work on this doctoral project resulted in a number of publications, which are listed below:

Published Papers:

1. M. Usman Iftikhar, D. Sadarnac, C. Karimi, "Conducted EMI Suppression and Stability Issues in Switch-mode DC-DC Converters", *10th IEEE International Multitopic Conference (INMIC'06)*, 23-24 Dec. 2006, Islamabad (Pakistan), pp. 389-394.

2. M. Usman Iftikhar, D. Sadarnac, C. Karimi, "Input Filter Damping Design for Control Loop Stability of DC-DC Converters", *IEEE International Symposium on Industrial Electronics (ISIE'07)*, 4-7 June 2007, Vigo (Spain), pp. 353-358.

3. M. Usman Iftikhar, A. Bilal, D. Sadarnac, P. Lefranc, C. Karimi, "Analysis of Input Filter Interactions in Cascade Buck Converters", *IEEE International Conference on Industrial Technology (ICIT'08)*, 21-24 April 2008, Chengdu (China), pp. 1-6.

4. M. Usman Iftikhar, P. Lefranc, D. Sadarnac, C. Karimi, "Theoretical and Experimental Investigation of Averaged Modeling of Non-ideal PWM DC-DC Converters Operating in DCM", *39th IEEE Power Electronics Specialists Conference (PESC'08)*, 15-19 June 2008, Rhodes Island (Greece), pp. 2257-2263.

5. M. Usman Iftikhar, E. Godoy, P. Lefranc, D. Sadarnac and C. Karimi, "A Control Strategy to Stabilize PWM DC-DC Converters with Input Filters Using State-Feedback and Pole-Placement", *30th IEEE International Telecommunications Energy Conference (INTELEC'08)*, 14-18 Sep. 2008, San Diego, CA (USA), pp. 1-5.

Submitted Papers:

6. M. Usman Iftikhar, P. Lefranc, D. Sadarnac, C. Karimi, "Efficiency Investigation of DC-DC Converters with Passively Damped Input Filter Circuit", *to appear in the International Journal of Electronics.*

LIST OF FIGURES

LIST OF TABLES

RÉSUMÉ ÉTENDU EN FRANÇAIS

Chapitre 1 : Introduction

Présentation générale

Les convertisseurs continu/continu sont devenus une composante essentielle des applications industrielles et militaires au cours des dernières décennies. Grâce à leur rendement de plus en plus élevé, leur encombrement, leur poids et leur coût réduits, ils ont remplacé les alimentations classiques linéaires, même pour de faibles niveaux de puissance. Un convertisseur de puissance peut être caractérisé comme un système périodique, non-linéaire et variant au cours du temps en raison de son fonctionnement basé sur le découpage. La topologie des éléments dynamiques du système dépend de l'état instantané de chaque interrupteur commandé, ce qui rend la modélisation complexe. Toutefois, les modèles analytiques des convertisseurs continu/continu à commande PWM sont essentiels pour leur conception et leur analyse dans de nombreuses applications telles que l'automobile, l'aéronautique, l'espace, les télécommunications, la marine, les ordinateurs, les équipements médicaux… Beaucoup d'efforts ont été faits au cours des dernières années pour modéliser les convertisseurs continu/continu. De nombreux modèles ont été proposés. Ces modèles sont très largement utilisés pour étudier les caractéristiques statiques et dynamiques des convertisseurs ainsi que pour concevoir leur système de régulation.

Les modèles dits « modèles moyennés » supposent que les effets du découpage sont « moyennés » durant une période de commutation. Ils sont employés usuellement pour analyser un système basé sur l'électronique de puissance. Les modèles continus grands-signaux sont généralement non-linéaires et peuvent être linéarisés autour d'un point de fonctionnement donné. Les modèles moyennés ne sont qu'une approximation mais sont intéressants pour étudier les convertisseurs continu/continu : ils permettent de déterminer simplement des fonctions de transfert locales, de simuler la réponse transitoire aux perturbations grands-signaux, de linéariser les modèles des convertisseurs pour dimensionner la commande feedback… En outre, l'emploi de modèles moyennés dans un simulateur numérique réduit fortement les temps de calculs, notamment dans l'étude au niveau système.

Typiquement un convertisseur continu/continu peut fonctionner suivant deux modes: le mode de conduction continue (le courant dans l'inductance ne s'annule jamais) et le mode de conduction discontinue (le courant est nul dans l'inductance durant une partie de la période de découpage). La conduction discontinue (DCM : Discontinuous Conduction Mode) s'observe toujours dans le cas d'un faible courant dans la charge et diffère de la conduction continue (CCM : Continuous Conduction Mode) par trois phases de fonctionnement, au lieu de deux, pendant la période de découpage. Les premiers modèles moyennés des convertisseurs PWM fonctionnant dans le mode CCM, basés sur la technique de moyennage en espace d'état, ont été introduits pendant les années 1970. Ensuite, cette méthode a aussi été appliquée au mode DCM, ce qui a abouti au modèle « d'ordre réduit » et ne caractérise le comportement qu'à basse fréquence. Les modèles « d'ordre complet » qui ont été proposés par la suite ont amélioré la précision, même à fréquence élevée. Une méthode unifiée pour les deux modes de

conduction a également été développée : elle aboutit effectivement à la même formulation pour CCM et DCM comme précédemment. Toutefois, la précision de ces modèles à fréquence élevée est discutable.

Même si les développements en matière de topologies de convertisseur et de semi-conducteurs de puissance ont conduit à des rendements et des fréquences de commutation plus élevés, les convertisseurs d'aujourd'hui ont encore des imperfections qui posent des problèmes au niveau de la commande feedback. L'un de ces problèmes est l'ondulation inévitable du courant d'entrée qui est à la source de perturbations électromagnétiques (EMI : Electromagnetic Interferences) et nécessite l'emploi d'un filtre approprié à l'entrée. En outre, un système de régulation de tension ou de courant équipe la plupart des convertisseurs. Or la caractéristique d'entrée d'un convertisseur régulé en sortie est celle d'une charge dynamique à puissance constante pour le filtre d'entrée, autrement dit, celle d'une résistance négative : toute variation de la tension au niveau de la source d'énergie du convertisseur se répercute en aval du filtre d'entrée et se traduit par une variation en sens contraire du courant en aval du filtre d'entrée. Il est clair que cette résistance négative a un effet déstabilisant sur le filtre d'entrée. Ainsi, la présence d'un filtre d'entrée n'accroît pas seulement la complexité et le coût du circuit mais peut également provoquer l'instabilité du système. Un problème similaire d'instabilité peut se produire aussi dans des architectures de puissance distribuées, où plusieurs convertisseurs continu/continu doivent être connectés en cascade.

Les problèmes liés aux filtres-EMI ont été examinés dès le début des années 1970. La recherche en ce domaine a mené au développement de la méthodologie de moyennage en espace d'état et à diverses solutions. La raison principale des débats animés sur ce thème est l'application du formalisme de l'interaction et des règles de dimensionnement aux différents modes de fonctionnement et de contrôle. Généralement, la stabilité en boucle fermée ne peut pas être garantie pour un filtre mal amorti à l'entrée. Ainsi, d'une part, le problème d'interaction du filtre d'entrée a considérablement compliqué la conception du régulateur et, d'autre part, elle a posé de nouveaux défis pour les techniques de modélisation sur lesquelles la loi de commande doit être fondée. Un filtre d'entrée est inévitable en raison de problèmes d'EMI[1]/EMC[2] dans la plupart des applications contemporaines de convertisseur continu/continu mais il doit aussi assurer la stabilité du système global. Compte tenu de ces objectifs, les techniques classiques de modélisation moyennée sont confrontées à de nouveaux défis et les débats sur la modélisation et la commande des convertisseurs continu/continu occupent une place centrale dans le domaine de l'électronique de puissance. Toutefois, les performances des modèles moyens pour l'analyse, la conception de la commande et pour la stabilité globale doivent encore être évaluées. Leurs capacités et leurs limites doivent être clairement définies avant de passer à des modèles plus complexes.

Motivations et objectifs

Il est admis que les propriétés dynamiques d'un convertisseur peuvent être exprimées de manière efficace en utilisant un modèle de circuit « équivalent en moyenne », lequel permet d'identifier la source de divers phénomènes dynamiques. Les modèles moyens en temps-continu ont été largement acceptés parce qu'ils sont faciles à comprendre et à mettre en œuvre. Lorsqu'ils ont été appliqués au mode DCM, ils ont abouti à des résultats s'écartant un peu de la réalité à des fréquences plus élevées que 1/10 de la fréquence de découpage. En conséquence, plus récemment, quelques modifications du moyennage classique en espace

[1] Electromagnetic Interference
[2] Electromagnetic Compatibility

d'état ont été proposées pour le DCM [sun01], ce qui se traduit par des modèles moyens d'ordre complet. Cependant, la validation expérimentale de ces modèles manque encore dans la littérature. La méthode du moyennage en espace d'état ou celle du circuit équivalent a aussi été appliquée à l'analyse des interactions du filtre d'entrée et à la conception de la commande. Cependant, la littérature ne fait pas encore état de l'analyse expérimentale qui devrait accompagner toute évolution du modèle et permettre de juger de son domaine de validité et de sa précision. En outre, le convertisseur est toujours considéré comme idéal.

Par ailleurs, il est difficile de prédéterminer les régulateurs nécessaires à cause du filtre d'entrée qui intervient lourdement et de manière non évidente dans les fonctions de transfert. Il est cependant possible d'effectuer une simulation numérique du convertisseur équipé de son filtre et de ses régulateurs mais il n'est pas évident d'optimiser l'ensemble de la sorte. Une littérature fournie porte sur le sujet et attribue au filtre d'entrée une cause potentielle d'instabilité des régulations. Des auteurs préconisent l'emploi de circuits amortisseurs dans le filtre pour résoudre ce problème mais la détermination des composants à implanter n'est pas toujours exacte (pas systématiquement confirmée par l'expérience) car les méthodes proposées supposent des modèles idéaux. Par ailleurs, la puissance dissipée dans les résistances d'amortissement n'est pas forcément négligeable et n'est pas souhaitable en raison de son impact sur le rendement du convertisseur.

Il reste beaucoup de questions liées à la modélisation moyenne et à son application à la conception de la boucle de commande qui doit être abordée de manière approfondie. Notre but est de contribuer à améliorer les modèles et la commande des convertisseurs continu/continu en présence d'un filtre d'entrée. Les principaux objectifs de cette thèse sont résumés ci-dessous :

- Faire une étude bibliographique pour comprendre et analyser les différents modèles moyens développés dans la littérature. Rétablir ces modèles en introduisant les pertes de circuit dans les équations des modèles.
- Effectuer des recherches sur la modélisation moyenne d'un convertisseur continu/continu non-idéal dans le mode DCM, sur le plan théorique mais aussi expérimental. Formuler et démontrer une méthodologie expérimentale pour la mesure de la fonction de transfert (sortie / commande) avec une précision raisonnable.
- Comparer la validité des différents modèles moyens développés dans la littérature et étudier les influences parasites comme prévu par les différents modèles d'ordre complet en incluant toutes les imperfections des composants dans les équations du modèle. Afin d'affronter la difficulté de manipulation des expressions compliquées, un programme d'analyse symbolique, Mathematica®, pourra être utilisé pour la détermination et la simplification des fonctions de transfert d'ordre élevé.
- Faire l'état de l'art des interactions du filtre d'entrée et examiner les différentes solutions actives et passives qui ont été proposées pour résoudre les problèmes. Analyser les interactions du filtre d'entrée dans toutes les topologies de base des convertisseurs (abaisseur, élévateur et inverseur) à l'aide de leur modèle moyen non-idéal et de formuler systématiquement certaines règles de dimensionnement pour éviter les effets néfastes sur la dynamique du convertisseur. Déduire les conditions de stabilité généralisée pour chacun de ces convertisseurs et identifier un domaine de fonctionnement stable en fonction des paramètres du circuit d'amortissement.
- Étendre cette étude à un cas de convertisseurs en cascade et déterminer les conditions de la stabilité en présence du filtre d'entrée. L'analyse doit se baser sur les fonctions de transfert en petits signaux. Valider expérimentalement cette approche.

- Étudier de manière approfondie le circuit passif d'amortissement qui est le plus utilisé dans le filtre d'entrée afin d'évaluer les critiques soulignées dans la littérature. Quantifier les pertes dans l'amortisseur et son influence sur le rendement global du système dans différentes conditions de fonctionnement. Généraliser cette étude à toutes les topologies fondamentales et vérifier expérimentalement les résultats obtenus.
- Proposer une solution alternative pour la commande d'un convertisseur continu/continu avec un filtre d'entrée mal-amorti, ce qui éviterait les pertes dans des résistances d'amortissement. Par exemple, concevoir et étudier une commande par retour d'état et le placement des pôles, et adapter cette commande avec les points de fonctionnament variants. Ensuite comparer les performances de la commande proposée avec celles d'une commande déjà existante dans la litérature par exemple, commande par mode-glissant. Évaluer les limites de la modélisation moyenne à haute fréquence pour la conception de la commande.

Chapitre 2 : Modélisation moyenne espace-état des convertisseurs continu/continu non-idéaux avec filtre d'entrée

Introduction générale

N'importe quel convertisseur de puissance utilise un système de commande. Par exemple, dans un convertisseur continu/continu, la tension de sortie doit typiquement être maintenue constante, indépendante de la tension d'entrée et des variations de la charge. Pour concevoir un tel système de commande, il est important de disposer d'un modèle dynamique du convertisseur. En particulier, il faut savoir comment les variations de la tension d'entrée, du courant dans la charge et le rapport cyclique affectent la tension de sortie. Il faut connaître les fonctions de transfert en petits signaux. Pour trouver ces informations, il est souhaitable de modéliser le comportement du système, au moins dans ses grandes lignes, en négligeant certains phénomènes peu influents. Malheureusement, la compréhension du comportement dynamique du convertisseur est gênée par la nature non-linéaire et le caractère temporel des processus de commutation et de modulation de largeur d'impulsion (PWM[1]). Toutefois, ces difficultés peuvent être aplanies grâce à l'utilisation de techniques consistant à « moyenner » en petits signaux. Ces techniques impliquent des approximations qui visent à négliger des phénomènes relativement complexes mais d'influence secondaire au profit d'une meilleure compréhension de l'essentiel. Ces approximations peuvent toujours être minimisées en réintroduisant ultérieurement ce qui a été négligé comme des éléments de second ordre. Cette façon de procéder, en deux étapes, permet de réduire considérablement les développements mathématiques. Cela mène aussi à une meilleure compréhension qualitative de l'influence de chacun des paramètres.

Les ondulations résiduelles dues au découpage sont relativement faibles par rapport à la variation des signaux dans un convertisseur bien dimensionné. Par conséquent, il est possible d'ignorer ces ondulations et de modéliser uniquement les variations à basse fréquence des signaux (courants et tensions) dans le convertisseur. Par exemple, supposons qu'une variation $d(t)$ soit introduite dans le rapport cyclique du convertisseur, de telle sorte que:

$$d(t) = D + D_m \cos \omega_m t \tag{1}$$

Dans cette expression, D et D_m sont constants, $|D_m| << D$, la pulsation ω_m de modulation est très petite par rapport à la pulsation de découpage $\omega_s = 2\pi f_s$. Dans ces conditions, le spectre du signal de sortie comporte des composantes à la fréquence de découpage ainsi que ses harmoniques et des bandes latérales. Toutefois, ces composantes sont de petite amplitude tant que les ondulations à cause du découpage sont faibles. En outre, ce spectre contient aussi une composante à basse fréquence à la pulsation de modulation ω_m. L'amplitude et la phase de cette composante dépend non seulement de la variation de rapport cyclique, mais aussi de la réponse fréquentielle du convertisseur. Les ondulations dues au découpage relatives au courant dans l'inductance et à la tension aux bornes du condensateur sont négligées pour moyenner sur une période de commutation. Par conséquent, le modèle qui en découle prévoit le comportement à basse fréquence du convertisseur.

L'approche moyennée en espace d'état pour les convertisseurs de puissance est utilisée couramment. Cela se justifie principalement par l'évidence apparente de cette méthode, par la simplicité de sa mise en œuvre, par la pertinence de ses résultats et par son aptitude à la généralisation [kis94, kre90, mit88]. Un modèle moyen petit-signal peut toujours être trouvé,

[1] Pulse Width Modulation

étant donné que les équations d'état du convertisseur peuvent être écrites. La théorie du calcul de la moyenne offre un cadre permettant d'aborder les questions se rapportant à des problèmes de la stabilité en raison des interactions avec le filtre d'entrée (qui seront étudiées au chapitre 3). Les résultats obtenus fournissent des outils pour le développement et le perfectionnement des méthodes visant à la conception et la commande des systèmes électroniques de puissance. Les méthodologies analytiques conventionnelles consistant à moyenner ont été largement étudiées et décrites dans la littérature [ben94, mak01, mid77b, san91a, san91b, ver81]. Toutefois, le convertisseur est toujours supposé idéal. Considérer les composants idéaux, sans pertes, simplifie le développement du modèle mais peut parfois conduire à des erreurs dans la prévision des instabilités [maz01]. Cependant, inclure les pertes inhérentes aux éléments du circuit électrique pour améliorer la précision du modèle n'est pas une tâche triviale ; celle-ci consiste habituellement à manipuler des expressions mathématiques complexes [dav06a].

Ce chapitre décrit l'état de l'art sur la modélisation moyenne dans les deux cas de mode de conduction : continu (CCM) et discontinu (DCM). Le cas du mode continu ayant largement été développé [eri01, mid77a, sun92, sun97] et étant relativement simple, nous n'y revenons que brièvement dans ce chapitre. Les modèles relatifs aux trois topologies de base de convertisseur (abaisseur, élévateur et inverseur) en CCM sont établis. Ils prennent en compte le filtre d'entrée et les imperfections des éléments du circuit. La modélisation moyenne en DCM occupe une place importante dans ce chapitre. La modélisation moyenne dans l'espace d'état des convertisseurs fonctionnant en DCM a aussi été bien développée dans la littérature récente et plusieurs modèles ont été présentés [cuk77, eri01, mak91, sun01, sun98, tym86, vor90]. Tous ces modèles s'expriment sous une forme analytique ou comme un circuit équivalent et peuvent être classés en trois catégories : 1) modèles d'ordre réduit, 2) modèles d'ordre complet, 3) modèles corrigés d'ordre complet. Dans la deuxième partie de ce chapitre, les divers aspects des modèles représentatifs de chacune de ces catégories sont analysés : influence des éléments parasites, caractéristiques petits-signaux dans le domaine fréquentiel. Afin de mieux cerner la validité de ces modèles, un prototype a été réalisé. Une méthodologie simple d'injection petit-signal et de mesure de la réponse fréquentielle est proposée et mise en œuvre pour déterminer la fonction de transfert commande/sortie du prototype expérimental. L'intérêt de cette méthode de mesure expérimentale a été démontré jusqu'à environ 1/3 de la fréquence de découpage.

Modélisation en mode de conduction continue (CCM)

Comme indiqué précédemment, la technique consistant à moyenner dans l'espace d'état fournit des équations petit-signaux basse-fréquence relatives au convertisseur. Les fonctions de transfert du convertisseur et les modèles à circuits équivalents peuvent ensuite être obtenus à partir de ces modèles d'état petits-signaux. La mise en équations du convertisseur fait apparaitre des variables d'état indépendantes telles que le courant dans une inductance et la tension aux bornes d'un condensateur. Ces variables constituent un vecteur d'état $x(t)$. Le convertisseur est alimenté par des sources indépendantes qui constituent le vecteur d'entrée $u(t)$. Le vecteur de sortie est constitué par $y(t)$. Au cours du premier intervalle, lorsque l'interrupteur est fermé pour la période dT_s, le convertisseur se réduit à un circuit linéaire dont les équations d'état peuvent être écrites dans la forme suivante :

$$\dot{x}(t) = A_1 x(t) + B_1 u(t) \ , \quad y(t) = C_1 x(t) + E_1 u(t) \tag{2}$$

Les matrices A_1, B_1, C_1, et E_1 décrivent les connexions de circuit au cours du premier intervalle. Au cours du deuxième intervalle, le convertisseur se réduit à un autre circuit linéaire, dont les équations d'état sont les suivants:

$$\dot{x}(t) = A_2 x(t) + B_2 u(t) \ , \quad y(t) = C_2 x(t) + E_2 u(t) \tag{3}$$

Les matrices A_2, B_2, C_2, et E_2 décrivent les connexions de circuit au cours du deuxième intervalle de durée $(1–d)T_s$. Un modèle non-linéaire à temps-continu est obtenu en moyennant (2) et (3) sur un cycle entier de commutation T_s et est représenté sous la forme suivante:

$$\dot{\bar{x}}(t) = A(d)\bar{x}(t) + B(d)u(t) \ , \quad y(t) = C(d)\bar{x}(t) + E(d)u(t) \tag{4}$$

Dans ce modèle, x est le vecteur d'état et $\bar{x}$ indique la moyenne de x sur un cycle entier de découpage T_s. Les matrices d'état correspondant à ce modèle non-linéaire sont données ci-dessous:

$$\begin{aligned} A(d) &= dA_1 + (1-d)A_2 \ , \ B(d) = dB_1 + (1-d)B_2 \\ C(d) &= dC_1 + (1-d)C_2 \ , \ E(d) = dE_1 + (1-d)E_2 \end{aligned} \tag{5}$$

La représentation ci-dessus est non-linéaire car les matrices du système dépendent du signal de commande $d(t)$. Il est supposé que les fréquences naturelles du convertisseur sont bien inférieures à la fréquence de découpage. Cette hypothèse coïncide avec l'approximation petites-ondulations et se justifie généralement dans un convertisseur bien dimensionné. Elle permet de négliger les composantes haute-fréquence liées au découpage. En outre, les variations sont linéarisées autour d'un point statique de fonctionnement. Les signaux sont exprimés comme la superposition d'un état de repos et de petites variations alternatives :

$$x(t) = X + \tilde{x}(t) \ , \ u(t) = U + \tilde{u}(t) \ , \ y(t) = Y + \tilde{y}(t) \ , \ d(t) = D + \tilde{d}(t) \tag{6}$$

Cette linéarisation petit-signal est justifiée si:

$$\|X\| > \|\tilde{x}(t)\| \ , \ \|U\| > \|\tilde{u}(t)\| \ , \ \|Y\| > \|\tilde{y}(t)\| \ , \ D > \left\|\tilde{d}(t)\right\| \tag{7}$$

$||x||$ représente la norme du vecteur x. Le modèle moyen espace-état qui décrit le convertisseur en régime statique est :

$$0 = AX + BU \ , \quad Y = CX + EU \tag{8}$$

La solution en régime statique est la suivante :

$$X = -A^{-1}BU \ , \quad Y = (-CA^{-1}B + E)U \tag{9}$$

Les équations d'état du modèle petit-signal sont :

$$\begin{aligned} \dot{\tilde{x}}(t) &= A\,\tilde{x}(t) + B\,\tilde{u}(t) + G\,\tilde{d}(t) \\ \tilde{y}(t) &= C\,\tilde{x}(t) + E\,\tilde{u}(t) + H\,\tilde{d}(t) \end{aligned} \tag{10}$$

A, B, C, E, G et H sont des matrices constantes qui dépendent de la topologie du convertisseur. En général, en CCM, G et H peuvent s'exprimer par :

$$G = \left(A_1 - A_2\right)X + \left(B_1 - B_2\right)U \ , \quad H = \left(C_1 - C_2\right)X + \left(E_1 - E_2\right)U \tag{11}$$

L'équation (10) décrit comment les petites variations de signal dans le vecteur d'entrée et le rapport cyclique excitent les variations dans l'état et la sortie. Maintenant, des modèles sous forme de circuits équivalents des convertisseurs continu/continu peuvent être construits en utilisant les équations moyennées espace-état. En suivant les étapes décrites ci-dessus, nous avons construit les modèles moyens linéarisés des trois convertisseurs de base (abaisseur, élévateur et inverseur) en incluant le filtre d'entrée et les imperfections du circuit. Les détails peuvent être consultés dans le chapitre 2 du manuscrit.

Modélisation en mode de conduction discontinu (DCM)

Etat de l'art

Les modèles analytiques concernant le fonctionnement en DCM sont essentiels pour l'analyse et la conception des convertisseurs continu/continu dans la plupart des applications. Beaucoup d'efforts ont été faits au cours des deux dernières décennies pour modéliser les convertisseurs fonctionnant en DCM [sun98]. Contrairement au CCM, des modèles moyens d'ordres différents sont présentés en cas de DCM. Certains de ces modèles sont obtenus en moyennant directement le circuit [eri01, vor90], d'autres en moyennant les équations d'état [cuk77, sun01]. Cependant, tous les modèles moyens en DCM peuvent être classés en trois principales catégories :

1. Modèles d'ordre réduit [cuk77, sun00, sun01]
2. Modèles d'ordre complet [mak91, vor90]
3. Modèles corrigés d'ordre complet [nir01, sun01, sun97]

Bien que ces modèles soient obtenus en moyennant dans l'espace-état ou par l'intermédiaire d'un circuit moyenné, les équations qui en résultent sont souvent identiques ou équivalentes. Le modèle est par conséquent d'ordre réduit ou d'ordre complet. Pour une topologie de convertisseur donnée, les modèles moyens d'ordre réduit sont généralement obtenus par une approche de moyennage espace-état [cuk77] ou par d'autres approches similaires [tym86], pour lesquelles le courant discontinu dans l'inductance est considéré comme une variable dépendante. Il n'apparaît donc pas comme une variable d'état. Bien que les modèles d'ordre réduit puissent prédire correctement le comportement basse-fréquence d'un convertisseur, de grandes divergences apparaissent à des fréquences plus élevées (au-dessus environ 1/10 de la fréquence de découpage). L'absence de courant dans l'inductance d'un modèle moyen est aussi très gênante dans certaines applications : par exemple, dans un PFC[1] monophasé, le courant dans l'inductance est la variable à contrôler. Afin de surmonter les difficultés liées à ces modèles, des modèles moyens d'ordre complet ont été présentés pour analyser le fonctionnement en DCM d'un convertisseur [vor90] et [mak91]. Ces modèles maintiennent toutes les variables d'état du convertisseur, y compris le courant discontinu dans l'inductance. Ainsi ils se traduisent par une amélioration de précision par rapport aux modèles d'ordre réduit. Toutefois, certaines divergences ont toujours été observées à hautes fréquences comme il sera montré ultérieurement dans ce chapitre [sun01].

Plus récemment, des modèles moyens corrigés d'ordre complet ont été proposés. Ils prennent en compte très précisément les dynamiques haute-fréquences du courant dans l'inductance. Ces modèles sont développés dans l'espace d'état [sun01], ainsi que pour la moyenne du circuit [eri01, sun00]. Ainsi, en utilisant une nouvelle contrainte de rapport-cyclique et en corrigeant le modèle espace-état avec une matrice spéciale, des modèles corrigés d'ordre complet ont été obtenus pour un convertisseur idéal. Toutefois, aucun des modèles visés ci-dessus n'a été validé expérimentalement alors que le convertisseur est toujours supposé idéal.

Dans une deuxième partie de ce chapitre, les limites de validité des modèles moyens en DCM sont évaluées. Leurs précisions respectives sont analysées par des simulations ainsi que par des mesures expérimentales sur un prototype de convertisseur abaisseur. Pour uniformité de l'étude, seuls les modèles représentatifs de chaque groupe sont comparés, et les parasites du

[1] Power Factor Corrector

circuit sont inclus dans les équations du modèle. Pour la simplicité et la clarté de cette étude comparative, nous n'avons pas immédiatement examiné l'effet du filtre d'entrée (qui sera incorporé dans les équations du modèle plus loin dans ce chapitre). Afin de résoudre la difficulté de traiter des expressions complexes, un outil d'analyse symbolique, Mathematica, est utilisé dans le calcul et la simplification des modèles petits-signaux non-idéaux.

Paradoxe de moyenne en DCM

En CCM, un cycle de commutation T_s est divisé en deux sous-intervalles, et les rapports respectives de ces intervalles sont d_1 et $d_2 = 1 - d_1$. Il est supposé que le rapport cyclique d_1 de l'interrupteur actif est contrôlé de façon externe. Il est également supposé que la moyenne du produit est égale au produit des moyennes, en particulier

$$\overline{Bu} = \overline{B} \cdot \overline{u} \tag{12}$$

$$\overline{Ax} = \overline{A} \cdot \overline{x} \tag{13}$$

L'approximation (12) est généralement acceptable lorsque l'ondulation de source est négligée. L'approximation (13) est acceptable si les variables ne s'écartent pas sensiblement de la moyenne de leurs valeurs (approximation faible-ondulation) et donc seules les matrices A_1 et A_2 commutent. Ces deux hypothèses sont couramment utilisées pour la modélisation des convertisseurs fonctionnant en CCM [mid77a] et ont également été appliquées au mode de conduction à la frontière (BCM : Boundary Conduction Mode) [che01].

En DCM, il y a trois configurations topologiques. Dans ce mode, un cycle de commutation est divisé en trois sous-intervalles correspondant respectivement à d_1, d_2 et $d_3 = 1 - d_1 - d_2$. La modélisation moyenne conventionnelle pour un convertisseur fonctionnant en DCM a été résumée dans [cuk77, sun01] et ([eri01], Chap. 7). Pour ce mode, l'application direct de (2)-(4) conduit à :

$$\dot{\bar{x}} = [d_1 A_1 + d_2 A_2 + d_3 A_3]\bar{x} + [d_1 B_1 + d_2 B_2 + d_3 B_3]v_{in} \tag{14}$$

Cette expression n'est plus exacte. La méthode classique représentée par (14) consiste à moyenner uniquement les matrices du système mais pas nécessairement les variables d'état [sun01]. L'hypothèse simplificatrice faite dans (13) présente maintenant un problème pour la variable d'état rapide i_L, laquelle est égale à zéro dans le troisième sous-intervalle. En particulier, la moyenne de i_L dans le troisième sous-intervalle est égale à zéro, alors qu'une moyenne classique en espace-état implique que cette valeur soit $d_3\bar{i}_L$. Puisque $\bar{i}_L$ n'est pas nulle, le résultat de la moyenne classique n'est pas nul à moins que la longueur du sous-intervalle d_3 soit nul, ce qui n'est vrai que dans le CCM ou à la limite CCM/DCM.

Une analyse détaillée se rapportant à l'inexactitude de (14) peut être trouvée dans [sun01]. Cette étude explique que le courant moyen dans l'inductance (comme un composant de $\bar{x}$) diffère de sa véritable moyenne d'un facteur $(d_1 + d_2)$. Une modification de (14) est donc proposée dans [sun01] pour le cas DCM. Cette correction peut être réalisée en divisant le(s) courant(s) d'inductance(s) dans la partie droite de (14) par un facteur $(d_1 + d_2)$. Une approche systématique à cet égard est de réorganiser le vecteur d'état $\boldsymbol{x}$ tel que $\boldsymbol{x} = \begin{bmatrix} \boldsymbol{i}_L & \boldsymbol{v}_C \end{bmatrix}^T$, où les sous-vecteurs $\boldsymbol{i}_L$ et $\boldsymbol{v}_C$ contienent les courants dans toutes les inductances (n_L) du convertisseur en DCM et les tensions des condensateurs respectivement, et de définir une matrice **M** comme il suit :

$$\mathbf{M} = diag\left[\underbrace{\frac{1}{d_1+d_2},\cdots,\frac{1}{d_1+d_2}}_{n_L},\overbrace{1,\cdots,1}^{N-n_L}\right], \quad \dim(\mathbf{M}) = N \tag{15}$$

En utilisant cette matrice, le modèle moyen modifié qui prédit correctement le comportement en DCM est le suivant :

$$\dot{\bar{x}} = [d_1A_1 + d_2A_2 + (1-d_1-d_2)A_3]\mathbf{M}\,\bar{x} + [d_1B_1 + d_2B_2 + (1-d_1-d_2)B_3]v_{in} \tag{16}$$

En outre, d_2 devient une variable dépendante qui peut maintenant être exprimée comme une fonction algébrique des autres variables du système. Cette dépendance de d_2 est souvent appelée la « contrainte du rapport-cyclique » [eri01, sun01].

Obtention des modèles moyens des différents ordres

1) Modèles d'ordre réduit

La dynamique rapide de i_L en DCM peut être négligée lors de l'examen des réponses dans la gamme des basses fréquences. Dans ce cas, la valeur moyenne de i_L et d_2 peut être exprimée comme une fonction algébrique du signal d_1 et la valeur moyenne des autres variables. Une relation volt-seconde du courant dans l'inductance est utilisée dans ce cas pour définir la dépendance de d_2 sur d'autres variables. L'ordre du modèle moyen résultant est ainsi réduit d'une unité par rapport à celui du modèle espace-état d'origine. Pour une topologie abaisseur idéale, l'équilibre volt-seconde sur un cycle de commutation implique la contrainte suivante sur le rapport-cyclique [cuk77, sun01]:

$$d_2 = \frac{v_{in} - \bar{v}_o}{\bar{v}_o} \cdot d_1 \tag{17}$$

En outre, il est démontré dans [sun01] que le même modèle d'ordre réduit est obtenu quel que soit l'approche utilisée, [cuk77] ou [sun01]. C'est parce que les deux méthodes utilisent la relation de l'équilibre volt-seconde (17) (voir titre « contrainte du rapport-cyclique ») pour obtenir le modèle moyen. En fait, il peut être facilement vérifié que l'utilisation de la relation d'équilibre volt-seconde mène toujours à un modèle d'ordre réduit. Dans cette étude, nous suivons l'approche classique de [cuk77] pour déduire les modèles d'ordre réduit.

2) Modèles d'ordre complet

La dynamique du courant d'inductance est incluse dans les modèles moyens d'ordre complet (e.g. méthode du rapport-cyclique équivalent [mak91], et modèle à circuit-équivalent [vor90]). Ces modèles démontrent une amélioration significative par rapport aux modèles d'ordre réduit. La référence [mak91] présente une approche unifiée qui se fonde sur la définition d'un rapport-cyclique équivalent, m, en fonction du rapport cyclique réel d_1. Le convertisseur est ensuite traité comme s'il travaillait en mode de conduction continue avec le rapport cyclique m au lieu de d_1. Pour un convertisseur abaisseur idéal, ce rapport cyclique équivalent m est :

$$m = \frac{d_1^2}{d_1^2 + \frac{2L}{T_s}\left(\frac{\bar{i}_L}{v_{in}}\right)} \tag{18}$$

Contrairement à [mak91], le modèle d'ordre complet présenté dans [vor90] est basé sur une approche circuit-équivalent d'une cellule de commutation. Cette cellule, comme définie dans [vor90] et [eri01], est un dispositif non-linéaire à trois-terminaux contenant l'interrupteur et la

diode avec un des terminaux commun entre les deux. Toutefois, malgré une approche différente de modélisation, les deux [vor90] et [mak91] donnent exactement le même modèle moyen d'ordre complet pour une topologie de convertisseur donné.

3) Modèles corrigés d'ordre complet

Comme expliqué plus haut, un problème d'incohérence a été détecté dans l'approche classique consistant à moyenner en espace-état lorsqu'elle est appliquée au DCM. Cela est dû au fait que la moyenne est effectuée sur les paramètres de matrices d'état mais pas sur les variables d'état. Ainsi, une moyenne espace-état classique, lorsqu'elle est appliquée au DCM, résulte dans un retard de phase et une chute de gain, lesquels diffèrent sensiblement de la véritable réponse du convertisseur [mak00, sun01]. Une modification a été proposée dans [sun01] pour corriger cette erreur : elle consiste à diviser le courant de l'inductance dans le modèle espace-état par le facteur d_1+d_2. Une approche systématique à cet égard est de réorganiser le vecteur d'état tels que $x=[i_L \quad v_C]^T$ et de le multiplier avec une matrice de correction **M** définie par (15). Ensuite, en utilisant une nouvelle contrainte du rapport-cyclique (19) qui provient de la moyenne du courant d'inductance sur un cycle de commutation, un modèle moyen corrigé d'ordre complet a été obtenu à partir de (16). Cette approche traduit très précisément les dynamiques hautes-fréquences dues au courant dans l'inductance i_L.

$$d_2 = \frac{2L\bar{i}_L}{d_1 T_s (v_{in} - \bar{v}_o)} - d_1 \tag{19}$$

Les termes $\bar{i}_L$ et T_s désignent respectivement le courant moyen dans l'inductance et la période de commutation. Une approche équivalente basée sur un circuit moyenné a également été présentée dans ([eri01], chap. 11). Elle a mené au « modèle à résistance sans-perte » (loss-free resistor model). Toutefois, elle exploite la même contrainte de rapport-cyclique (19). Ainsi, elle conduit au même modèle d'ordre complet que celui présenté par [sun01]. Nous avons utilisé [sun01] à fin de comparaison dans ce chapitre.

Comparaisons des modèles

Pour fournir un modèle moyen espace-état en DCM, la contrainte de rapport-cyclique d_2 a été constatée comme une distinction essentielle entre les modèles d'ordre réduit, modèles d'ordre complet et les modèles corrigés d'ordre complet. Pour faciliter la lecture, les modèles représentatifs de chaque groupe sont résumés dans les tableaux 2.1, 2.2 et 2.3 du manuscrit, lequel est détaillé pour les trois structures idéales : abaisseur, élévateur et inverseur. Malgré une différence d'ordre, tous les modèles moyens présentés ci-dessus prédisent le même état de repos. Une étude comparative porte donc uniquement sur le comportement dynamique petit-signal de ces modèles dans le domaine-fréquentiel. Pour cette comparaison, un convertisseur abaisseur est choisi comme une référence. Dans une étape ultérieure, tous les parasites du circuit sont inclus dans les équations d'état ainsi que dans l'expression de d_2 pour reformuler plus précisément les modèles respectifs de l'abaisseur. Les diagrammes de Bode sont ensuite tracés pour la fonction de transfert commande/sortie. Afin de comparer les réponses des trois types des modèles et étudier l'influence des parasites, leurs gains et phases sont superposés sur une seule figure.

Il est à noter que les modèles d'ordre réduit fournissent une réponse au premier ordre, ce qui sous-estime considérablement la phase. D'autre part, les modèles d'ordre complet et les modèles corrigés d'ordre complet possèdent un pôle supplémentaire à haute fréquence (à une fréquence proche ou supérieure à la fréquence de découpage). Cependant, à basse fréquence, jusqu'à environ 1/10 de la fréquence de découpage, une réponse cohérente est donnée par les

trois modèles comparés. Leur différence devient plus importante à des fréquences plus élevées, particulièrement dans leur phase. La précision améliorée du modèle corrigé d'ordre complet par rapport aux modèles précédents d'ordre complet et d'ordre réduit est validée expérimentalement jusqu'à environ 1/3 de la fréquence de découpage, comme il sera montré plus loin dans cette section. Néanmoins, à des fréquences plus élevées (au dessus de 1/2 de la fréquence de découpage), la validité des modèles moyens est généralement douteuse. L'influence des pertes, en particulier l'effet de l'ESR (Equivalent Series Resistance) des condensateurs, sur la fonction de transfert et sur la position de son pôle haute-fréquence est discuté en détail dans le manuscrit. Il apparaît une différence importante entre les prédictions des modèles d'ordre complet et celles des modèles corrigés d'ordre complet.

Validation expérimentale des modèles

Afin d'étudier expérimentalement l'exactitude de ces modèles moyens, nous avons proposé une méthode simple pour mesurer la fonction de transfert commande/sortie sur un prototype réel de abaisseur. Cette méthode expérimentale, dont le schéma utilisé et les étapes de mesure sont détaillés dans le manuscrit, consiste principalement en l'injection de petites perturbations sinusoïdales dans le signal de commande et dans la mesure des variations correspondantes provoquées en sortie. Les deux signaux, commande et tension de sortie, sont mesurés et traités par Matlab® pour calculer le déphasage moyen et l'atténuation respective. En définitive, ces relevés expérimentaux sont comparés avec les résultats de simulation (prenant en compte les éléments parasites) pour démontrer la validité des modèles. Comme on pouvait s'y attendre, le modèle corrigé d'ordre complet correspond mieux à la réalité que les autres modèles.

La fonction de transfert est évaluée jusqu'à 30*k*Hz, ce qui est environ 1/3 de la fréquence de découpage (100*k*Hz). Plus près ou au-delà de la fréquence de découpage les résultats de mesures deviennent de plus en plus perturbés en raison de l'interaction entre l'injection des perturbations et du bruit de commutation. De plus, l'accroissement de l'atténuation, à des fréquences plus élevées d'environ 1/3 de la fréquence de découpage, rend la mesure du signal de sortie très difficile. En général, à proximité et au-dessus de la fréquence de découpage, les modèles moyens ont une utilité limitée puisque les hypothèses de base de la moyenne ne sont plus valables. Bien que l'approche expérimentale présentée soit assez simple, elle donne d'assez bon résultats dans la gamme de fréquences visée (c'est-à-dire jusqu'à environ 1/3 de la fréquence de découpage). Toutefois, pour effectuer des mesures au-delà de cette gamme de fréquence, des techniques plus sophistiquées de filtrage sont indispensables pour limiter la problématique du bruit et atteindre une précision raisonable.

Conclusions

Dans ce chapitre, divers aspects de la modélisation moyenne petit-signal pour des convertisseurs continu/continu non-idéaux en CCM et particulièrement en DCM font l'objet d'une analyse approfondie. Les expressions analytiques des modèles représentatifs de la littérature sont reformulées pour inclure les parasites. Les modèles moyens d'ordre variable en DCM, fréquemment cités dans la littérature, sont comparés non seulement entre eux mais aussi avec un prototype réel dotés de ses parasites. En plus de confirmer la quasi-exactitude des modèles corrigés d'ordre complet, nous avons testé une technique expérimentale pour mesurer la fonction de transfert commande/sortie petit-signal. L'efficacité de cette technique expérimentale est démontrée dans la gamme de fréquences visée dans la plupart des applications pratiques. En outre, l'influence des éléments parasites sur les caractéristiques des convertisseurs est étudiée dans le domaine de fréquence comme cela est prévu dans le cadre des différents modèles moyens étudiés.

Chapitre 3 : Interactions avec le filtre d'entrée et problématique de la commande : Une solution passive pour la stabilité

Introduction générale

Ce chapitre analyse les interactions entre la commande et le filtre d'entrée. La tendance naturelle en matière de convertisseurs continu/continu est de minimiser leur poids et leur encombrement. Cela incite à augmenter la fréquence de découpage car la taille des composants passifs ainsi que leur coût diminuent avec la fréquence de fonctionnement plus élevée. Par contre, pour une topologie donnée, dans une application donnée, le choix d'une fréquence de découpage plus élevée mène à des perturbations électromagnétiques (EMI), donc généralement plus gênantes. Les alimentations à découpage sont considérées comme perturbatrices dans la mesure où le découpage rapide des tensions et courants génère des champs électromagnétiques pouvant provoquer des interférences avec le fonctionnement du système et de son environnement [jos98, wil98]. Le bruit EMI s'impose notamment dans le courant d'entrée d'un convertisseur à découpage qui interagit avec l'impédance de source primaire [art01]. Combinée avec le bruit rayonné, les perturbations résultantes peuvent polluer sensiblement la source d'alimentation et peuvent également provoquer une dégradation dans les systèmes où de multiples modules convertisseurs sont alimentés par un bus de puissance commun, par exemple dans le cas d'un réseau de distribution en courant continu [art01]. Les topologies Flyback et abaisseur sont particulièrement connues pour leurs courants d'entrée bruyants, car un interrupteur semi-conducteur est directement connecté en série avec l'entrée. D'autres topologies comme l'élévateur et la structure de Cuk sont intrinsèquement plus « propres » à l'entrée.

Afin de combattre les EMI, un filtre d'entrée de type LC est habituellement employé entre un convertisseur continu/continu et sa source d'énergie non-régulée. Une part assez importante du coût d'un convertisseur de puissance correspond aux filtres : il s'agit de le rendre obligatoirement conforme aux diverses normes EMI/EMC. Toutefois, un filtre d'entrée qui a été correctement dimensionné pour répondre aux seules exigences de compatibilité électromagnétique (CEM) peut provoquer certains dysfonctionnements et réduire les performances du convertisseur en régime dynamique [mid76]. Une impédance du filtre d'entrée, vue de l'aval, trop forte à la fréquence de résonance peut interagir avec les boucles de régulation [mid78]. Certains justifient qualitativement cette interaction complexe entre les régulations et le filtre d'entrée par la caractéristique de « résistance dynamique négative » que présente un convertisseur de type continu/continu régulé vu de son entrée : si pour une raison quelconque la tension d'entrée vient à augmenter, le convertisseur réagit de manière à ce que la charge continue à fonctionner à puissance constante, ceci en consommant lui-même moins de courant ; cette évolution en sens inverse du courant et de la tension en aval du filtre d'entrée se traduit bien par l'équivalent d'une « résistance négative » peu propice à amortir ce filtre ! Tout cela conduit à la dégradation des performances dynamiques du système, voire à son instabilité [mid76, mid78, sad04]. Ce chapitre traite de ce problème d'instabilité due à l'interaction des filtres d'entrée avec la boucle de commande.

La cause de l'instabilité en présence d'un filtre en entrée

De par leur nature, les convertisseurs continu/continu sont considérés comme « charges à puissance constante ». Cela signifie que pour un régulateur idéal à découpage, la puissance moyenne consommée reste constante. Si la tension vient à augmenter en entrée, le circuit de commande PWM réduit le rapport cyclique de l'interrupteur pour maintenir une tension

constante en sortie. Cela se traduit par une diminution du courant d'entrée dans la même proportion. En régime de variations, un changement positif dans la tension d'entrée produit un changement négatif dans le courant d'entrée et vice-versa : le convertisseur peut ainsi être considéré comme une « résistance différentielle négative » à ses bornes d'entrée. La valeur de cette résistance dépend du point de fonctionnement du convertisseur :

$$R_{in} = -\frac{\Delta v_{CF}}{\Delta i_{in}} \tag{20}$$

R_{in} est la résistance d'entrée du convertisseur ; Δv_{CF} et Δi_{in} sont les changements progressifs (variations lentes) de la tension et du courant en entrée du convertisseur. Pour analyser le comportement du convertisseur et les diverses interactions dans le système, un modèle simplifié est nécessaire.

Autour d'un point de fonctionnement, lorsque R_{in} peut être considéré comme constante, le système peut être considéré comme linéaire et il est possible d'écrire :

$$s^2 - \frac{s}{R_{in}C_F} + \frac{1}{L_F C_F} = 0 \tag{21}$$

où L_F et C_F sont l'inductance et la condensateur respectivement du filtre d'entrée. Le terme négatif dans cette expression polynomiale caractéristique correspond à une exponentielle positive dans le domaine temporel, ce qui représente un système sans-bornes, donc instable. Ainsi, un filtre non amorti ou légèrement amorti connecté à l'entrée du régulateur peut interagir avec la caractéristique de résistance négative du régulateur. Cela se traduit par l'équivalent d'un oscillateur et explique pourquoi un filtre d'entrée peut conduire à des instabilités. Il faut noter que lorsque la charge est maximale et que la tension d'entrée est minimale, la valeur de la résistance R_{in} est minimale, ce qui représente le pire des cas. En outre, l'impédance d'entrée du convertisseur apparaît comme une résistance négative uniquement aux basses fréquences. À des fréquences plus élevées, cette impédance est influencée par les éléments parasites du filtre.

Amortissement du filtre d'entrée – une solution passive

Une méthode simple proposée dans la littérature pour résoudre le problème d'instabilité est de mettre en place une résistance (évidemment positive) suffisante dans le filtre d'entrée afin de neutraliser l'effet de la résistance négative d'entrée du convertisseur. En conséquence, l'influence du filtre d'entrée sur les fonctions de transfert du convertisseur devient moins sensible, voire négligeable. Toutefois, il n'est pas toujours possible d'ajouter la résistance nécessaire à l'amortissement du filtre : selon sa valeur, elle peut être le siège de pertes énergétiques importantes. Plusieurs configurations sont possibles : une résistance en série avec L_F est traversée par le courant d'entrée dont la seule composante moyenne peut être à l'origine de pertes importantes ; une résistance en série avec C_F pose moins de problèmes de pertes mais dégrade le filtrage ; une résistance R_d en parallèle avec le condensateur C_F est pratiquement soumise à la tension d'entrée et à des pertes prohibitives ; une résistance R_d en parallèle avec L_F mène à des pertes bien moindres mais le filtrage est dégradé [eri01].

En vue de limiter ces problèmes de dissipation, une solution est illustrée à la Fig. 3.4 : un condensateur est connecté en série avec la résistance R_d. Le condensateur empêche la circulation d'un courant continu dans la résistance R_d et limite ainsi les pertes. La valeur du condensateur C_d peut être exprimée comme un multiple de la capacité de filtrage : $C_d = kC_F$. Elle est normalement choisie très importante par rapport à C_F de sorte que l'impédance de la

branche R_d-C_d corresponde essentiellement à la résistance R_d pour la fréquence de résonance f_F du filtre.

L'amortisseur R_d-C_d parallèle, comme illustré Fig. 3.4, trouve des applications importantes dans les convertisseurs continu/continu. Puisqu'une résistance doit être connectée en série avec C_d, ce condensateur peut être choisi parmi ceux dont la résistance série équivalente (ESR) est relativement importante : par exemple les condensateurs électrolytiques ou de type tantale. Cette méthode n'est toutefois guère envisageable dans les convertisseurs alimentés en alternatif à cause de la dissipation énergétique dans la résistance. Dans ces cas, les associations parallèle et série de type R_d-L_d peuvent conduire à un dimensionnement plus favorable.

Interactions avec le filtre d'entrée en CCM

Dans ce résumé de thèse, nous analysons seulement le convertisseur abaisseur. Les résultats relatifs à l'élévateur et à l'inverseur sont détaillés dans le manuscrit complet. En supposant une source de tension constante V_{in} et une charge purement résistive, la fonction de transfert commande/sortie en boucle ouverte d'un convertisseur continu/continu non-idéal peut s'exprimer selon son modèle linéaire petit-signal sous la forme suivante:

$$G(s) = \frac{\tilde{v}_o}{\tilde{d}} = K \frac{A_3 s^3 + A_2 s^2 + A_1 s + A_0}{B_4 s^4 + B_3 s^3 + B_2 s^2 + B_1 s + B_0} \tag{22}$$

Dans cette expression : $K = V_{in}/m$; m et les coefficients A_k et B_k de $G(s)$ dépendent de la famille et du mode de conduction du convertisseur. Pour un convertisseur abaisseur non-idéal équipé d'un filtre d'entrée, ces coefficients sont donnés dans le manuscrit. Le gain et la phase de cette fonction de transfert y sont tracés pour un fonctionnement avec et sans filtre d'entrée.

Il est évident que l'incidence du filtre de sortie sur cette fonction de transfert se traduit par un déphasage de -180° à fréquence élevée. Or, le tracé de la phase montre que l'ajout d'un filtre d'entrée mène à une résonance supplémentaire à la fréquence de résonance de ce filtre et à une nouvelle rotation de phase de -360°. Lorsqu'une régulation classique de tension est réalisée, sa bande passante est généralement inférieure à la fréquence de coupure du filtre de sortie. Sans tenir compte du filtre d'entrée, le correcteur peut être de type PI et dimensionné sans tenir compte du retard de 180° dû au filtre de sortie. Toutefois, si la brutale rotation de phase causée par le filtre d'entrée à sa fréquence de coupure se situe également à une fréquence inférieure à la fréquence de coupure du filtre de sortie, le risque est grand d'observer une instabilité dans la boucle. Un correcteur de type PID ne peut pas suffire à combattre un retard de phase trop important et à ramener à la stabilité. Il est démontré dans le manuscrit que $G(s)$ comprend désormais une paire de pôles complexes et une paire de RHP (Right Hand Plane) zéro associée à la dynamique du filtre d'entrée. Comme mentionné précédemment, le système à boucle fermée peut être stabilisé en ajoutant un amortissement suffisant dans le filtre d'entrée. Un critère peut alors être défini pour le dimensionnement de l'amortissement nécessaire de façon à déplacer tous les zéros de la fonction de transfert du côté droit vers le côté gauche du plan complexe. Toutefois, les contraintes de dimensionnement doivent être calculées pour le cas le plus défavorable, ce qui correspond à un convertisseur idéal sans pertes internes. Nous avons d'abord exprimé la fonction de transfert en négligeant tous les éléments parasites des composants mais en incluant l'amortisseur de type R_d-C_d (celui montré en Fig. 3.4). Ensuite nous avons appliqué le critère de Routh au numérateur de cette fonction de transfert afin d'obtenir les conditions nécessaires pour amener tous ses zéros vers le côté

gauche du plan *s*. Ces conditions de stabilité peuvent généralement être exprimées sous la forme générale suivante :

$$a_0 + a_1 R_d > 0 \tag{23a}$$

$$b_0 + b_1 R_d + b_2 R_d^2 > 0 \tag{23b}$$

Les coefficients a_k et b_k sont constants et peuvent être exprimés en fonction des paramètres du circuit. Pour un convertisseur abaisseur idéal ces coefficients sont donnés ci-dessous :

$$\begin{aligned} &a_0 = (1+k)L_F C_F \ , \quad a_1 = -kL_F C_F D^2 / R \\ &b_0 = (1+k)D^2 L_F^2 C_F / R \ , \quad b_1 = -kL_F C_F \left(\frac{D^4 L_F}{R^2} + kC_F \right) , \quad b_2 = \frac{k^2 D^2 L_F C_F^2}{R} \end{aligned} \tag{24}$$

Afin de déterminer la région de fonctionnement stable, ces conditions (23) sont tracées sur un plan dont l'axe horizontal représente la valeur normalisée de la résistance d'amortissement R_d, et l'axe vertical correspond à la valeur du rapport k des condensateurs. Cependant, cette région de stabilité dépend des paramètres du convertisseur donné et varie si un des composants L_F ou C_F est modifié.

Interactions avec le filtre d'entrée en DCM

En suivant la même procédure que celle présentée ci-dessus, les conditions de stabilité peuvent aussi être déterminées pour le mode de conduction discontinue (DCM). Toutefois, en général, les observations et les conclusions tirées de l'analyse des interactions avec le filtre d'entrée en CCM peuvent être également appliquées aux mêmes convertisseurs mais fonctionnant en DCM. Les modèles moyens espace-état d'ordre variant en DCM ont déjà été traités dans le chapitre précédent, et nous avons sélectionné les modèles d'ordre réduit pour l'étude des interactions avec le filtre d'entrée en DCM. Toutefois, il est à rappeler ici que ce type de modèles ignore la dynamique rapide du courant d'inductance en DCM. En raison de cette approximation les pôles haute-fréquence et les zéros du côté-droit (dans le cas de l'élévateur et celui de l'inverseur) n'apparaissent pas dans la fonction de transfert du convertisseur. Par conséquent, les conditions de stabilité obtenues sont assez simples en DCM par rapport à celles de la CCM, en particulier pour l'élévateur et l'inverseur. Ce qui est intéressant est que le numérateur de la fonction de transfert des trois convertisseurs (abaisseur, élévateur et inverseur) est identique en fonctionnement DCM. Ainsi, les conditions de stabilité obtenues pour la DCM sont également les mêmes pour l'abaisseur, l'élévateur et l'inverseur. Ces conditions peuvent aussi être exprimées dans la forme générale (23) pour chacun de ces trois convertisseurs idéaux, et les coefficients a_k et b_k de (23) pour DCM sont donnés ci-dessous :

$$\begin{aligned} &a_0 = (1+k)L_F C_F \ , \quad a_1 = -kL_F C_F M^2 / R \\ &b_0 = (1+k)M^2 L_F^2 C_F / R \ , \quad b_1 = -kL_F C_F \left(M^4 L_F / R^2 + kC_F \right) , \quad b_2 = k^2 M^2 L_F C_F^2 / R \end{aligned} \tag{25}$$

Il est à noter, cependant, que les coefficients a_k et b_k de (23) en DCM sont exactement les mêmes (pour les trois convertisseurs de base) que ceux, donnés par (24), qui ont déjà été obtenus pour un convertisseur abaisseur fonctionnant en CCM. La seule différence : au lieu d'utiliser la valeur d'équilibre du rapport-cyclique D comme en (24), la valeur d'équilibre du rapport de tension $M = V_{out}/V_{in}$ apparaît dans (25) pour la DCM. Cela implique que la région de stabilité sera la même que celle tracée précédemment pour le convertisseur abaisseur

opérant en CCM. Une autre remarque est que la condition d'ordre supérieur (23b) est une condition nécessaire et suffisante. Si la condition (23b) est satisfaite, la première inégalité (23a) sera alors naturellement satisfaite. En outre, la même condition s'applique à l'élévateur et à l'inverseur fonctionnant en DCM. La raison en est que le zéro haute-fréquence du côté-droit, le même pour les deux types de convertisseurs, n'apparaît plus dans leur modèle moyen d'ordre réduit. Par conséquent, le nombre de conditions requises est également réduit à deux pour ces deux convertisseurs en DCM (contrairement à trois conditions en cas de CCM).

Interactions avec le filtre d'entrée de convertisseurs en cascade

Le problème d'instabilité se pose aussi dans le cas où deux convertisseurs (ou plus) sont connectés en cascade. Une des applications de ce type de configuration est la situation où un rapport cyclique trop petit ou trop grand serait nécessaire pour obtenir une certaine tension en sortie. La configuration cascade fournit une solution assez pratique pour accéder à cet objectif. Toutefois, des oscillations peuvent se produire à cause non seulement des interactions entre un filtre d'entrée et un convertisseur mais aussi par les interactions possibles entre plusieurs étages en cascade.

Dans une deuxième partie de ce chapitre nous avons tout d'abord présenté un modèle moyen généralisé des convertisseurs en cascade à n étages avec un filtre d'entrée et incluant toutes les imperfections du circuit. Puis en utilisant ce modèle moyen nous avons traité un exemple où deux convertisseurs abaisseurs sont connectés en cascade avec un filtre LC en entrée et une charge résistive. Le but était de rectifier l'influence du filtre d'entrée en se basant sur la fonction de transfert en boucle ouverte, ce qui va ramener, par conséquence, la conception du régulateur un problème classique. Il est validé expérimentalement que avec un filtre bien-amorti, le système reste stable même avec un régulateur classique (e.g. correcteur PI). Les mêmes démarches, comme elles sont présentées dans la première partie de ce chapitre, permettent d'obtenir les conditions de stabilité en fonction des paramètres de l'amortisseur R_d-C_d dans ce cas particulier. Il a été démontré que la procédure de dimensionnement de l'amortisseur proposé dans ce chapitre est aussi applicable à cet exemple. Les mêmes types d'interactions existent entre le premier et le deuxième étage du convertisseur. Cependant l'ensemble peut être stabilisé en ajoutant l'amortissement suffisant uniquement au circuit du filtre d'entrée. Une région stable pour cet exemple particulier a été obtenue et validée expérimentalement. Les résultats détaillés sont dans le manuscrit.

Conclusions

Le problème d'instabilité associé à la présence du filtre d'entrée dans les convertisseurs continu/continu est traité dans ce chapitre. Une solution purement passive à ce problème d'instabilité est étudiée. Une procédure de dimensionnement d'amortisseur de type R_d-C_d connecté en parallèle du condensateur dans le filtre est proposée. Elle est basée sur la fonction de transfert en boucle ouverte. Les conditions de la stabilité sont déduites pour les topologies de convertisseur de base (abaisseur, élévateur, inverseur). Ainsi, une région de stabilité est identifiée. Elle fixe les limites minimales et maximales de la résistance d'amortissement qui doit être ajoutée si les résistances parasites du filtre d'entrée ne sont pas suffisantes. Certaines considérations pour optimiser cet amortissement sont également discutées. À la fin, une étude particulière porte sur des convertisseurs abaisseurs en cascade et fonctionnant avec filtre d'entrée.

Chapitre 4 : Influence d'un amortissement passif sur le rendement du convertisseur : Étude critique

Introduction et motivations

L'amortissement passif des filtres d'entrée dans les convertisseurs continu/continu est critiquable en raison des pertes pas forcément négligeables qu'il implique dans des résistances. Toutefois, une évaluation quantitative précise de son impact sur le rendement semble n'avoir jamais été présentée. Le mode de fonctionnement doit influencer les pertes dans les résistances d'amortissement mais cette influence reste à chiffrer. Dans le cas de l'amortisseur de type R_d-C_d série, le condensateur empêche la circulation d'un courant moyen dans la résistance R_d, ce qui minimise les pertes énergétiques. Toutefois, il subsiste une composante alternative de courant dans la résistance, d'où des pertes. Nous pouvons penser à sophistiquer la commande du convertisseur afin de limiter ce besoin en résistance d'amortissement mais au détriment de la simplicité de réalisation. Un système de commande plus complexe implique d'autres contraintes ainsi que des difficultés de conception et de mise en œuvre. Considérant que l'implication des amortisseurs passifs constitue encore un domaine peu exploré, nous avons poussé l'analyse du circuit R_d-C_d plus en détail au cours de cette thèse afin d'en déduire l'influence sur le rendement de conversion. Les résultats de cette étude constituent ce chapitre.

Ce chapitre comprend donc l'analyse généralisée des pertes dues à l'amortissement. L'approche proposée étant simple et directe, elle permet de mieux cerner qualitativement les conséquences de l'utilisation de résistances d'amortissement, généralement ignorées dans la littérature consacrée à ce sujet, tout en les chiffrant assez précisément. Le cas pratique du réseau R_d-C_d, le plus utilisé dans les convertisseurs continu/continu, est étudié théoriquement et expérimentalement. Les conditions de fonctionnement capables de porter les pertes d'amortissement à un niveau inacceptable sont identifiées. Par exemple, il apparaît que le rendement du convertisseur se dégrade nettement pour les charges élevées lorsque les résistances d'amortissement sont assez faibles. En outre, il est démontré que ces pertes sont considérablement plus importantes pour les convertisseurs de type abaisseur que pour les convertisseurs élévateurs. Il est aussi constaté que ces pertes dépendent du point de fonctionnement du convertisseur. En conséquence de ces résultats, une attention toute particulière doit être portée à l'aspect énergétique lors du dimensionnement de l'amortisseur. Dans l'hypothèse où l'optimisation de l'amortisseur mènerait à des pertes intolérables, il faudrait envisager l'utilisation d'une solution active pour assurer la stabilité. Le choix final se traduit généralement par un compromis entre la complexité du système de commande et le rendement de conversion.

Analyse des pertes énergétiques

Généralités

Afin d'évaluer le rendement, nous devons d'abord calculer le courant circulant dans la branche R_d-C_d. La figure 4.2 situe cette branche dans son contexte. Nous supposons que le courant consommé de la source $i_{LF}(t)$ en régime statique soit maintenu constant et puisse être exprimé comme $I_{LF} = f(d, I_o)$. Le paramètre d est le rapport cyclique de l'interrupteur ; I_o est la valeur du courant de sortie en régime statique, lequel est donné par $I_o = V_o / R$.

Dans cette dernière expression, V_o est la valeur de la tension de sortie en régime statique et R est la résistance de charge. En outre, le courant total $i_s(t)$ entrant dans la branche parallèle peut être toujours exprimé comme ci-dessous :

$$i_s(t) = i_{LF}(t) - i_{in}(t) \tag{26}$$

Partant du principe de conservation des courants au nœud n (voir Fig. 4.2), il est possible de déterminer une équation différentielle linéaire non-homogène du premier ordre :

$$\frac{di_2(t)}{dt} + a \cdot i_2(t) = b(t) \tag{27}$$

avec :

$$\begin{aligned} a &= \frac{1+1/k}{R_d C_F} \\ b(t) &= \frac{i_s(t)}{R_d C_F} \end{aligned} \tag{28}$$

La solution de l'équation (27) est la valeur instantanée du courant recherché, lequel dépend de la topologie du convertisseur.

Convertisseur abaisseur

Dans le cas d'un convertisseur abaisseur idéal, l'évolution du courant d'entrée $i_{in}(t)$, celle du courant de source $i_{LF}(t)$ et celle du courant dans la branche parallèle $i_s(t)$ peuvent être tracées. En utilisant ces courants, une solution de l'équation (27) peut être déterminée pour les deux sous-intervalles du cycle de commutation comme suit :

Intervalle t_{on} : $0 < t < dT$

$$i_{2(on)}(t) = A + \lambda_1 \cdot e^{-at} \tag{29a}$$

Intervalle t_{off} : $0 < t < (1-d)T$

$$i_{2(off)}(t) = B + \lambda_2 \cdot e^{-at} \tag{29b}$$

Avec :

$$\begin{aligned} A &= -\frac{(1-d)I_o}{aR_d C_F} \quad , \quad B = \frac{dI_o}{aR_d C_F} \\ \lambda_1 &= \frac{I_o}{aR_d C_F}\left(1 - \frac{(e^{-adT}-1)}{(e^{-aT}-1)} \cdot e^{-a(1-d)T}\right) \\ \lambda_2 &= -\frac{I_o}{aR_d C_F} \cdot \frac{(e^{-adT}-1)}{(e^{-aT}-1)} \end{aligned} \tag{30}$$

Il est à noter que λ_1 et λ_2 sont des constantes d'intégration dont les valeurs peuvent être déterminées en imposant les conditions limites suivantes :

$$i_{2(on)}(0) = i_{2(off)}\left((1-d)T\right)$$
$$i_{2(off)}(0) = i_{2(on)}(dT) \tag{31}$$

La valeur efficace du courant $i_2(t)$ est calculable en utilisant la relation suivante :

$$I_{2RMS} = \sqrt{\frac{1}{T}\left(\int_0^{dt} i_{2(on)}^2(t)\cdot dt + \int_0^{(1-d)T} i_{2(off)}^2(t)\cdot dt\right)} \tag{32}$$

Les pertes instantanées et les pertes moyennes peuvent alors être déterminées : $i_2^2(t)R_d$ et $I_{2RMS}^2 R_d$, respectivement. Les pertes résultantes peuvent ainsi être calculées pour différentes valeurs de R_d en conservant le courant de charge constant et vice versa. Les résultats sont donnés dans le manuscrit en fonction de R_d et I_o pour un convertisseur abaisseur de puissance nominale égale à 10W. Les pertes, la résistance d'amortissement et le courant de sortie sont normalisés par rapport à la puissance nominale, la résistance de charge et le courant nominal de sortie, respectivement. Il s'agit d'un moyen pour évaluer la réduction du rendement en fonction de R_d et du courant de sortie.

Il apparaît ainsi que le rendement global de conversion d'abord tend à augmenter avec R_d, pour de très petites valeurs de R_d, puis atteint un maximum, puis diminue pour des valeurs plus élevées de R_d. Pour un convertisseur donné, la valeur de R_d qui correspond aux pertes maximales peut facilement être déterminée en dérivant l'expression de $R_d I_{2RMS}^2$. Il est souhaitable de s'écarter autant que possible de cette valeur critique, au moment de la conception de l'amortisseur, tout en respectant les conditions de stabilité requises. Il faut également noter que le rendement tend à diminuer lorsque le courant de charge augmente.

À l'heure actuelle, de nombreux convertisseurs de puissance sont alimentés par des sources d'énergie renouvelables non-régulées (par exemple des panneaux solaires, piles à combustible…). Ces types de sources imposent de grandes variations de tension qui peuvent entrainer le rapport cyclique d à s'écarter sensiblement de la valeur nominale dans les convertisseurs en aval. Ainsi, il peut être utile d'étudier l'effet de d sur les pertes dans l'amortisseur. Dans le manuscrit, nous avons tracé l'évolution des pertes normalisées relatives au convertisseur abaisseur cité précédemment, en fonction de d et R_d, pour une même puissance nominale de 10W, un courant nominal de 0.8A en sortie, et pour une variation de d entre 0.2 et 0.8. Il s'avère ainsi que le rendement du convertisseur a tendance à décroitre lorsque d s'approche de 0.5, les pertes maximales se produisant quand d = 0.5. Ainsi, il apparaît qu'une résistance d'amortissement correctement dimensionnée pour fonctionner au point nominal n'est pourtant pas optimale si le point de fonctionnement varie sensiblement. L'importance de la dégradation du rendement est liée aux valeurs de d et de R_d.

Convertisseur élévateur

Suivant la même méthode que celle décrite précédemment, une solution de l'équation différentielle (27) peut être déterminée pour un convertisseur élévateur :

Intervalle t_{on} : $0 < t < dT$

$$i_{2(on)}(t) = A(t) + \lambda_1 \cdot e^{-at} \tag{33a}$$

Intervalle t_{off} : $0 < t < (1-d)T$

$$i_{2(off)}(t) = B(t) + \lambda_2 \cdot e^{-at} \tag{33b}$$

où

$$A(t) = \frac{(1-d)(2-2at+adT)I_o}{2a^2 LRR_d C_F}$$
$$B(t) = -\frac{d(2-2at+a(1-d)T)I_o}{2a^2 LRR_d C_F}$$
$$\lambda_1 = -\frac{I_o}{a^2 LRR_d C_F} \cdot \frac{(e^{-a(1-d)T}-1)}{(e^{-aT}-1)} \tag{34}$$
$$\lambda_2 = \frac{I_o}{a^2 LRR_d C_F} \cdot \left(1 - \frac{(e^{-a(1-d)T}-1)}{(e^{-aT}-1)} \cdot e^{-adT}\right)$$

Les mêmes conditions aux limites, comme indiqué par (31), sont appliquées pour évaluer les constantes d'intégration λ_1 et λ_2. Comme précédemment, la simulation des pertes normalisées, leur influence sur le rendement et l'effet de *d* sur le rendement d'un convertisseur élévateur de puissance nominale 10W, sont présentés dans le manuscrit. Nous constatons les mêmes tendances qu'avec l'abaisseur. Toutefois, les pertes sont moins importantes et varient beaucoup moins dans l'amortisseur de l'élévateur. Par exemple, lorsque le courant de charge est doublé par rapport à sa valeur nominale, les pertes maximales peuvent aller jusqu'à 1.3% dans l'amortisseur de l'élévateur alors qu'elles atteignent 4% dans celui de l'abaisseur. Cette différence de comportement provient de la nature discontinue du courant en entrée des convertisseurs abaisseurs et de leurs dérivés. L'influence du condensateur du filtre d'entrée C_F sur les pertes d'amortissement est aussi étudiée dans ce chapitre. Une augmentation de la valeur de C_F entraîne une diminution de la tension efficace aux bornes de la branche d'amortissement, d'où une réduction des pertes d'amortissement. Afin de pouvoir mieux visualiser cet effet, les pertes d'amortissement sont simulées dans le manuscrit pour différentes valeurs de C_F dans un abaisseur et dans un élévateur.

Conclusions

Une analyse générale du rendement des convertisseurs continu/continu avec filtre d'entrée amorti par un moyen passif est présentée dans ce chapitre. Les résultats expérimentaux et ceux des simulations révèlent que l'utilisation d'un amortissement passif doit être conçue avec beaucoup d'attention, en particulier lorsque la charge du convertisseur est amenée à varier dans de grandes proportions. Généralement, un compromis est à trouver entre la complexité du système de commande et le rendement. L'impact des résistances d'amortissement n'est jamais à négliger d'emblée. Ce travail a permis de démontrer que la dégradation du rendement est plus importante dans un abaisseur que dans un élévateur (parce que le courant est découpé en aval du filtre de l'abaisseur), lorsque le rapport cyclique est proche de 0,5 (parce que les ondulations sont plus fortes dans le filtre pour cette valeur), lorsque le courant de charge augmente (parce que les ondulations augmentent avec la charge) et passe par un maximum pour une certaine résistance d'amortissement critique (une résistance nulle et une résistance infinie mèneraient à des pertes nulles).

L'emploi de résistances d'amortissement est critiquable. Il permet toutefois de conserver une commande assez simple (par exemple un correcteur de type PI). L'analyse systématique présentée dans ce chapitre apporte certains éléments en vue de statuer sur la structure d'ensemble pour une application donnée : filtre, convertisseur et commande.

Chapitre 5 : Commande des convertisseurs continu/continu avec filtre en entrée : Une solution active pour la stabilité

Introduction et motivations

Une alimentation à découpage se doit d'être stable et précise. Sa réponse dynamique doit être optimisée, notamment dans les domaines des télécommunications, de l'aéronautique et de l'espace. Toutefois, comme cela a été vu dans le chapitre 3, un convertisseur est toujours associé à un filtre d'entrée et à un système de régulation, cette association pouvant provoquer l'instabilité du système si le filtre n'est pas suffisamment amorti [mid76]. Dans de nombreux convertisseurs continu/continu, la solution consiste à amortir les oscillations du filtre par des résistances dans le filtre d'entrée pour assurer la stabilité [mid78, usm07]. Différentes méthodes d'amortissement passif sont examinées en détail au chapitre 3. Bien que ces amortisseurs soient efficaces pour stabiliser le système, les pertes qui en résultent dans le filtre peuvent dégrader le rendement comme cela est décrit au chapitre 4. En outre, le risque d'instabilité dépend du régulateur : il est accru pour un régulateur rapide. Il est difficile de trouver une loi de commande permettant de surmonter ces difficultés en raison de la présence de non-linéarités et l'ordre élevé ($n > 2$) du système. La suppression totale de toute résistance (non parasite) dans le filtre d'entrée est encore bien plus difficile à atteindre. Il s'agit de trouver des lois de commande capables d'assurer à elles seules la stabilité d'un système naturellement instable. Peu de données existent à ce sujet dans les publications.

Dans ce chapitre, nous présentons certaines solutions actives comme alternatives à l'amortissement passif du filtre d'entrée. Dans un premier temps, une commande par retour d'état combinée avec une régulation de type PI est proposée pour assurer la stabilité des convertisseurs continu/continu en présence du filtre d'entrée. La résonance du filtre rend la commande très difficile. Toutefois, l'algorithme de commande proposé assure effectivement la stabilité du système sans l'aide d'aucun composant passif, donc sans pertes énergétiques inutiles. La loi de commande est basée sur un retour d'état complet. Pour ajuster la réponse du système, le calcul des gains de retour d'état est effectué par un placement des pôles du système en boucle fermée. Des simulations sont présentées pour confirmer l'efficacité de la stratégie de commande proposée en présence de grandes variations de la charge et de l'entrée. Afin d'annuler l'erreur dans la réponse en régime établi, un intégrateur de l'erreur entre la consigne et la tension de sortie est également ajouté à ce retour d'état. Le calcul des gains feedback est adapté à différents points de fonctionnement par une évolution continue du vecteur des gains. Ceci est obtenu en utilisant des tableaux indexés par la tension d'entrée et la résistance de la charge.

Ensuite, dans un deuxième temps, une commande par mode-glissement basée sur l'approche de la fonction de Lyapunov [nic95] est discutée. Cette approche est déjà présentée en [nic95] et si nous avons choisi cette méthode c'est uniquement afin de pouvoir comparer avec notre proposition de retour d'état.

Commande par retour d'état

Modèle utilisé pour la commande

Un convertisseur abaisseur avec un filtre non-amorti à l'entrée est utilisé à titre d'exemple pour introduire la commande par retour d'état dans ce chapitre. En général, un convertisseur

peut facilement être représenté par un modèle moyen linéarisé en espace d'état comme indiqué ci-après:

$$\dot{\tilde{x}} = A\tilde{x} + B\tilde{d} + G\tilde{v}_{in} \ , \quad \tilde{v}_o = C\tilde{x} \tag{35}$$

Dans cette expression, $\tilde{x}$ représente le vecteur d'état du système linéarisé prenant en compte les courants dans toutes les inductances et les tensions aux bornes de tous les condensateurs. Pour un convertisseur tel que celui de la Fig. 5.1, ce vecteur d'état peut être défini par : $\tilde{x} = \begin{bmatrix} \tilde{i}_{LF} & \tilde{i}_L & \tilde{v}_{CF} & \tilde{v}_o \end{bmatrix}^T$. Le signe "~" au-dessus de *x* désigne de petites variations dans les signaux correspondants. D'autre part, $\tilde{d}$, $\tilde{v}_o$ et $\tilde{v}_{in}$ sont les quantités scalaires qui représentent les petites variations du rapport cyclique, la tension de sortie et la tension d'entrée, respectivement.

Une intégration de la différence entre la tension de sortie et celle de référence peut être incluse dans la boucle de commande feedback afin de pouvoir supprimer l'erreur en sortie dans le régime établi. Afin de pouvoir réaliser systématiquement la boucle comprenant l'intégrateur et la commande par retour d'état, l'état du système représenté par (35) doit être augmenté et la commande doit être conçue pour ce système d'ordre élevé. Le nouveau système ainsi obtenu peut être décrit par :

$$\dot{\tilde{x}}_a = A'\tilde{x}_a + B'\tilde{d} + G'\tilde{v}_{in} + H'\tilde{v}_{ref} \ , \quad \tilde{v}_o = C'\tilde{x}_a \tag{36}$$

Dans cette expression, $\tilde{x}_a$ représente le vecteur d'état augmenté qui contient également le terme intégral comme une variable d'état. Le nouvel état du système peut s'écrire : $\tilde{x}_a = \begin{bmatrix} \tilde{i}_{LF} & \tilde{i}_L & \tilde{v}_{CF} & \tilde{v}_o & \tilde{e} \end{bmatrix}^T$, où $\tilde{e}$ est définie comme suit :

$$\tilde{e} = \int_0^t (\tilde{v}_{ref} - \tilde{v}_o)\, dt \tag{37}$$

Le modèle (36) peut alors être utilisé pour la synthèse de la commande par retour d'état.

Conception da la commande

L'objectif de la commande est de garantir l'asservissement de la tension de sortie à une référence constante et d'assurer la stabilité du système en présence du filtre d'entrée. Elle doit également être suffisamment robuste pour rejeter les faibles perturbations dues à la tension d'entrée, le courant de charge et la tension de la référence, tout en s'adaptant à l'évolution du point de fonctionnement.

1) Stabilisation avec retour d'état

À l'aide de la technique du retour d'état linéaire, une loi de commande peut être définie comme:

$$\tilde{d} = -k \cdot \tilde{x}_a \tag{38}$$

Dans cette expression, $k = \begin{bmatrix} k_1 & k_2 & \cdots & k_5 \end{bmatrix}$ représente le vecteur des gains qui est à déterminer. Les équations d'état et celle de la sortie du système en boucle fermée se ramènent à :

$$\dot{\tilde{x}}_a = (A' - B'k)\tilde{x}_a + G'\tilde{v}_{in} + H'\tilde{v}_{ref} \ , \quad \tilde{v}_o = C'\tilde{x}_a \tag{39}$$

En supposant que l'ensemble (A' , B') est commandable, la dynamique du système en boucle fermée peut être stabilisée par un choix approprié des valeurs propres de $(A' - B'k)$.

2) Placement des pôles

Pour évaluer les gains k_i, les valeurs propres de $(A' - B'k)$ peuvent être désignées par un placement des pôles du système en boucle fermée. Une méthode simple consiste à calculer le polynôme caractéristique de $(A' - B'k)$ et à identifier ses coefficients en utilisant un autre polynôme qui a les pôles dominants souhaités p_i comme ses racines :

$$\det\left(sI - (A' - B'k)\right) = \prod_{i=1}^{n} (s - p_i) \tag{40}$$

Dans cette expression, n est le nombre de pôles dominants qui sont à placer. Pour n'importe quel système avec tous les zéros du côté gauche dans le plan-s, les valeurs propres peuvent éventuellement être assignées de telle façon que les pôles dominants soient à proximité des zéros du système. Toutefois, lorsque les zéros sont dans la partie droite du plan-s (comme dans notre exemple de l'ensemble filtre-convertisseur), les pôles dominants ne peuvent pas être choisis à proximité des zéros "instables" du système [fra91]. Dans ce cas, pour tout zéro, $z_i = \sigma_i + j\omega_i$, du côté droit dans le plan-s, le pôle correspondant peut être situé à proximité de la position $s_i = -\sigma_i + j\omega_i$. Néanmoins, le cas échéant, l'emplacement des pôles dominants peut être modifié pour les éloigner suffisamment de la frontière de stabilité.

3) Adaptation du vecteur des gains aux variations de la charge et de l'entrée

Le calcul des gains de retour d'état peut être adapté à différents points de fonctionnement par une évolution continue du vecteur des gains. Cet objectif peut être atteint en utilisant des tableaux de recherche (à deux dimensions) indexés par la tension d'entrée et la résistance de charge. La méthode de recherche utilisée pour les points situés entre ou au-delà des valeurs stockées est l'interpolation ou l'extrapolation. La valeur de la résistance de charge peut être estimée en mesurant le courant de charge. Toutefois, à cette fin, un capteur de courant supplémentaire peut être nécessaire.

Exemple d'application : Abaisseur avec filtre d'entrée

Un convertisseur abaisseur opérant dans le mode CCM avec un filtre en entrée est choisi à titre d'exemple pour illustrer la conception de la commande et l'évaluation de ses performances. Pour ce convertisseur, la matrice A' et les vecteurs B' , C' , G' et H' de son modèle d'état élevé sont présentés dans le manuscrit.

Afin d'obtenir la réponse dynamique désirée, les pôles du système en boucle fermée sont placés en -0.5×10^4, $-2(1 \pm i)\times10^4$ et $-3(1 \pm i)\times10^4$ respectivement. Ici, il convient de mentionner que les modèles moyens linéarisés sont généralement valables jusqu'à environ 1/3 de la fréquence de découpage [dav06b] (f_s = 100kHz dans notre cas). Par conséquent, les pôles dominants du système sont placés dans cette gamme de fréquence. Les gains du retour d'état et celui de l'intégrateur sont calculés en utilisant (40). Ces gains sont à faire varier afin d'adapter les changements au point de fonctionnement. Cela est réalisé à l'aide d'un tableau de recherche pour chaque élément du vecteur des gains, tableau qui est indexé par la tension d'entrée et la résistance de charge.

Afin d'étudier les performances de cette commande pour un convertisseur à découpage, le système en boucle fermée est simulé dans MATLAB/Simulink® en utilisant un modèle de commutation du convertisseur (dont les résultats sont détaillés dans le manuscrit). Cette commande se compose essentiellement de deux boucles : une première boucle d'intégration et une deuxième boucle de retour d'état. Les sorties des deux boucles sont additionnées avant d'être appliquées à l'entrée du modulateur de type PWM, lequel agit par l'intermédiaire d'un buffer sur l'interrupteur. Les résultats des simulations démontrent que ce type de commande fournit une erreur nulle en sortie dans le régime établi et un fonctionnement stable, même en présence d'un filtre non-amorti. Aucun composant passif n'a été utilisé dans le circuit du filtre. Les performances de ce retour d'état avec les gains variables ont été comparées avec celles d'un retour d'état fixe : elles sont bien meilleures. La mise en œuvre du système complet de commande par retour d'état, incluant les capteurs de mesure et un processeur numérique de signal (DSP) peu performant, est réalisable et devrait prochainement faire l'objet d'une étude particulière.

Commande par mode-glissant

Commande à structures variables des systèmes non-linéaires

Auparavant, nous avons fondé notre loi de commande sur le modèle moyen linéarisé [usm08c]. Ce type de modèle repose sur l'hypothèse que la fréquence de commutation est beaucoup plus grande que la fréquence naturelle du système et suppose aussi que les ondulations des variables d'état sont petites. D'autre part, l'approche mode-glissant des systèmes à structures variables (VSS : Variable Structure Systems) offre une façon alternative de mettre en œuvre une action de commande qui exploite la possibilité de réglage inhérente aux convertisseurs de puissance [hun93, spi97]. En particulier, les interrupteurs du convertisseur sont commandés en fonction des valeurs instantanées des variables d'état, de telle manière que la trajectoire du système soit forcée de rester sur une surface sélectionnée dans l'espace d'état. Cette surface est appelée "surface de glissement" (ou « surface de commutation »). Ce qui est le plus remarquable dans ce type de commande par mode-glissant, c'est la capacité de mener à des systèmes très robustes. En outre, la conception d'une commande par mode-glissant utilise une approche systématique permettant de garantir la stabilité et des performances satisfaisantes malgré l'imprécision de la modélisation. La théorie de la commande par mode-glissant (SMC : Sliding-Mode Control) a été largement discutée dans la littérature pour diverses applications [ahm03, hun93, mat97, utk93]. Cette approche a aussi démontré son efficacité pour commander les alimentations à découpage. Son application aux structures de base des convertisseurs est examinée dans un certain nombre de publications [ahm03, bay03, nic95, ven85]. Nous ne rentrons donc pas dans le détail de la méthode et nous présentons seulement une brève introduction de la commande par mode-glissant avant de présenter son application à l'ensemble filtre-convertisseur.

Prenons l'exemple d'un système non-linéaire avec une seule entrée, représenté par l'équation d'état suivante :

$$\dot{x} = f(x) + g(x) \cdot u \ , \qquad u = \{0, 1\} \tag{41}$$

Dans cette expression, x est l'état du système d'ordre n, $f(x)$ et $g(x)$ sont des champs vectoriels de dimension n. Cette équation décrit le comportement dynamique du convertisseur de puissance avec les interrupteurs réversibles. L'entrée, sous la forme de la commande u, définit la position des interrupteurs dans la cellule de commutation. Les deux interrupteurs doivent être dans des états complémentaires.

Une loi de commande à structure variable permet un comportement grand-signal stable du système non-linéaire représenté par (41). En mode de glissement, la trajectoire tend asymptotiquement au point d'équilibre avec un comportement dynamique imposé par l'emplacement de la surface de commutation dans l'état-espace. La conception de cette commande consiste à choisir une surface de glissement $s(x)$ associée à une loi de commutation sur laquelle un mouvement glissant avec la dynamique de performance désirée peut être créé. Idéalement, une fois interceptée, la loi de commande maintient la trajectoire d'état sur la surface à tout moment et la trajectoire glisse de long de cette surface. La tâche la plus importante est de concevoir une loi de commande qui conduit l'état du système à la surface de commutation, puis le maintien à la surface lors de l'interception. Une approche de Lyapunov est habituellement utilisée pour caractériser cette tâche.

Conception de la Commande basée sur la fonction de Lyapunov

Plusieurs méthodes ont été proposées pour la conception de la surface de commutation $s(x)$ [hun93, nic95, san92]. Dans cette thèse, nous avons choisi une approche par la fonction de Lyapunov, laquelle est présentée dans [nic95] pour l'ensemble abaisseur-filtre. Nous discutons les performances de la commande par retour d'état, présentée dans ce chapitre, comparées à celles d'un contrôleur mode-glissant [nic95]. La conception de la surface de glissement de [nic95] est décrite ici pour la facilité de compréhension. Dans cette approche, en choisissant une fonction de Lyapunov définie positive $V(x)$, ce qui représente une quantité d'énergie, une condition de l'accessibilité peut être donné par:

$$\dot{V}(x) < 0 \qquad \text{quand} \quad s(x) \neq 0 \tag{42}$$

Une transformation linéaire est nécessaire pour décrire le comportement dynamique du système (41) en termes d'écart par rapport à des valeurs nominales:

$$x = X + \Delta x\ , \quad u = U_{eq} + \Delta u = \{0,1\} \tag{43}$$

Dans cette expression, U_{eq} représente la commande équivalente qui, en cas d'une action de commutation infiniment rapide (c'est-à-dire cas idéale), maintient le système en son point d'équilibre X. Il est à noter que l'entrée, sous la forme de la commande Δu, reste toujours une valeur discontinue. La description du système se réduit maintenant à :

$$\dot{x} = \Delta\dot{x} = f(x) + g(x)U_{eq} + g(x)\Delta u \qquad \text{avec} \ \ \Delta u = \{-U_{eq}, 1 - U_{eq}\} \tag{44}$$

La quantité d'énergie stockée dans les éléments réactifs du convertisseur est donnée par :

$$W(t) = \frac{1}{2} x^T Q x\ , \qquad Q = Q^T > 0 \tag{45}$$

où Q est une matrice symétrique definie positive. De manière équivalente, cette expression (45) peut aussi s'écrire (en utilisant (43) dans (45)) :

$$W(t) = \frac{1}{2} X^T Q X + \frac{1}{2} \Delta x^T Q \Delta x + \Delta x^T Q X \tag{46}$$

Le second terme $V(\Delta x) = ½\ \Delta x^T Q \Delta x$ est une fonction quadratique positive qui peut être choisie comme une fonction de Lyapunov [nic95, san92]. Selon le théorème de Lyapunov, le système non-linéaire (41) sera asymptotiquement stable si la dérivée temporelle de V est négative. En différenciant V le long de la trajectoire du système et en utilisant (44), il vient :

$$\dot{V}(\Delta x) = \Delta x^T Q f(x) + \Delta x^T Q g(x) U_{eq} + \Delta x^T Q g(x) \Delta u \tag{47}$$

Supposant que dans le cas idéal le système (41), composé des élements linéaires passifs et réactifs, est stable en boucle ouverte avec une commande constante (i.e. $\Delta u = 0$). Il semble évident que dans ces conditions :

$$\Delta x^T Q f(x) + \Delta x^T Q g(x) U_{eq} \le 0 \tag{48}$$

Une commande stabilisante pour un convertisseur régulé peut alors être obtenue en choisissant la commande Δu selon la valeur de $\Delta x^T Q\, g(x)$, de telle manière que le résultat de l'expression (47) soit toujours négatif. La loi de commande feedback prend ainsi la forme :

$$\Delta u = \begin{cases} 0 - U_{eq} & \Delta x^T Q g(x) > 0 \\ 1 - U_{eq} & \Delta x^T Q g(x) < 0 \end{cases} \quad \text{où} \quad 0 < U_{eq} < 1 \tag{49}$$

Avec :

$$u = \begin{cases} 1 & \mathrm{s}(x) > 0 \\ 0 & s(x) < 0 \end{cases} \quad \text{avec} \quad s(x) = -\Delta x^T Q g(x) \tag{50}$$

La position des interrupteurs est définie en fonction du signe de $s(x)$. Si la fréquence pouvait être infinie, cette loi de commutation induirait un mouvement de glissement sur la surface de commutation $s(x) = 0$.

Exemple d'application : Abaisseur avec filtre d'entrée

Les équations d'état dans la forme (41) décrivant l'opération d'un abaisseur avec filtre d'entrée en mode CCM sont données dans le manuscrit. L'application de la surface de commutation donnée par (50) à cet exemple abaisseur-filtre induit un mouvement de glissement sur la surface suivant [nic95] :

$$s(x) = I_{ref} \frac{v_{CF}}{v_{in}} - i_L \tag{51}$$

Toutefois, cette solution présente un inconvénient : la régulation de la tension de sortie est effectuée en imposant un courant de référence $I_{ref} = V_{ref}/R$. En modifiant (51), la surface de glissement devient indépendante du courant d'inductance actuel i_L. En remplaçant i_L par ($i_C + v_C/R$), on obtient :

$$s = \frac{1}{R}\left(V_{ref} \frac{v_{CF}}{v_{in}} - v_C \right) - i_C \tag{52}$$

Dans cette expression, i_C est le courant qui traverse le condensateur de sortie C. La résistance R de charge détermine le comportement dynamique du système en boucle fermée (à la place d'un courant de référence I_{ref}). Par conséquent, ce système de commande présente un autre inconvénient : les performances en régime dynamique dépendent du point de fonctionnement. Toutefois, dans [nic95] ce paramètre R est remplacé par une valeur constante c_1 en vue d'imposer les performances en régime dynamique pour une charge nominale R_N :

$$s = c_1 C\left(V_{ref} \frac{v_{CF}}{v_{in}} - v_C \right) - i_C \quad \text{avec} \quad c_1 = \frac{1}{R_N C} \tag{53}$$

L'accessibilité de la surface de glissement (53) est maintenant réalisée par la loi de commande (50) pour une valeur spécifique de la résistance de charge $R = R_N$. En conséquence, le système en boucle fermée sera stable, même si le filtre d'entrée ne présente pas d'amortissement. Étant donné que la stabilité est également assurée pour une résistance de charge plus élevée que R_N, la valeur de R_N doit être choisie comme une charge dissipant une puissance maximale en sortie.

Une commande par hystérésis constitue un moyen simple de réalisation de cette loi de commande résultant en un fonctionnement à fréquence variable. En outre, la loi de commande (50) est basée sur l'hypothèse d'une fréquence infinie. Cependant, dans la pratique, ce type de commande souffre d'un phénomène dit « chattering », lequel consiste en des oscillations de trajectoire d'état autour de la surface de glissement (voir Fig. 5.12b dans le manuscrit). La réponse dynamique de ce contrôleur est simulée à l'aide d'un modèle de commutation du convertisseur avec un filtre d'entrée non-amorti (dont les résultats se trouvent dans le manuscrit).

Comparaison des deux commandes et conclusions

En comparant les deux commandes présentées dans ce chapitre, il apparaît clairement que les performances en régime dynamique de la commande par retour d'état semblent bien meilleures que celles du mode-glissant (en particulier en termes de temps d'établissement), à l'exception de la réponse aux variations de tension d'entrée (pour laquelle la commande par mode-glissant est meilleure). La commande par mode-glissant a d'autres inconvénients. Notamment, elle est une commande à fréquence de commutation variable, ce qui n'est pas souhaitable dans certaines applications. Le phénomène de « chattering » est également génant car il s'agit de haute activité de contrôle. Il y a deux autres problèmes liés à la commande par mode-glissant (celle présentée en [nic95]) : l'utilisation d'une référence de courant pour réguler la tension de sortie et l'influence du point de fonctionnement sur ses performances. De plus, il apparaît une erreur dans sa réponse transitoire car la référence est modifiée par un facteur v_{CF}/v_{in}. Tous ces problèmes n'existent pas avec la commande par retour d'état proposée dans cette thèse. L'adaptation au point de fonctionnement est obtenue par des tableaux de recherche. L'erreur dans la sortie est éliminée en utilisant une action intégrale combinée avec le retour d'état. La régulation est réalisée en imposant directement une tension de la référence (au lieu d'un courant). Le seul inconvénient de cette commande dans sa forme actuelle est que sa réalisation nécessite une mesure d'état du système en utilisant des capteurs. Ses performances en utilisant un observateur (pour reconstruire l'état du système) peuvent être étudiées dans des travaux futurs afin d'éviter les capteurs.

Chapitre 6 : Conclusions générales et perspectives

Contributions de cette thèse

Les principaux thèmes développés dans cette thèse sont les suivants :

- L'état de l'art sur la modélisation dite « moyenne » des convertisseurs continu/continu est décrit dans cette thèse, avec une attention particulière portée au fonctionnement de type DCM. L'analyse qui en découle porte pratiquement sur tous les types de modèles moyens qui ont été proposés depuis les débuts jusqu'à l'heure actuelle : modèles d'ordre réduit et modèles d'ordre complet, modèles corrigés d'ordre complet. Chaque modèle moyenné (qu'il s'agisse d'un modèle en espace-état ou un modèle sous forme de circuit équivalent) peut être classé dans un de ces groupes. Les principales caractéristiques de chacun de ces groupes sont examinées dans cette thèse.
- La méthodologie du calcul de la moyenne est examinée en vue de son application à la DCM. Des modèles de différents ordres sont étudiés et leurs équations espace-état sont reformulées, y compris en ce qui concerne les effets parasites. Une comparaison dans le domaine fréquentiel est alors effectuée entre ces modèles dans un cas idéal mais aussi en étant plus réaliste. Les précisions de ces modèles sont évaluées expérimentalement au moyen d'une maquette construite à cet effet. En conséquence, le domaine fréquentiel de validité de chaque type de modèle est clairement défini. Les effets des pertes, éventuellement importantes, sur le comportement fréquentiel et sur l'emplacement des pôles à haute fréquence sont également étudiés. Les prédictions des différents types de modèles à cet égard sont comparées.
- Une méthode expérimentale simple est proposée pour la validation systématique des modèles moyens dans le domaine de fréquence. Cette technique est basée sur l'injection de petites perturbations dans le signal de commande et sur la mesure des variations qui en résultent pour en déduire des phases et des gains. La validité de cette méthode est démontrée dans la gamme de fréquences intéressante (jusqu'à environ 1/3 de la fréquence de commutation).
- Le problème de l'interaction entre la régulation et le filtre d'entrée est traité en utilisant les modèles moyens petits-signaux. L'instabilité qui en résulte est expliquée. Une étude bibliographique en ce domaine recense divers travaux de recherche. Dans un premier temps, une solution classique d'amortissement « passif », en vue de combattre toute instabilité, est examinée en détail. Une nouvelle approche est proposée pour le dimensionnement de ce circuit d'amortissement, laquelle est fondée sur l'application du critère de Routh-Hurwitz au polynôme correspondant au numérateur de la fonction de transfert en boucle ouverte. En conséquence, les conditions de stabilité sont déterminées pour chacune des topologies de base des convertisseurs. Ces conditions sont également validées expérimentalement. Les frontières entre fonctionnements stable et instable sont clairement définies selon les paramètres du circuit d'amortissement.
- L'analyse des interactions avec le filtre d'entrée est étendue à des convertisseurs connectés entre eux en cascade. Le cas de deux convertisseurs abaisseur avec un filtre d'entrée est analysé en détail. La procédure de dimensionnement du circuit d'amortissement, déjà décrite pour un convertisseur seul, est évaluée puis validée en vue de son application au cas spécifique des convertisseurs en cascade. Toutefois, de nouvelles conditions de stabilité sont proposées, puis validées expérimentalement.

- L'influence des résistances d'amortissement sur le rendement du convertisseur est analysée. La puissance dissipée dans ces résistances est quantifiée pour différents points de fonctionnement. La chute du rendement est chiffrée, paramétrée par la résistance d'amortissement, le courant de charge et le rapport cyclique. Ces résultats sont exploitables lors de la conception d'un convertisseur, lorsqu'il s'agit de faire des compromis entre le rendement et la complexité des systèmes de commande.
- Afin de supprimer tout amortisseur passif et les pertes énergétiques qui y sont associées, une commande active est proposée dans cette thèse. Cette solution met en œuvre un retour d'état avec placement des pôles. La conception de cette commande est basée sur un modèle moyen d'état augmenté, alors que ses performances en régime dynamique sont évaluées en utilisant un modèle de commutation du convertisseur. Ce système de commande est robuste et bien adapté aux variations de la charge et en entrée. Sa réponse à des perturbations grands-signaux est intéressante. Une commande à structure variable basée sur le mode-glissant est comparée à l'approche par fonction de Lyapunov. Cette dernière approche est présentée en détail dans cette thèse et le comportement en régime transitoire qui en résulte est simulé.

Orientation possible de la recherche en ce domaine

La recherche est un processus continu et il n'est jamais évident de conclure que la solution proposée est définitive. Les recherches menées dans cette thèse ont contribué à répondre à certaines questions posées depuis longtemps, concernant la modélisation, les interactions avec le filtre d'entrée, les pertes dues à l'amortissement, la stabilité et la commande des convertisseurs. Certaines solutions, des techniques et des méthodes déjà existantes ont été améliorées. Toutefois, des efforts sont encore nécessaires dans certains domaines. Tout au long de cette thèse, plusieurs idées ont émergé et de nouvelles questions se sont posées. Sur la base de ces réflexions, voici quelques suggestions pour de futurs travaux (une liste plus exhaustive des perspectives est donnée dans le chapitre 6 du manuscrit) :

- Tout au long de ce travail, nous avons supposé une charge purement résistive. Ce n'est évidemment pas toujours le cas dans la pratique. Les interactions avec le filtre d'entrée devraient également être étudiées en présence d'une charge plus complexe, voire active.
- À l'avenir, le formalisme établi dans cette thèse pour les interactions avec le filtre d'entrée pourrait être étendu à des réseaux de distribution d'énergie continue dans lesquels se trouvent plusieurs convertisseurs connectés en cascade et des combinaisons parallèles, avec un filtre LC entre deux convertisseurs. Toutefois, de nombreux travaux de recherche sur l'analyse de la stabilité de ces systèmes de distribution d'énergie peuvent être cités et différents auteurs utilisent des approches différentes.
- Bien que les pertes énergétiques dues à l'amortissement aient été quantifiées dans le circuit de type R_d-C_d au cours de cette thèse, aucun critère d'optimisation n'a été proposé pour le dimensionnement de l'amortisseur : il s'agit d'atteindre la stabilité et une réponse optimale en régime dynamique avec un minimum de pertes énergétiques. La recherche doit être poursuivie sur les circuits d'amortissement passif, à commencer par la structure même des amortisseurs, de façon à dégager des règles précises de conception et de dimensionnement.
- La commande par retour d'état telle que présentée dans ce travail repose sur la mesure de l'état du système. Toutefois, dans de futurs travaux, sa faisabilité devrait également être étudiée. L'estimation de l'état (observateur) constitue une autre piste dans le but de réduire

le nombre de capteurs dans le circuit et pour éliminer les problèmes liés aux retards de ces mesures. La performance de cette commande par retour d'état devrait également être évaluée sur une maquette.

- Les performances de la commande par modes glissants dépendent essentiellement du choix de la surface de commutation. Par introduction de termes dérivés pondérés, et en introduisant les incertitudes liées au point de fonctionnement et aux paramètres du système il est possible d'améliorer ses performances. Par ailleurs, une autre commande possible pour ce problème est la commande passive avec sa variante adaptative qui lève le problème des incertitudes paramétriques et donne une maîtrise de la convergence vers le point de fonctionnement, donc de l'amortissement des oscillations induites par le filtre.

Chapter 1

INTRODUCTION

In this chapter a general introduction and background of the subject is presented. Motivations behind this thesis and its research objectives are described. Structure of this dessertation is also outlined briefly.

1.1 GENERAL BACKGROUND

Over the past few decades, switch-mode dc-dc converters have eventually become an essential element of widespread commercial and military applications. Due to their high efficiency, light weight and relatively low cost, the switching dc-dc converters have raised a significant research interest in the area of their modeling, analysis, and control. Among various types of dc-dc converters, the Pulse-Width Modulated (PWM) converters constitute by far the largest group. They have displaced conventional linear power supplies even at low power levels. Switch-mode dc-dc converters can be categorized as non-linear periodic time-variant systems due to their inherent switching operation. The topology of the dynamical elements of such a system depends on instantaneous positions of the power switches. This is what makes their modeling a complex task. Nevertheless, accurate analytical models of PWM dc-dc converters are essential for the analysis and design of converters in a variety of applications e.g., automobiles, aeronautics, aerospace, telecommunications, submarines, naval ships, mainframe computers and medical equipements. Many efforts have been made in the past few decades to model dc-dc converters and several new models have been proposed. These models are widely used to study the static and dynamic characteristics of the converters as well as to design their regulation control system [che01, dav06b, mak91, mid77a, mid77b, sun01, sun92, sun98].

The so-called averaged models, wherein the effects of fast switching are “averaged” over a switching interval, are most frequently applied when investigating power-electronics-based systems. Continuous large-signal models are typically non-linear and can be linearized around a desired operating point. Averaged models of dc-dc converters offer several advantages over the switching models. These advantages are straightforward approach in determining local transfer-functions, faster simulation of transient response to large-signal perturbations and to allow general-purpose simulators to linearize converters for designing the feedback controller. Moreover, fast execution of averaged models makes them ideal for representing the respective components in system-level studies.

Typically a dc-dc converter can operate in two modes. One is the Continuous Conduction Mode (CCM) in which inductor current never falls to zero and the second mode is

Discontinuous Conduction Mode (DCM) allowing inductor current to become zero for a portion of switching period. DCM typically occurs at light load and differs from CCM since this mode results into three different switched networks over one switching cycle (as opposed to two switched networks in case of CCM operation). Models for PWM converters, operating in CCM (based on famous state-space averaging technique), were first introduced in 1970's [mid77a, mid77b]. Since then, several circuit-oriented averaging approaches have also been proposed [che81, mak91]. However, all of the averaged models in CCM predict only the low frequency behavior correctly (up to about 1/2 of switching frequency). Then these averaging methods were also applied to DCM which resulted into reduced-order models [cuk77]. These reduced-order models were valid only at very low-frequencies (from steady-state to about 1/10 of switching frequency). The full-order models for DCM were derived later [mak91, vor90], which have improved accuracy also at higher frequencies (upto about 1/3 of switching frequency). A unified method for both conduction modes has also been developed giving actually the same formulation for CCM and DCM as reported previously. However, the accuracy of these models at even higher frequencies is still questionable (i.e. beyond 1/2 of switching frequency).

Even though, advanced technological developments in converter topologies and high-speed power semiconductors have led to improved conversion efficiencies and high switching frequencies, present switching converters still possess several undesirable characteristics due to which additional problems are imposed for complex feedback control circuitry. One such problem is originated from rapid switching of input currents that cause severe electromagnetic interference (EMI). This issue required addition of an appropriate input-filter to smooth out substantial current ripple components at switching frequency. Moreover, many power converters exhibit an important characteristic of almost-perfect regulation at the output terminals independent of input perturbations. This characteristic reflects at the input terminals as a constant-power load. In particular, an increase of input voltage causes a decrease in input current, and hence results into a dynamic negative resistance at input. This negative resistance characteristic of the regulator can interact with the input filter to form a negative resistance oscillator. Thus the presence of input filters not only increase the complexity and cost of the circuit but can also induce instability in the system. Similar instability problem can appear in the distributed power architectures, wherein several dc-dc converters are to be connected in cascade.

The EMI-filter problems were first recognized and discussed in the early seventies [mid76]. The topic has been under intense research and discussion since the development of state-space averaging methodology and several solutions have also been proposed [eri99, mid78, phe79]. The main reason for continuing discussions on this issue has been the applicability of interaction formulation and design rules to various operation- and control-modes. Normally, closed-loop stability cannot be guaranteed for an underdamped input filter. Thus on one hand the input-filter interaction problem has considerably complicated the regulator design and on the other hand it has posed additional challenges for the modeling techniques on which the control law has to be based. Although using input filters is unavoidable due to EMI/EMC reasons in most of contemporary applications, assuring converter stability in the presence of input filters is also of crucial importance. In view of the aforementioned issues and problems, conventional averaged modeling techniques face new challenges. An increasingly complex debate on the modeling and control of dc-dc converters has occupied a center stage in the field of advanced power electronics. Nevertheless, the performance of averaged models for the analysis, control and stabilization still need to be evaluated and their capabilities and

limitations need to be clearly defined before moving to the more complex models. That is the main focus of this manuscript.

1.2 MOTIVATIONS AND OBJECTIVES

It is well known that the low-frequency dynamic properties of a converter can be expressed effectively using an averaged model, providing useful physical insights which help in identifying the source of various dynamical phenomena. Continuous-time averaged models have been widely accepted among the practicing engineers because they are easy to understand and implement in industry. The popularity of the state-space averaging approach is due largely to its clear justification, simple methodology, analytical nature of results and demonstrated practical utility. However, there still remain the following fundamental questions unresolved.

- Under what conditions do averaged models give a useful system approximation ?
- Are the stability properties of approximate models are identical to those of original system ?
- How can one quantify the errors incurred by the approximation ?
- Is the approximation valid for large signals ?
- What is the upper limit of the frequency for averaging to be valid ?
- Can the open-loop approximate model be used for closed-loop design ?

The research carried out in this thesis offers a framework to deal with these and other associated questions. Performance of averaging methodology is investigated for the stability analysis and control design of dc-dc converters. Moreover, the application of conventional state-space averaging method to DCM raised several apprehensions, because it resulted in reduced-order low-frequency models that appear to be inaccurate at frequencies greater than about 1/10 of the switching frequency [sun98]. As a consequence, in some recent literature, modifications in the conventional state-space averaging method were proposed for DCM which resulted into several full-order averaged models [eri01, sun00, sun01]. However, related work still lacks experimental validation of these models. State-space averaging method or equivalent-circuit method was also applied to the analysis of input-filter interactions and control-loop design. However, none of the model developments in literature include an experimental validation of the obtained models and the converter is always assumed ideal in such studies. Such fundamental deficiencies and unresolved issues in traditional averaged models are addressed in this research work.

As far as control is concerned, it is difficult to predetermine the suitable regulator for a given converter application because of the input filter which heavily interferes with the control-loop in a very complex way. Although it is possible to carry out a digital simulation of closed-loop converter (equipped with its filter), it is still not easy to optimize the whole system. Consequently, several compromises are to be made. Literature provides a door to this subject and the input filters are accused of being the potential cause of instability in output voltage regulation [mid76]. Some authors recommend the use of passive damping in the filter circuits to resolve this problem and suggest adding some external resistance for this purpose to the filter circuit [eri99, mid78]. However, the value of required resistance is not systematically confirmed through experiments. Furthermore, the power dissipation in such damping resistors is another undesirable issue which needs considerable attention because it affects conversion efficiency.

In addition to the above mentioned challenges, there are still many issues related to averaged modeling and its application to control-loop design, which need to be addressed thoroughly. The scope of this work is motivated by the need to improve the modeling and control of dc-dc converters in presence of input filter. The main objectives of the research work carried out during this thesis are summarized below:

- Carry out a detailed bibliographic study of various averaged models developed in related literature. Reestablish these models by introducing circuit parasitics into model equations.
- Investigate the averaged modeling of non-ideal dc-dc converters in DCM both theoretically and experimentally. Formulate and demonstrate an experimental methodology for the measurement of control-to-output transfer function with a reasonable accuracy. Deal with the enormously increased complexity of non-ideal model expressions using a symbolic analysis package such as Mathematica®.
- Compare the relative validity of various averaged models developed in literature and study the parasitic effects as predicted by models of different orders, including all imperfections of the components into model equations.
- State-of-the-art study of input-filter interactions and review of different passive and active solutions that have been proposed to resolve this interaction problem. Analyze input-filter interactions in all basic converter topologies (buck, boost and buck-boost) using their non-ideal averaged models and systematically formulate some design rules to avoid its adverse impact on converter dynamics. Derive generalized stability conditions for each of these converters and identify a safe operating region in terms of its damping circuit parameters.
- Extend the study of filter-converter interactions to the case of cascade converters and determine the conditions for stability in the presence of input filter. The analysis is to be based on the small-signal control-to-output transfer function. Practical validation of the above derived conditions on experimental prototypes.
- Realize thorough efficiency investigation of dc-dc converters with the passive damping solution which is most commonly employed to damp input-filter oscillations. Systematically respond to the criticism and apprehensions that have been raised in the literature regarding passive damping method. Quantify the effect of damping losses on overall system efficiency under varying operating conditions. Generalization to all fundamental topologies and subsequent experimental verification of the obtained results.
- Propose some alternate control solution for the stability of dc-dc converter with an underdamped input filter, thus avoiding the use of dissipative resistors in the circuit. Introduce a state-feedback controller in which feedback gain vector adapts to the changing operating point. Design and explore the performance of a control system based on state-feedback and pole-placement and then compare this method with another existing scheme such as sliding-mode control. Evaluate the performance of averaged modeling for high-frequency control design.

1.3 OUTLINE OF DISSERTATION

The organization of this dissertation is as follows. ***Chapter 2*** starts with a detailed review of literature on the averaged modeling especially in DCM and most recent developments in this area. Analytical expressions of state-space models are re-established by including element parasitics of the circuit. A comparison of representative models from the literature in DCM has been carried out for ideal as well as for non-ideal converters and their predictions

regarding parasitic effects; small-signal frequency domain characteristics and high frequency poles have been analyzed. Then the validity of these models is further investigated experimentally. A simple experimental methodology is proposed to measure control-to-output transfer function from a hardware prototype which helps in systematically analyzing the accuracy of averaged modeling by comparing theoretical results with those of experiments.

In ***Chapter 3***, based on the non-ideal averaged models derived in the preceding chapter, instability problem due to input filters is explained using open-loop control-to-output transfer functions and their pole-zero locations. Input-filter interactions and their control related issues are analyzed for three basic converter topologies (buck, boost and buck-boost). Stability conditions are derived and consequently a safe operating region is identified for each basic converter followed by its experimental verifications. Then in the second part of this chapter, a case-study is presented in which the above developed formulation of input-filter interactions is further extended to a special case of cascade buck converters using its non-ideal model. The use of damping resistors in the input-filter circuit is analyzed for this particular case and subsequent stability conditions and safe operating region are defined. Finally these conditions are also validated through an experimental prototype of closed-loop cascade buck converter (with an input filter) while regulating the output with a conventional voltage-mode control.

Before proposing a control solution for stability, ***Chapter 4*** is explicitly dedicated to efficiency investigation of dc-dc converters with passive damping circuit and to respond systematically to various critics and doubts raised in literature regarding the use of passive dampers. The chapter starts with a comprehensive literature survey of several passive and active methods and then a generalized analysis of efficiency of dc-dc converters (with passively damped input filters) is presented in detail for buck-type and boost-type converters. Damping resistor power losses are quantified and their impact on converter efficiency is examined under varying operating conditions. The theoretical predictions of this chapter are also validated experimentally.

In ***Chapter 5***, an alternate control solution using state-feedback and pole-placement is proposed. A new state-feedback control scheme is introduced in which feedback gains can be adapted to the changing operating point. The closed-loop system is simulated in the presence of a lossless input filter and its performance is analyzed in comparison with another control scheme already presented in literature, which is based on sliding-mode control.

Finally, the main contributions of this thesis are outlined in ***Chapter 6***, together with suggestions for future research topics.

Chapter 2

STATE-SPACE AVERAGED MODELING OF NON-IDEAL DC-DC CONVERTERS WITH INPUT FILTER

In this chapter, we formulate and investigate state-space averaged models of dc-dc converters separately in CCM[1] and DCM[2]. Different averaged models for DCM, presented in the literature, are studied and their state equations are re-established by including necessary circuit parasitics. An experimental technique is proposed to validate these models using a prototype converter. Limitations of averaged models in DCM are discussed in detail.

2.1 INTRODUCTION

Converter systems invariably require feedback control systems. For example, in a typical dc-dc converter application, the output voltage must be kept constant, regardless of changes in input voltage or in the effective load resistance. To design such a control system, we need a dynamic model of the switching converter. In particular, how do variations in the input voltage, the load current, and the duty cycle affect the output voltage? What are the small-signal transfer functions? To answer these questions, it is desired to model the important dominant behavior of the system, while neglecting other insignificant phenomena. Unfortunately, understanding of converter dynamic behavior is hampered by the nonlinear time-varying nature of switching and pulse-width modulation process. However, these difficulties can be overcome through the use of waveform averaging and small-signal modeling techniques. Such a modeling process involves approximations to neglect small but complicating phenomena, in an attempt to understand what is most important. Once this basic insight is gained, it may be desirable to carefully refine the model, by accounting for some of the previously ignored phenomena. It is a fact of life that real, physical systems are complex, and their detailed analysis can easily lead to an intractable and useless mathematical mess. Approximate averaged models are an important tool for gaining understanding and physical insight.

The switching ripples are small in a well-designed converter. Hence, we may ignore the switching ripple and model only the underlying ac variations in the converter waveforms. For example, suppose that some ac variation is introduced into the converter duty cycle $d(t)$, such that:

[1] Continuous Conduction Mode
[2] Discontinuous Conduction Mode

$$d(t) = D + D_m \cos \omega_m t \tag{2.1}$$

where D and D_m are constants, $|D_m| << D$, and the modulation frequency ω_m is much smaller than the converter switching frequency $\omega_s = 2\pi f_s$. The spectrum of the output voltage waveform will contain components at the switching frequency as well as its harmonics and sidebands. However, these components are small in magnitude as long as the switching ripple is small. In addition, the spectrum would also contain a low-frequency component at the modulation frequency ω_m. The magnitude and phase of this component depends not only on the duty cycle variation, but also on the frequency response of the converter. Switching ripples in the inductor current and capacitor voltage waveforms are removed by averaging over one switching period. Hence, an ac model is obtained which predicts the low-frequency behavior of the converter.

Averaged modeling of dc-dc converters is indispensable for small-signal frequency-domain characterization and/or for computationally efficient system-level time-domain transient studies. A number of ac converter modeling techniques have appeared in the literature [che81, che82, lee85, leh96, mah97, mid73, mid77a, vor89], including the current-injected approach [che81, che82], switching-frequency dependent averaged models [leh96], circuit averaging [vor89], and the state-space averaging method [mah97]. Although the proponents of a given method may prefer to express the end result in a specific form, the end results of nearly all methods are equivalent. Averaged switch modeling is also applied to the boundary conduction mode of dc-dc converters [che01].

The state-space description of dynamical systems is a mainstay of modern control theory and is also adopted in the power electronics field. The popularity of the state-space averaging approach for power converters is due largely to its clear justification, generality of its result, simple methodology, and demonstrated practical utility [kis94, kre90, mit88]. A small-signal averaged model can always be obtained, provided that the state equations of the original converter can be written. Averaging theory offers a framework for addressing the questions related to stability issues due to input-filter interactions (which will be discussed in chapter 3). The available results then provide tools for the development and refinement of methods for the design and control of power electronic systems. Conventional analytical averaged methodologies have been extensively investigated in the literature [ben94, mak01, mid77b, san91a, san91b, ver81]. However, the converter is always assumed to be ideal. Although considering ideal/lossless components significantly simplifies the model development, neglecting the parasitic effects in averaged models may sometimes lead to failure in predicting the fast-scale instabilities [maz01]. Therefore including the internal losses of the circuit elements for improving the model accuracy is sometimes necessary. However, this is not a trivial task often requiring laborious derivations that produce complicated expressions [dav06a].

In this chapter, the state-of-the-art state-space averaging is described and both conduction modes CCM and DCM are considered separately. Since application of averaging methodologies in CCM are relatively straight-forward and has been presented previously in numerous publications [eri01, mid77a, sun92, sun97], we have discussed it only briefly in this chapter. Models for the three basic converter topologies (buck, boost and buck-boost) in CCM are re-established by including input filter and appropriate imperfections of the circuit elements. Whereas, averaged modelling in DCM has been paid special consideration in this chapter because model development in DCM is more delicate as compared to that in CCM. State-space averaged modeling of PWM converters in DCM has received significant attention

in the recent literature and several models have been developed [cuk77, eri01, mak91, sun01, sun98, tym86, vor90]. All of these models are given either in analytical form or as equivalent circuits, and can be classified into three categories: 1) reduced-order models, 2) full-order models, 3) corrected full-order models. In the second part of this chapter, various aspects of the representative models of each category have been investigated in DCM. A discussion is proposed to explain the differences between these models especially considering their bandwidths. Several previously established models are compared based on their predictions of parasitic effects as well as the small-signal frequency-domain characteristics. In order to further analyze their relative validity, these models are compared to a hardware prototype. A simple methodology of small signal-injection and subsequent frequency-response measurement is proposed and implemented to extract the small-signal control-to-output transfer function from a hardware prototype. Experimental effectiveness of this method has been demonstrated up to about 1/3 of the switching frequency. The non-ideal models formulated in this chapter provide the basis to derive small-signal transfer functions and subsequent stability analysis which is the subject of next chapter.

2.2 MODELING IN CONTINUOUS CONDUCTION MODE (CCM)

2.2.1 General Framework

Switched converters are often modelled as piecewise linear networks in which topology changes at the boundaries between subsequent subintervals within a switching cycle [pej95]. Based on the state of each switching element, such as transistor and diode, the appropriate state-space equations can be derived. The state variables are generally associated with the energy storage components. In addition there are well-defined algorithms [chu75], and software tools [asm02, jat00, jat04, mer08] that automatically generate and dynamically update the state-space model for each new topological state of the system being studied. Regardless of the approach or tool used, it is assumed that inside each subinterval the system state-model may be expressed by the system matrices.

The state-space averaging technique generates the low-frequency small-signal equations of PWM dc-dc converters. Converter transfer functions and equivalent-circuit models can then be obtained from these small-signal models. The converter contains independent state variables such as inductor currents and capacitor voltages, that form the state vector $x(t)$, and the converter is driven by independent sources that form the input vector $u(t)$. The output vector $y(t)$ contains dependent signals of interest. During the first subinterval, when the switches are closed for time dT_s, the converter reduces to a linear circuit whose equations can be written in the following state-space form:

$$\begin{aligned} \dot{x}(t) &= A_1 x(t) + B_1 u(t) \\ y(t) &= C_1 x(t) + E_1 u(t) \end{aligned} \tag{2.2}$$

The matrices A_1, B_1, C_1, and E_1 describe the network connections during the first subinterval. During the second subinterval, the converter reduces to another linear circuit, whose state-space equations are:

$$\begin{aligned} \dot{x}(t) &= A_2 x(t) + B_2 u(t) \\ y(t) &= C_2 x(t) + E_2 u(t) \end{aligned} \tag{2.3}$$

The matrices A_2, B_2, C_2, and E_2 describe the network connections during the second subinterval of length $(1 - d)T_s$. A continuous-time low-frequency nonlinear model is obtained

by averaging (2.2) and (2.3) over an entire switching cycle T_s and is represented in the following form:

$$\begin{aligned} \dot{\bar{x}}(t) &= A(d)\bar{x}(t) + B(d)u(t) \\ y(t) &= C(d)\bar{x}(t) + E(d)u(t) \end{aligned} \tag{2.4}$$

where x is the state vector and $\bar{x}$ denotes the average of x over an entire switching period T_s. The corresponding averaged state matrices are given below:

$$\begin{aligned} A(d) &= dA_1 + (1-d)A_2 \\ B(d) &= dB_1 + (1-d)B_2 \\ C(d) &= dC_1 + (1-d)C_2 \\ E(d) &= dE_1 + (1-d)E_2 \end{aligned} \tag{2.5}$$

The above representation is nonlinear since system matrices depend on the control signal $d(t)$. It is assumed that the natural frequencies of the converter network are much smaller than the switching frequency. This assumption coincides with the small-ripple approximation, and is usually satisfied in well-designed converters. It allows the high-frequency switching harmonics to be removed by an averaging process. In addition, the waveforms are linearized about a dc quiescent operating point. The converter waveforms are expressed as quiescent values plus small ac variations, as follows:

$$\begin{aligned} x(t) &= X + \tilde{x}(t) \\ u(t) &= U + \tilde{u}(t) \\ y(t) &= Y + \tilde{y}(t) \\ d(t) &= D + \tilde{d}(t) \end{aligned} \tag{2.6}$$

This small-signal linearization is justified provided that:

$$\begin{aligned} \|X\| &> \|\tilde{x}(t)\| \\ \|U\| &> \|\tilde{u}(t)\| \\ \|Y\| &> \|\tilde{y}(t)\| \\ D &> \left\|\tilde{d}(t)\right\| \end{aligned} \tag{2.7}$$

where $||x||$ represents the norm of vector x. The state-space averaged model that describes the quiescent converter waveforms is:

$$\begin{aligned} 0 &= AX + BU \\ Y &= CX + EU \end{aligned} \tag{2.8}$$

The steady-state solution of the converter is:

$$\begin{aligned} X &= -A^{-1}BU \\ Y &= (-CA^{-1}B + E)U \end{aligned} \tag{2.9}$$

The state equations of the small-signal model can be represented as:

$$\begin{aligned} \dot{\tilde{x}}(t) &= A\,\tilde{x}(t) + B\,\tilde{u}(t) + G\,\tilde{d}(t) \\ \tilde{y}(t) &= C\,\tilde{x}(t) + E\,\tilde{u}(t) + H\,\tilde{d}(t) \end{aligned} \tag{2.10}$$

Where A, B, C, E, G and H are constant matrices which depend on the converter topology. In general, for continuous conduction mode G and H are given as below:

$$\begin{aligned} G &= (A_1 - A_2)X + (B_1 - B_2)U \\ H &= (C_1 - C_2)X + (E_1 - E_2)U \end{aligned} \tag{2.11}$$

The equation (2.10) describes how small-signal variations in the input vector and duty cycle excite variations in the state and output vectors. By taking Laplace transform of (2.10), all small-signal transfer functions can now be derived. These transfer function are given below in their general form:

$$\left.\frac{X(s)}{U(s)}\right|_{\tilde{d}=0} = (sI - A)^{-1} B \tag{2.12a}$$

$$\left.\frac{X(s)}{D(s)}\right|_{\tilde{u}=0} = (sI - A)^{-1} G \tag{2.12b}$$

$$\left.\frac{Y(s)}{U(s)}\right|_{\tilde{d}=0} = C(sI - A)^{-1} B + E \tag{2.12c}$$

$$\left.\frac{Y(s)}{D(s)}\right|_{\tilde{u}=0} = C(sI - A)^{-1} G + H \tag{2.12d}$$

For the stability analysis, only control-to-output transfer function (2.12d) is of interest in this thesis. The numerators and denominators of this transfer function for specific cases will be represented in the next chapter. Equivalent circuit models of dc-dc converters can also be constructed using the state-space averaged equations, which can represent the physical properties of PWM dc-dc converters.

2.2.2 Buck Converter Model with Input Filter

Fig. 2.1 presents a simple buck converter with a purely resistive load and an LC filter at its input. All parasitics of the circuit are included. The parasitics are modeled here by constant equivalent series resistors. With such resistors we model only the Joule effect in conductors (capacitor, inductor, diode, MOSFET).

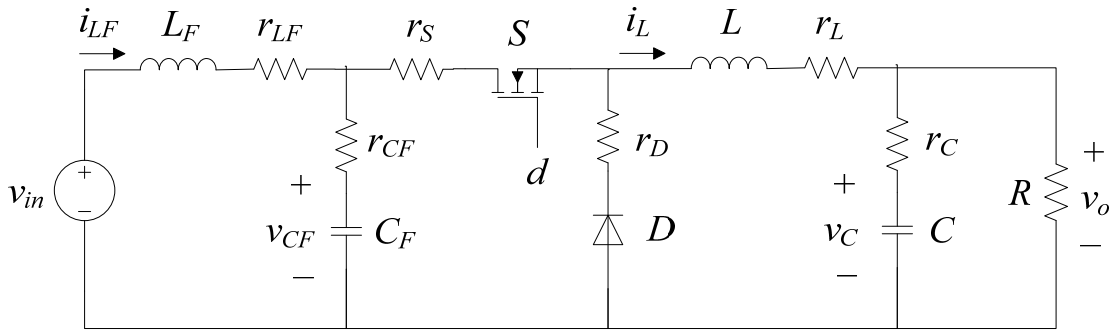

Fig. 2.1. Non-ideal buck converter circuit with input filter.

The state vector of this system contains all inductor currents and capacitor voltages and can be represented as: $x = \begin{bmatrix} i_{LF} & i_L & v_{CF} & v_C \end{bmatrix}^T$. The nonlinear model matrices as given by (2.5) can be written for this buck converter as below:

$$A(d)=\begin{bmatrix} -\frac{r_0}{L_F} & \frac{d\,r_{CF}}{L_F} & -\frac{1}{L_F} & 0 \\ \frac{d\,r_{CF}}{L} & -\frac{r_1}{L} & \frac{d}{L} & -\frac{R'}{L} \\ \frac{1}{C_F} & -\frac{d}{C_F} & 0 & 0 \\ 0 & \frac{R'}{C} & 0 & -\frac{R'}{RC} \end{bmatrix},\ B(d)=\begin{bmatrix} \frac{1}{L_F} \\ 0 \\ 0 \\ 0 \end{bmatrix} \qquad (2.13)$$

$$C(d)=\begin{bmatrix} 0 & R'r_C & 0 & R' \end{bmatrix},\ E(d)=0$$

Where r_0 and r_1 are the equivalent loss resistances which can be defined as:

$$r_0 = r_{LF} + r_{CF} \qquad (2.14)$$

$$r_1 = r_L + d(r_{CF} + r_S) + (1-d)r_D + r_C R' \qquad (2.15)$$

Here r_{LF} and r_{CF} are the equivalent series resistances (ESR) of the input-filter inductor and capacitor respectively and R' is defined as:

$$R' = \frac{R}{R + r_C} \qquad (2.16)$$

After the linearization of state-space model given by (2.13), the matrices of the corresponding small-signal linear model are obtained as below:

$$A=\begin{bmatrix} -\frac{r_0}{L_F} & \frac{D\,r_{CF}}{L_F} & -\frac{1}{L_F} & 0 \\ \frac{D\,r_{CF}}{L} & -\frac{r_1}{L} & \frac{D}{L} & -\frac{R'}{L} \\ \frac{1}{C_F} & -\frac{D}{C_F} & 0 & 0 \\ 0 & \frac{R'}{C} & 0 & -\frac{R'}{RC} \end{bmatrix},\ B=\begin{bmatrix} \frac{1}{L_F} \\ 0 \\ 0 \\ 0 \end{bmatrix},\ G=\begin{bmatrix} \frac{r_{CF}\bar{I}_L}{L_F} \\ \frac{\bar{V}'_{CF}}{L} \\ -\frac{\bar{I}_L}{C_F} \\ 0 \end{bmatrix} \qquad (2.17)$$

$$C=\begin{bmatrix} 0 & R'r_C & 0 & R' \end{bmatrix},\ E=H=0$$

Once again referring to steady-state values by capitalized quantities and assuming that the output current and voltage have negligible ripples, the steady-state relationships of this non-ideal converter can be derived from (2.9) as below:

$$\begin{aligned} &\frac{V_o}{V_{in}} = \frac{D}{1+\left(\frac{r_L + D(r_{LF}+r_S) + (1-D)r_D}{R}\right)} \\ &\bar{V}_{CF} = V_{in} - r_{LF}\bar{I}_{LF} \\ &\bar{V}_C = V_o \\ &\bar{I}_L = \frac{V_o}{R} \\ &\bar{I}_{LF} = \frac{DV_o}{R} \\ &\bar{V}'_{CF} = \bar{V}_{CF} + r_{CF}(\bar{I}_{LF} - \bar{I}_L) - (r_S - r_D)\bar{I}_L \end{aligned} \qquad (2.18)$$

This shows that the dc output voltage is the same as the capacitor voltage; dc inductor current is the same as the dc load current, and the voltage gain is the familiar ideal gain D reduced by a correction factor less than 1. Note that when parasitic resistances are set to zero this correction factor goes to unity. However, the dc current gain is unaffected by parasitics. The averaged equivalent circuit model of this buck converter is shown in Fig. 2.2.

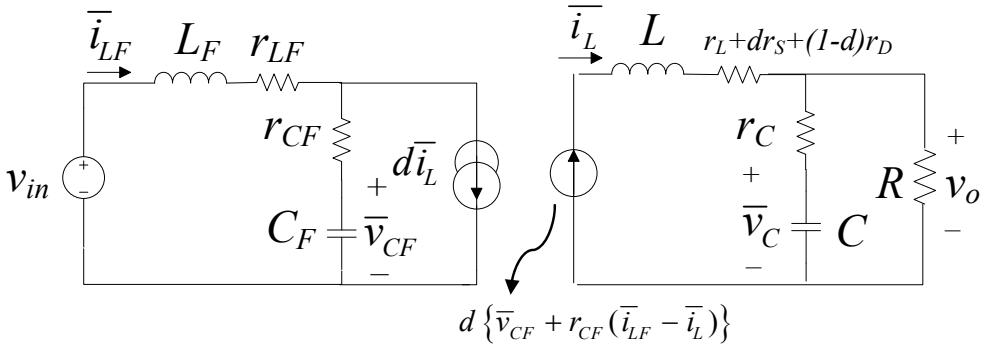

Fig. 2.2. Averaged nonlinear equivalent-circuit model of buck converter with input filter.

2.2.3 Boost Converter Model with Input Filter

Fig. 2.3 presents a simple boost converter with an input filter and resistive load, wherein all parasitics of the circuit are represented by constant equivalent series resistors. The state vector for this circuit is again given by $x=\left[i_{LF} \quad i_L \quad v_{CF} \quad v_C\right]^T$.

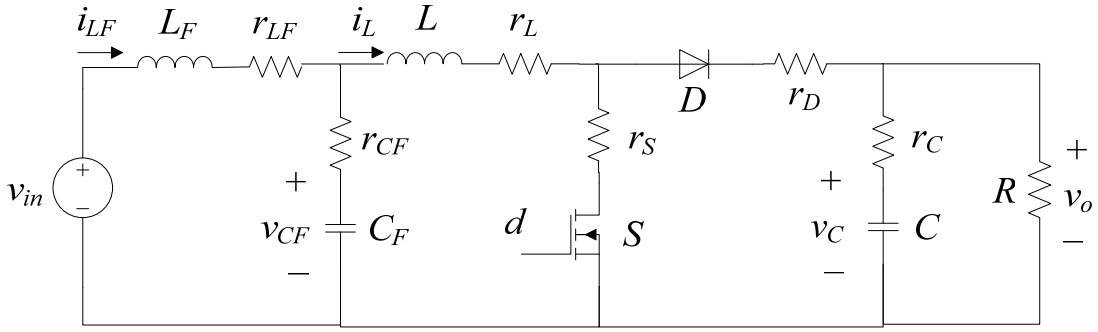

Fig. 2.3. Non-ideal boost converter circuit with input filter.

The nonlinear model matrices as given by (2.5) can be written for this boost converter as below:

$$A(d)=\begin{bmatrix} -\frac{r_0}{L_F} & \frac{r_{CF}}{L_F} & -\frac{1}{L_F} & 0 \\ \frac{r_{CF}}{L} & -\frac{r_1}{L} & \frac{1}{L} & -\frac{(1-d)R'}{L} \\ \frac{1}{C_F} & -\frac{1}{C_F} & 0 & 0 \\ 0 & \frac{(1-d)R'}{C} & 0 & -\frac{R'}{RC} \end{bmatrix},\quad B(d)=\begin{bmatrix} \frac{1}{L_F} \\ 0 \\ 0 \\ 0 \end{bmatrix} \tag{2.19}$$

$$C(d)=\begin{bmatrix} 0 & (1-d)R'r_C & 0 & R' \end{bmatrix},\quad E(d)=0$$

Where r_0 and R' are the same as give by (2.14) and (2.16) respectively. However, r_1 for the boost converter is defined as:

$$r_1 = r_L + r_{CF} + dr_S + (1-d)(r_D + r_C R') \tag{2.20}$$

The matrices corresponding to the small-signal linear model (2.10) are given as:

$$A = \begin{bmatrix} -\frac{r_0}{L_F} & \frac{r_{CF}}{L_F} & -\frac{1}{L_F} & 0 \\ \frac{r_{CF}}{L} & -\frac{r_1}{L} & \frac{1}{L} & -\frac{(1-D)R'}{L} \\ \frac{1}{C_F} & -\frac{1}{C_F} & 0 & 0 \\ 0 & \frac{(1-D)R'}{C} & 0 & -\frac{R'}{RC} \end{bmatrix}, \quad B = \begin{bmatrix} \frac{1}{L_F} \\ 0 \\ 0 \\ 0 \end{bmatrix}, \quad G = \begin{bmatrix} 0 \\ \frac{\bar{V}_C'}{L} \\ 0 \\ -\frac{\bar{I}_L'}{C} \end{bmatrix}$$
$$C = \begin{bmatrix} 0 & (1-D)R'r_C & 0 & R' \end{bmatrix}, \quad E = 0, \quad H = \begin{bmatrix} -r_C R' \bar{I}_L \end{bmatrix} \tag{2.21}$$

Assuming that the output current and voltage have negligible ripples, the steady-state relationships for this non-ideal boost converter can be represented as:

$$\begin{aligned} \frac{V_o}{V_{in}} &= \frac{1}{1-D+\left(\frac{r_{LF}+r_L+Dr_S+(1-D)r_D}{(1-D)R}\right)} \\ \bar{V}_{CF} &= V_{in} - r_{LF}\bar{I}_{LF} \\ \bar{V}_C &= V_o \\ \bar{I}_L &= \frac{V_o}{R(1-D)} \\ \bar{I}_{LF} &= \bar{I}_L \\ \bar{V}_C' &= \bar{V}_C R' - \bar{I}_L(r_S - (r_D + r_C R')) \\ \bar{I}_L' &= \bar{I}_L R' \end{aligned} \tag{2.22}$$

The averaged equivalent circuit model of this boost converter is shown in Fig. 2.4.

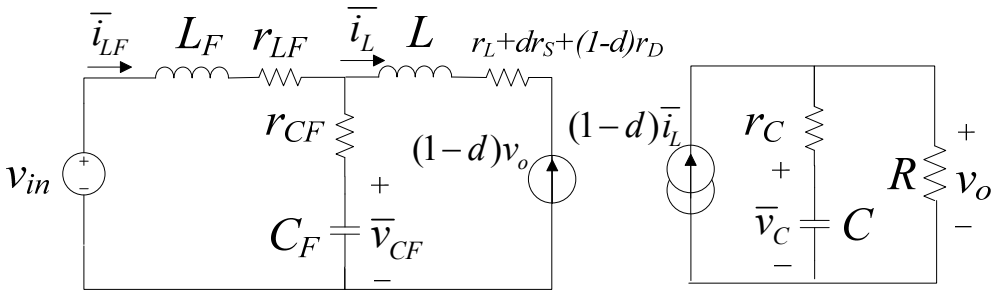

Fig. 2.4. Averaged nonlinear equivalent-circuit model of boost converter with input filter.

2.2.4 Buck-Boost Converter Model with Input Filter

Fig. 2.5 shows the schematic of a buck-boost converter with an input filter and resistive load, wherein all parasitics of the circuit are also included as equivalent series resistor models. The state vector is defined as: $x = \begin{bmatrix} i_{LF} & i_L & v_{CF} & v_C \end{bmatrix}^T$.

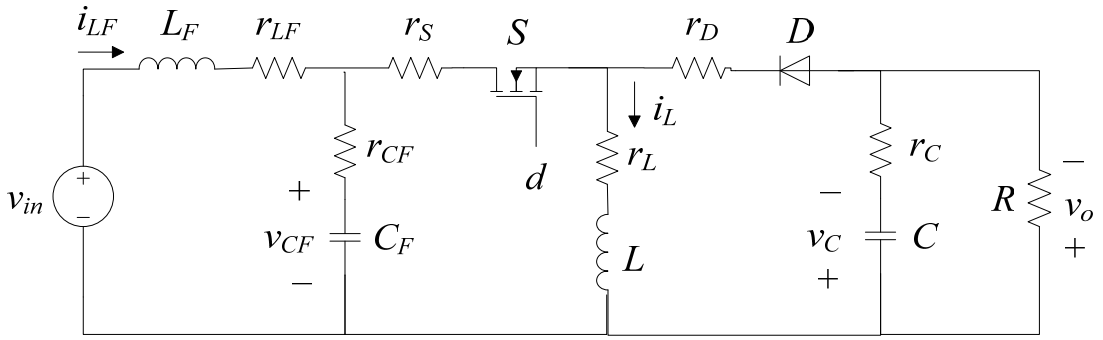

Fig. 2.5. Non-ideal buck-boost converter circuit with input filter.

The nonlinear model matrices as given by (2.5) can be written for this boost converter as below:

$$A(d)=\begin{bmatrix} -\frac{r_0}{L_F} & \frac{dr_{CF}}{L_F} & -\frac{1}{L_F} & 0 \\ \frac{dr_{CF}}{L} & -\frac{r_1}{L} & \frac{d}{L} & -\frac{(1-d)R'}{L} \\ \frac{1}{C_F} & -\frac{d}{C_F} & 0 & 0 \\ 0 & \frac{(1-d)R'}{C} & 0 & -\frac{R'}{RC} \end{bmatrix},\quad B(d)=\begin{bmatrix} \frac{1}{L_F} \\ 0 \\ 0 \\ 0 \end{bmatrix} \tag{2.23}$$

$$C(d)=\begin{bmatrix} 0 & (1-d)R'r_C & 0 & R' \end{bmatrix},\quad E(d)=0$$

Where r_0 and R' are the same as give by (2.14) and (2.16) respectively. However, r_1 for the buck-boost converter is defined as:

$$r_1 = r_L + d(r_{CF}+r_S)+(1-d)(r_D+r_C R') \tag{2.24}$$

The matrices of the small-signal linear model (2.10) are given as:

$$A=\begin{bmatrix} -\frac{r_0}{L_F} & \frac{Dr_{CF}}{L_F} & -\frac{1}{L_F} & 0 \\ \frac{Dr_{CF}}{L} & -\frac{r_1}{L} & \frac{D}{L} & -\frac{(1-D)R'}{L} \\ \frac{1}{C_F} & -\frac{D}{C_F} & 0 & 0 \\ 0 & \frac{(1-D)R'}{C} & 0 & -\frac{R'}{RC} \end{bmatrix},\quad B=\begin{bmatrix} \frac{1}{L_F} \\ 0 \\ 0 \\ 0 \end{bmatrix},\quad G=\begin{bmatrix} \frac{r_{CF}\bar{I}_L}{L_F} \\ \frac{\bar{V}'_{CF}}{L} \\ -\frac{\bar{I}_L}{C_F} \\ -\frac{\bar{I}'_L}{C} \end{bmatrix} \tag{2.25}$$

$$C=\begin{bmatrix} 0 & (1-D)R'r_C & 0 & R' \end{bmatrix},\quad E=0,\quad H=\begin{bmatrix} -r_C R'\bar{I}_L \end{bmatrix}$$

Assuming that the output current and voltage have negligible ripples, the steady-state values for this buck-boost converter are obtained from (2.9) as:

$$
\begin{aligned}
&\frac{V_o}{V_{in}} = \frac{D}{1-D+\left(\dfrac{r_L + D(r_{LF}+r_S)+(1-D)r_D}{(1-D)R}\right)} \\
&\bar{V}_{CF} = V_{in} - r_{LF}\bar{I}_{LF} \\
&\bar{V}_C = V_o \\
&\bar{I}_L = \frac{V_o}{R(1-D)} \\
&\bar{I}_{LF} = D\bar{I}_L = \frac{DV_o}{R(1-D)} \\
&\bar{V}'_{CF} = \bar{V}_{CF} + \bar{V}_C R' + r_{CF}(\bar{I}_{LF} - \bar{I}_L) - \bar{I}_L(r_S - (r_D + r_C R')) \\
&\bar{I}'_L = \bar{I}_L R'
\end{aligned}
\tag{2.26}
$$

The averaged equivalent circuit model of this buck-boost converter is shown in Fig. 2.6.

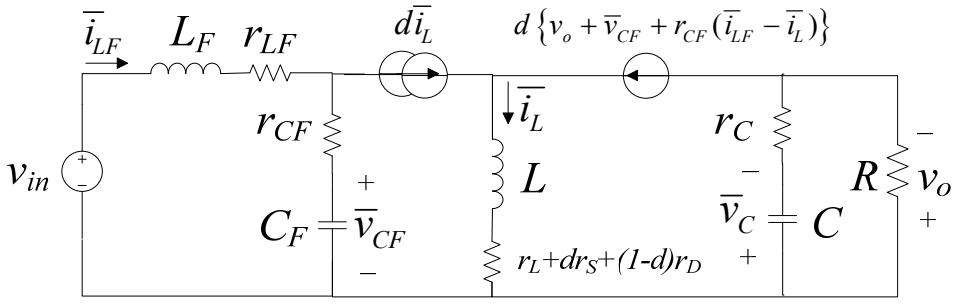

Fig. 2.6. Averaged nonlinear equivalent-circuit model of buck-boost converter with input filter.

2.3 MODELING IN DISCONTINUOUS CONDUCTION MODE (DCM)

2.3.1 State of the Art

Accurate analytical models for DCM operation of PWM converters are essential for the analysis and design of converters in a variety of applications. Many efforts have been made in the past two decades to model PWM converters in DCM [sun98]. Contrary to CCM, averaged models of varying orders are reported in case of DCM. Some of these averaged models are obtained by circuit-averaging [eri01, vor90] and others by state-space averaging [cuk77, sun01]. However, all the averaged models in DCM can be classified into three main categories:

1. Reduced-order models [cuk77, sun00, sun01]
2. Full-order models [mak91, vor90]
3. Corrected full-order models [nir01, sun01, sun97]

Although these models can be provided either through state-space averaging or circuit averaging, the resulting system equations are often identical or equivalent, consequently giving a model which is either reduced-order or full-order. For a given converter topology, the reduced-order averaged models are generally obtained by conventional state-space averaging method [cuk77] or by other similar approaches [tym86] in which discontinuous inductor current is treated as a dependent variable hence it does not appear as a state variable. Therefore the order of the model is reduced by one degree. Although reduced-order models

can correctly predict the low-frequency behavior of a converter, large discrepancies appear at high frequencies (above about 1/10 of the switching frequency). Nevertheless, these models can be suitable in some cases depending upon the control system used and the bandwidth of the closed-loop. Absence of inductor current from averaged model is, however, undesirable in some applications such as single-phase PFC, wherein inductor current is the ultimate control variable. In order to overcome the shortcomings of these models, full-order averaged models have been reported for DCM operation of PWM converters in [vor90] and [mak91]. These models retain all the state variables of the converter, including the discontinuous inductor current, thus show improved accuracy over reduced-order models. However, some discrepancies have still been observed at high frequencies as illustrated later in this chapter [sun01].

More recently, corrected full-order averaged models that very accurately capture the high frequency dynamics of the inductor current were proposed for state-space averaging [sun01] as well as for circuit averaging [eri01, sun00]. Thus using a new duty-ratio constraint and correcting the state-space model with a special correction matrix, corrected full-order models for an ideal dc-dc converter were obtained. Thus a better accuracy is also attained above 1/10 of the switching frequency.

However, none of the above referred model developments include an experimental analysis of accuracy and the converter is always assumed to be ideal. Although considering ideal/lossless components significantly simplifies the model development, neglecting the parasitic effects in averaged models may sometimes lead to failure in predicting the fast-scale instabilities [maz01]. Including the internal losses of the circuit elements for improving the model accuracy is not a trivial task often requiring laborious derivations that produce complicated expressions. Furthermore, not all of the parasitics can be included easily in all of the models [nir01].

In the rest of this chapter, a rigorous investigation of the validity and limitations of the above mentioned averaged models for DCM is presented. Their comparative accuracy is analyzed by simulations as well as by experimental tests on hardware prototype of a buck converter. For consistency, only the representative models from each group are compared, wherein all the parasitic effects of the circuit elements are included into model equations. For simplicity and clarity of this comparative study, we have not considered the input-filter effect right away (which will be incorporated into model equations later in this chapter). In order to deal with the difficulty of handling complicated expressions, a symbolic analysis package Mathematica® is used in the derivation and simplification of the non-ideal small-signal models.

2.3.2 Averaging Paradox in DCM

In CCM, switching interval T_s is divided into two subintervals, and the respective duty cycles are d_1 and $d_2 = 1 - d_1$. It is assumed that the active switch duty cycle d_1 is controlled externally. It is also assumed that the average of the product is equal to the product of the averages, especially

$$\overline{Bu} = \overline{B} \cdot \overline{u} \tag{2.27}$$

$$\overline{Ax} = \overline{A} \cdot \overline{x} \tag{2.28}$$

Assumption (2.27) is usually accepted when the source ripple is neglected. Assumption (2.28) is acceptable if the original switching variables do not deviate significantly from their average

values (small-ripple approximation) and system matrices A_1 and A_2 commute. These two assumptions are commonly used for converters working in CCM [mid77a] and have also been applied to the Boundary Conduction Mode (BCM) [che01].

In DCM, there are three topological states. In this mode, a switching interval is divided into three subintervals corresponding to d_1, d_2 and $d_3 = 1 - d_1 - d_2$, respectively. The inductor current i_L in this mode is shown in Fig. 2.7 for a lossless buck converter, wherein i_L goes to zero when both switch and diode are off. Conventional state-space averaging for converters working in DCM has been summarized in [cuk77, sun01] and ([eri01], Chap. 7). For this mode, the direct extension of (2.2)-(2.4) results in

$$\dot{\bar{x}} = [d_1 A_1 + d_2 A_2 + d_3 A_3]\bar{x} + [d_1 B_1 + d_2 B_2 + d_3 B_3]v_{in} \tag{2.29}$$

which is no longer accurate. The conventional state-space averaging method in (2.29) averages only the system matrices and not necessarily the state variables themselves [sun01]. The simplifying assumption made in (2.28) now present a problem for the fast state variable i_L, which is zero in the third subinterval. In particular, the local average of i_L in the third subinterval is zero (see Fig. 2.7), whereas the conventional state-space averaging implies that this value should be $d_3 \bar{i}_L$. Since $\bar{i}_L$ is not zero, the result of the conventional state-space averaging is not zero unless the length of the discontinuous subinterval d_3 is zero, which is only true in CCM or BCM (i.e. at boundary of CCM and DCM).

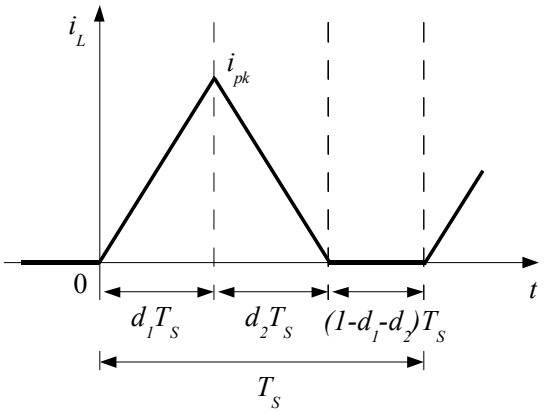

Fig. 2.7. Idealized inductor-current waveform for a converter in DCM.

A comprehensive discussion revealing the inconsistency of (2.29) can also be found in [sun01]. It explains that the average inductor current $\bar{i}_L$ in (2.29) (as an element of $\bar{x}$) differs from its true average by a factor of $(d_1 + d_2)$. Hence a modification of (2.29) is proposed in [sun01] for DCM case to deliberately correct this mismatch. This is achieved by dividing inductor current(s) on the right-hand side of (2.29) by the factor $(d_1 + d_2)$. A systematic approach to correct this inconsistency is to rearrange the state vector $\boldsymbol{x}$ such that $\boldsymbol{x} = [\boldsymbol{i}_L \quad \boldsymbol{v}_C]^T$, where subvector $\boldsymbol{i}_L$ contains all (n_L) inductor currents of the converter in DCM, and define a matrix $\mathbf{M}$ as follows:

$$\mathbf{M} = diag\left[\underbrace{\frac{1}{d_1 + d_2}, \cdots, \frac{1}{d_1 + d_2}}_{n_L}, \overbrace{1, \cdots, 1}^{N - n_L}\right], \quad \dim(\mathbf{M}) = N \tag{2.30}$$

Using this matrix, the modified averaged model that would correctly predict the behavior in DCM becomes:

$$\dot{\bar{x}} = [d_1 A_1 + d_2 A_2 + (1 - d_1 - d_2) A_3]\mathbf{M}\,\bar{x} + [d_1 B_1 + d_2 B_2 + (1 - d_1 - d_2) B_3] v_{in} \qquad (2.31)$$

This model is also called "corrected full-order model". Moreover, d_2 becomes a dependent variable that can now be expressed as an algebraic function of other system variables. This dependency of d_2 is frequently called the "duty-ratio constraint" [eri01, sun01].

2.3.3 Averaged Modeling of an Ideal Converter

In the following, we first describe various ideal models from literature by ignoring all the parasitics of the circuit shown in Fig. 2.8. Then in the next step, the parasitics will be included and the state-space equations of the respective models will be reformulated to improve their accuracy. Finally a comparison will be shown in frequency-domain. For consistency, only buck converter (Fig. 2.8) is considered here as a reference for model comparison and detailed illustrations. However, the control-to-output transfer function of an ideal model in DCM can be expressed in the following generalized form for any of the three basic converters (i.e. buck, boost or buck-boost):

$$\frac{\tilde{v}_C(s)}{\tilde{d}_1(s)} = \frac{K_o(s - z_1)}{(s + p_1)(s + p_2)} \qquad (2.32)$$

where z_1 represent the RHP[1] zero and p_1 and p_2 are the two complex poles of this transfer function. For quick reference, the representative models of each group are summarized in Table 2.1, Table 2.2 and Table 2.3 for lossless buck, boost and buck-boost converters, respectively. In these tables M denotes duty-ratio in DCM (i.e. $M = V_{out}/V_{in}$). A general analytical result for pole and zero location of these converters is also presented in their corresponding tables. To provide a state-space averaged model in DCM, the duty-ratio constraint d_2 has been found to be the key distinction between the reduced-order, full-order and corrected full-order models.

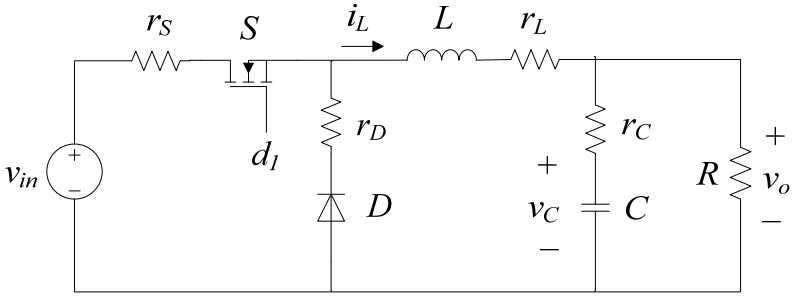

Fig. 2.8. Buck converter circuit diagram with parasitic included.

2.3.3.1 Reduced-Order Models

The fast dynamics of i_L in DCM can sometimes be neglected when considering responses in the range of low frequencies. In this case, the average value of i_L and d_2 can be expressed as an algebraic function of the control signal d_1 and the average value of the remaining variables. A volt-second balance relation of inductor current is used in this case to define the dependency of d_2 on other variables. The order of the resulting averaged model is therefore reduced by one from that of the original state-space model. For an ideal buck topology, volt-

[1] Right Hand s-Plane

second balance over a switching cycle implies the following duty-ratio constraint [cuk77, sun01]:

$$d_2 = \frac{v_{in} - \bar{v}_o}{\bar{v}_o} \cdot d_1 \tag{2.33}$$

Moreover, it is demonstrated in [sun01] that same reduced-order model is obtained regardless of which one of the two approaches [cuk77] or [sun01] is used. This is because of the fact that both of these methods use volt-second balance relation (2.33) (as duty-ratio constraint) to derive their reduced-order models. In fact, it can be readily verified that use of the volt-second balance relation will always result in a reduced model. In this study, we follow the conventional approach of [cuk77] to derive reduced-order models.

2.3.3.2 Full-Order Models

The inductor current dynamics are included in the full-order averaged models (equivalent duty-ratio method [mak91] and averaged-switch model [vor90]). These models show great improvement over the reduced-order models. Ref. [mak91] presents a unifying approach which is based on the definition of an equivalent duty-ratio, m, as a function of the actual duty ratio d_1. The converter is then treated as if it worked in CCM with the duty ratio of the switch at m rather than d_1. For ideal buck converter this equivalent duty-ratio m is given as follow:

$$m = \frac{d_1^2}{d_1^2 + \frac{2L}{T_s}\left(\frac{\bar{i}_L}{v_{in}}\right)} \tag{2.34}$$

Unlike [mak91], the full-order model presented in [vor90] is based on an equivalent circuit model of PWM switch-cell. The PWM switch-cell, as defined in [vor90] and [eri01], is a three-terminal nonlinear device containing the switch and the diode with one of the terminals as their common point. However, in spite of a different modeling approach, both [vor90] and [mak91] give exactly the same full-order averaged model for any given converter topology.

2.3.3.3 Corrected Full-Order Models

As explained earlier, an inconsistency problem was observed in the formal state-space averaging approach when applied to DCM. It was due to the fact that averaging is being performed on the state-space matrix parameters but not on the state variables themselves. Thus the conventional state-space averaging when applied in DCM results in an overestimated phase-lag and magnitude-drop which differ significantly from the true averaged response of the converter [mak00, sun01]. A modification was proposed in [sun01] to correct this mismatch and it was achieved by dividing the inductor current(s) in the state-space model by the factor d_1+d_2. A systematic approach to this is to rearrange the state vector such that $x = [i_L \quad v_C]^T$ and multiply it with a special correction matrix **M** as defined by (2.30). Then by using a different duty-ratio constraint (2.35) that comes from averaging the inductor current waveform over a switching cycle, a corrected full-order model for state-space averaging was obtained from (2.31) that very accurately capture the high frequency dynamics of inductor current i_L.

$$d_2 = \frac{2L\bar{i}_L}{d_1 T_s (v_{in} - \bar{v}_o)} - d_1 \tag{2.35}$$

where $\bar{i}_L$ and T_s denote the average inductor current and the switching period respectively. An equivalent circuit-averaging approach was also presented in ([eri01], Ch. 11) which was named as “loss-free resistor model”. However it exploits the same duty-ratio constraint as

given by (2.35). Thus, it results into same full-order model as of [sun01]. We have used [sun01] for comparison purpose in this chapter.

Table 2.1. Summary of conventional averaged models for an ideal buck converter in DCM.

Averaged Model	Averaged state-space equations	Low-frequency pole (p_1)	High-frequency pole (p_2)	RHP zero (z_1)
Reduced-order models [cuk77, sun01, sun97]	$\frac{d\bar{i}_L}{dt} = 0$ $\frac{d\bar{v}_C}{dt} = \frac{d_1^2 T_s (v_{in} - \bar{v}_C) v_{in}}{2LC\bar{v}_C} - \frac{\bar{v}_C}{RC}$	$\frac{2-M}{1-M} \cdot \frac{1}{RC}$	none	none
Full-order models [mak91, vor90]	$\frac{d\bar{i}_L}{dt} = \frac{T_s d_1^2 v_{in}^2}{L(T_s d_1^2 v_{in} - 2L\bar{i}_L)} - \frac{\bar{v}_C}{L}$ $\frac{d\bar{v}_C}{dt} = \frac{\bar{i}_L}{C} - \frac{\bar{v}_C}{RC}$	$\frac{2-M}{1-M} \cdot \frac{1}{RC}$	$\frac{2}{T_s} \cdot \left(\frac{M}{D_1}\right)^2$	none
Corrected full-order models [nir01, sun00, sun01]	$\frac{d\bar{i}_L}{dt} = \frac{d_1 v_{in}}{L} - \frac{2\bar{i}_L \bar{v}_C}{d_1 T_s (v_{in} - \bar{v}_C)}$ $\frac{d\bar{v}_C}{dt} = \frac{\bar{i}_L}{C} - \frac{\bar{v}_C}{RC}$	$\frac{2-M}{1-M} \cdot \frac{1}{RC}$	$\frac{2M}{D_1(1-M)T_s}$	none

Table 2.2. Summary of conventional averaged models for an ideal boost converter in DCM.

Averaged Model	Averaged state-space equations	Low-frequency pole (p_1)	High-frequency pole (p_2)	RHP zero (z_1)
Reduced-order models [cuk77, sun01, sun97]	$\frac{d\bar{i}_L}{dt} = 0$ $\frac{d\bar{v}_C}{dt} = \frac{v_{in}^2}{2LC} \cdot \frac{d_1^2 T_s^2}{\bar{v}_C - v_{in}} - \frac{\bar{v}_C}{RC}$	$\frac{2M-1}{M-1} \cdot \frac{1}{RC}$	none	none
Full-order models [mak91, vor90]	$\frac{d\bar{i}_L}{dt} = \frac{v_{in}}{L} - \frac{2\bar{i}_L \bar{v}_C}{d_1^2 T_s \bar{v}_C + 2L\bar{i}_L}$ $\frac{d\bar{v}_C}{dt} = \frac{2L\bar{i}_L^2}{C(d_1^2 T_s \bar{v}_C + 2L\bar{i}_L)} - \frac{\bar{v}_C}{RC}$	$\frac{2M-1}{M-1} \cdot \frac{1}{RC}$	$\frac{2(M-1)^2}{D_1^2 M^2 T_s}$	$\frac{2(M-1)}{D_1^2 M T_s}$
Corrected full-order models [nir01, sun00, sun01]	$\frac{d\bar{i}_L}{dt} = \frac{2\bar{i}_L}{d_1 T_s}(1 - \frac{\bar{v}_C}{v_{in}}) + \frac{d_1 \bar{v}_C}{L}$ $\frac{d\bar{v}_C}{dt} = \frac{\bar{i}_L}{C} - \frac{d_1^2 T_s v_{in}}{2LC} - \frac{\bar{v}_C}{RC}$	$\frac{2M-1}{M-1} \cdot \frac{1}{RC}$	$\frac{2(M-1)}{D_1 T_s}$	$\frac{2}{D_1 T_s}$

Table 2.3. Summary of conventional averaged models for an ideal buck-boost converter in DCM.

Averaged Model	Averaged state-space equations	Low-frequency pole (p_1)	High-frequency pole (p_2)	RHP zero (z_1)
Reduced-order models [cuk77, sun01, sun97]	$\frac{d\bar{i}_L}{dt} = 0$ $\frac{d\bar{v}_C}{dt} = \frac{v_{in}^2 d_1^2 T_s}{2LC\bar{v}_C} - \frac{\bar{v}_C}{RC}$	$\frac{2}{RC}$	none	none
Full-order models [mak91, vor90]	$\frac{d\bar{i}_L}{dt} = \frac{d_1 T_s v_{in}}{d_1^2 T_s (v_{in}+\bar{v}_C) + 2L\bar{i}_L}\left(\frac{d_1(v_{in}+\bar{v}_C)}{L} - \frac{2\bar{i}_L\bar{v}_C}{d_1 v_{in} T_s}\right)$ $\frac{d\bar{v}_C}{dt} = \frac{2L\bar{i}_L^2}{C\left(d_1^2 T_s (v_{in}+\bar{v}_C) + 2L\bar{i}_L\right)} - \frac{\bar{v}_C}{RC}$	$\frac{2}{RC}$	$\frac{2M^2}{D_1^2 T_s (M+1)^2}$	$\frac{R}{M(M+1)L}$
Corrected full-order models [nir01, sun00, sun01]	$\frac{d\bar{i}_L}{dt} = \frac{d_1(v_{in}+\bar{v}_C)}{L} - \frac{2\bar{i}_L\bar{v}_C}{d_1 v_{in} T_s}$ $\frac{d\bar{v}_C}{dt} = \frac{\bar{i}_L}{C} - \frac{d_1^2 T_s v_{in}}{2LC} - \frac{\bar{v}_C}{RC}$	$\frac{2}{RC}$	$\frac{2M}{D_1 T_s}$	$\frac{2}{D_1 T_s}$

2.3.4 Reformulation of Models for Non-Ideal Converter

Including the effect of parasitics is important for improving model accuracy. Conduction losses are often modeled as appropriate equivalent series resistances (ESR) associated with the circuit components. The duty-ratio constraints and subsequent state-space model equations must be modified to include the effect of parasitics. Ideal averaged models reviewed in the previous section are reformulated in this section to account for parasitics. In order to avoid the unnecessary complexity of the analytical expressions, model equations are shown by including only those parasitics whose effect on converter dynamics is more pronounced (i.e. $r_L \neq 0$, $r_C \neq 0$, $r_S \neq 0$ and $r_D = 0$). Moreover, for the simplicity of all non-ideal model representations in this section we define the following equivalent loss resistances:

$$\begin{aligned} r_a &= r_S + r_L + r_C R' \\ r_b &= r_a - r_S \end{aligned} \tag{2.36}$$

where R' is given by (2.16).

2.3.4.1 Reduced-Order Model with Parasitics

In the non-ideal case, the conventional state-space averaging method [cuk77] that uses a volt-second relation of the inductor results in the following modified duty-ratio constraint:

$$d_2 = \frac{d_1\left(v_{in} - \bar{i}_L(r_a - r_b)\right)}{\bar{v}_C R' + \bar{i}_L r_b} - d_1 \tag{2.37}$$

It can be readily verified that taking $r_C = r_L = r_S = 0$ in (2.36) and (2.16) will make r_a, r_b and R' as 0, 0 and 1 respectively, which would subsequently reduce (2.37) to the duty-ratio constraint of the ideal converter as given by (2.33). Now by substituting (2.37) into (2.29) the modified state-space averaged model of a non-ideal buck converter in DCM is obtained as below:

$$\begin{aligned} \frac{d\bar{i}_L}{dt} &= 0 \\ \frac{d\bar{v}_C}{dt} &= \frac{d_1\bar{i}_L\left(v_{in} - \bar{i}_L(r_a - r_b)\right)R'}{C(\bar{v}_C R' + \bar{i}_L r_b)} - \frac{\bar{v}_C R'}{RC} \end{aligned} \tag{2.38}$$

This is a conventional reduced-order averaged model of a non-ideal converter where the dynamics of the inductor current disappear. Since the inductor current is no longer a state variable, it must be expressed as an algebraic function of other variables. The average of the inductor current, as reported in [cuk77], is given as:

$$\bar{i}_L = \frac{i_{pk}}{2} \tag{2.39}$$

where peak inductor current i_{pk} for a non-ideal buck converter can be given as:

$$i_{pk} = \frac{d_1 T_S}{L}(v_{in} - \bar{i}_L r_a - \bar{v}_C R') \tag{2.40}$$

Here an inconsistency can be noticed between the true average of the inductor current $\bar{i}_L$ and the one given by (2.39). This is because of the fact that $\bar{i}_L$ in (2.39) is defined as the average over the first two subintervals of a switching cycle and differs from the true average by a factor of d_1+d_2. These two quantities are treated in [cuk77] as if they were interchangeable. However, a correction of this mismatch is proposed in [sun01] by dividing inductor current in (2.38) by (d_1+d_2) and then using the correct average of the inductor current as given below:

$$\bar{i}_L = \frac{i_{pk}}{2}(d_1 + d_2) \tag{2.41}$$

Since, it has been demonstrated in [sun98] that in case of reduced-order models the resulting state-space equations are identical whether we use the conventional averaging approach of [cuk77] or corrected averaging method as described in [sun01]; we follow [cuk77] for consistency. Hence using (2.40), the relation (2.39) can be solved for $\bar{i}_L$ as below:

$$\bar{i}_L = \frac{d_1 T_S(v_{in} - \bar{v}_C R')}{2L + d_1 T_S r_a} \tag{2.42}$$

This can now be substituted into model expressions (2.38) to eliminate its dependency on $\bar{i}_L$.

2.3.4.2 Full-Order Model with Parasitics

By taking account of the circuit parasitics, the equivalent duty-ratio m given by (2.34) remains unchanged. Nevertheless, final state-space model is modified significantly. For the non-ideal buck converter, the full-order averaged model derived using the method presented in [mak91] and [vor90] is:

$$\begin{aligned} \frac{d\bar{i}_L}{dt} &= \frac{T_S d_1^2 v_{in}\left(v_{in} - \bar{i}_L(r_a - r_b)\right)}{L(T_S d_1^2 v_{in} + 2L\bar{i}_L)} - \frac{\bar{i}_L r_b}{L} - \frac{\bar{v}_C R'}{L} \\ \frac{d\bar{v}_C}{dt} &= \frac{\bar{i}_L R'}{C} - \frac{\bar{v}_C R'}{RC} \end{aligned} \tag{2.43}$$

2.3.4.3 Corrected Full-Order Model with Parasitics

As described in the previous section, the use of a new representation of d_2 and correcting the state-space model with a special correction matrix [sun01], a corrected full-order model can be obtained. For the non-ideal buck converter case, inclusion of the circuit parasitics results into following modified duty-ratio constraint d_2:

$$d_2 = \frac{2L\bar{i}_L}{d_1 T_s (v_{in} - \bar{v}_C R' - \bar{i}_L r_a)} - d_1 \tag{2.44}$$

Substituting this into (2.31) now gives the following full-order state-apace averaged model of non-ideal buck-converter in DCM:

$$\begin{aligned} \frac{d\bar{i}_L}{dt} &= \frac{d_1 v_{in}}{L} - \frac{d_1 T_S (v_{in} - \bar{v}_C R' - \bar{i}_L r_a)}{2L^2}\left(\frac{4L^2 \bar{i}_L \bar{v}_C R'}{d_1^2 T_s^2 (v_{in} - \bar{v}_C R' - \bar{i}_L r_a)^2} - d_1 (r_a - r_b) \right) - \frac{\bar{i}_L r_b}{L} \\ \frac{d\bar{v}_C}{dt} &= \frac{\bar{i}_L R'}{C} - \frac{\bar{v}_C R'}{RC} \end{aligned} \tag{2.45}$$

It can be easily verified that the same state-space ideal models as listed in Table 2.1 can be obtained directly from their respective non-ideal models derived in this section if r_S, r_L and r_C are ignored.

2.3.5 Model Comparisons

Since all of the aforementioned averaged models predict the same DC voltage transfer ratio and steady-state average inductor current, a comparative study is carried out in frequency-domain to investigate the small-signal behavior of these converter models. Buck converter is again taken as an example for this comparison.

2.3.5.1 Frequency Responses

In order to evaluate the small-signal behavior of various converter models in DCM, control-to-output transfer function responses of reduced-order model, full-order model and corrected full-order model are superimposed in Fig. 2.9 for easy comparison. Ideal models are simulated by dashed lines in this figure whereas solid lines correspond to their respective non-ideal models. The parameter values used for these simulations are: L=168μH, C=6μF, f_s=100kHz, v_{in}=24V, v_o=14V, R=120Ω, r_L=50mΩ, r_C=20mΩ and r_S=30mΩ. It is noteworthy that the reduced-order models (plot a and b) portray a first-order response that significantly underestimates the phase. Whereas the full-order models (plot c and d) and corrected full-order models (plot e and f) exhibit an additional high-frequency pole near or exceeding the switching frequency. However, at low frequencies up to about 1/10 of the switching frequency a consistent response can be observed in all of the three compared models. Their difference becomes more prominent at higher frequencies, especially in their phase. The accuracy of corrected full-order models over previous full-order and reduced-order models has been verified experimentally up to about 1/3 of the switching frequency, as will be shown later in the next section. Nevertheless, at frequencies higher than about 1/2 of the switching frequency the validity of all types of averaged models is generally questionable.

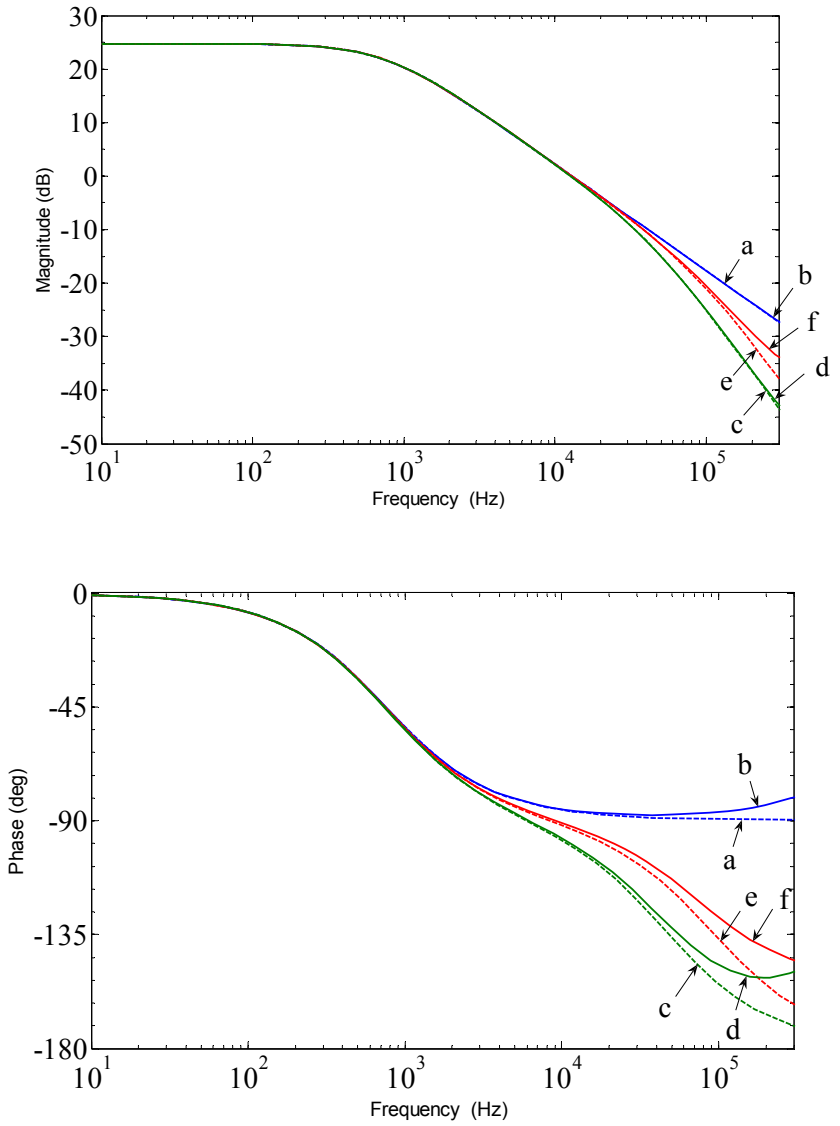

Fig. 2.9. Control-to-output transfer function magnitude and phase plot comparison; (a): reduced-order model for ideal converter [**cuk77**], (b): reduced-order model with parasitics included, (c): full-order models for ideal converter [**vor90**] and [**mak91**], (d): full-order models with parasitics included, (e): corrected full-order model for ideal converter [**sun01**], (f) corrected full-order model with parasitics included. (Parameter values: L=168μH, C = 6μF, f_s = 100kHz, v_{in} = 24V, v_o = 14V, R = 120Ω, r_L = 50mΩ, r_C = 20mΩ and r_S = 30mΩ)

2.3.5.2 Effect of Capacitor ESR

Since the ESR of output capacitor can strongly influence the converter's control-loop crossover frequency and the phase margins, we have investigated its effect on small-signal characteristics of the buck converter. Fig. 2.10(a) and (b) show the control-to-output transfer function phase variations as predicted by full-order models (i.e. circuit-averaging [vor90] and state-space averaging [mak91]) and corrected full-order models (i.e. [sun01]) respectively. These variations are shown as a function of r_C while fixing r_L = 50mΩ, r_S = 10mΩ and r_D = 0 (since r_D has little influence on frequency-domain characteristics). Likewise, Fig. 2.11 shows the magnitude responses with varying r_C. Through an examination of Fig. 2.11 it can be noticed that the attenuation at high frequencies tends to decrease due to r_C. It is also worth mentioning that capacitor ESR causes the non-ideal buck converter models to exhibit a zero at very high frequencies. Since this frequency is usually much higher than the switching frequency, these zeros are primarily inconsequential. Furthermore, a significant difference can

be observed between the predictions of full-order and corrected full-order models at high frequencies, especially in their phase plot. This difference becomes even more noticeable above about 1/3 of the switching frequency (f_s=100kHz).

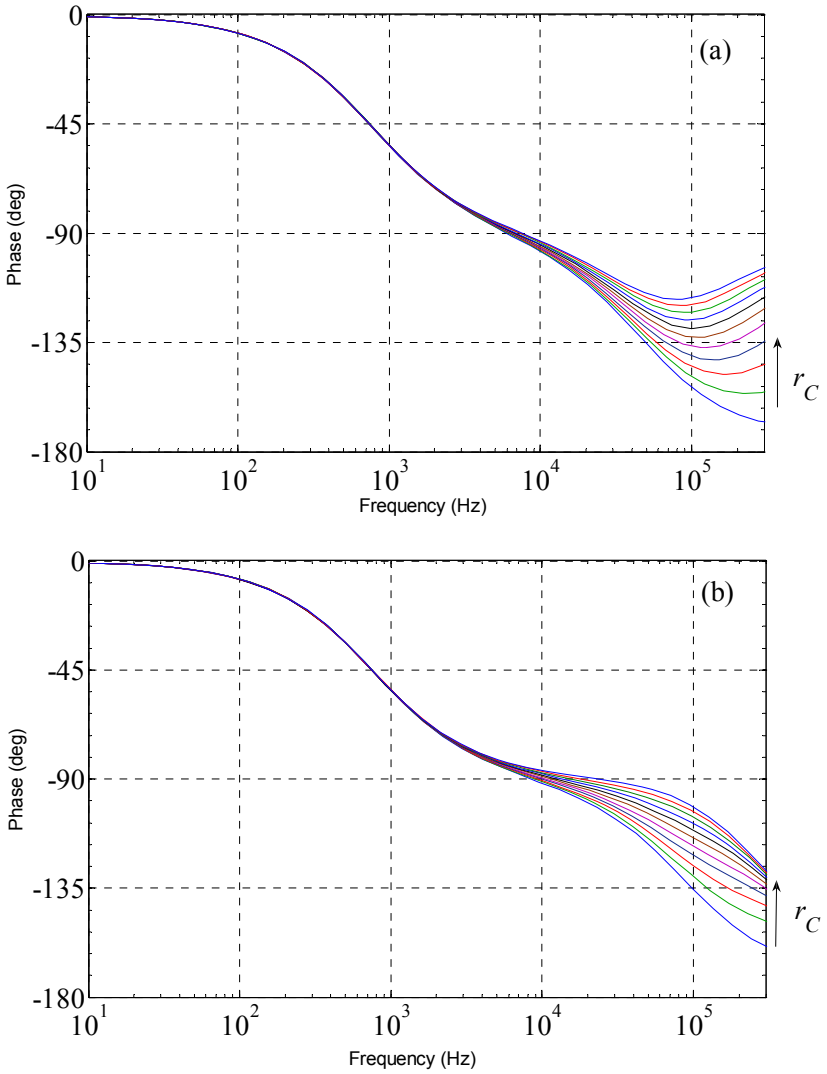

Fig. 2.10. Effect of r_C on phase response as predicted by (a): full-order models [**vor90**] and [**mak91**], (b): corrected full-order model [**sun01**]. (Parameter values: $r_C \in [0, 0.2]\Omega$, $r_L = 50m\Omega$, $r_S = 10m\Omega$, $r_D = 0$, L=168μH, $C = 6\mu$F, $f_s = 100k$Hz, $R = 120\Omega$).

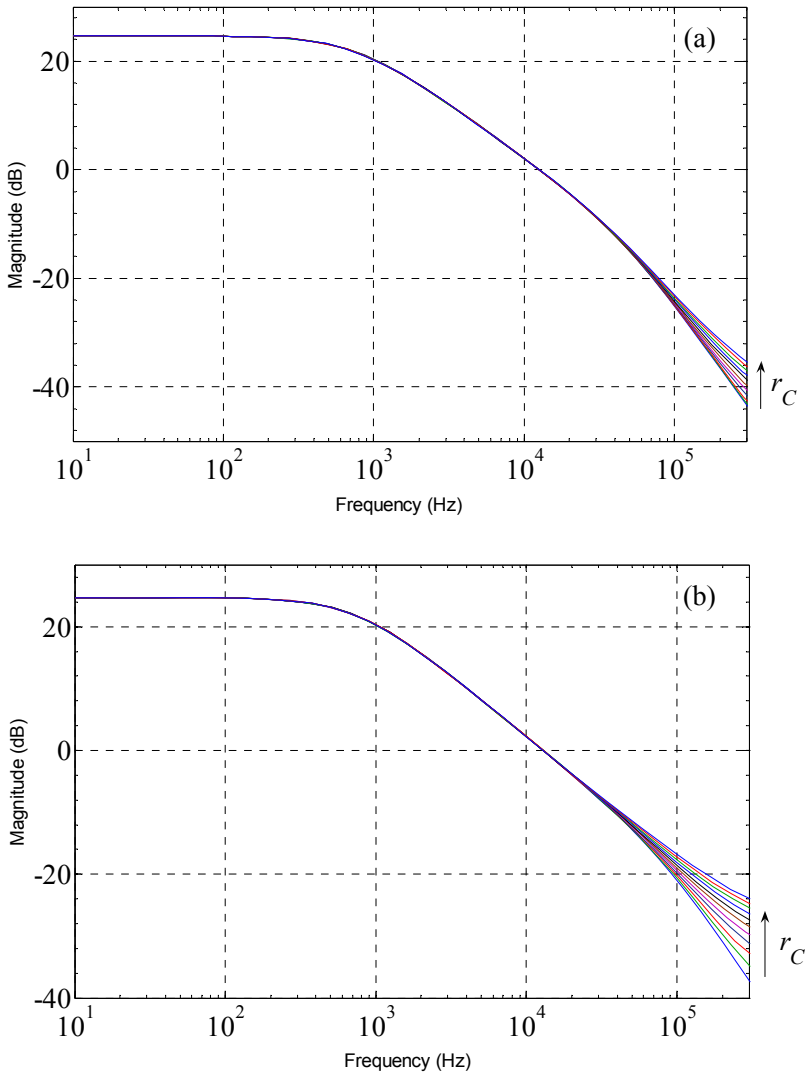

Fig. 2.11. Effect of r_C on magnitude response as predicted by (a): full-order models [**vor90**] and [**mak91**], (b): corrected full-order model [**sun01**]. (Parameter values: $r_C \in [0, 0.2]\Omega$, $r_L = 50m\Omega$, $r_S = 10m\Omega$, $r_D = 0$, $L = 168\mu$H, $C = 6\mu$F, $f_s = 100k$Hz, $R = 120\Omega$).

2.3.5.3 High-Frequency Pole in DCM

Location of the high-frequency pole of buck converter as predicted by full-order and corrected full-order models is shown in Fig. 2.12 as a function of DC operating point. It can be seen that corrected full-order models usually predict this pole at much higher frequency than that predicted by full-order models (except for very small values of duty cycle). This can also be confirmed from the fact that second pole in corrected full-order lossless model (see Table 2.1) is located at $2Mf_S/D_1(1-M)$, which can easily exceed the switching frequency. This fact often justifies the use of reduced-order models which completely neglect the dynamics of inductor current.

Capacitor ESR also effects the location of high-frequency pole. This effect is demonstrated in Fig. 2.13 using a plot of differential high-frequency pole-location with increasing values of r_C while keeping all other parameters constant. This differential pole-location is normalized with respect to the pole-frequencies predicted by their respective lossless models (i.e. where $r_C = r_L = r_S = r_D = 0$).

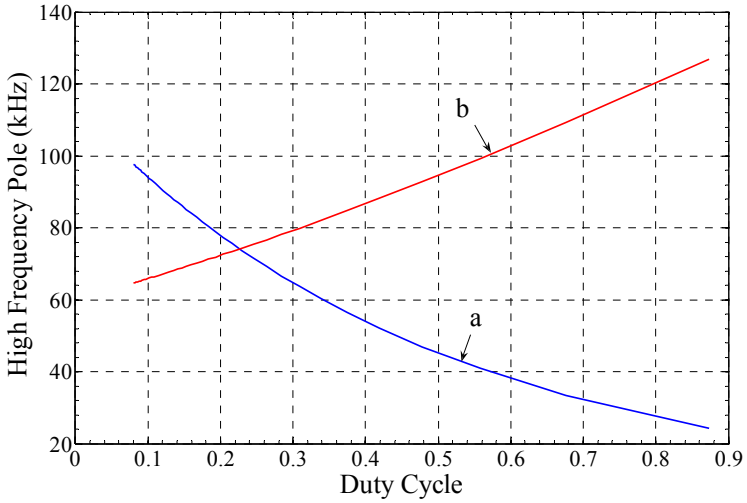

Fig. 2.12. High-frequency pole of buck converter at different operating points as predicted by (a): full-order models [**vor90**] and [**mak91**], (b): corrected full-order model [**sun01**]. (Parameter values: r_C= 10$m\Omega$, r_L =50$m\Omega$, r_S = 10$m\Omega$, r_D = 0, L = 168μH, C = 6μF, f_s = 100kHz, R = 120Ω)

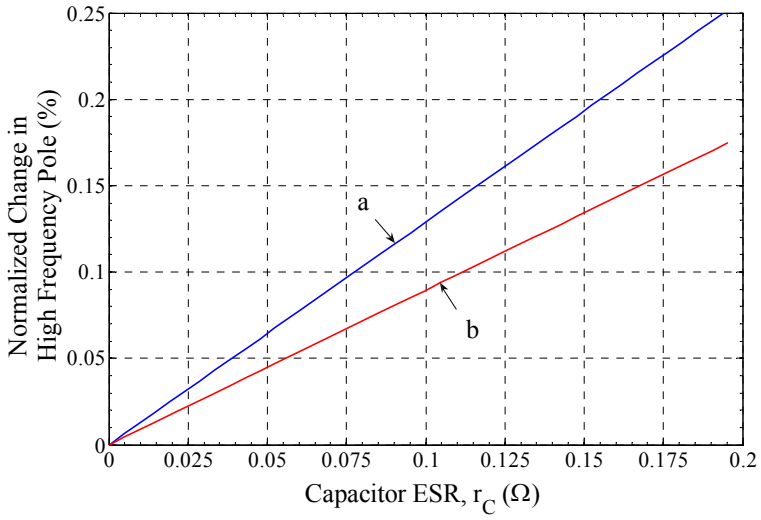

Fig. 2.13. Effect of r_C on high-frequency pole as predicted by (a): full-order models [**vor90**] and [**mak91**], (b): corrected full-order model [**sun01**]. (Parameter values: $r_C \in [0, 0.2]\Omega$, r_L = 50$m\Omega$, r_S = 10$m\Omega$, r_D = 0, L =168μH, C = 6μF, f_s = 100kHz, R = 120Ω)

2.3.6 Experimental Investigation of Averaged Modeling in DCM

In order to extract the small-signal control-to-output transfer function from a hardware prototype, a systematic procedure is implemented for small signal-injection and subsequent frequency response measurement of buck converter. The simplified schematic used for this purpose is shown in Fig. 2.14.

2.3.6.1 Small-Signal Measurement Procedure

The following step-by-step procedure has been applied for small-signal measurements:

1. A sinusoidal signal having peak-to-peak amplitude of about 200mV was superimposed on an appropriate constant DC voltage level.
2. The resultant signal was then applied to the input of PWM control circuitry.

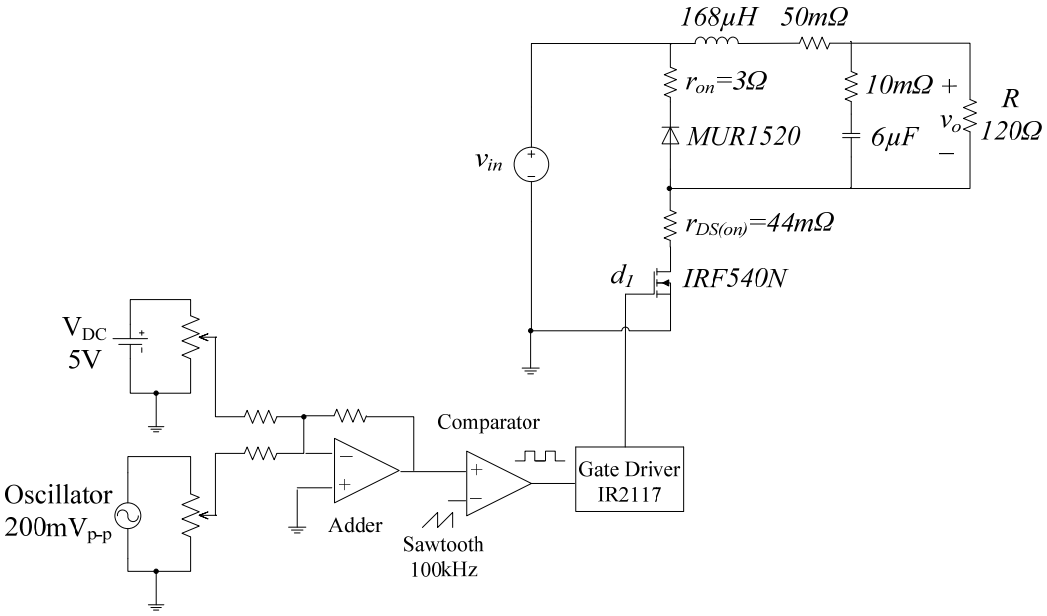

Fig. 2.14. Simplified schematic used for small-signal experimental measurements.

3. Corresponding output voltage variations were recorded along with their respective input perturbations for each frequency point and both signals were then treated in MATLAB/Simulink® environment for further analysis and to extract the necessary magnitude and phase information (see Appendix C for details).
4. To remove the undesired switching noise from the data values obtained in Step 3, a zero-phase digital filtering was performed in both the forward and reverse directions. Thus the resulting sequences have precisely zero-phase distortion.
5. Next, peaks of these input and output variables were detected using the well-known zero-derivative method. Knowing the exact locations of peaks in time-domain, phase-shift was then calculated using $360\times\Delta t/T$. Here T is the measured time-period of the input perturbation signal and Δt is the time-delay between the corresponding peaks of the output and input signals.
6. To avoid any possible measurement error in the necessary phase information for each frequency point, step 4 and 5 were repeated over a sufficiently large number of successive cycles and a mean phase was then calculated as follows:

$$\frac{1}{nT}\sum_{k=1}^{n}360\times\Delta t_k \tag{2.46}$$

This approach, albeit quite simple, works sufficiently good in the frequency range of interest (i.e. upto about 1/3 of the switching frequency). However in order to make measurements beyond this frequency range more sophisticated filtering techniques need to be employed to nullify the problematic noise, yet achieving reasonable accuracy.

2.3.6.2 Model Validations

A buck converter prototype having typical parasitics (see Fig. 2.14) was developed corresponding to an operating point defined by v_{in}=24V, v_o=14V (d_1=0.5). The DCM operation of this converter is assured for any load greater than 80.64Ω. The magnitude and phase of the measured transfer function are compared with model simulations in Fig. 2.15. In

order to achieve the best possible match with the measurements these model simulations also include the same values of parasitics as shown in Fig. 2.14. As expected, corrected full-order model matches the hardware prototype more accurately than others. The transfer function is evaluated up to 30*k*Hz, which is about 1/3 of the switching frequency (100*k*Hz). Closer to the switching frequency the results become more and more distorted due to the interaction between injected perturbations and switching noise. Furthermore, increased attenuation makes it harder to accurately capture the desired output signal at frequencies higher than about 1/3 of the switching frequency. In general, considering frequencies close to and above the switching frequency has limited use for the averaged models since the basic assumptions of averaging are no longer valid.

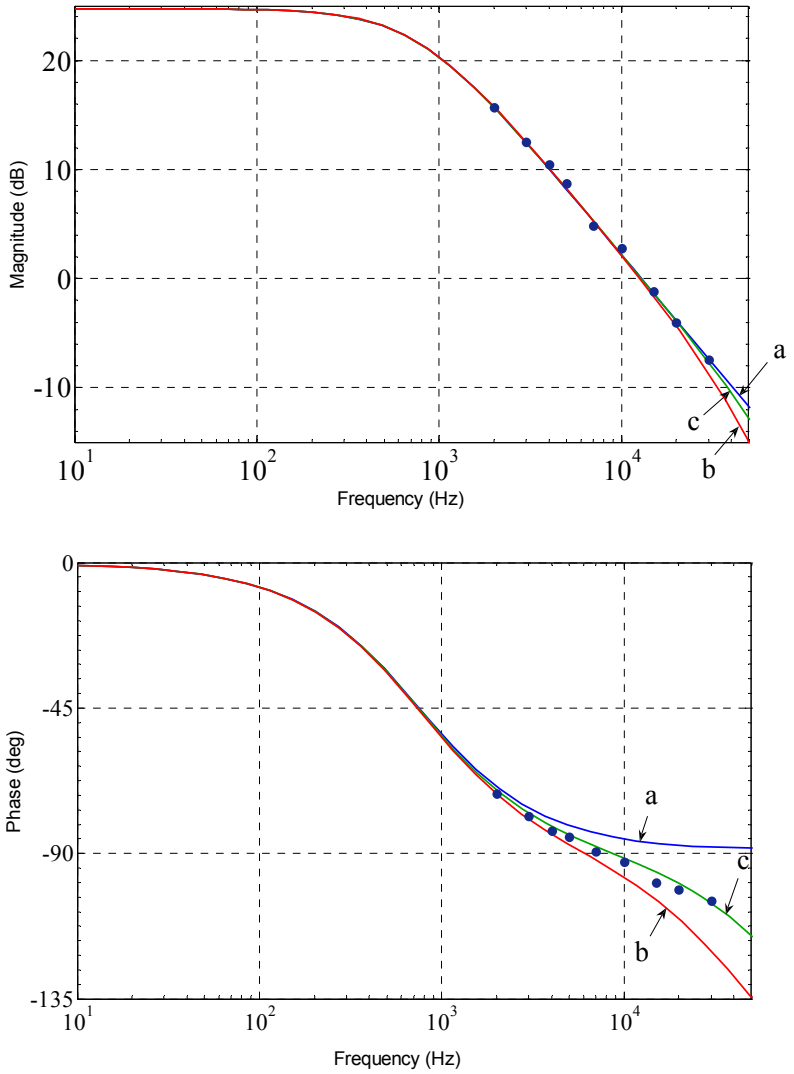

Fig. 2.15. Control-to-output transfer function magnitude and phase plots; Dotes: Measurements; Lines: Simulations; (a) reduced-order model [**cuk77**], (b) full-order models [**vor90**] and [**mak91**], (c) corrected full-order model [**sun01**]. (Parameter values: $L = 168\mu$H, $C = 6\mu$F, $f_s = 100k$Hz, $v_{in} = 24$V, $v_o = 14$V, $R = 120\Omega$, $r_L = 50m\Omega$, $r_C = 10m\Omega$, $r_D = 3\Omega$ and $r_S = 44m\Omega$)

2.3.6.3 Limitations of Averaged Modeling in DCM

Averaging is a valuable tool for both analysis and design, but one should be aware of the hazards of its incorrect applications. Due to the inherent sampling property of averaging method, the proper interpretation and use of averaging method is uncertain if the frequency

range of interest is extended beyond 1/2 of the switching frequency. Moreover, in DCM the agreement between measured and theoretical curves (as shown in Fig. 2.15) is found to be a function of model order and the definition of duty-ratio constraint d_2. Since the starting differential equations for the derivation of reduced-order and full-order models are the same, so the difference can only originate from the use of two different duty-ratio constraints. Note that averaging process and the duty-ratio constraint are the two major steps in which approximations have been introduced. Since the full-order model is much more accurate than the reduced-order model, it can be concluded that the accuracy of the final averaged model depends largely on the duty-ratio constraint. Though averaging step also introduces error, but this error is less significant, at least in the frequency range of interest.

This conclusion is in agreement with results from CCM modeling where averaging is the only approximation made. It is indicative, that in some cases the discrepancies observed in frequency-response of the converters operating in DCM are larger than discrepancies commonly found in applications of the state-space averaging in CCM. However, if we could find a "perfect" duty-ratio constraint, the resulting averaged model for DCM operation would be as accurate as CCM averaged models. The fact that averaging in DCM is taken over three intervals rather than two (as in CCM) is not responsible for the deteriorated accuracy in most previous models. There are two points worth noting with respect to validity of the averaged models for discontinuous modes. One of the assumptions in the derivation of the state-space averaged model is that the converter's corner frequencies are well below the switching frequency. With respect to the circuit waveforms, this assumption implies that ac ripples in capacitor voltages and inductor currents are relatively small. In the DCM, however, the ac ripple of either inductor current or capacitor voltage is relatively large. The second remark is concerned with the consistency between the premises and implications of the model. A general result derived from the averaged model implies that the high-frequency pole of the converter in DCM is at the frequency higher than approximately 1/3 of the switching frequency. Moreover, for boost and buck-boost converters in DCM, it can be shown that the predicted RHP zero is at even higher frequencies. Thus, the predicted corner frequencies are not well below the switching frequency, as originally assumed in the derivation of the model.

In conclusion, when averaged models are applied to cases in which the basic assumptions are not well satisfied and/or when the predicted corner frequencies are comparable to the switching frequency, the accuracy of the predicted response cannot be guaranteed. However, all of the three categories of models discussed above, exhibit approximately the same frequency-response up to about 1/10 of f_s. Beyond this frequency range, corrected full-order model conforms better to the real hardware; however some control designers may still find full-order model a more suitable choice for their control design since it exhibits the maximum phase-lag (thus represents the worst case in terms of loop phase-margins).

The relevant case in which accuracy can be guaranteed is an exact sampled-data model [alm04, chu99, hul89]. However in the low-frequency range, which is mostly of interest for closing a feedback loop around the converter's power stage, the accuracy of the averaged model is quite satisfactory (see Fig. 2.15). Simplicity of averaged models is the major advantage over the more accurate sampled-data models.

2.3.7 Formulation of Averaged Models in DCM with Input Filters

For the study of input-filter interactions and subsequent stability analysis in DCM we have a choice of various averaged models of different orders as presented in the previous section. The resonance of input filter, however, occurs at frequencies much lower than the switching

frequency (usually less than 1/10 of f_s). Since, it has been observed that in this frequency range somewhat consistent response is exhibited by all three types of averaged models discussed above [usm08b] (i.e. reduced-order, full-order and corrected full-order models). Hence we can reasonably choose reduced-order models [cuk77] to derive stability conditions for filter-converter system wherein the converter operates in DCM. Although detailed stability investigation is the subject of Chapter 3, this section derives the reduced-order state-space models of the basic converter topologies (buck, boost and buck-boost), modified to include input-filter effect. These models will be exploited in the next chapter to derive respective small-signal transfer functions and to carry out subsequent stability analysis. It is assumed that the current in input filter inductor L_F is continuous. Furthermore, for the sake of simplicity the on-resistance of diode r_D is neglected in the following model derivations.

2.3.7.1 Buck Converter Model with Input Filter

Including the effect of input filter and its parasitics, the duty-ratio constraint d_2 (based on volt-second balance over a switching cycle) as given by (2.33) is modified to yield the following expression of d_2 for buck converter [cuk77]:

$$d_2 = \frac{d_1\left(\overline{v}_{CF} + r_{CF}\overline{i}_{LF} - \overline{i}_L(r_a - r_b)\right)}{\overline{v}_C R' + \overline{i}_L r_b} - d_1 \tag{2.47}$$

where the equivalent loss resistances r_a and r_b for this nonideal buck converter are redefined as follows:

$$r_a = r_S + r_{CF} + r_L + r_C R' \tag{2.48}$$

$$r_b = r_a - r_S - r_{CF} \tag{2.49}$$

Here r_{LF} and r_{CF} are the ESR of filter inductor and capacitor respectively. Furthermore, r_0 and R' are the same as defined for CCM by (2.14) and (2.16), respectively. Now writing state-space equations for the buck-converter with input filter (as shown in Fig. 2.1) and using the duty-ratio constraint (2.47) to replace d_2, the following nonlinear averaged model is obtained:

$$\begin{aligned}
\frac{d\overline{i}_{LF}}{dt} &= \frac{v_{in} - r_0\overline{i}_{LF} + d_1 r_{CF}\overline{i}_L - \overline{v}_{CF}}{L_F} \\
\frac{d\overline{i}_L}{dt} &= 0 \\
\frac{d\overline{v}_{CF}}{dt} &= \frac{\overline{i}_{LF} - d_1\overline{i}_L}{C_F} \\
\frac{d\overline{v}_C}{dt} &= \frac{d_1\overline{i}_L\left(\overline{v}_{CF} + r_{CF}\overline{i}_{LF} - \overline{i}_L(r_a - r_b)\right)R'}{C(\overline{v}_C R' + \overline{i}_L r_b)} - \frac{\overline{v}_C R'}{RC}
\end{aligned} \tag{2.50}$$

This is a degenerate model where the dynamics of the inductor current i_L automatically disappear. Since the inductor current is no longer a state variable in this model, it must be expressed as an algebraic function of other variables, resulting in a reduced-order averaged model that is independent of inductor dynamics. For the non-ideal buck converter with input filter, the peak value of inductor current is:

$$i_{pk} = \frac{d_1 T_s}{L}(\overline{v}_{CF} + r_{CF}\overline{i}_{LF} - r_a\overline{i}_L - \overline{v}_C R') \tag{2.51}$$

Using (2.51) in (2.39) and subsequently solving for $\bar{i}_L$ (i.e. using the approach of [cuk77]), we obtain the following expression of average inductor current:

$$\bar{i}_L = \frac{i_{pk}}{2} = \frac{d_1 T_s (\bar{v}_{CF} + r_{CF}\bar{i}_{LF} - \bar{v}_C R')}{2L + r_a d_1 T_s} \tag{2.52}$$

which can now be substituted into (2.50) to eliminate its dependence on $\bar{i}_L$. The result is a conventional reduced-order averaged model in DCM for buck converter with its input filter.

Steady-state analysis:

The dc operating point of the buck converter with input filter with a constant duty cycle $d_1 = D_1$ can be determined by letting the right-hand sides of differential equations (2.50) equal to zero and solving the resulting algebraic equations for $\bar{I}_{LF}$, $\bar{V}_{CF}$ and $\bar{V}_C$. Let the scalar value of M be the intended output-input voltage ratio. The results can be expressed as:

$$\begin{aligned} M &= \frac{V_o}{\bar{V}_{CF}} = \frac{2}{1+\sqrt{1+4K/D_1^2}} \\ \bar{I}_{LF} &= D_1 \bar{I}_L \\ \bar{I}_L &= \frac{D_1(\bar{V}_{CF} - \bar{V}_C R')}{KR} \\ \bar{V}_{CF} &= V_{in} - r_{LF}\bar{I}_{LF} \\ \bar{V}_C &= V_o = M\bar{V}_{CF} \end{aligned} \tag{2.53}$$

where K is a dimensionless parameter which plays a key role in the DCM since it combines uniquely all the parameters responsible for discontinuous behavior. For non-ideal converter it can be defined as below:

$$K = \frac{2L + D_1 T_s (r_a - D_1 r_{CF})}{RT_s} \tag{2.54}$$

It can be verified that (2.53) represents the same dc operating point as that predicted by full-order model [mak91, vor90] as well as by corrected full-order model [sun00, sun01]. Using standard linearization techniques, a small-signal model can now be derived from (2.50).

2.3.7.2 Boost Converter Model with Input Filter

Including the effect of input filter and its parasitics, the duty-ratio constraint d_2 (based on volt-second balance relation) for boost converter yields the following expression:

$$d_2 = \frac{\bar{v}_{CF} + r_{CF}\bar{i}_{LF} - \bar{i}_L r_a}{\bar{v}_C R' + \bar{i}_L r_b - \bar{v}_{CF} - r_{CF}\bar{i}_{LF}} \cdot d_1 \tag{2.55}$$

where the equivalent loss resistances r_a and r_b in case of boost converter are defined as follows:

$$r_a = r_S + r_{CF} + r_L \tag{2.56}$$

$$r_b = r_a - r_S + r_C R' \tag{2.57}$$

Now writing state-space equations for the boost-converter with input filter (as shown in Fig. 2.3) and using the duty-ratio constraint defined by (2.55) to replace d_2, the following nonlinear averaged model is obtained:

$$\begin{aligned}
\frac{d\bar{i}_{LF}}{dt} &= \frac{v_{in} - r_0\bar{i}_{LF} - \bar{v}_{CF}}{L_F} + \frac{d_1\bar{i}_L r_{CF}\left(\bar{v}_C R' - \bar{i}_L(r_a - r_b)\right)}{L_F(\bar{v}_C R' + \bar{i}_L r_b - \bar{i}_{LF} r_{CF} - \bar{v}_{CF})} \\
\frac{d\bar{i}_L}{dt} &= 0 \\
\frac{d\bar{v}_{CF}}{dt} &= \frac{\bar{i}_{LF}}{C_F} - \frac{d_1\bar{i}_L\left(\bar{v}_C R' - \bar{i}_L(r_a - r_b)\right)}{C_F(\bar{v}_C R' + \bar{i}_L r_b - \bar{i}_{LF} r_{CF} - \bar{v}_{CF})} \\
\frac{d\bar{v}_C}{dt} &= \frac{d_1\bar{i}_L(\bar{v}_C R' + \bar{i}_{LF} r_{CF} - \bar{i}_L r_a)R'}{C(\bar{v}_C R' + \bar{i}_L r_b - \bar{i}_{LF} r_{CF} - \bar{v}_{CF})} - \frac{\bar{v}_C R'}{RC}
\end{aligned} \tag{2.58}$$

Following the same procedure for the non-ideal boost converter with input filter, the peak value of inductor current can be expressed as:

$$i_{pk} = \frac{d_1 T_s}{L}(\bar{v}_{CF} + r_{CF}\bar{i}_{LF} - r_a\bar{i}_L) \tag{2.59}$$

Using (2.59) in (2.39) and then solving for $\bar{i}_L$, we obtain the following expression [cuk77]:

$$\bar{i}_L = \frac{i_{pk}}{2} = \frac{d_1 T_s(\bar{v}_{CF} + r_{CF}\bar{i}_{LF})}{2L + r_a d_1 T_s} \tag{2.60}$$

This can now be substituted into (2.58) to eliminate its dependence on $\bar{i}_L$. The result is a conventional reduced-order averaged model in DCM for boost converter with input filter.

Steady-state analysis:

By equating right-hand sides of equations (2.58) to zero and making use of (2.60), we can determine the steady-state solution for boost converter in DCM as shown below:

$$\begin{aligned}
M &= \frac{V_o}{\bar{V}_{CF}} = \frac{1 + \sqrt{1 + 4D_1^2/K}}{2} \\
\bar{I}_{LF} &= D_1\bar{I}_L + \frac{\bar{V}_C}{R} \\
\bar{I}_L &= \frac{D_1(\bar{V}_{CF}R + r_{CF}\bar{V}_C)}{KR^2} \\
\bar{V}_{CF} &= V_{in} - r_{LF}\bar{I}_{LF} \\
\bar{V}_C &= V_o = M\bar{V}_{CF}
\end{aligned} \tag{2.61}$$

where K is the same as given by (2.54).

2.3.7.3 Buck-Boost Converter Model with Input Filter

The duty-ratio constraint d_2 for buck-boost converter (based on volt-second balance of inductor current) yields the following expression [cuk77]:

$$d_2 = \frac{\bar{v}_{CF} + r_{CF}\bar{i}_{LF} - \bar{i}_L r_a}{\bar{v}_C R' + \bar{i}_L r_b} \cdot d_1 \tag{2.62}$$

The equivalent loss resistances r_a and r_b in case of buck-boost converter are defined as below:

$$r_a = r_S + r_{CF} + r_L \tag{2.63}$$

$$r_b = r_L + r_C R' \tag{2.64}$$

Now writing state-space equations for the buck-boost-converter with input filter (as shown in Fig. 2.5) and substituting the duty-ratio constraint (2.62) to replace d_2, the following reduced-order nonlinear averaged model is obtained:

$$\begin{aligned}
\frac{d\bar{i}_{LF}}{dt} &= \frac{v_{in} - r_0 \bar{i}_{LF} + d_1 r_{CF} \bar{i}_L - \bar{v}_{CF}}{L_F} \\
\frac{d\bar{i}_L}{dt} &= 0 \\
\frac{d\bar{v}_{CF}}{dt} &= \frac{\bar{i}_{LF} - d_1 \bar{i}_L}{C_F} \\
\frac{d\bar{v}_C}{dt} &= \frac{d_1 \bar{i}_L (\bar{v}_{CF} + r_{CF} \bar{i}_{LF} - \bar{i}_L r_a) R'}{C(\bar{v}_C R' + \bar{i}_L r_b)} - \frac{\bar{v}_C R'}{RC}
\end{aligned} \tag{2.65}$$

For the non-ideal buck-boost converter with input filter, the peak value of inductor current can be written as:

$$i_{pk} = \frac{d_1 T_s}{L} (\bar{v}_{CF} + r_{CF} \bar{i}_{LF} - r_a \bar{i}_L) \tag{2.66}$$

Substituting (2.66) into (2.39) and then solving for $\bar{i}_L$, we get the following expression of average inductor current:

$$\bar{i}_L = \frac{i_{pk}}{2} = \frac{d_1 T_s (\bar{v}_{CF} + r_{CF} \bar{i}_{LF})}{2L + r_a d_1 T_s} \tag{2.67}$$

This can now be substituted into (2.65) to eliminate its dependence on $\bar{i}_L$. The result is a conventional reduced-order averaged model in DCM for buck-boost converter with input filter.

Steady-state analysis:

Following the same procedure as described above, the dc operating point of this buck-boost converter with input filter is obtained as below:

$$\begin{aligned}
M &= \frac{V_o}{\bar{V}_{CF}} = \frac{D_1}{\sqrt{K}} \\
\bar{I}_{LF} &= D_1 \bar{I}_L \\
\bar{I}_L &= \frac{D_1 \bar{V}_{CF}}{KR} \\
\bar{V}_{CF} &= V_{in} - r_{LF} \bar{I}_{LF} \\
\bar{V}_C &= V_o = M \bar{V}_{CF}
\end{aligned} \tag{2.68}$$

with K having the same value as given by (2.54).

2.4 SUMMARY

In this chapter, various aspects of small-signal averaged modeling of non-ideal PWM converters are investigated. Since averaged models of varying order exist in literature for DCM, therefore more attention has been paid to the averaged modeling in DCM (rather than in CCM). Analytical expressions of the representative models from the literature are reformulated by including necessary parasitics. These commonly-cited averaged models are compared not only among themselves but also with a hardware prototype having typical parasitics. Besides confirming the relative accuracy of corrected full-order models, we have tested an experimental technique for measuring small-signal control-to-output transfer function and demonstrated its effectiveness in the frequency range which is usually of interest in most of the applications. More importantly, the parasitic effects on frequency-domain characteristics of the PWM converters as predicted by various averaged models are studied. Furthermore, it has been shown that r_C has the most significant influence on converter performance than any other parasitic of the circuit. Another remark is that from a control designer's point of view the feasibility of different modeling methods on high-frequency control-loop design is important. Although corrected full-order model conforms better to the real hardware, some control designers may still find full-order model a more suitable choice for their control design since it exhibits the maximum phase-lag (thus represents the worst case in terms of loop phase-margins).

Chapter 3

INPUT-FILTER INTERACTIONS AND CONTROL ISSUES: A PASSIVE SOLUTION FOR STABILITY

In this chapter, problem of input-filter interactions is explained using averaged models of dc-dc converters. A comprehensive state-of-the-art study of input-filter interaction problem is presented. A passive damping solution is discussed to assure stability of dc-dc converters in presence of input filter. Design criteria are proposed for the dimensioning of damping resistance without over sizing or under sizing. A case study of cascade buck converters with input filter is also presented.

3.1 INTRODUCTION

The trend in next generation dc-dc converters is to achieve smaller size and lighter weight. This trend naturally pushes to increase the switching frequency because at higher operating frequencies not only the size and weight of the passive components are dramatically reduced but the relevant operational costs are also lessened. However, besides providing compact high-density dc-dc converters, the high-frequency switching operation also raises electromagnetic interaction (EMI) issues. Switched-mode power converters are typically considered sources of electromagnetic noise as their high-frequency switching of voltage and current generates higher order harmonics that have a potential to cause interference with system operation [jos98, wil98]. The problematic conducted input EMI noise generally comprises of reflected ripples in the input current of a switch-mode power converter which interacts with the source impedance of the raw supply voltage [art01]. Combined with any radiated noise, the resultant disturbance can significantly pollute the power-mains and can also cause degradation in systems wherein multiple dc-dc converter modules are fed by a common power bus as in case of dc distribution networks [art01]. Flyback and buck topologies are particularly notorious for noisy input currents, since a semiconductor switch is directly in series with the input power line; whereas other topologies such as boost and Cuk converters inherently produce lesser conducted noise at input.

In order to combat EMI, an LC filter is usually employed between a dc-dc converter and its unregulated power source. A substantial part of manufacturing cost for power converters in critical applications involves designing filters to conform to the varying EMI/EMC norms for various military and commercial applications. However, a presumably well-designed input filter, satisfying aforementioned requirements of EMI/EMC, when combined with a switching converter, can often cause significant performance degradation [mid76], such as reduction in loop gain, output impedance and instability. Excessive peak of output impedance at the

resonant frequency of the filter can interact with the regulator control-loop [mid78]. The cause of this complex interaction is diagnosed to be the negative dynamic resistance characteristic exhibited by dc-dc converters at their input terminals, which leads to degradation in loop gain, output impedance and even possible instability of the system [mid76, mid78, sad04]. Thus on one hand, input filters serve to suppress the EMI, but on the other hand the control-loop design must take into account this input filter in order to assure stability. As a consequent, the control-loop design process becomes more complicated than in the case when no input filter is present, and additional challenges and constraints are imposed on the control system to assure stability.

This chapter addresses this instability problem originated from the interaction of input-filter with converter's control-loop and is structured as follows:

- Explanation of the interaction between the converter and input filter
- Thorough review of literature describing state of the art on this subject
- Review of various passive damping configurations to resolve the issue
- Influence of input filter on basic converter topologies (in both CCM and DCM) and derivation of the required conditions to achieve stable regulation
- A case-study of cascade buck converters with input filter to confirm the effectiveness of the suggested design criteria

3.2 WHY INPUT FILTERS CAN CAUSE INSTABILITY ?

By their very nature, dc-dc converters are classified as constant-power loads. This means that for an ideal switching regulator, with no losses, the average input power remains constant. If the input voltage increases by some factor, the PWM closed-loop control circuitry cuts back the duty cycle of the controlled switch to maintain a constant output voltage. This, in turn, causes the input current to decrease by the same proportion. In incremental terms, a positive incremental change in the input voltage results in a negative incremental change in the input current and vice versa, causing the converter to look like a negative differential resistance at its input terminals. The value of this negative resistance depends on the operating point of the converter according to:

$$R_{in} = -\frac{\Delta v_{CF}}{\Delta i_{in}} \tag{3.1}$$

where R_{in} is the input resistance, and Δv_{CF} and Δi_{in} are the incremental changes in the input voltage and input current to the dc-dc converter. To analyze the behavior of the converter and its interaction with the rest of the system, a simplified model of the system is necessary. A simple L-C filter, combined with negative dynamic resistance model of the switching regulator, is shown in Fig. 3.1.

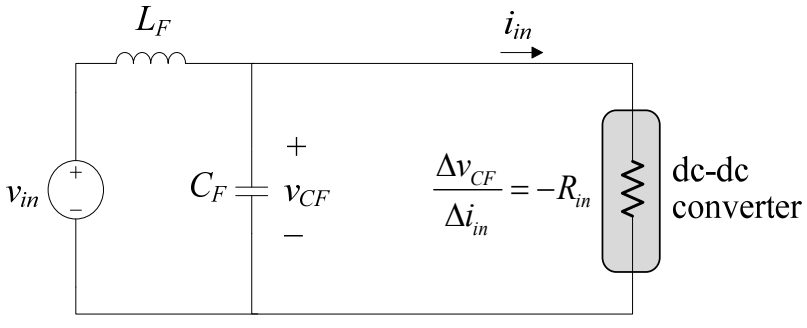

Fig. 3.1. Low frequency ac model of LC input filter with dc-dc converter as load.

In the vicinity of a given operating point, where R_{in} can be considered constant and the system can therefore be considered linear, the characteristic polynomial of this circuit (Fig. 3.1) is:

$$s^2 - \frac{s}{R_{in}C_F} + \frac{1}{L_F C_F} = 0 \tag{3.2}$$

The negative term in this characteristic polynomial transforms to a positive exponential in the time domain, representing an unbounded, hence unstable system. Thus an undamped or lightly damped input filter connected to the regulator input port, can interact with the negative resistance characteristics of the regulator to form a negative-resistance oscillator. This further explains why addition of an input filter tends to lead to instability. It is noteworthy that at full load and lowest input voltage the magnitude of R_{in} is the minimum which represents the worst case. Moreover, the converter's input impedance appears as a negative resistance only at low frequencies. At higher frequencies this impedance is influenced by the converter's own internal filter elements and the limited bandwidth of its feedback loop.

However, despite the theoretical arguments presented above, it is still possible that in some practical applications a dc-dc converter with a simple L-C input filter do not exhibit instability. There are several possible reasons why a switching regulator combined with an input filter might not oscillate in practice:

1. The L-C filter components or even the power line itself may include enough parasitic resistance to provide sufficient damping.
2. The input filter is designed such that its resonant frequency is well above the switching regulator bandwidth.

Under any one of these conditions it is fairly possible that a dc-dc converter may not oscillate even in presence of an input filter. However, a comprehensive understanding of the problem is important from practical point of view because most of the designers realize a dc-dc converter design in two distinct steps. First the converter itself is designed according to its given performance specifications, and then in the second step a low-pass filter having sufficient attenuation, to alleviate various noise problems, is added at the input of the converter “black box”. There arises a new complication from the fact that the presence of an input filter affects the dynamics of the converter, which otherwise performed well. Apparently it seems that an added input filter is outside the converter feedback loop, and therefore should not affect the converter properties, such as loop-gain, output impedance or transfer functions (except for the direct affect of the filter forward voltage transfer function). However, this is not true, because the input filter is, in fact, not “outside” the feedback loop but interacts with it. It was shown that the input filter actually affects all transfer functions of the converter, including the control-to-output transfer function, the line-to-output transfer function as well as the output impedance of the converter [mid76, mid78]. As a consequence, additional criteria need to be established in order to avoid this harmful influence of an input filter upon the regulator terminal properties. The choice is not whether or not to use an input filter but to find an optimum way of minimizing its adverse impact on overall system performance. Although, the potential instability is only one aspect of a broader question concerning the influence of an input filter upon regulator properties, but the emphasis and scope of this thesis is mainly confined to the instability issue.

3.3 STATE OF THE ART

Before 1970's

In the old days, when 20kHz switch-mode power supplies first began to be used in the mid 1960's usually the only EMI specification imposed was for conducted emissions above 150kHz. This requirement of EMI was somewhat lenient and therefore placed the input filter beyond the negative input-resistance frequency of the switching regulator, so adding a filter never caused instability. Later MIL-STD-461 standards, such as CS01[1] and CE03[2], were invoked and filters had to meet new conducted susceptibility and emission requirements down to frequencies as low as 30Hz [mil86]. The need of getting sufficient attenuation at the switching frequency forced the filter resonance to migrate into the region of instability. Thus a new complication arose from the fact that this input filter impairs all other properties of the regulator itself, in extreme cases to the point of causing instability. Since then, an increasing interest in calculating and measuring stability of complex power systems has originally taken the form of input-filter interactions in power supplies.

1970 – 1980:

The problem of EMI-filter interactions with switching converters was first identified and brought into spotlight in the early seventies. The papers on this subject extend back to as early as 1971 [bie71]. The detailed treatment of this problem was first given by Dr. R. D. Middlebrook in [mid76] and [mid78], the former of which has now become a classic in the field. In [mid76] input-filter design criteria were established leading to some impedance inequalities which not only ensured stability, but also specified qualitative impairment of the performance properties caused by this interaction. Middlebrook pointed out that oscillations could be positively prevented by assuring that the magnitude of the output impedance $|Z_S|$ of the source (filter) remains lower than the magnitude of the input impedance $|Z_{in}|$ of downstream converter as shown in Fig. 3.2.

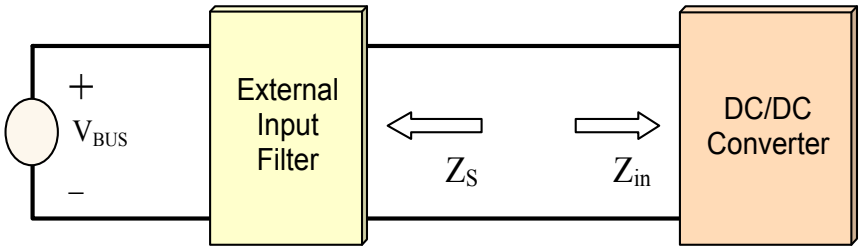

Fig. 3.2. Definition of the source impedance Z_S, and the converter's input impedance Z_{in}.

In the subsequent years, considerable progress in the small-signal modeling and analysis methods for dc-dc converters greatly facilitated the understanding of various dynamical phenomena of switching converters. In particular, the development of averaging methods, such as [mid77a, mid77b] and [cuk77], motivated the research and discussions on the problem of input-filter interactions with switch-mode power supplies. In [mid78], the results of [mid76] are established by physical reasoning using a more circuit-oriented approach of dealing with the system stability problem. The analysis was based on an ac equivalent

[1] This "Conducted Susceptibility" requirement is applicable to equipment and subsystem input power leads (AC and DC), over a frequency range of 30 Hz to 50 kHz.
[2] This "Conducted Emission" requirement defines the limits of the current that can be put back on the power bus in the frequency range of 15 kHz to 50 MHz.

averaged circuit model of the dc-dc converter, called "canonical model". It also introduced some guidelines to achieve optimal damping of the input filter to assure stability.

One undesirable characteristic of a simple L-C filter is that the output impedance of the filter approaches a maximum peak (ideally infinity) at the resonance of this filter. However, if this peak of filter output impedance is greater than the open-loop input impedance of the converter at any frequency, then sustained oscillations are likely to commence at that frequency which can lead to instability. The criterion proposed in both [mid76] and [mid78] is a graphical method in which frequency curves of the output impedance Z_S of input-filter (see Fig. 3.2) and the open-loop input impedance Z_{in} of the dc-dc converter are superimposed in the same plot. These curves (impedances vs. frequency) are plotted for the worst-case condition of low-line and full-load. As a result, a fairly simple criterion to insure stability was worked out and it imposed following constraint on the input filter design for all frequencies:

$$|Z_S| << |Z_{in}| \tag{3.3}$$

For the realization of this input-filter design constraint, it was proposed to add some extra damping resistance to the filter circuit, either in parallel or in series with L_F or C_F, if their natural parasitics are insufficient for this purpose. A qualitative comparison between various possible damping circuit configurations was also presented leading to simple design criteria; for details the reader is referred to [mid76, mid78].

Later in [phe79], the results of [mid78] were extended to several commonly used single-section L-C filters as well as to two configurations of two-section L-C filters. Various damping arrangements were investigated with a view of optimizing the performance of switching power converters. Parameters considered for optimization were peaking, output impedance, weight, volume and cost of the filters. The effect of input filter on loop stability, transient response and audio-susceptibility were also investigated in [lee79] based on the small-signal averaged model, and an optimum low-pass and light-weight filter configuration was proposed.

1980 – 1990:

In the 1980's, the major contribution to the input-filter interaction problem was made by S. S. Kelkar and F. C. Lee. A new concept of input-filter compensation via pole-zero cancellation was proposed in [kel82, kel83] to minimize peaking effect of the filter output impedance. This compensation scheme was implemented using a feedforward loop in addition to the existing feedback loop of a buck converter in CCM with constant duty-cycle control. Feedforward compensation effectively isolated the switching converter from its source hence avoided any detrimental interactions. In this feedforward method, the input-filter inductor current and capacitor voltage were multiplied by some gains and then subtracted from the feedback signal generated at the output of the integrator in the feedback-loop. The result was then fed to the pulse width modulator. However, this scheme required measurement of the small-signal variations in the input-filter inductor current and capacitor voltage. Moreover the gain of the feedforward circuit was also dependent on the supply voltage and the type of duty-cycle control used.

The input-filter compensation scheme as initially presented in [kel82] and [kel83] was designed for a fixed input-voltage. Later this concept was extended to introduce an adaptive compensation which tracked the input voltage variations by including an additional feedforward of the input voltage [kel84a]. Although this modified compensation scheme

retained all other features of earlier non-adaptive circuit for single-loop controlled regulator, its design was considerably different for multi-loop controlled regulators having different types of duty-cycle control. This is due to the fact that duty-cycle modulator gain in this method was a function of particular multi-loop implementation. However, this approach allows significant reduction of the damping resistance size, provided that the input filter contains a sufficient minimal amount of natural damping. Complete stability analysis of a buck regulator employing this input-filter compensation scheme was presented in [kel84b]

1990 – 2000:

The criterion (3.3) is generally necessary and sufficient for the stability of voltage-mode controlled PWM converters operating in CCM. However, this criterion was found inappropriate for current-programmed control. So, after some initial work by [eri92] and [koh92], an addition to this criterion was worked out in 1992 by [jan92] for current-programmed converters. The resulting criteria for current-programmed converters were found to coincide with previous voltage-mode design criteria, except that one additional criterion is necessary to guarantee stability of the input voltage feedforward loop. A useful discussion on the input-filter design for current-programmed converters can also be found in [wu92], and the dynamic response of current-programmed dc-dc converters with input filters (using a switched-inductor model) is explained in [tsa92].

In the late 1990's, the conventional input-filter-interaction formulation was further extended to obtain specific results for several discrete applications. For instance, input-filter design issues for power factor correction (PFC) circuits were discussed in detail in [vla96] and [ora03]. Similar criteria for cascaded converters with intermediate filters have also been developed by [cho95] and [liz96]. In [eri99], the optimal damping approach of [mid78] was extended to two other filter topologies, and application of the results to multiple-section cascaded filters was illustrated. The extension [eri99] made use of Middlebrook's extra element theorem [mid89, mid98] to demonstrate how addition of an input filter modifies the converter's loop-gain and other important quantities. Similarly a specific design example of two-section RC-damped input filter was presented in [mit99] using the same analytical design criteria presented in the earlier literature. Ref. [alf99] has used large-signal nonlinear discrete-time averaged model to explain classical input-filter interactions in dc-dc converters. Nonlinear techniques are employed for the stability analysis; however, no new criteria are derived. In [bar96], filter-converter system is first investigated for its small-signal stability by replacing the converter with a constant current source. Then a large-signal model is used to obtain limit cycles of stability applying numerical calculations.

An increased trend in the dc power distribution networks led the filter-converter interaction concept to be further applied on other interconnected systems. For example, in many applications, such as spacecrafts, aeronautics and telecommunication power systems, several converters are usually required to be connected in cascade. In such configuration, a downstream dc-dc converter appears as constant-power load to the source converter, hence causing an analogous interaction problem leading to system instability. Numerous published papers address this instability problem in dc distribution networks based on interconnected switching power converters [art01, byu99, cho91, lew89, sch90, tab92, wan03]. The stability and loading effects of such integrated systems are usually studied using the "minor-loop gain", which is generally defined as the ratio of the output impedance of the source subsystem (e.g. input filter) and the input impedance of the load subsystem (e.g. dc-dc converter) [cho91, gho96, lew89, sch90].

2000 – Present:

In the recent years, besides exploring various passive and active damping solutions, new modeling techniques have been introduced and applied for the analysis of input-filter interactions. For instance, a two-port unterminated modeling technique was introduced in [sun02a] for the analysis of input-filter interactions in telecommunication power distribution system. This approach known as "unterminated modeling" (also known as "hybrid model" or "G-parameter representation") was demonstrated to be more suitable for complicated dynamical systems composed of cascaded switched-mode converters [sun03, sun04]. The method is based on the use of two-port model of a converter where the input and output ports are modelled using *Norton*'s equivalent circuit and *Thevenin*'s equivalent circuit, respectively. The name "unterminated" signifies that the load is usually treated as an external element that is not included into the model of converter. This approach was first applied to the formulation of the input-filter interactions in peak-current-mode controlled (PCMC) buck converters [sun02b, sun02c], and later to the voltage-mode controlled (VMC) buck converters [han06a, han06b]. However, the results obtained using this approach cannot be easily generalized to be valid for types of converters other than buck converter. An other similar algebraic approach to modeling of dc-dc converters with input filters was introduced in [alt04] for voltage-mode controlled (VMC) as well as for peak-current-mode controlled (PCMC) buck converter, which also resulted into similar results.

Instabilities in power converters with input filters were also discussed by [tsu01] for railway vehicle applications. Three different damping methods were analyzed for input filters, but the need for further study on damping networks was emphasized. Ref. [kim05] reported some important results regarding the comparison of voltage-mode control and current-mode control. It stated that the impedance constraints for a minimal input-filter interaction are significantly easier to meet in the current-mode controlled converters rather than in voltage-mode controlled converters. However it focused more on the analysis and shed little light on the design of damping circuits. A different technique for input-filter damping design was suggested in [cal02] based on the zero dynamics analysis. However, the results yielded by this method were equivalent to those obtained using the classical approach [mid78] based on minimizing the filter output impedance.

It is observed that most of the above mentioned papers specify that to guarantee system stability the magnitude of the source impedance, Z_S, should be small compared to the magnitude of the converter's input impedance, Z_{in} (see Fig. 3.2). Since the external filter impedance usually dominates the source impedance, thus $|Z_S| << |Z_{in}|$ requirement mainly becomes a constraint on the design of input filter.

Although the $|Z_S| << |Z_{in}|$ requirement is a relatively well-known "rule of thumb" in the industry, it is not always easy to implement. One reason is that very few dc-dc converter vendors provide $|Z_{in}|$ in their data sheets, which forces the designer to make complicated measurements to determine this value. Also, in achieving a satisfactory level of stability it is not clear how much $|Z_S|$ must be kept smaller as compared to $|Z_{in}|$. Nevertheless, in practice most power system engineers successfully create stable distributed power systems by placing a relatively large electrolytic capacitor across the input terminals of each dc-dc converter. The Equivalent Series Resistance (ESR) of this capacitor provides the positive resistance needed to compensate for the destabilizing effects of the converter's negative input resistance. But this method is not satisfactory for high-reliability applications.

In [kar03, sad04] and [usm06, usm07], a different and more practical approach was presented to design input-filter damping solely based on the open-loop control-to-output transfer function. It was highlighted that a second order input filter causes two RHP[1] zeros in the open-loop transfer function of the converter, and these zeros are the source of instability in the closed-loop. A design criterion was proposed to shift these zeros to the LHP[2] by adding R-C parallel damping to the filter circuit. In [usm06, usm07] it was found that not only there exist a minimum value of damping resistance required for stability but there also exists an upper limit on this resistance value. These lower and upper limits on damping resistance were determined accurately in these papers. Thus they permit to define a stable operating region in the damping-circuit parameters space. The required stability conditions, for which all zeros of the transfer-function remain on the LHP, were intuitively obtained by application of Routh-Hurwitz criterion to the numerator polynomial of the transfer function.

It is also worth mentioning here that most of the approaches presented above propose passive damping of input filters to solve the instability problem. Nevertheless, some other authors have also suggested active damping methods [dah02, lac08] or control solutions [bar02, nic95, usm08c] to avoid excessive power dissipation in passive damping components. Some of these active alternatives will be discussed in the next chapters along with a detailed quantitative assessment of the efficiency degradation by passive dampers.

In the current chapter, we focus on the passive damping solution and follow the approach presented in [usm06, usm07] to design parallel R-C damping without over sizing or under sizing. The objective of this chapter is to complete the work presented in these papers for all basic topologies (i.e. buck, boost and buck-boost) for both CCM and DCM. The state-space averaging technique, as presented in the preceding chapter, is applied throughout for the derivation of small-signal transfer functions and subsequent stability analysis. New design rules are formulated which provide the exact values of the damping resistance to be inserted in the input filter from a practical viewpoint. Furthermore, these analytical design rules are systematically verified through experiments. The internal parasitics of the filter components are taken into account for the stability analysis and their effect on frequency-domain characteristics is studied quantitatively. The analysis is carried out and experimentally tested for voltage-mode controlled converters; however the implications of the results for both CCM and DCM are discussed. The extension of these results to a particular example of cascade buck converter will also be treated later in this chapter.

3.4 DAMPING OF INPUT FILTER – A PASSIVE SOLUTION

Review of Various Damping Configurations:

As evident from the literature survey presented above, an easy method to mitigate the instability problem is to simply introduce adequate resistance into the input filter to counteract the negative input resistance of the dc-dc converter. As a result, the detrimental effect of input filter on converter transfer functions becomes negligible. However, it is not practical to add a damping resistance arbitrarily to the filter circuit, because a damping resistor in series with L_F would decrease converter efficiency since it must pass all of the dc input current. While a damping resistor in series with C_F would seriously degrade its attenuation characteristic as well as the efficiency since it must essentially pass entire ac input current component.

[1] Right Hand *s*-Plane
[2] Left Hand *s*-Plane

One possible approach of damping the filter is to add a damping resistance R_d in parallel with capacitor C_F, as shown in Fig. 3.3(a). Unfortunately, this configuration also suffers from power dissipation problem in R_d. One solution to power dissipation problem is to place R_d in parallel with L_F as illustrated in Fig. 3.3(b). Since the dc voltage across inductor L_F is ideally zero, there is now no dc power loss in resistor R_d. Nevertheless, the main problem with this circuit is that its transfer function contains a high-frequency zero. Addition of R_d degrades the slope of the high-frequency asymptote from -40dB/decade to -20dB/decade [eri01]. Hence this circuit effectively behaves as a single-pole R-C low-pass filter with no attenuation provided by inductor L_F.

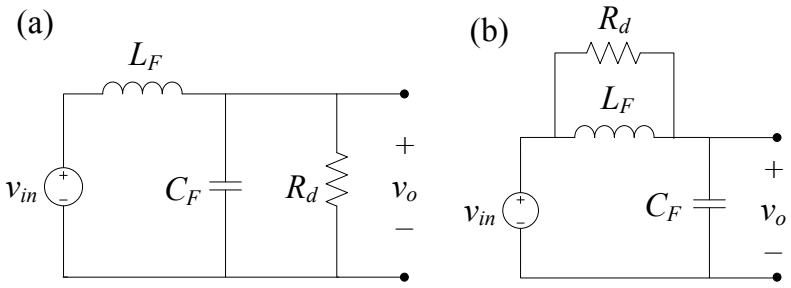

Fig. 3.3. Two attempts to damp the input filter; (a): Addition of damping resistance across C_F; (b): Addition of damping resistance in parallel with L_F.

To deal with these issues, a practical solution for damping the input filter is illustrated in Fig. 3.4. In this configuration, a dc blocking capacitor is connected in series with resistance R_d. Since no dc current can flow through R_d, its dc power loss is ideally eliminated. The value of the dc blocking capacitor C_d can be expressed as $C_d = kC_F$ and is chosen to be very large as compared to C_F so that at filter resonant frequency f_F, the impedance of R_d-C_d branch is dominated by resistor R_d.

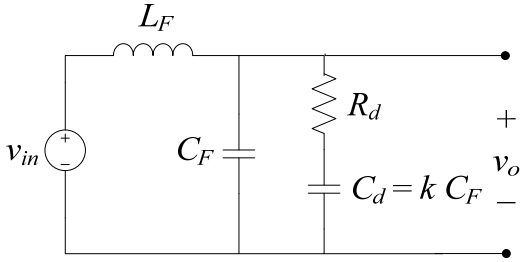

Fig. 3.4. A practical method of damping the input filter, including the damping resistance R_d and dc blocking capacitor C_d.

The R_d-C_d parallel damping approach, as shown in Fig. 3.4, finds significant application in dc-dc converters. Since a resistor is to be placed in series with C_d, this capacitor can be realized using capacitor types having substantial equivalent series resistance (ESR), such as electrolytic and tantalum types. However this method is not desirable in ac power converters as large capacitor C_d can cause excessive dissipation at line frequency because of the ac current flowing through the damping branch. In such applications, the parallel and series R_d-L_d approaches presented in Fig. 3.5 can lead to smaller designs. This method eliminates the excessive dissipation in resistor and is, therefore, widely used in ac power converter filters. The design and optimization of these damping networks is discussed in [phe79] and [eri99].

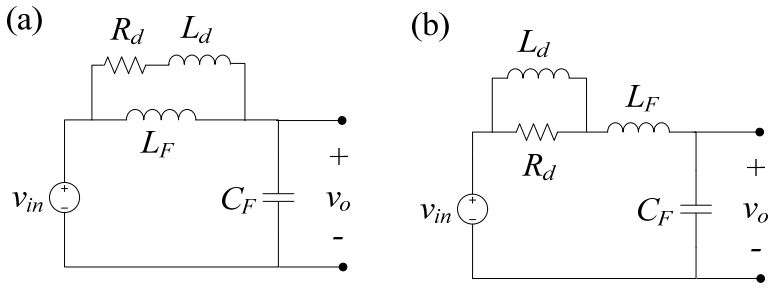

Fig. 3.5. Several practical approaches to damp the input filter oscillations in ac power converters; (a): R_d-L_d parallel damping; (b): R_d-L_d series damping.

Effect of R_d–C_d Parallel Damping on Filter Characteristics:

Being the most practical damping approach for dc-dc converter applications [mid78], we consider only the R_d-C_d parallel damping in our study. The input-to-output transfer function and the output impedance of an L-C filter with R_d-C_d shunt damping (as shown in Fig. 3.4) can be expressed as below:

Input-to-output transfer function:

$$G_F(s) = \frac{v_o(s)}{v_{in}(s)} = \frac{s(R_dC_d)+1}{s^3(L_FC_FC_dR_d)+s^2\left[L_F(C_F+C_d)\right]+s(R_dC_d)+1} \tag{3.4}$$

Output impedance:

$$Z_{out}(s) = \frac{sL_F\left[s(R_dC_d)+1\right]}{s^3(L_FC_FR_dC_d)+s^2\left[L_F(C_F+C_d)\right]+s(R_dC_d)+1} \tag{3.5}$$

Plot of the filter transfer function and output impedance are shown in Fig. 3.6 for varying values of damping resistance R_d while keeping other parameters constant. Below the resonant frequency of the filter $f_F = 1/2\pi\sqrt{L_FC_F}$, the input voltage passes through the filter without significant attenuation. Above this resonant frequency, voltages are attenuated and the attenuation increases at a slop of 40dB/decade. At the resonant frequency, there is a peak in gain where the output voltage of the filter is actually higher than the input voltage. The amount of this peak is determined by the series and parallel losses associated with various elements as well as those of source and load. The effect of these losses is normally consolidated into a damping factor. With a damping factor of 1, there is no peak whereas the highest peak occurs for zero damping.

The highest peak in the output impedance occurs when the filter is undamped. The output impedance of the filter is low at low frequency because the inductor impedance is low and the power bus is essentially a short circuit. At high frequencies, the output impedance of the filter is again low because of the low impedance of the capacitor at high frequency. However, at resonance, the impedance of the filter can be significantly high, especially if there is little damping.

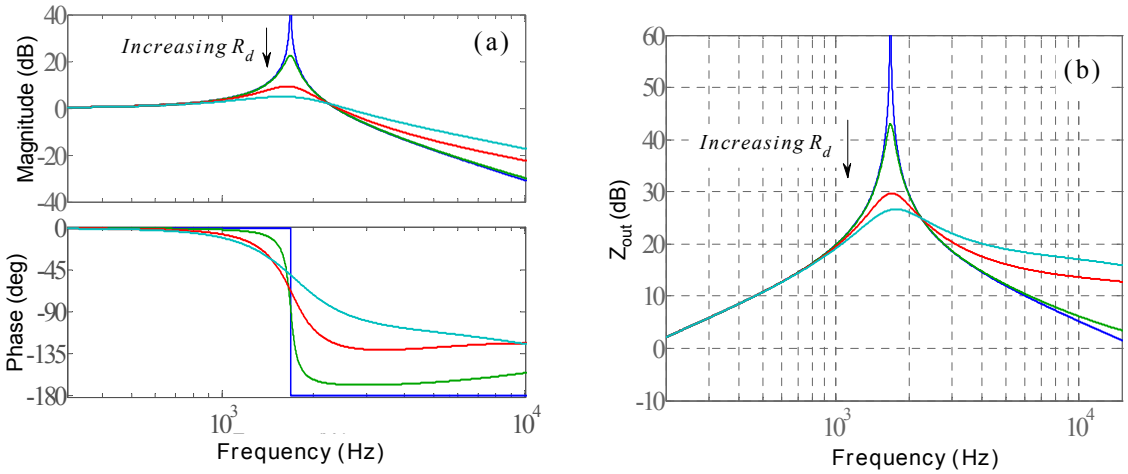

Fig. 3.6. (a): Bode plot of filter transfer function (3.4), (b): Output impedance (3.5) plot of input filter. (Parameter values: $L_F = 1mH$, $C_F = 1\mu F$, $k = 10$, $R_d \in [0, 8]\ \Omega$).

3.5 INPUT-FILTER INTERACTIONS IN CCM

3.5.1 Buck Converter with Input Filter

Circuit Diagram:

The circuit diagram of a non-ideal buck converter with input filter is shown below:

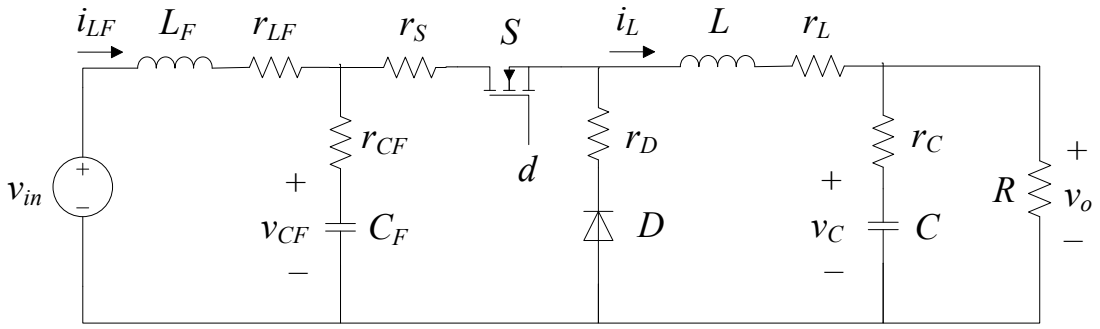

Fig. 3.7. Non-ideal buck converter circuit with input filter.

Effect of Filter Poles on Converter Transfer Function:

Assuming a constant input voltage V_{in}, the open-loop control-to-output transfer function of a non-ideal dc-dc converter can be obtained from its small-signal linear model in the following form:

$$G(s) = \frac{\tilde{v}_o}{\tilde{d}} = K \frac{A_3 s^3 + A_2 s^2 + A_1 s + A_0}{B_4 s^4 + B_3 s^3 + B_2 s^2 + B_1 s + B_0} \tag{3.6}$$

Where $K = V_{in}/m$. Here m and the coefficients A_k and B_k of $G(s)$ depend on the converter family and conduction mode. For a non-ideal buck converter with input filter (see Fig. 3.7) these coefficients are found to be as follows:

$$
\begin{aligned}
m &= \left(r_1 + D^2(r_{LF} - r_{CF}) + R'R\right) \Big/ R'R \\
A_0 &= r_1 - D^2(r_{LF} - r_{CF}) + R'R \\
A_1 &= r_C C\left(r_1 - D^2(r_{LF} - r_{CF}) + R'R\right) + D^2(r_{CF}^2 C_F - L_F) + r_0 C_F(r_1 + R'R) \\
A_2 &= C_F L_F(r_1 + R'R) + r_C C\left(D^2(r_{CF}^2 C_F - L_F) + r_0 C_F(r_1 + R'R)\right) \\
A_3 &= r_C L_F C_F C(r_1 + R'R) \\
B_0 &= mR' \\
B_1 &= RC\left(r_1 + D^2(r_{LF} - r_{CF})\right) + R'\left(L + D^2(L_F - r_{CF}^2 C_F) + r_0 C_F(r_1 + R'R)\right) \\
B_2 &= RC\left(L + r_0 r_1 C_F + D^2(L_F - r_{CF}^2 C_F)\right) + R'C_F\left(r_0 L + L_F(r_1 + R'R)\right) \\
B_3 &= C_F\left(RC(r_0 L + r_1 L_F) + R'L_F L\right) \\
B_4 &= RCC_F LL_F
\end{aligned}
\tag{3.7}
$$

Where r_0 and r_1 for this buck converter are defined in Chapter 2 by equation (2.14) and (2.15) respectively, and R' is generally defined by (2.16) for every converter. However, for the ease of reading, these expressions are repeated here:

$$r_0 = r_{LF} + r_{CF} \tag{3.8}$$

$$r_1 = r_L + d(r_{CF} + r_S) + (1-d)r_D + r_C R' \tag{3.9}$$

$$R' = \frac{R}{R + r_C} \tag{3.10}$$

Fig. 3.8 contains bode plot showing magnitude and phase of this open-loop transfer function of buck converter with and without input filter. In order to demonstrate the effects of parasitics both ideal and non-ideal cases are superimposed in this figure and are represented by dashed lines and continuous lines respectively. For this simulation, the circuit parameters are chosen to be: $L_F = 1m\text{H}$, $C_F = 2\mu\text{F}$, $L = 0.1m\text{H}$, $C = 1\mu\text{F}$, $R = 30\Omega$, $f_s = 100k\text{Hz}$, $V_{in} = 48\text{V}$ and $D = 0.5$. Moreover, for non-ideal case the values of parasitics chosen are: $r_S = r_D = 50m\Omega$ and $r_{LF} = r_{CF} = r_L = r_C = 0.5\Omega$.

It is obvious that complex poles of the buck converter output filter cause its phase to approach -180° at high frequency. However, Fig. 3.8 shows that after addition of the input filter an additional resonance mode exists at the resonant frequency of the input filter, which introduces an additional -360° phase shift into the phase. While regulating the output voltage with a classical voltage-mode control, the bandwidth is usually lower than the cutoff frequency of the output filter. So, we easily avoid the 180° phase lag introduced by the output filter and the corrector is only a simple PI. However the actual constraint on the regulator design is imposed by the input filter resonance which lies inside or close to the loop bandwidth. If the crossover frequency of regulator feedback loop is near to or greater than the resonant frequency of input filter, then the loop phase margin will become negative and instability will occur (since PID corrector with 360° phase lead is unfeasible). It can also be shown that $G(s)$ now contains an additional complex pole pair and a complex RHP zero pair, associated with the input filter dynamics. That is why input filters are notorious for destabilizing switching regulator systems.

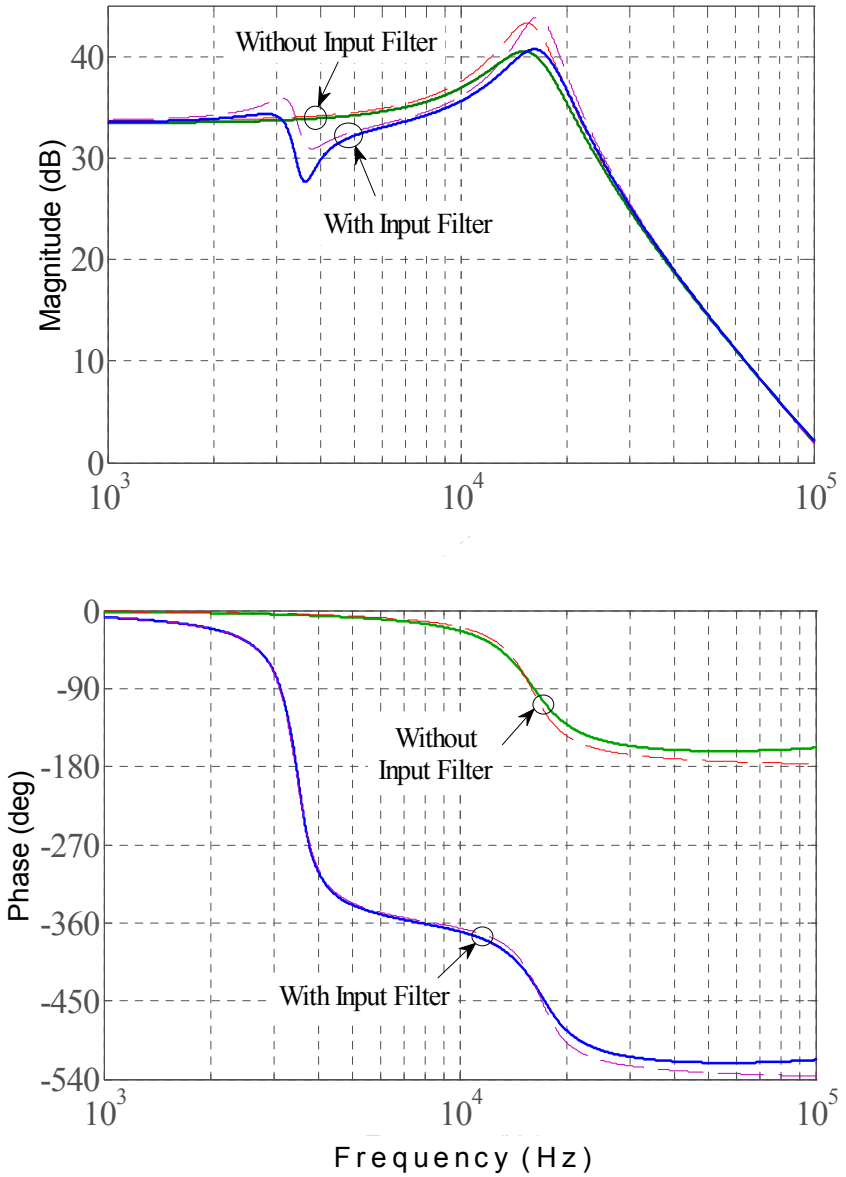

Fig. 3.8. Bode plot of control-to-output transfer function of buck converter with and without input filter; *Dashed Lines*: ideal case; *Continuous Lines:* non-ideal case. (Parameter values: $L_F = 1m\text{H}$, $C_F = 2\mu\text{F}$, $L = 0.1m\text{H}$, $C = 1\mu\text{F}$, $R = 30\Omega$, $f_s = 100k\text{Hz}$, $V_{in} = 48\text{V}$ and $D = 0.5$)

Stability Analysis Using Nyquist Criteria:

Nyquist plots of the open-loop transfer function (3.6) for the non-ideal buck converter without input filter and with an undamped input filter are shown in Fig. 3.9 and Fig. 3.10, respectively. The parameter values for this plot are the same as used in Fig. 3.8. It can be observed that in buck converter without any input filter, the open-loop control-to-output transfer function has no zeros in the right-half *s*-plane. Therefore the system is of minimum phase type. The addition of an L-C filter at converter input introduces two complex conjugate zeros in the right-half plane of that transfer function, which is apparent from two encirclements of the origin in the Nyquist plot of Fig. 3.10, and the instability is evident since the critical point is enclosed by this plot. These zeros represent a poorly damped system and cause instability in the closed loop. However next subsection shows how these zeros of $G(s)$ can be moved to the left-half plane by adding proper damping to the filter circuit, thus avoiding unstable behavior in the closed loop.

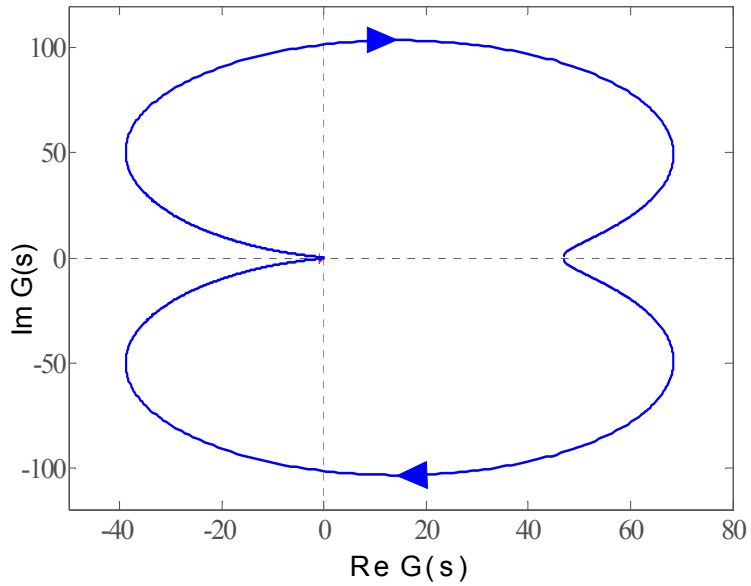

Fig. 3.9. Nyquist plot of $G(s)$ without input filter. (Parameter values: $L = 0.1m\text{H}$, $C = 1\mu\text{F}$, $R = 30\Omega$, $f_s = 100k\text{Hz}$, $V_{in} = 48\text{V}$, $D = 0.5$, $r_{LF} = r_{CF} = r_L = r_C = 0.5\Omega$ and $r_S = r_D = 50m\Omega$)

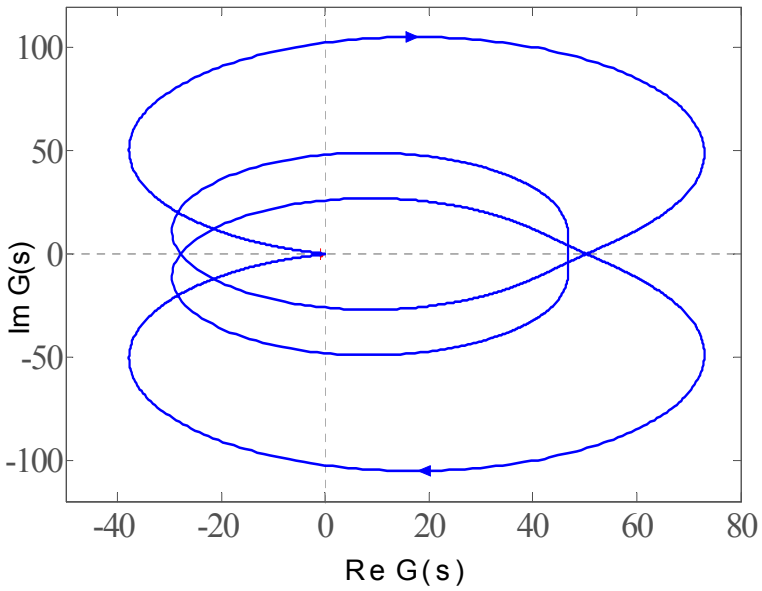

Fig. 3.10. Nyquist plot of $G(s)$ with undamped input filter (only natural parasitics are included). (Parameter values: $L_F = 1m\text{H}$, $C_F = 2\mu\text{F}$, $L = 0.1m\text{H}$, $C = 1\mu\text{F}$, $R = 30\Omega$, $f_s = 100k\text{Hz}$, $V_{in} = 48\text{V}$, $D = 0.5$, $r_{LF} = r_{CF} = r_L = r_C = 0.5\Omega$ and $r_S = r_D = 50m\Omega$)

Influence of Natural Parasitic Losses:

It is evident from Fig. 3.8 that the nominal internal losses of the circuit are not sufficient to damp the input-filter oscillations. However, if the natural losses of the circuit are significantly high then they can play an important role in the damping of input filter. In order to further clarify the influence of natural parasitics on the phase lag of $G(s)$ we have plotted the phase response of this transfer function for varying value of r_{LF} in Fig. 3.11(a), while keeping all other parasitics constant at: $r_S = r_D = 50m\Omega$ and $r_L = r_C = r_{CF} = 0$.

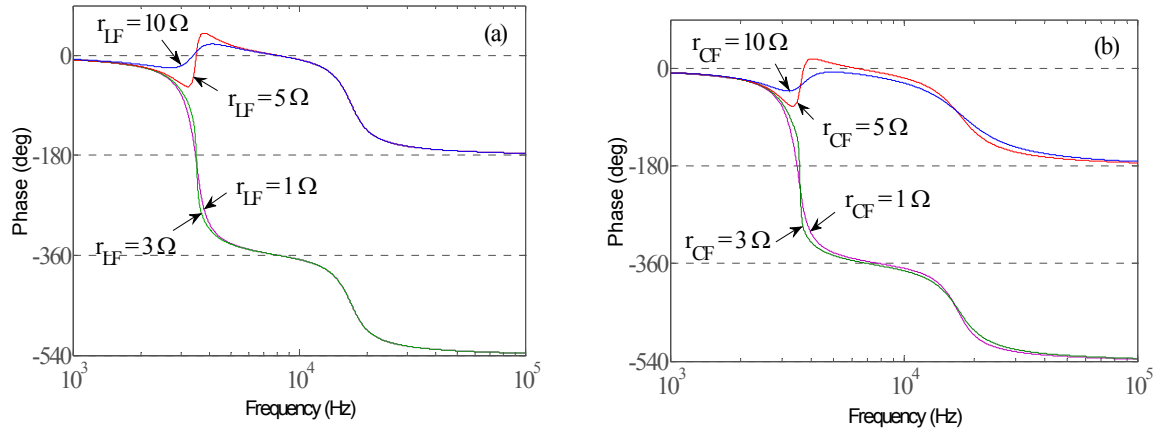

Fig. 3.11. Effect of input filter natural losses on phase lag of $G(s)$; (a): Effect of r_{LF} keeping $r_{CF} = 0$, (b): Effect of r_{CF} keeping $r_{LF} = 0$. (Parameter values: $L_F = 1mH$, $C_F = 2\mu F$, $L = 0.1mH$, $C = 1\mu F$, $R = 30\Omega$, $f_s = 100kHz$, $V_{in} = 48V$, $D = 0.5$, $r_S = r_D = 50m\Omega$ and $r_L = r_C = 0$)

From Fig. 3.11(a), it can be noticed that the phase lag, due to input filter resonance, remains 360° as long as r_{LF} is smaller than a certain minimum value. However, when the value of r_{LF} is increased further, then almost no phase lag occurs at this frequency (actual phase transition in this particular example occurs at $r_{LF} = 3.6\Omega$). Similarly, in Fig. 3.11(b) the phase response is plotted for different values of r_{CF} while keeping other parasitics constant at their previous values, except r_{LF} is now fixed at 0. It can be observed that r_{CF} has more or less the same influence on the response as that of r_{LF} because stabilization is mainly due to the sum of both r_{LF} and r_{CF} [kar03]. So, with a proper choice of the sum of r_{LF} and r_{CF} the bandwidth limitation imposed by the input filter can be overcome. In Fig. 3.12, the phase of the same buck converter is plotted for different values of r_L while keeping all other parasitics constant. This shows that the losses in the output filter components have almost no influence on the first phase rotation. The output-filter parasitics effect the phase only at higher frequencies.

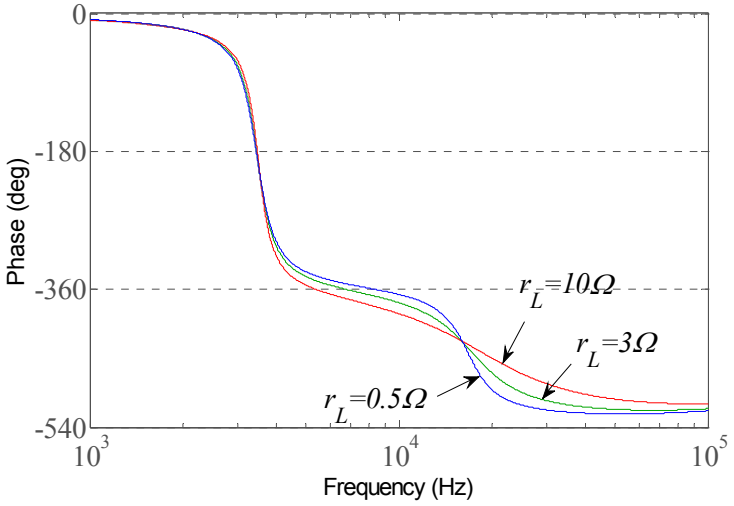

Fig. 3.12. Effect of output filter inductor losses on phase lag of $G(s)$. (Parameter values: $L_F = 1mH$, $C_F = 2\mu F$, $L = 0.1mH$, $C = 1\mu F$, $R = 30\Omega$, $f_s = 100kHz$, $V_{in} = 48V$, $D = 0.5$, $r_S = r_D = 50m\Omega$, $r_{LF} = r_{CF} = 0$ and $r_C = 0.5\Omega$)

As discussed earlier, both of the input-filter parasitics (r_{LF} and r_{CF}) contribute to significant power dissipation due to the dc and/or ac current flowing through these resistances. Therefore, in this thesis we have considered the most practical approach of damping suggested for dc-dc converter applications which consists of R_d-C_d shunt circuit as shown in Fig. 3.4.

Conditions for Stability:

The closed-loop system can be stabilized by adding adequate damping to the input filter. A criterion can then be defined for the design of required damping in such a way so as to bring all right-hand side zeros of the open-loop transfer function to the left-hand side of *s*-plane. However, the design constraints must be derived for the worst case situation, which obviously corresponds to an ideal converter having no internal losses. Such ideal buck converter with a damped input filter using R_d-C_d parallel damping is shown in Fig. 3.13.

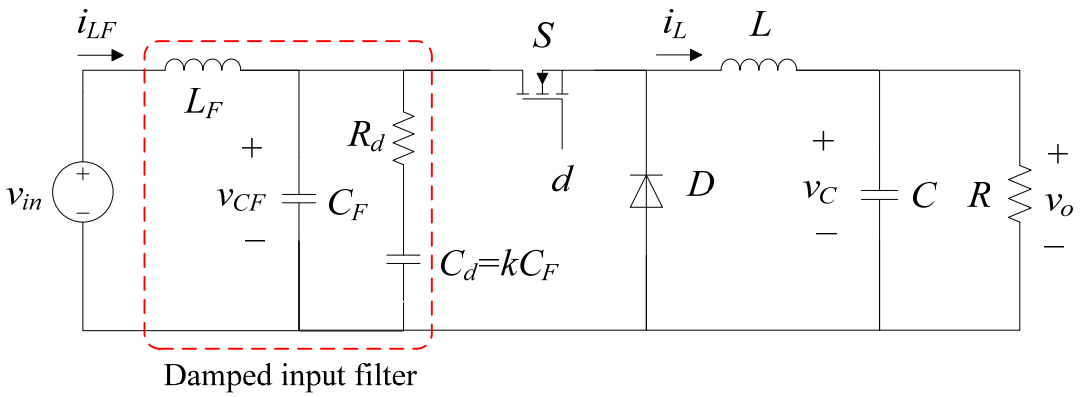

Fig. 3.13. Ideal buck converter with damped input filter using R_d-C_d parallel damping.

We now proceed to design this R_d-C_d parallel damping (see Fig. 3.13) for an ideal converter case (i.e. the worst case). Inclusion of R_d-C_d branch in a lossless filter-converter circuit, however, modifies all the coefficients of its open-loop transfer function, therefore we denote this new transfer function by $G'(s)$ which can be represented in the following form:

$$G'(s) = \frac{\tilde{v}_o}{\tilde{d}} = K' \frac{A'_3 s^3 + A'_2 s^2 + A'_1 s + A'_0}{B'_5 s^5 + B'_4 s^4 + B'_3 s^3 + B'_2 s^2 + B'_1 s + B'_0} \tag{3.11}$$

This transfer function essentially corresponds to a converter in which the damping branch is included, but all natural losses of the circuit elements are ignored (to represent the worst case). Therefore, the coefficients of $G'(s)$ can be obtained directly from those of G(s) shown in (3.7) by first setting all parasitic resistances equal to zero and then replacing sC_F with the following impedance:

$$sC_F \leftarrow \frac{1}{\frac{1}{sC_F} \left\| \left(\frac{1}{skC_F} + R_d \right) \right.} = \frac{s(1+k)C_F + s^2(kC_F^2 R_d)}{1 + s(kC_F R_d)} \tag{3.12}$$

The resulting coefficients A'_k and B'_k of $G'(s)$ can then be expressed as follows:

$$
\begin{aligned}
K' &= V_{in} \\
A_0' &= 1 \\
A_1' &= kC_F R_d - D^2 L_F / R \\
A_2' &= L_F C_F \left(1 + k - kD^2 R_d / R\right) \\
A_3' &= kL_F C_F^2 R_d \\
B_0' &= 1 \\
B_1' &= kC_F R_d + (L + D^2 L_F)/R \\
B_2' &= C\left(L + D^2 L_F\right) + (1+k) L_F C_F + kC_F R_d (L + D^2 L_F)/R \\
B_3' &= L_F C_F L(1+k)/R + kC_F R_d \left(C_F L_F + CL + D^2 L_F C\right) \\
B_4' &= L_F C_F LC(1+k) + kL_F C_F^2 L R_d / R \\
B_5' &= kL_F C_F^2 LCR_d
\end{aligned}
\tag{3.13}
$$

Now using these coefficients, application of the Routh-Hurwitz criterion to the numerator polynomial of the transfer function (3.11) would give us the conditions for which all the zeros of $G'(s)$ are on the left-hand side of s-plane. Application of this criterion results into following two conditions:

$$a_0 + a_1 R_d > 0 \tag{3.14a}$$

$$b_0 + b_1 R_d + b_2 R_d^2 > 0 \tag{3.14b}$$

where

$$
\begin{aligned}
a_0 &= (1+k) L_F C_F \\
a_1 &= -kL_F C_F D^2 / R \\
b_0 &= (1+k) D^2 L_F^2 C_F / R \\
b_1 &= -kL_F C_F \left(\frac{D^4 L_F}{R^2} + kC_F\right) \\
b_2 &= \frac{k^2 D^2 L_F C_F^2}{R}
\end{aligned}
\tag{3.15}
$$

The fulfillment of two inequalities given by (3.14) assures that the signs of real parts of the zeros of $G'(s)$ are now negative. These conditions must be fulfilled if we want to have a bandwidth higher than the input filter cutoff frequency (to avoid the 360° phase lag). It is also noticeable that these conditions depend only on the input filter parameters and are independent of the output filter values. This fact reconfirms the observations made previously in Fig. 3.11 and Fig. 3.12.

In order to find the possible range of R_d and k for which the conditions (3.14) are satisfied, both of these conditions can be plotted on (R_d, k) plane for a given converter. We have plotted these conditions for the same converter parameters as used in the simulation of Fig. 3.8. In this plot, horizontal axis represents the damping resistance which is normalized with respect to the load resistance, and vertical axis represents the capacitor ratio k. Moreover, the plot is shown for three different value of L_F (1mH, 10mH, 20mH).

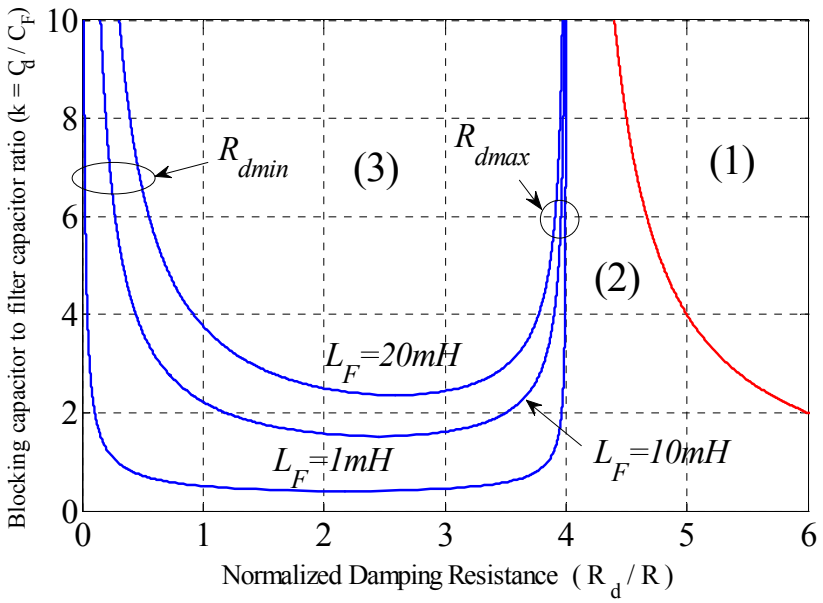

Fig. 3.14. Region of stability for buck converter example; *Dashed Line*: plot of condition (3.14a), *Solid Lines*: plot of condition (3.14b). (Parameter values: $C_F = 2\mu\text{F}$, $L = 0.1m\text{H}$, $C = 1\mu\text{F}$, $R = 30\Omega$, $f_s = 100k\text{Hz}$ and $D = 0.5$)

Plots of Fig. 3.14 are obtained by tracing loci of all the points where one of the conditions (3.14a) and (3.14b) equals to zero[1]. Then three different zones on this (R_d, k) plane can be distinguished. Zone (1) represents the region where none of the two conditions is satisfied. Zone (2) where only condition (3.14a) is satisfied and zone (3) where both conditions are satisfied simultaneously. For all the points contained in this zone, closed-loop stability is assured. Therefore we call this zone as "region of stability". Moreover, the influence of the value of L_F can also be observed from the plots of Fig. 3.14. The smaller the value of L_F, larger is the range of R_d and k which assures stability.

A careful examination of this stability region reveals that condition (3.14b) is a rather sufficient condition for the small-signal stability of buck converter, since fulfilling this condition assures that the first inequality is also satisfied. Moreover, for any given capacitor-ratio k, there exist a minimum limit R_{dmin} as well as a maximum limit R_{dmax} on the permissible value of damping resistance. Furthermore, both of these boundary values can be determined analytically by finding the two roots of the quadratic condition (3.14b). So for any application, the value of damping resistance must be chosen from within this range, but the selected value should be kept sufficiently away from the boundaries of the stable zone. However; choosing an optimum value of R_d is not so evident. It requires some trade-offs depending upon several considerations such as its influence on efficiency as well as its effect on the output impedance characteristics of the filter. Such considerations for the optimization of damping resistance will be discussed later in this and the next chapter.

Fig. 3.15 illustrates how addition of a well-damped input filter modifies magnitude and phase of the control-to-output transfer function. In this example, parallel R_d-C_d damping circuit of Fig. 3.4 is employed with $R_d = 2.5\Omega$ and $C_d = 5C_F$ which is chosen from well within the stability region shown in Fig. 3.14. It can be noted that there is now very little modification of the phase and gain of $G(s)$ due to input filter. Thus we can expect that performance of converter feedback loop will now be unaffected by addition of this input filter.

[1] In other words, by plotting roots of (3.14a) and (3.14b) in k–R_d plane.

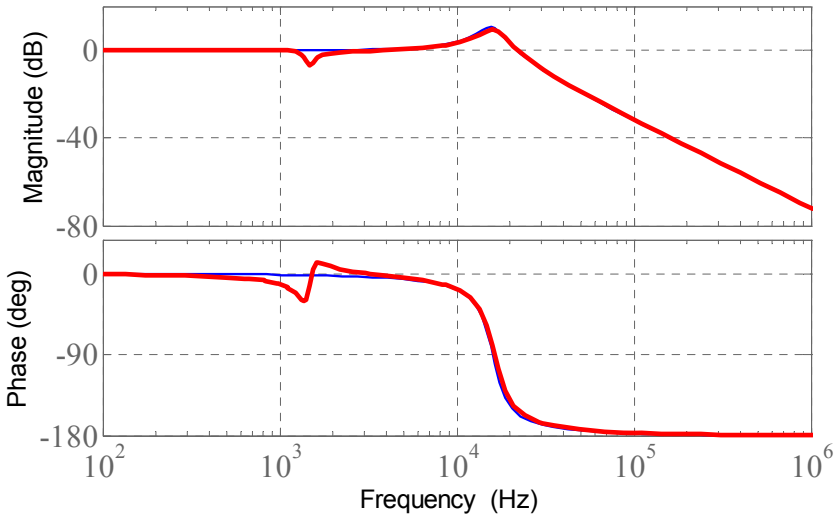

Fig. 3.15. Effect of a well-damped input filter on open-loop transfer function; *Thin lines*: without input filter, *Solid lines*: with R_d-C_d damped input filter (R_d = 2.5Ω and C_d = 5C_F).
(Parameter values: $L_F = 1m\text{H}$, $C_F = 2\mu\text{F}$, $L = 0.1m\text{H}$, $C = 1\mu\text{F}$, $R = 30\Omega$, $f_s = 100k\text{Hz}$ and $D = 0.5$)

3.5.2 Boost Converter with Input Filter

Circuit Diagram:

The circuit diagram of a non-ideal boost converter with input filter is shown below:

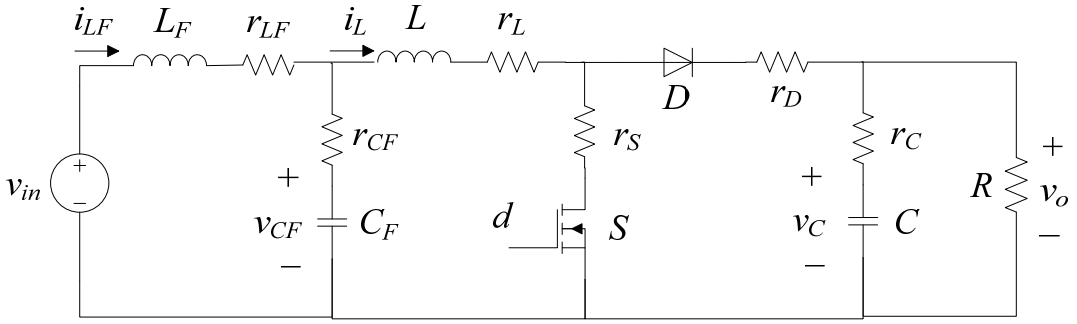

Fig. 3.16. Non-ideal boost converter circuit with input filter.

Effect of Filter Poles on Converter Transfer Function:

Similar to the buck converter case, the open-loop control-to-output transfer function of a non-ideal boost converter with input filter (as shown in Fig. 3.16) can be obtained in the following form:

$$G(s) = \frac{\tilde{v}_o}{\tilde{d}} = K\,\frac{A_4 s^4 + A_3 s^3 + A_2 s^2 + A_1 s + A_0}{B_4 s^4 + B_3 s^3 + B_2 s^2 + B_1 s + B_0} \tag{3.16}$$

Where $K = V_{in}/m$. The coefficients A_k and B_k of this transfer function and the corresponding value of m for a boost converter operating in CCM are obtained as given below:

$$
\begin{aligned}
m &= \left(r_1 + r_{LF} - r_{CF} + (1-D)^2 RR'\right) \big/ RR' \\
A_0 &= r_{CF} - r_{LF} - r_1 + (1-D)^2 RR' \\
A_1 &= r_C C\left(r_{CF} - r_{LF} - r_1 + (1-D)^2 RR'\right) - L - L_F - C_F\left(r_0\left(r_1 - (1-D)^2 RR'\right) - r_{CF}^2\right) \\
A_2 &= -C_F\left(r_0 L + L_F\left(r_1 - (1-D)^2 RR'\right)\right) - r_C C\left(L + L_F + C_F\left(r_0\left(r_1 - (1-D)^2 RR'\right) - r_{CF}^2\right)\right) \\
A_3 &= -C_F\left(L_F L + r_C C\left(r_0 L + L_F\left(r_1 - (1-D)^2 RR'\right)\right)\right) \\
A_4 &= -r_C C_F L_F CLRR' \\
B_0 &= mR' \\
B_1 &= RC(r_{LF} + r_1) + R'\left(L + L_F + C_F\left(r_0\left(r_1 + (1-D)^2 RR'\right) - r_{CF}^2\right)\right) \\
B_2 &= RC\left(L + L_F + r_0 r_1 C_F - r_{CF}^2 C_F\right) + C_F R'\left(r_0 L + L_F\left(r_1 + (1-D)^2 RR'\right)\right) \\
B_3 &= C_F\left(RC(r_0 L + r_1 L_F) + L_F LR'\right) \\
B_4 &= C_F L_F CLR
\end{aligned}
\tag{3.17}
$$

where r_0 and r_1 are the same as defined for a boost converter in Chapter 2 by equation (2.14) and (2.20) respectively. Bode plot of this non-ideal boost converter is now plotted in Fig. 3.17 with and without input filter. For this simulation, the circuit parameters are chosen to be: $L_F = 1m\text{H}$, $C_F = 4.7\mu\text{F}$, $L = 0.1m\text{H}$, $C = 0.1\mu\text{F}$, $R = 100\Omega$, $V_{in} = 24\text{V}$ and $D = 0.5$. Moreover, the nominal values of parasitics are chosen as: $r_{LF} = r_{CF} = r_L = r_C = 0.5\Omega$ and $r_S = r_D = 50m\Omega$.

In boost converter, the open-loop control-to-output transfer function has an RHP zero even in the absence of input filter; therefore the system is of nonminimum phase type. This additional zero is also depicted by the increased numerator degree of $G(s)$ represented by (3.16) as compared to that of buck converter (see equation (3.6)). The phase plot in Fig. 3.17 shows that complex poles of the converter output filter cause its phase to approach -270° at high frequency. Usually, when regulating the output voltage with classical voltage-mode control, the converter feedback loop bandwidth is lower than the cutoff frequency of output filter, so we avoid this phase lag introduced by the output filter and the corrector can be a simple PI. However, an additional -360° of phase shift is introduced into the phase at the resonant frequency of the input filter. This rotation of phase is problematic from controls point of view and can be mitigated by using passive damping and then accomplishing some inequalities as in case of buck converter.

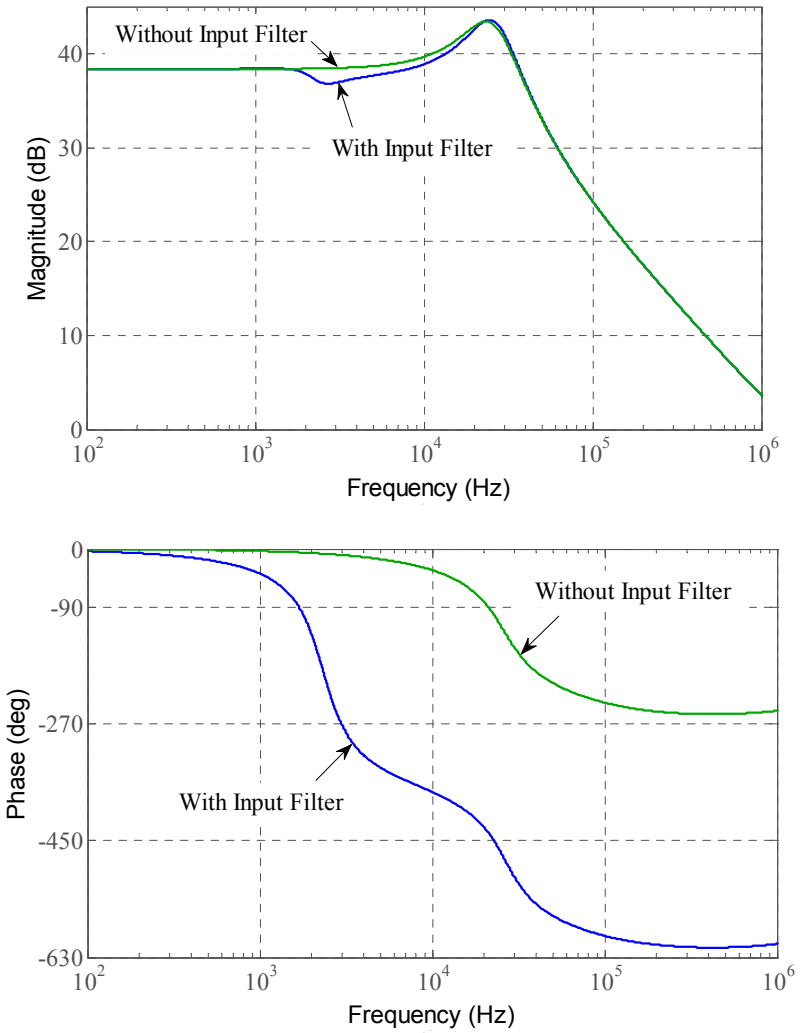

Fig. 3.17. Bode plot of non-ideal boost converter with and without input filter. (Parameter values: $L_F = 1mH$, $C_F = 4.7\mu F$, $L = 0.1mH$, $C = 0.1\mu F$, $R = 100\Omega$, $V_{in} = 24V$, $D = 0.5$, $r_S = r_D = 50m\Omega$ and $r_{LF} = r_{CF} = r_L = r_C = 0.5\Omega$)

Conditions for Stability:

Damping the input filter using the R_d-C_d parallel circuit adds another zero to the open loop transfer function and modifies all of its coefficients given by (3.17). Neglecting all natural circuit parasitics in (3.17) and then substituting (3.12), the resulting modified coefficients A'_k and B'_k of $G'(s)$ for an ideal boost converter are obtained as below:

$$
\begin{aligned}
K' &= V_{in}/(1-D)^2 \\
A_0' &= (1-D)^2 R \\
A_1' &= kC_F R_d R(1-D)^2 - L - L_F \\
A_2' &= L_F C_F R(1-D)^2 + kC_F \left(L_F \left(R(1-D)^2 - R_d \right) - LR_d \right) \\
A_3' &= L_F \left(kC_F \left(C_F R_d R(1-D)^2 - L \right) - LC_F \right) \\
A_4' &= -kC_F^2 L_F L R_d \\
B_0' &= (1-D)^2 R \\
B_1' &= L + L_F + (1-D)^2 kC_F R R_d \\
B_2' &= C_F L_F R(1-D)^2 + RC(L+L_F) + kC_F \left(LR_d + L_F \left(R(1-D)^2 + R_d \right) \right) \\
B_3' &= L_F C_F L + kC_F \left(L_F R R_d \left(C + C_F (1-D)^2 \right) + L(L_F + RCR_d) \right) \\
B_4' &= L_F L \left(C_F RC(1+k) + kC_F^2 R_d \right) \\
B_5' &= kC_F^2 L_F LCRR_d
\end{aligned}
\tag{3.18}
$$

Now using these coefficients, application of Routh-Hurwitz criterion to the numerator polynomial of this transfer function would give us the conditions for a lossless boost converter, which assure that all zeros of $G'(s)$ are on the left-hand side of *s*-plane. This results into following three inequalities:

$$a_0 + a_1 R_d > 0 \tag{3.19a}$$

$$b_0 + b_1 R_d + b_2 R_d^2 > 0 \tag{3.19b}$$

$$c_0 + c_1 R_d + c_2 R_d^2 + c_3 R_d^3 > 0 \tag{3.19c}$$

where

$$
\begin{aligned}
a_0 &= -C_F L_F L(1+k) \\
a_1 &= kC_F^2 L_F R(1-D)^2 \\
b_0 &= -C_F^2 L_F^2 LR(1-D)^2 (1+k)^2 \\
b_1 &= kC_F^2 L_F \left(kL^2 + kL_F L + C_F L_F R^2 (1-D)^4 (1+k) \right) \\
b_2 &= -k^2 C_F^3 L_F^2 R(1-D)^2 \\
c_0 &= C_F^2 L_F^3 LR(1-D)^2 (1+k)^2 \\
c_1 &= -kC_F^2 L_F \left(kL^3 + 2kL^2 L_F + C_F L_F^2 R^2 (1-D)^4 (1+k) + kL_F L \left(L_F + C_F R^2 (1-D)^4 (1+k) \right) \right) \\
c_2 &= k^2 C_F^3 L_F R(1-D)^2 \left(kL^2 + L_F L(1+k) + L_F \left(L_F + kC_F R^2 (1-D)^4 \right) \right) \\
c_3 &= -k^3 C_F^3 L_F^2 R^2 (1-D)^4
\end{aligned}
\tag{3.20}
$$

It can be noticed that contrary to two stability constraints in case of buck converter, the number of conditions to be fulfilled for a boost converter is three (see (3.19)). This is because boost converter is a nonminimum phase type system and it contains an RHP zero even when no filter is present at its input. So, addition of a second order input-filter increases the total number of RHP zeros to three. Now in order to find exact range of R_d and k for which all of

the three conditions are to be satisfied, the conditions (3.19a), (3.19b) and (3.19c) are plotted on a common (R_d, k) plane by fixing R, L, C, D and C_F. Fig. 3.18 shows these plots for three different values of L_F (1mH, 2mH, 3mH). The values of the circuit parameters for this plot are taken the same as used for bode-plot in Fig. 3.17.

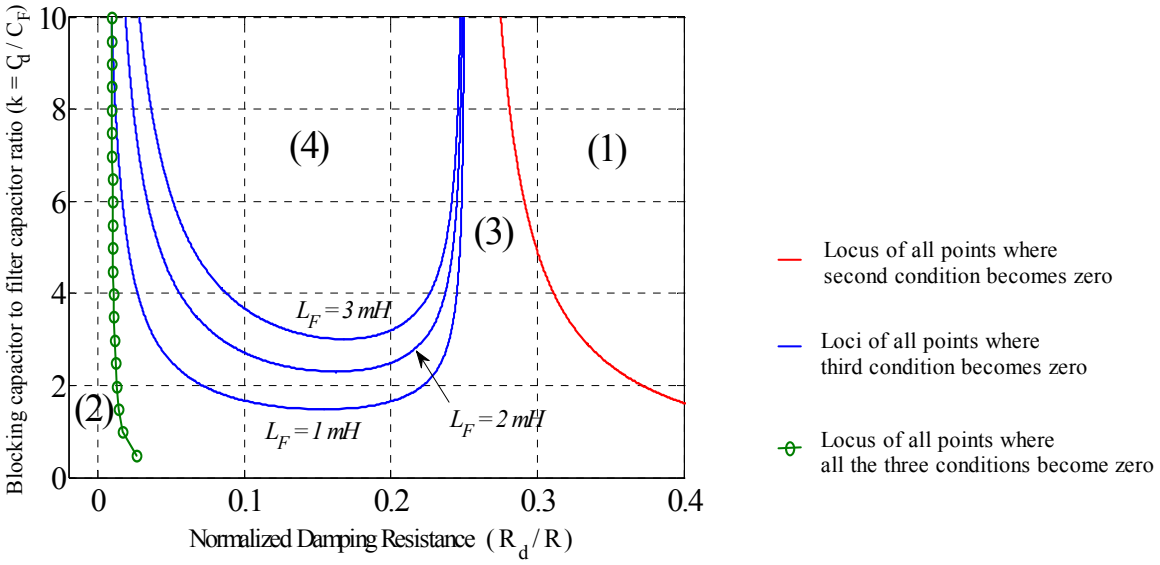

Fig. 3.18. Plot of stability conditions for boost converter. (Parameter values: $C_F = 4.7\mu\text{F}$, $L = 0.1m\text{H}$, $C = 0.1\mu\text{F}$, $R = 100\Omega$, $V_{in} = 24\text{V}$, $D = 0.5$, $r_S = r_D = 50m\Omega$ and $r_{LF} = r_{CF} = r_L = r_C = 0.5\Omega$)

The plots of Fig. 3.18 correspond to the loci of the points where any one or more of the three conditions, given by (3.19), are zero. Thus four distinct zones on this (R_d, k) plane can be distinguished. Zone (1) where only condition (3.19a) is satisfied exclusively. Zone (2) where only condition (3.19c) is satisfied exclusively. Zone (3) where conditions (3.19a) and (3.19b) both are satisfied but (3.19c) gives a negative value and zone (4) where all of the three conditions are positive. Thus, for all the points contained in this zone, the small-signal stability is assured. Moreover, a careful reader would note that condition (3.19c) is a rather sufficient condition for boost converter because it guarantees the fulfillment of other two conditions as well. The influence of the value of L_F on the stable zone can also be observed. The smaller the value of L_F, larger is the range of R_d and k that assures stability. Although this result is consistent with the buck converter case; however, the region of stability is much more sensitive to the value of filter inductor in case of boost converter. Furthermore, it is also evident from Fig. 3.18 that in case of boost converter the region of stability is significantly smaller than that of buck converter.

3.5.3 Buck-Boost Converter with Input Filter

Circuit Diagram:

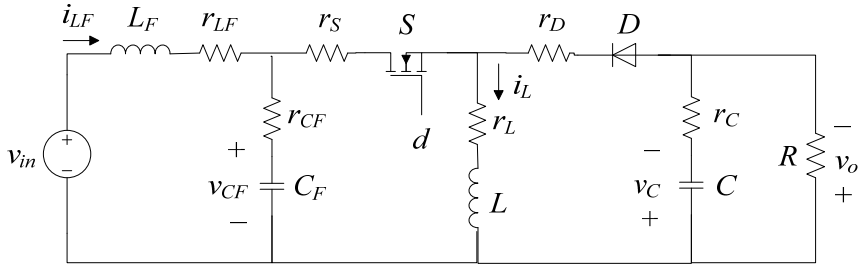

Fig. 3.19. Non-ideal buck-boost converter circuit with input filter.

Effect of Filter Poles on Converter Transfer Function:

Similar to the buck and boost converter cases, the open-loop control-to-output transfer function of a non-ideal buck-boost converter with input filter (as shown in Fig. 3.19) can be obtained from its small-signal linear model in the following form:

$$G(s) = \frac{\tilde{v}_o}{\tilde{d}} = K\,\frac{A_4 s^4 + A_3 s^3 + A_2 s^2 + A_1 s + A_0}{B_4 s^4 + B_3 s^3 + B_2 s^2 + B_1 s + B_0} \tag{3.21}$$

Where $K = V_{in}/m$. The coefficients A_k and B_k of this transfer function and the corresponding value of m for this converter are obtained as below:

$$\begin{aligned}
m &= \left(r_1 + D^2(r_{LF} - r_{CF}) + (1-D)^2 RR'\right)\Big/ RR' \\
A_0 &= (1-2D)r_1 + D^2(r_{CF} - r_{LF}) + (1-D)^2 RR' \\
A_1 &= r_C C\left((1-2D)r_1 + D^2(r_{CF} - r_{LF}) + (1-D)^2 RR'\right) + r_0 C_F(r_1 + RR') \\
&\quad - D\left(L + 2r_0 C_F(r_1 + RR')\right) + D^2\left(C_F(r_{CF}^2 + r_0 RR') - L_F\right) \\
A_2 &= C_F\left(D^2 L_F RR' + L_F(r_1 + RR') - D\left(r_0 L + 2L_F(r_1 + RR')\right)\right) + r_C C\left(r_0 C_F\left(r_1 + RR'\right)\right. \\
&\quad \left. - D\left(L + 2r_0 C_F(r_1 + RR')\right) + D^2\left(C_F(r_{CF}^2 + r_0 RR') - L_F\right)\right) \\
A_3 &= C_F\left(-DL_F L + r_C C\left(D^2 L_F RR' + L_F(r_1 + RR') - D\left(r_0 L + 2L_F(r_1 + RR')\right)\right)\right) \\
A_4 &= -r_C D C_F C L_F L \\
B_0 &= mR' \\
B_1 &= RC\left(r_1 + D^2(r_{LF} - r_{CF})\right) + R'\left(L - 2r_0 DC_F RR' + r_0 C_F\left(r_1 + RR'\right)\right. \\
&\quad \left. + D^2(L_F - r_{CF}^2 C_F + r_0 C_F RR')\right) \\
B_2 &= RC\left(L + r_0 r_1 C_F + D^2(L_F - r_{CF}^2 C_F)\right) + C_F R'\left(r_0 L + L_F\left(r_1 + (1-D)^2 RR'\right)\right) \\
B_3 &= C_F\left(RC(r_0 L + r_1 L_F) + L_F LR'\right) \\
B_4 &= C_F C L_F LR
\end{aligned} \tag{3.22}$$

where r_0 and r_1 for this buck-boost converter are the same as already defined in Chapter 2 by equation (2.14) and (2.24), respectively. Bode plot of this non-ideal buck-boost converter is now plotted in Fig. 3.20 for both cases: with and without input filter. For this simulation, the circuit parameters are chosen to be: $L_F = 1m\text{H}$, $C_F = 4.7\mu\text{F}$, $L = 0.1m\text{H}$, $C = 1\mu\text{F}$, $R = 50\Omega$, $V_{in} = 24\text{V}$ and $D = 0.5$. The nominal values of parasitics chosen are: $r_S = r_D = 50m\Omega$ and $r_{LF} = r_{CF} = r_L = r_C = 0.5\Omega$. Buck-boost converter is also an example of nonminimum phase type system since it contains an RHP zero in its transfer function (even when no input filter is present)

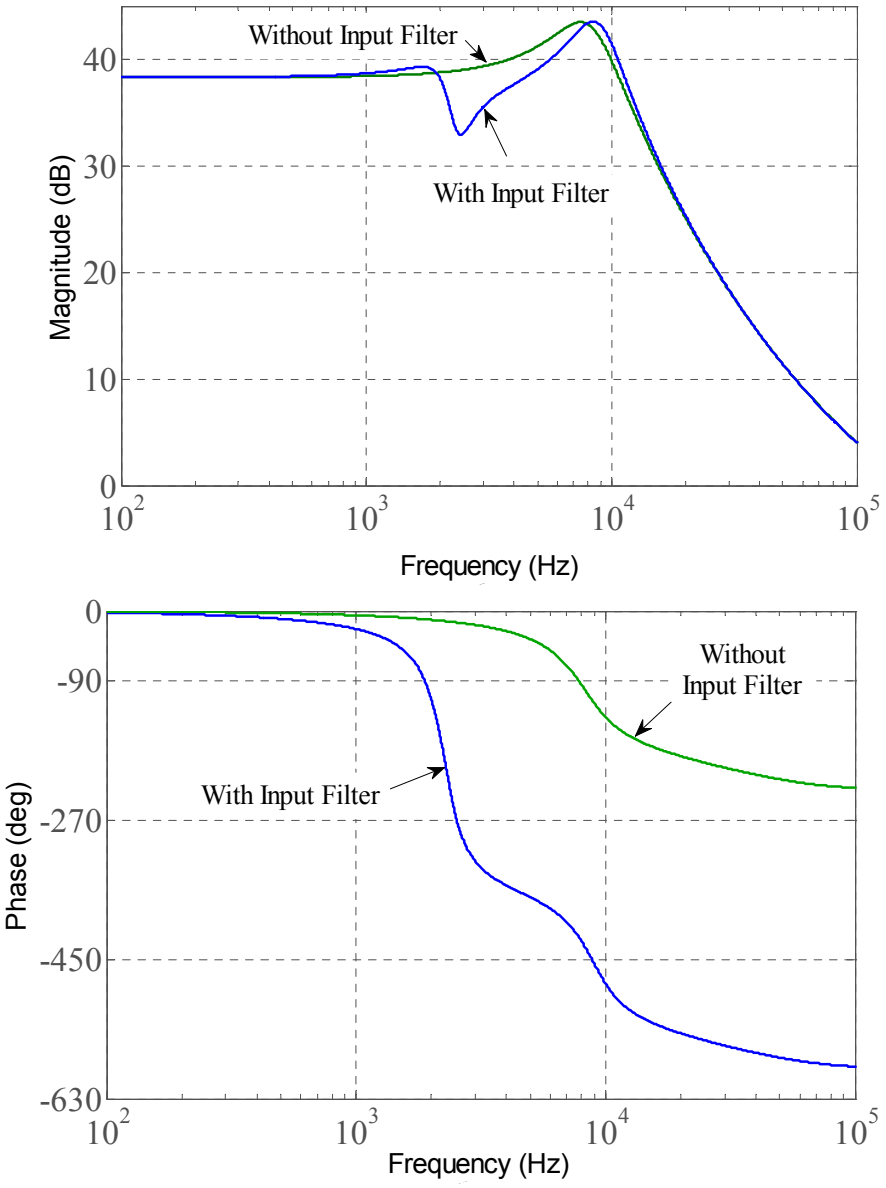

Fig. 3.20. Bode plot of non-ideal buck-boost converter with and without input filter. (Parameter values: $L_F = 1mH$, $C_F = 4.7\mu F$, $L = 0.1mH$, $C = 1\mu F$, $R = 50\Omega$, $V_{in} = 24V$, $D = 0.5$, $r_S = r_D = 50m\Omega$, $r_{LF} = r_{CF} = r_L = r_C = 0.5\Omega$)

.

Conditions for Stability:

In order to derive the stability conditions for the worst case situation of an ideal buck-boost converter, we follow the same steps as described previously for the buck and boost converters. Ignoring all natural parasitics in (3.22) and then substituting (3.12) into (3.22), the new coefficients A'_k and B'_k corresponding to $G'(s)$ for the buck-boost converter are obtained as shown below:

$$
\begin{aligned}
K' &= V_{in}/(1-D)^2 \\
A_0' &= (1-D)^2 R \\
A_1' &= \left(kC_F R_d R + D^2\left(kC_F R_d R - L_F\right) - D\left(L + 2kC_F R_d R\right)\right) \\
A_2' &= C_F L_F R(1-D)^2 + kC_F\left(L_F\left((1-D)^2 R - D^2 R_d\right) - DLR_d\right) \\
A_3' &= C_F L_F\left(kC_F R_d R(1-D)^2 - DL(1+k)\right) \\
A_4' &= -kDC_F^2 L_F L R_d \\
B_0' &= (1-D)^2 R \\
B_1' &= L + kC_F R_d R - 2kDC_F R_d R + D^2(L_F + kC_F R_d R) \\
B_2' &= RC(L + D^2 L_F) + C_F\left(kLR_d + L_F\left((1-D)^2(1+k)R + kD^2 R_d\right)\right) \\
B_3' &= C_F L_F L + kC_F\left(L_F R_d R\left(C_F(1-D)^2 + D^2 C\right) + L(L_F + RCR_d)\right) \\
B_4' &= C_F L_F L\left(RC(1+k) + kC_F R_d\right) \\
B_5' &= kC_F^2 L_F CLRR_d
\end{aligned}
\tag{3.23}
$$

Now applying Routh-Hurwitz criterion to the numerator polynomial of this transfer function would give us the conditions for a buck-boost converter which assure that all the zeros of $G'(s)$ are on the left-hand side of *s*-plane (even if no natural damping is provided by parasitics). Application of this criterion to $G'(s)$, using the coefficient values given by (3.23), results into following three conditions:

$$a_0 + a_1 R_d > 0 \tag{3.24a}$$

$$b_0 + b_1 R_d + b_2 R_d^2 > 0 \tag{3.24b}$$

$$c_0 + c_1 R_d + c_2 R_d^2 + c_3 R_d^3 > 0 \tag{3.24c}$$

where

$$
\begin{aligned}
a_0 &= -DL(1+k)\ ,\ a_1 = kC_F R(1-D)^2\ ,\ b_0 = -(1-D)^2(1+k)^2 DL_F LR \\
b_1 &= k\left((1+k)R^2 C_F L_F\left(1-4D+D^4\right) + D^3 L_F\left(kL - 4C_F R^2(1+k)\right)\right. \\
&\quad \left. + D^2\left(kL^2 + 6C_F L_F(1+k)R^2\right)\right) \\
b_2 &= -D^2(1-D)^2 k^2 C_F L_F R \\
c_0 &= (1-D)^2 D^3 L_F^2 L(1+k)^2 R \\
c_1 &= -kD\left(C_F L_F(1+k)R^2\left(D^5 L_F + kL + D(L_F - 4kL)\right) + 2D^3 L_F\left(kL^2 + 3C_F L_F(1+k)R^2\right.\right. \\
&\quad \left. -2kC_F L(1+k)R^2\right) + D^2\left(kL^3 - 4C_F L_F^2(1+k)R^2 + 6kC_F L_F L(1+k)R^2\right) \\
&\quad \left. + D^4 L_F\left(kL(L_F + C_F(1+k)R^2) - 4C_F L_F(1+k)R^2\right)\right) \\
c_2 &= (1-D)^2 k^2 C_F R\left(kC_F L_F R^2 - 4kDC_F L_F R^2 + kD^2(L^2 + 6C_F L_F R^2)\right. \\
&\quad \left. + D^3 L_F((1+k)L - 4kC_F R^2) + D^4 L_F(L_F + kC_F R^2)\right) \\
c_3 &= -D^2(1-D)^4 k^3 C_F^2 L_F R^2
\end{aligned}
\tag{3.25}
$$

Three conditions (3.24) are required to be fulfilled in case of buck-boost converter to assure its stability in presence of input filter. To find possible range of R_d and k for which all of these three conditions are satisfied, the conditions (3.24a), (3.24b) and (3.24c) are plotted on a (R_d, k) plane by fixing R, L, C, D and C_F. Fig. 3.21 shows these plots for three different values of L_F (1mH, 5mH, 10mH). The values of the circuit parameters for this plot are the same as used for bode-plot in Fig. 3.20.

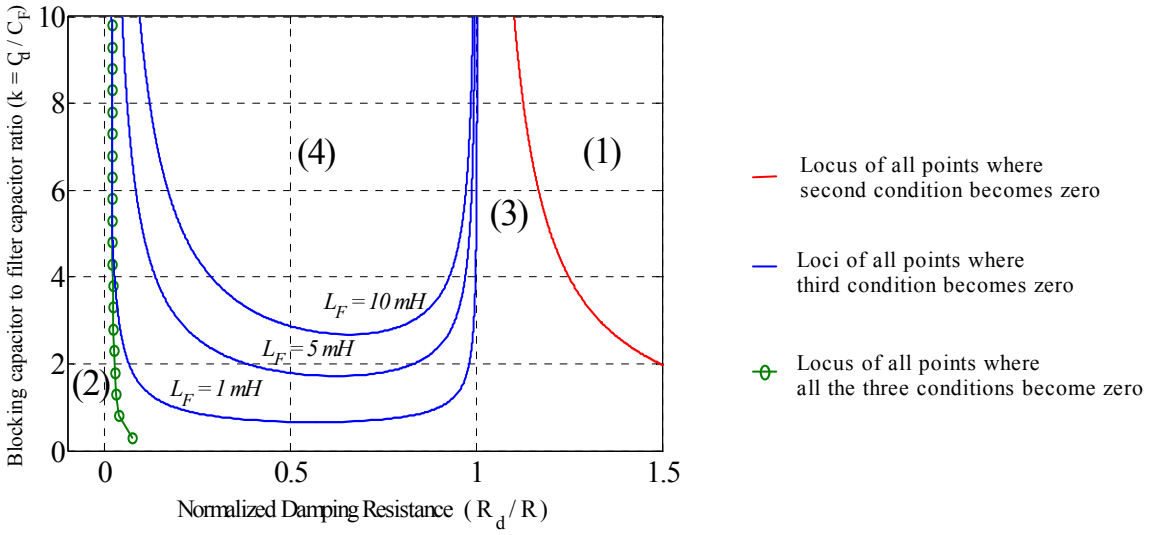

Fig. 3.21. Plot of stability conditions for buck-boost converter. (Parameter values: $C_F = 4.7\mu\text{F}$, $L = 0.1m\text{H}$, $C = 1\mu\text{F}$, $R = 50\Omega$, $V_{in} = 24\text{V}$, $D = 0.5$, $r_S = r_D = 50m\Omega$, $r_{LF} = r_{CF} = r_L = r_C = 0.5\Omega$)

Four distinct zones on this (R_d, k) plane can be distinguished. For instance, zone (1) where only condition (3.24a) is satisfied exclusively. Zone (2) where only condition (3.24c) is satisfied exclusively. Zone (3) where conditions (3.24a) and (3.24b) both are satisfied but (3.24c) gives a negative value and zone (4) where all the three conditions are positive simultaneously. Thus, for all the points contained in this zone, the small-signal stability is assured. It can be noticed that for the stability of buck-boost converter it is sufficient to satisfy condition (3.24c), because the other two conditions will then be satisfied automatically. The influence of the value of L_F can also be observed. The smaller the value of L_F, larger is the range of R_d and k that assures stability. This result is in agreement with our previous remarks for buck and boost converters.

3.5.4 Effect of Load on the Stability Conditions

All of the stability conditions (3.14), (3.19) and (3.24) are functions of the load resistance R. In order to study the influence of load on the region of stability, we have plotted the stability conditions (3.14b) for a buck converter using different values of R, while keeping all other parameters same as used in Fig. 3.8. In Fig. 3.22, a close-up of the obtained stability regions is shown to demonstrate the load effect on the lower boundary of the stable zone. This figure implies that a greater R_{dmin} is required to assure the stability at high load currents (i.e. for smaller values of R in Fig. 3.22). Moreover, for smaller load resistance there is also a slight increase in the minimum required value of capacitor-ratio k that must be employed. So in order to avoid any risk of instability in a given application, such R_d must be chosen which satisfies the stability conditions under full-load condition. Then even if the load current is decreased, the damping resistance would still be sufficient to assure system stability in that case.

As far as loading effect on the upper limit of R_d is concerned, apparently it seems that the value of R_{dmax} decreases with decrease in load resistance; however in relative terms (i.e. R_d/R) it remains essentially the same irrespective of the load (i.e. R_{dmax}/R = 400% for sufficiently large value of k, with every load). These conclusions are also true for boost and buck-boost converters operating in CCM as well as in DCM.

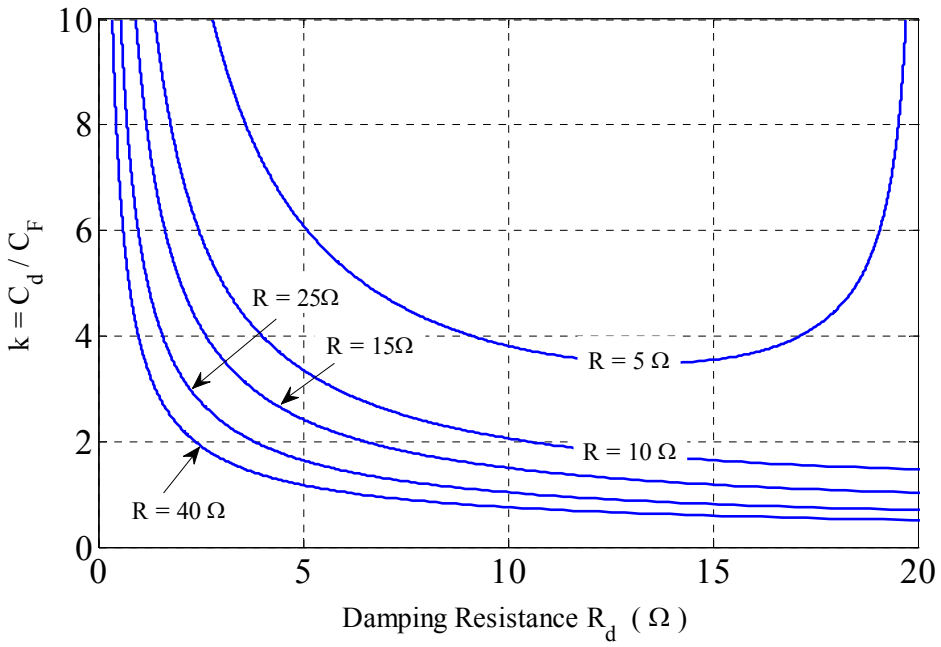

Fig. 3.22. Effect of load resistance on stability conditions for buck converter example. (Parameter values: $L_F = 1mH$, $C_F = 2\mu F$, $L = 0.1mH$, $C = 1\mu F$, $f_s = 100kHz$ and $D = 0.5$)

3.6 INPUT-FILTER INTERACTIONS IN DCM

Following the same procedure as presented above, stability conditions can also be determined for discontinuous conduction mode (DCM) operation. However, in general, the observations and conclusions derived from the analysis of input-filter interactions in CCM can be applied equally to the same converters operating in DCM. State-space averaged models of various orders for DCM have already been discussed in the preceding chapter, and we have selected reduced-order models for the study of input-filter interactions in DCM. However, it is recalled that reduced-order models ignore the fast inductor current dynamics in DCM. Due to this approximation the high frequency poles and the RHP zeros (in case of boost and buck-boost converter) do not appear in the converter transfer functions. Therefore the derived conditions of stability are rather simplified in case of DCM especially in case of boost and buck-boost converters. More interestingly the numerator of the transfer function of all of the three ideal converters is identical when operating in DCM. Thus the stability conditions obtained for DCM operation are also the same for buck, boost and buck-boost converters. These conditions can be expressed in the following generalized form for any of the three converters (buck, boost and buck-boost):

$$a_0 + a_1 R_d > 0 \tag{3.26a}$$

$$b_0 + b_1 R_d + b_2 R_d^2 > 0 \tag{3.26b}$$

where a_k and b_k are given below:

$$
\begin{aligned}
a_0 &= (1+k)L_F C_F \\
a_1 &= -kL_F C_F M^2 / R \\
b_0 &= (1+k)M^2 L_F^2 C_F / R \\
b_1 &= -kL_F C_F \left(M^4 L_F / R^2 + kC_F \right) \\
b_2 &= k^2 M^2 L_F C_F^2 / R
\end{aligned}
\tag{3.27}
$$

It can be noticed that these coefficients (3.27) are exactly the same as those already obtained for a buck converter operating in CCM given by (3.15). The only difference is that instead of steady-state duty-cycle D in (3.15), the steady-state voltage ratio $M = V_{out}/V_{in}$ appears in (3.27) for the DCM case. Hence the stability region will also be the same as plotted previously for buck converter operating in CCM (see Fig. 3.14). As usual, the higher order condition (3.26b) is a more decisive condition in this case because it is necessary and sufficient to fulfill this condition. And if (3.26b) is satisfied, the first inequality (3.26a) is then naturally fulfilled. Moreover the same condition is also applicable to boost and buck-boost converter operating in DCM. This is because the high-frequency RHP zero, which is inherent to these two types of converters, is no more present in their reduced-order averaged models. Therefore, the number of required conditions has also reduced to two for these converters in DCM (contrary to three conditions in case of CCM).

3.7 EXPERIMENTAL VALIDATION OF STABILITY CONDITIONS

In order to validate the theoretical stability conditions derived in this chapter, we developed an experimental prototype of buck converter with input filter operating in CCM. This prototype is used to observe converter behavior and validate stability relations (3.14a) and (3.14b). The converter was designed for voltage-mode control with following circuit parameters: v_{in} = 50V, v_o = 25V (D = 0.5) and f_s = 100kHz. An input filter with L_F = 14.7mH and C_F = 1μF is added. In order to test our stability conditions, a much bigger L_F and much smaller C_F are chosen so that the converter remains unstable unless no external damping is provided. Stability relation (3.14b) gives the minimum required value of R_d = 30.25Ω for k = 4.7. The inductor and capacitor ESR are measured at switching frequency using an impedance analyzer and are found to be 70mΩ and 50mΩ respectively. Moreover C_d is an electrolytic capacitor having ESR ≈ 1Ω. Thus a total of 1.2Ω (approximately) is already provided by the internal parasitics of the filter circuit.

Fig. 3.23 shows capacitor voltage v_{CF} across C_F vs. time. First there is 33Ω inserted as R_d, the voltage is stable and equal to 50V. Then we switch the resistance down to 12Ω. The voltage starts an oscillation at frequency equal to the cutoff frequency of input filter. The oscillation grows up very quickly to almost ±40V (i.e. 10 to 90V) where the converter is almost unable to work. This is of course observable in all stages of converter including the output voltage. To verify condition (3.14b) R_d was reduced in small steps and it was verified that as soon as R_d is reduced below 29Ω (i.e. approx. 30.25-1.2 ≈ 29Ω), the circuit start oscillating.

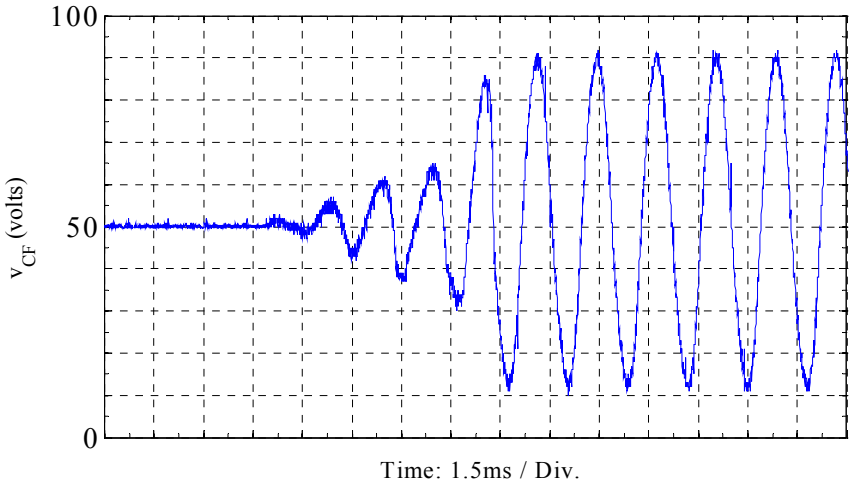

Fig. 3.23. Measured voltage across the filter capacitor C_F, (R_d is switched from 33Ω to 12Ω). (Parameter values: $L_F = 14.7m\text{H}$, $C_F = 1\mu\text{F}$, $L = 1m\text{H}$, $C = 1\mu\text{F}$, $k = 4.7$, $R = 33\Omega$, $f_s = 100k\text{Hz}$, $V_{in} = 50\text{V}$, $V_0 = 25\text{V}$, $D = 0.5$, $r_{LF} \approx 70m\Omega$, $r_{CF} \approx 50m\Omega$ and $ESR_{Cd} \approx 1\Omega$)

3.8 OPTIMUM DAMPING

Considerations for Optimization:

Although the conditions derived above provide us the minimum and maximum limits on the value of the damping resistance R_d for a given value of k but they do not provide any indication of their optimum values. The process of optimization depends on an engineering choice of the desired characteristics of the input filter. However, not all characteristics can be optimized simultaneously with the same set of parameters, hence some trade-offs are required. Several optimization criteria can be worked out depending upon which characteristics are the most crucial for a given application, while compromising on other factors. Some of the important factors which are to be considered for the optimization of input-filter damping are listed below:

- Size, weight and cost are obvious parameters to most designs. Usually, all three of these properties are interrelated. For instance, unless designed properly, a large dc blocking capacitor C_d would increase size, weight as well as cost of the circuit.
- Output impedance peak, as mentioned before, can be critical to the stability of dc-dc converter and it is almost always desirable to have the lowest output impedance of the input filters. Peak output impedance can invariably be reduced using large capacitance values or higher damping coefficients.
- Desired attenuation characteristics at a given frequency are important from two aspects. First the switching (current) noise generated by the converter must be kept off the lines. Second the noise on the lines must be kept away from the converter. Both of these two transfer functions are the same. So, the peak in the gain of this transfer function at the filter resonance frequency is an important parameter to be considered from attenuation point of view. And the choice of external damping parameters (R_d and C_d) should not have a significant effect on the attenuation characteristics of the filter.

- Power dissipation in the damping resistors should also be taken into consideration while designing input filter damping, since it can significantly deteriorate conversion efficiency. Besides, this negative aspect of passive damping has not been given proper attention in the relevant literature. We have dedicated Chapter 4 to the detailed efficiency analysis of such passive damping.

It is shown in [eri99, mid78] that the optimum value of damping resistance R_d is different depending upon which property of the input filter is to be optimized. For example, if the filter is damped to achieve the minimum peak of the transfer function gain, then the output impedance peak is substantially higher. On the other hand, if the input filter is damped to achieve the minimum peak of its output impedance then the transfer function gain will be higher than its minimum. This means that optimum design cannot be achieved simultaneously for all of these properties. If the damping of one property is optimized, then that of the others is not optimized.

However, in practice, minimizing the output impedance peak is probably the most desirable choice, because it alleviates the inequality requirements (3.14), (3.19) and (3.24) for the stability. Nevertheless, in spite of this compromise, the optimum results do allow a smaller value of blocking capacitance C_d to be used, which also save damping circuit from being over-sized and over-weight. Hence optimization in the folowing work refers to a selection of the damping elements (R_d and C_d) such that the peak filter-output impedance is minimized.

Optimum Damping for Minimal Filter-Output Impedance:

In order to find optimum value of damping, the criteria proposed in [mid78] can be used, which implies that the optimum damping corresponds to the parameter values for which the output impedance of the input filter $|Z_{out}|$ is minimized. It proposes a method to find this optimum value of k for a given value of R_d and vice versa. When such a damped filter is subsequently combined with negative dynamic input resistance of the converter, the resultant impact is that of a positive resistance and thus instability is avoided.

At first sight, it appears that a specified damping would be achieved by choosing a suitably low value of R_d. However, this is true only if the blocking capacitance C_d is infinitely large. Fig. 3.24 shows the magnitude plots of the output impedance (3.5) of the input filter for various values of R_d. If R_d is infinite, the maximum of $|Z_{out}|$ is infinite at resonant frequency. When R_d is reduced, $|Z_{out}|_{\max}$ comes down symmetrically with respect to the resonant frequency, but with a finite blocking capacitance further reduction in R_d causes $|Z_{out}|_{\max}$ to move to a lower frequency as shown in Fig. 3.24. In fact at a certain value of R_d, the maximum of $|Z_{out}|$ reaches a minimum and then further reduction in R_d causes $|Z_{out}|_{\max}$ to increase again. Such a behaviour is obvious because at $R_d = \infty$, the filter has zero damping at a resonant frequency of $f_F = 1/2\pi\sqrt{L_F C_F}$. Similarly, when $R_d = 0$, the filter again has zero damping but at a lower frequency $1/2\pi\sqrt{L_F(1+k)C_F} = f_F/\sqrt{1+k}$. The curves in Fig. 3.24 are plotted for $k = 10$. It is apparent, therefore, that there exists an optimum value of R_d for which maximum value of $|Z_{out}|$ is minimal.

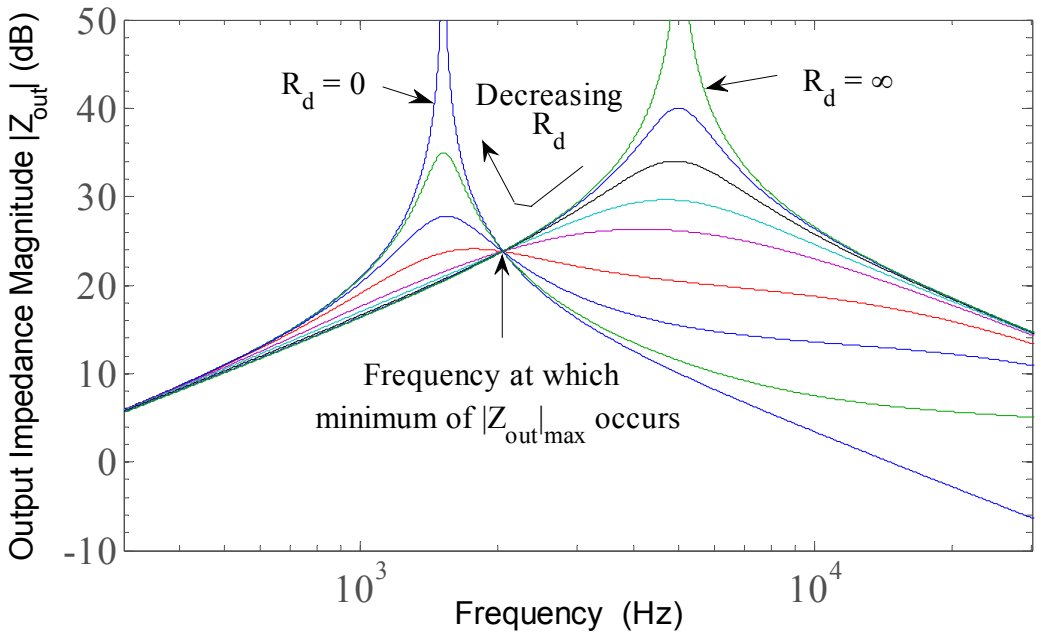

Fig. 3.24. Output impedance magnitude plot of input filter for varying values of damping resistance R_d. (Parameter values: $L_F = 1mH$, $C_F = 1\mu F$, $k = 10$, $R_d \in [0, \infty]\Omega$)

That value of C_d which leads to the minimum peak in $|Z_{out}|$, for a given value of R_d, will be the optimum C_d, and it can be found by first determining the frequency corresponding to this point. The key to a simple solution lies in the recognition that all curves of $|Z_{out}|$, for a given k, go through a common point, and this point must be the minimum of $|Z_{out}|_{\max}$. The frequency, at which this minimum peak occurs, is the frequency at which the magnitude of Z_{out} given by (3.5) is independent of R_d, and can be given by:

$$f_{opt} = f_F \sqrt{\frac{2}{2+k}} \tag{3.28}$$

where f_F is the filter resonant frequency. The value of the peak output impedance for optimum design is then $|Z_{out}|$ evaluated at f_{opt}, which is [mid78]:

$$|Z_{out}|_{\max} = R_0 \frac{\sqrt{2(2+k)}}{k} \tag{3.29}$$

where $R_0 = \sqrt{L_F / C_F}$. The value of damping resistance that leads to the optimum damping is then obtained by differentiating $|Z_{out}|$ with respect to R_d and the result is given by[1] :

$$(R_d)_{Opt} = R_0 \sqrt{\frac{(2+k)(4+3k)}{2k^2(4+k)}} \tag{3.30}$$

Now in order to visualize the location of this optimum damping relative to our stability region determined previously, the plot of (3.30) is superimposed on the stability region of buck converter in Fig. 3.25. It can be observed that this optimum value of R_d lies sufficiently away from the lower boundary of the stable region for all values of k.

[1] The derivation of these analytical results is outlined in [mid78].

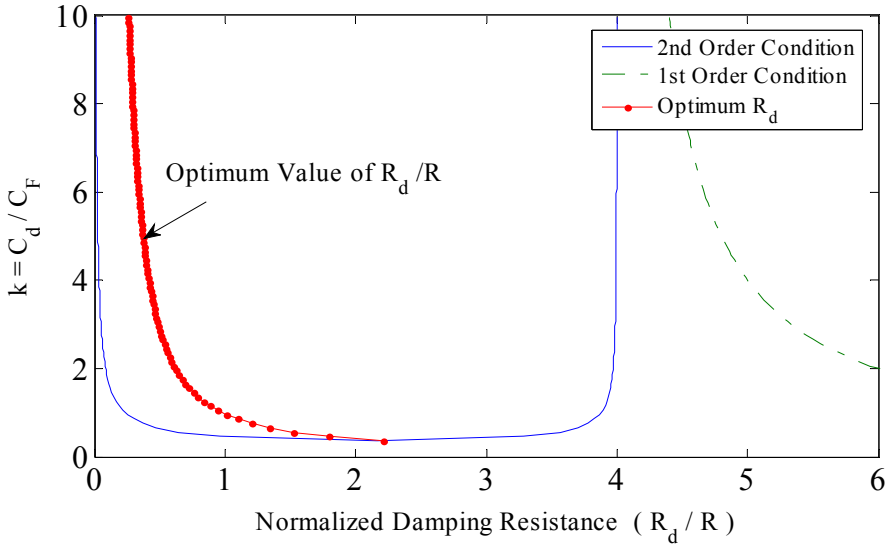

Fig. 3.25. Location of optimum damping resistance in the stable region for buck converter.
(Parameter values: $L_F = 1m\text{H}$, $C_F = 2\mu\text{F}$, $L = 0.1m\text{H}$, $C = 1\mu\text{F}$, $R = 30\Omega$, $f_s = 100k\text{Hz}$ and $D = 0.5$)

3.9 CASE STUDY: INPUT-FILTER INTERACTIONS IN CASCADE BUCK CONVERTERS

3.9.1 Introduction

Many applications of switch-mode dc-dc converters require high conversion ratios (V_{out}/V_{in}). In particular, low voltage and high current applications usually need a converter operating with very high or very low duty cycle. However, this demand can be better fulfilled by using a cascade converter, wherein *n*-stages can be connected in cascade, such that the total conversion ratio is increased by *n*. Higher dc conversion ratios are particularly needed in modern mainframe computers, aeronautics and telecommunication appliances, where the input bus voltage (usually 48V) has to be lowered to very low voltage levels with the help of load converters. One possible solution to fulfill this requirement can be the use of dc-dc converters with transformers (isolated converters). However, the use of transformer results in large switching surges that may damage the switching devices. Moreover, the use of transformer limits the switching frequency of the converter [mid88]. An alternative approach for realizing larger dc conversion ratios is cascading of the converters [mat76]. This scheme mainly uses multistage approach that consists of *n*-basic converters connected in cascade.

As discussed earlier, usually an EMI filter has to be employed at the input of any dc-dc converter to meet EMI/EMC requirements. Instability may also occur in the cascade converters not only due to interactions of input filter with converter [mid76, sad04] but also because of interactions among cascaded converter stages. In order to study stability issues in interconnected subsystems, most of the previously published analysis have been based on the minor-loop gain [cho91, lew89, raj02, sch90], which is defined as the ratio of the output impedance of the supply subsystem (e.g. EMI filter) and the input impedance of the load subsystem (e.g. dc-dc converter). Moreover, extensive research and discussions have been done on filter-converter interactions with pure resistive loads; however, little attention has been paid to the case where the load is active or another similar converter.

In this case-study, we investigate this interaction of input filters in cascaded buck converters. The problem is treated by using a small-signal averaged model of the converter in which natural parasitic resistances of the circuit elements are also taken into account. The open-loop control-to-output transfer function of the complete system is used for the analysis of the input-filter interactions in a buck converter which is loaded with another buck converter. It is shown that the closed-loop stability of such a cascaded system can be assured by damping only the input filter circuit [usm08a], and no damping is usually required to be added to converter output filters. The conditions of stability are derived in this section for a cascade buck converter, through which the lower and upper limits on the required value of this damping can be determined quantitatively. A classical PWM voltage-mode control is considered for this cascade converter with each stage operating at the same frequency and the switches are synchronized. Such a control scheme is also suitable for low voltage and high current applications [vee03].

The rest of the chapter is organized as follows: In the next subsection, first of all a generalized small-signal linear model is presented for *n*-stage cascade buck converter based on the state-space averaged modeling technique [mor02], wherein all natural parasitics of the circuit are included. From this state-space model an open-loop transfer function is then derived. Effect of filter poles on the converter transfer function is analyzed and the conditions of stability are derived in the subsequent subsections. Finally, the experimental results are presented.

3.9.2 Generalized Averaged Model of n-Stage Cascade Buck Converter

A simplified schematic of *n* basic buck converters connected in cascade with an L-C input filter is shown in Fig. 3.26. All converter stages are assumed to be in continuous conduction mode for this study.

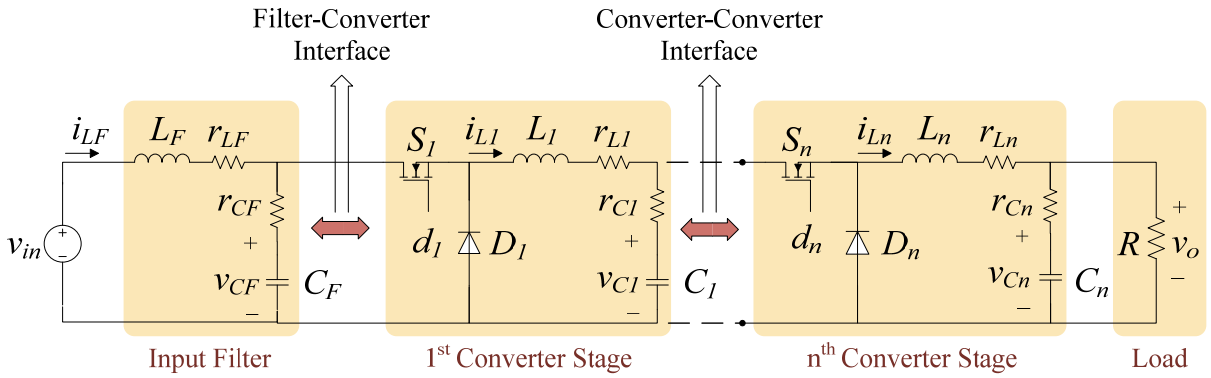

Fig. 3.26. Cascaded *n*-buck converters with input filter.

3.9.2.1 Nonlinear Model

For the *n*-buck cascade converters shown in Fig. 3.26, a continuous-time low-frequency model is obtained by writing state equations for each state and is represented in the following form:

$$\begin{aligned} \dot{x}(t) &= A(d)x(t) + B(d)v_{in}(t) \\ y(t) &= C(d)x(t) + E(d)v_{in}(t) \end{aligned} \tag{3.31}$$

where $x(t) = \begin{bmatrix} i_{LF} & i_{L1} & \cdots & i_{Ln} & v_{CF} & v_{C1} & \cdots & v_{Cn} \end{bmatrix}^T$ is the state vector of length $2(n+1)$, $v_{in}(t)$ is the input voltage, $y(t)$ is the output voltage v_o, and n is the number of stages. $A(d)$ is a

matrix of order 2(n+1)×2(n+1) and $B(d)$ and $C(d)$ are the vectors of length 2(n+1), as given below:

$$A(d)=\begin{bmatrix}
\frac{-r_0}{L_F} & \frac{d_1 r_{CF}}{L_F} & 0 & \cdots & 0 & \frac{-1}{L_F} & 0 & 0 & \cdots & 0 \\
\frac{d_1 r_{CF}}{L_1} & \frac{-r_1}{L_1} & \frac{d_2 r_{C1}}{L_1} & \cdots & 0 & \frac{d_1}{L_1} & \frac{-1}{L_1} & 0 & \cdots & 0 \\
0 & \frac{d_2 r_{C1}}{L_2} & \frac{-r_2}{L_2} & \ddots & 0 & 0 & \frac{d_2}{L_2} & \frac{-1}{L_2} & \cdots & 0 \\
\vdots & \vdots & \ddots & \ddots & \frac{d_n r_{C(n-1)}}{L_{n-1}} & 0 & \vdots & \ddots & \ddots & 0 \\
0 & 0 & 0 & \frac{d_n r_{C(n-1)}}{L_n} & \frac{-r_n}{L_n} & 0 & 0 & 0 & \frac{d_n}{L_n} & \frac{-1}{L_n} \\
\frac{1}{C_{CF}} & \frac{-d_1}{C_{CF}} & 0 & 0 & 0 & 0 & 0 & 0 & 0 & 0 \\
0 & \frac{1}{C_1} & \frac{-d_2}{C_1} & \cdots & 0 & 0 & 0 & 0 & 0 & 0 \\
0 & 0 & \frac{1}{C_2} & \ddots & 0 & 0 & 0 & 0 & 0 & 0 \\
0 & 0 & 0 & \ddots & \frac{-d_n}{C_{n-1}} & 0 & \vdots & \vdots & \vdots & 0 \\
0 & 0 & 0 & 0 & \frac{R'}{C_n} & 0 & 0 & 0 & 0 & \frac{-R'}{RC_n}
\end{bmatrix}$$

$$B(d)=\begin{bmatrix}\frac{1}{L_F} & 0 & 0 & 0 & \cdots & 0\end{bmatrix}^T \qquad (3.32)$$

$$C(d)=\begin{bmatrix}0 & 0 & 0 & 0 & \cdots & 1\end{bmatrix}$$

Where d_k is the duty ratio of the kth stage and $E(d)$ is zero in this case. In the above representation r_k is the equivalent loss resistance of the kth stage which is given as:

$$r_k=\begin{cases} r_{LF}+r_{CF} & \text{for } k=0 \\ r_{Lk}+r_{Ck}+d_k(r_{C(k-1)}+r_{Sk})+(1-d_k)r_{Dk} & \text{for } k=1,2,\cdots,(n-1) \\ r_{Ln}+R'r_{Cn}+d_n(r_{C(n-1)}+r_{Sn})+(1-d_n)r_{Dn} & \text{for } k=n \end{cases} \qquad (3.33)$$

where R' for the cascade converter is modified as:

$$R'=\frac{R}{R+r_{Cn}} \qquad (3.34)$$

Where r_{Sk} and r_{Dk} are the resistances of the switches and diodes respectively, of the kth stage. The above representation is nonlinear as the matrix A depends on the control signals d_k. A nonlinear averaged circuit model can also be obtained from this state-space model as below:

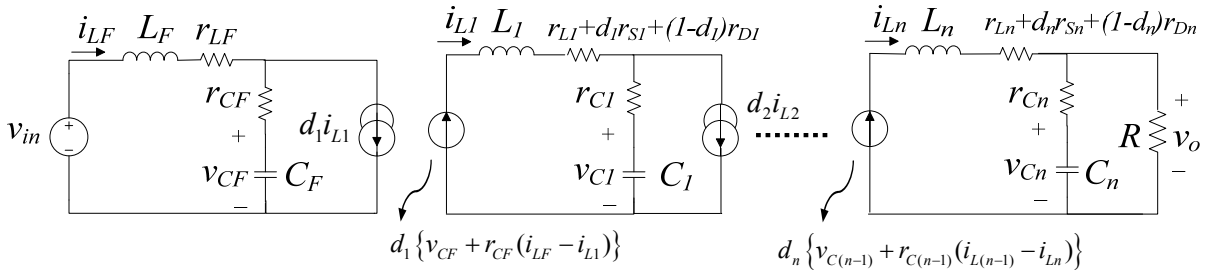

Fig. 3.27. Nonlinear averaged circuit model of *n*-stage cascade buck converter.

3.9.2.2 Linear Model

Linearization of the above nonlinear model is carried out by decomposing all the state variables, input, output and the control signals into two parts. The first part is the nominal value denoted by uppercase letters and the second part is the deviation from the nominal value denoted by an overhead mark "~". Thus $x(t)$, $d_k(t)$, $v_{in}(t)$ and $y(t)$ can be expressed as follows:

$$\begin{aligned} x(t) &= X + \tilde{x}(t) \\ d_k(t) &= D_k + \tilde{u}_k(t) \\ v_{in}(t) &= V_{in} + \tilde{v}_{in}(t) \\ y(t) &= Y + \tilde{y}(t) \end{aligned} \tag{3.35}$$

By substituting (3.35) into expressions (3.31) and assuming that deviations are sufficiently small that the nonlinear and second order terms can be neglected, it results in a small-signal linear model of the following form:

$$\begin{aligned} \dot{\tilde{x}}(t) &= A\tilde{x}(t) + B\tilde{e}(t) \\ \tilde{y}(t) &= C\tilde{x}(t) \end{aligned} \tag{3.36}$$

where $\tilde{e}(t) = \begin{bmatrix} \tilde{v}_{in} & \tilde{d}_1 & \tilde{d}_2 & \cdots & \tilde{d}_n \end{bmatrix}^T$ is a vector of length (n+1) containing input $\tilde{v}_{in}(t)$ and the control signals $\tilde{d}_k(t)$. In this linear model A and B are constant matrices of order $2(n+1)\times 2(n+1)$ and $2(n+1)\times(n+1)$ respectively. The resulting matrices A, B and vector C of this small-signal linear model (3.36) are given below:

$$A=\begin{bmatrix}
\frac{-r_0}{L_F} & \frac{D_1 r_{CF}}{L_F} & 0 & \cdots & 0 & \frac{-1}{L_F} & 0 & 0 & \cdots & 0 \\
\frac{D_1 r_{CF}}{L_1} & \frac{-r_1}{L_1} & \frac{D_2 r_{C1}}{L_1} & \cdots & 0 & \frac{D_1}{L_1} & \frac{-1}{L_1} & 0 & \cdots & 0 \\
0 & \frac{D_2 r_{C1}}{L_2} & \frac{-r_2}{L_2} & \ddots & 0 & 0 & \frac{D_2}{L_2} & \frac{-1}{L_2} & \cdots & 0 \\
\vdots & \vdots & \ddots & \ddots & \frac{D_n r_{C(n-1)}}{L_{n-1}} & 0 & \vdots & \ddots & \ddots & 0 \\
0 & 0 & 0 & \frac{D_n r_{C(n-1)}}{L_n} & \frac{-r_n}{L_n} & 0 & 0 & 0 & \frac{D_n}{L_n} & \frac{-1}{L_n} \\
\frac{1}{C_{CF}} & \frac{-D_1}{C_{CF}} & 0 & 0 & 0 & 0 & 0 & 0 & 0 & 0 \\
0 & \frac{1}{C_1} & \frac{-D_2}{C_1} & \cdots & 0 & 0 & 0 & 0 & 0 & 0 \\
0 & 0 & \frac{1}{C_2} & \ddots & 0 & 0 & 0 & 0 & 0 & 0 \\
0 & 0 & 0 & \ddots & \frac{-D_n}{C_{n-1}} & 0 & \vdots & \vdots & \vdots & 0 \\
0 & 0 & 0 & 0 & \frac{R'}{C_n} & 0 & 0 & 0 & 0 & \frac{-R'}{RC_n}
\end{bmatrix} \tag{3.37}$$

$$B=\begin{bmatrix}
\frac{1}{L_F} & \frac{r_{CF} I_{L1}}{L_F} & 0 & \cdots & 0 \\
0 & \frac{V'_{CF}}{L_1} & \frac{r_{C1} I_{L2}}{L_1} & \cdots & 0 \\
0 & 0 & \frac{V'_{C1}}{L_2} & \ddots & 0 \\
\vdots & \vdots & \vdots & \ddots & \frac{r_{C(n-1)} I_{Ln}}{L_{n-1}} \\
0 & 0 & 0 & 0 & \frac{V'_{C(n-1)}}{L_n} \\
0 & -\frac{I_{L1}}{C_0} & 0 & 0 & 0 \\
0 & 0 & -\frac{I_{L2}}{C_1} & \cdots & 0 \\
0 & 0 & 0 & \ddots & 0 \\
\vdots & \vdots & \vdots & \ddots & -\frac{I_{Ln}}{C_{n-1}} \\
0 & 0 & 0 & 0 & 0
\end{bmatrix}$$

$$C=\begin{bmatrix}0 & 0 & \cdots & 0 & R'r_{Cn} & 0 & 0 & \cdots & 0 & R'\end{bmatrix}$$

where

$$V'_{Ck} = V_{Ck} + r_{Ck}(I_{Lk} - I_{L(k+1)}) - (r_{S(k+1)} - r_{D(k+1)})I_{L(k+1)} \quad \text{for } \forall k \tag{3.38}$$

For the generality of (3.38) and for all following expressions we define $V_{CF} = V_{C0}$ and $I_{LF} = I_{L0}$, and thus k = 0 corresponds to the input filter stage. To further simplify the expressions we assume that:

$$\left| r_{S(k+1)} - r_{D(k+1)} \right| / R << 1 \tag{3.39}$$

Then (3.38) becomes:

$$V'_{Ck} \cong V_{Ck} + r_{Ck}(I_{Lk} - I_{L(k+1)}) \tag{3.40}$$

The following relations exist between the steady-state values I_{Lk}, V_{Ck}, V_o and the input voltage V_{in}:

$$I_{Lk} = \begin{cases} \prod_{i=k+1}^{n} D_i \cdot V_o / R & \text{for } k = 0,1,2,\cdots,(n-1) \\ V_o / R & \text{for } k = n \end{cases} \tag{3.41}$$

$$V_{Ck} = \begin{cases} E - r_0 I_{L0} + D_1 r_{CF} I_{L1} & \text{for } k = 0 \\ D_k[V_{C(k-1)} + r_{C(k-1)} I_{L(k-1)}] - r_k I_{Lk} + D_{k+1} r_{Ck} I_{L(k+1)} & \text{for } k = 1,2,\cdots,(n-1) \\ D_n[V_{C(n-1)} + r_{C(n-1)} I_{L(n-1)}] / (1 + \frac{r_n}{R}) & \text{for } k = n \end{cases} \tag{3.42}$$

From (3.41) and (3.42), the steady state output voltage can be expressed as:

$$V_o = \frac{D_n V_{C(n-1)}}{1 + r_n / R} \tag{3.43}$$

If the deviations in the input voltage are not desired (i.e. $\tilde{v}_{in}(t) = 0$), the corresponding column in B is eliminated. Moreover, when the same switching signal $d(t)$ is used for each stage then $\tilde{e}(t) = \tilde{d}(t)$ and the matrix B is further reduced to a column vector.

3.9.2.3 Open Loop Transfer Function:

In order to facilitate analytical evaluation of the effect of input filter on the cascade converter operation, we have confined our study to two converter stages (i.e. n = 2). Moreover, both stages are controlled with the same duty cycle $d(t)$. A 2-stage cascade buck converter with input filter is shown in Fig. 3.28:

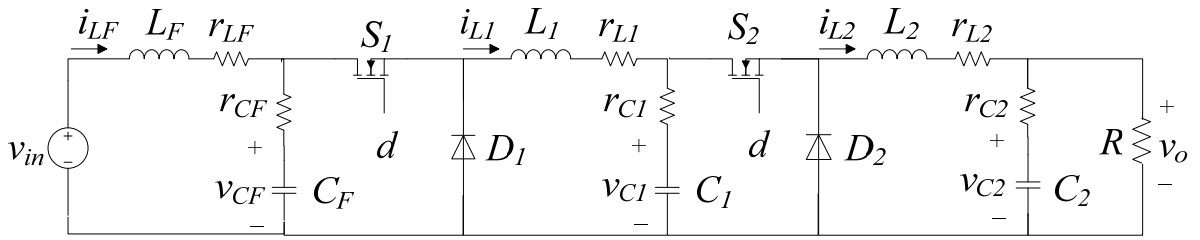

Fig. 3.28. A 2-stage cascade buck converter with input filter.

By taking the Laplace transform of (3.36) and using the same nominal control signal D for both stages, the open-loop control-to-output transfer function can be obtained from the above small-signal model as shown below:

$$G(s) = \frac{\tilde{v}_o}{\tilde{d}} = K \frac{A_5 s^5 + A_4 s^4 + A_3 s^3 + A_2 s^2 + A_1 s + A_0}{B_6 s^6 + B_5 s^5 + B_4 s^4 + B_3 s^3 + B_2 s^2 + B_1 s + B_0} \quad (3.44)$$

where $K=V_{in}/m$, and m is defined as below:

$$m = \left\{ r_2 + R'R + D^4 (r_{LF} - r_{CF}) + D^2 (r_1 - 2r_{C1}) \right\} \Big/ \left(R + r_{C2} \right) \quad (3.45)$$

The coefficients A_k and B_k of this $G(s)$ are functions of the circuit parameters, and depend on the converter family and conduction mode. For 2-stage buck converter with both stages operating in CCM, these coefficients are listed in Appendix-A.

3.9.3 Stability Analysis of Cascade Buck Converter

3.9.3.1 Effect of Filter Poles on Converter Transfer Function

Fig. 3.29 contains the bode plot showing the magnitude and phase of open-loop transfer function (3.44) for 2-stage buck converter with and without input filter. The circuit parameters used for this simulation are: $C_F = C_1 = C_2 = 1\mu$F, $L_F = 10m$H, $L_1 = 1m$H, $L_2 = 0.1m$H, $R = 33\Omega$, $D = 0.5$, $r_{LF} = 0.5\Omega$, $r_{CF} = 60m\Omega$, and $r_1 = r_2 = 0.65\Omega$.

Dashed lines in Fig. 3.29 are showing the magnitude and phase plots of $G(s)$ for the cascade buck converter when no filter is present at its input. It can be observed that converter stage-1 and stage-2 dynamics cause a phase shift of -360° and -180° respectively, at their respective resonant frequencies, thus causing its cumulative phase to approach -540° at higher frequencies. Thus a right-hand side zero pair which appeared due to cascading of the converters can cause instability if the loop bandwidth is near to or greater than either of the cutoff frequencies f_1 or f_2, even when no input filter is present.

Nevertheless, when an L-C filter is added at its input, it causes an additional phase shift of -360° at the resonant frequency f_F of this filter, as shown by the continuous line plot in Fig. 3.29. If the crossover frequency of the regulator feedback loop is near to or greater than this resonant frequency of the input filter (which is usually the case in practice), then the loop phase margin will become negative and can cause instability. It can be shown that addition of a second order input filter has introduced an additional complex pole pair and a complex right-half plane zero pair to $G(s)$. These right-hand side zeros are the cause of instability in the closed loop and thus can cause oscillations in the dc circuit. It is also evident from Fig. 3.29 that the nominal internal losses of the circuit are not sufficient to damp these oscillations. Hence we need to add some damping in addition to the natural internal losses. Next section shows how these right-hand side zeros of $G(s)$ can be moved to the left-half s-plane by adding proper damping to the filter circuit, thus avoiding the unstable behavior in the closed loop.

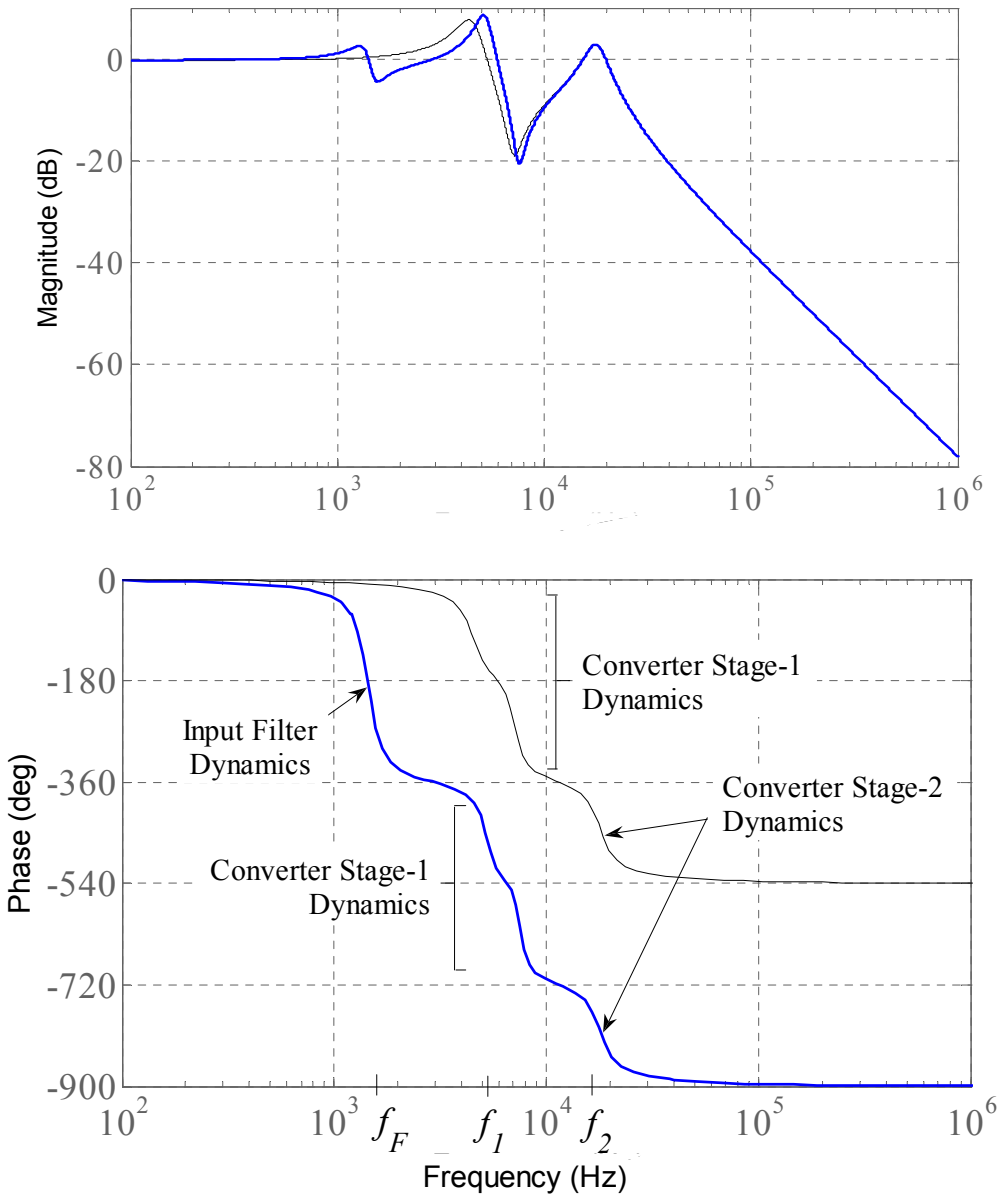

Fig. 3.29. Bode plot of open loop control-to-output transfer function of cascade buck converter, *Thin Lines:* without input filter; *Solid Lines:* with input filter. (Parameter values: $C_F = C_1 = C_2 = 1\mu$F, $L_F = 10m$H, $L_1 = 1m$H, $L_2 = 0.1m$H, $R = 33\Omega$, $D = 0.5$, $r_{LF} = 0.5\Omega$, $r_{CF} = 60m\Omega$ and $r_1 = r_2 = 0.65\Omega$)

3.9.3.2 Conditions for Stability

Following the same steps as presented earlier for single stage converters, in this section we formulate a similar design procedure for the cascade buck converter to dimension the R_d-C_d damping circuit shown in Fig. 3.4. For this purpose we first ignore all natural losses in (3.44), so that the resulting design equations would give us the minimum value of damping resistance required for the worst case (i.e. lossless converter). Then we add R_d-C_d damping branch to the circuit shown in Fig. 3.28, wherein the number of stages are still limited to two. The transfer function (3.44) is then modified to include the effect of an additional pole and zero due to R_d-C_d branch. As usual, this modified transfer function can be obtained by substituting (3.12) into (3.44), and the new transfer function is then denoted by $G'(s)$. The corresponding coefficients A'_k of its numerator polynomial are shown below:

$$
\begin{aligned}
A_0' &= A_0 \\
A_1' &= A_1 + 2kC_F R_d \\
A_2' &= A_2 + kDC_F \left\{ D^2 R_d (D^2 - L_1)/R + 2L_F \right\} \\
A_3' &= A_3 + kDC_F \left\{ (C_1 L_1 + 2C_F L_F) R_d - D^2 L_F (L_1/R - C_1 R_d) \right\} \\
A_4' &= A_4 + kDC_F L_F L_1 (C_1 - D^2 C_F R_d / R) \\
A_5' &= kDC_F^2 L_F C_1 L_1 R_d
\end{aligned}
\tag{3.46}
$$

where A_k is the numerator coefficients of $G(s)$ given by (3.44) with all parasitics put equal to zero. Now, by using coefficients (3.46) the application of Routh-Hurwitz criterion to the numerator polynomial of $G'(s)$ the conditions are derived for which its roots (i.e. zeros of $G'(s)$) will move to the left-hand side of the s-plane. As a result we get the following four inequalities:

$$a_0 + a_1 R_d > 0 \tag{3.47a}$$

$$b_0 + b_1 R_d + b_2 R_d^2 > 0 \tag{3.47b}$$

$$c_0 + c_1 R_d + c_2 R_d^2 + c_3 R_d^3 > 0 \tag{3.47c}$$

$$d_0 + d_1 R_d + d_2 R_d^2 + d_3 R_d^3 + d_4 R_d^4 + d_5 R_d^5 > 0 \tag{3.47d}$$

where a_k, b_k, c_k and d_k are all constants which can be expressed in terms of circuit parameters (L_k, C_k, D, R and k), and are listed in Appendix-A.

By fulfilling the four conditions given by (3.47) it is assured that the signs of the real parts of the zeros of $G'(s)$ will be now negative. Thus these inequalities can lead us to the determination of a boundary between stable and unstable operation of the converter. In order to find the possible range of R_d and k for which all of these inequalities hold true, these conditions are plotted on the (R_d, k) plane by fixing all other parameters (Fig. 3.30). Then for each plot two or more regions on this plane can be distinguished where the corresponding condition is either true or false. Finally the intersection of all the "true" regions is the region where all of the four conditions can be met simultaneously thus ensuring all the zeros of open loop transfer function to lie on the left-hand side of s-plane. This common region is the region of stable operation which is shown by the solid line in Fig. 3.30. The small signal stability is assured for all the points contained in this region. However in order to avoid only the -360° phase shift which is caused by the input filter, an other relatively larger region can be identified on this plane for which only those zeros are moved to the left-hand side which are associated to the input filter dynamics. The boundary of this larger zone is shown by the thin line in Fig. 3.30. For the sake of simplicity, only the stability boundaries are shown in this figure, while all other irrelevant plots of stability conditions (3.47) are eliminated from this figure. The parameter values used for this plot are: $C_1 = C_2 = 1\mu$F, $C_F = 0.47\mu$F, $L_F = 4m$H, $L_1 = L_2 = 0.8m$H, $R = 33\Omega$ and $D = 0.5$.

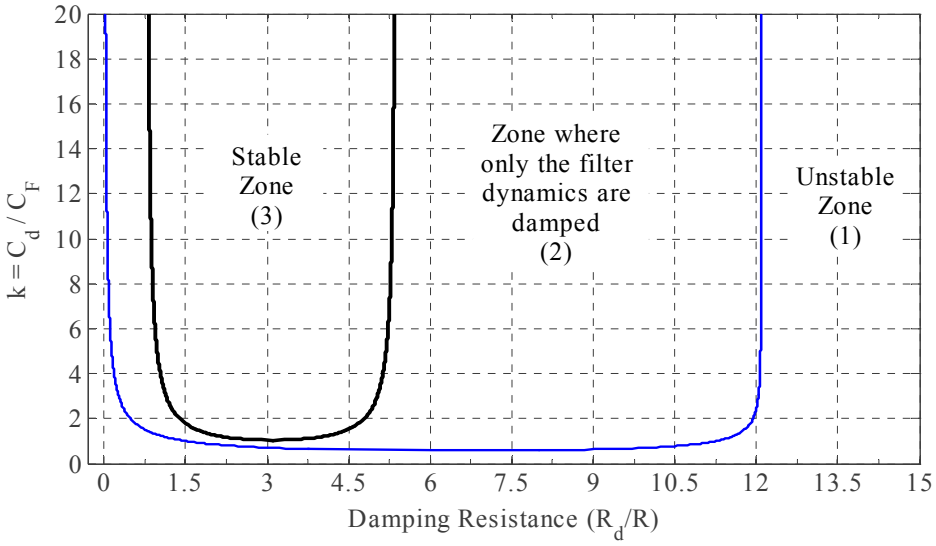

Fig. 3.30. Region of stability for cascade buck converter example; *Solid line*: boundary of the stable zone; *Thin line*: boundary of the zone where only the filter dynamics are damped. (Parameter values: $C_1 = C_2 = 1\mu$F, $C_F = 0.47\mu$F, $L_F = 4$mH, $L_1 = L_2 = 0.8$mH, $f_s = 100$kHz, $R = 33\Omega$ and $D = 0.5$)

Note that the internal losses are ignored in the derivation of stability conditions (3.47), so the stability region shown in Fig. 3.30 gives the lower and upper limits on the total value of the damping resistance that must be added in an ideal converter to assure close-loop stability. However in practice at least some part of the required damping resistance will be contributed by the natural internal losses of the circuit. These internal losses will be taken into account while the experimental verification. Bode plot of a cascade buck converter with a well damped input filter is simulated in Fig. 3.31, using the same circuit parameters as in Fig. 3.30 and damping parameters chosen from within the stable zone of Fig. 3.30 (k=10 and R_d=35Ω).

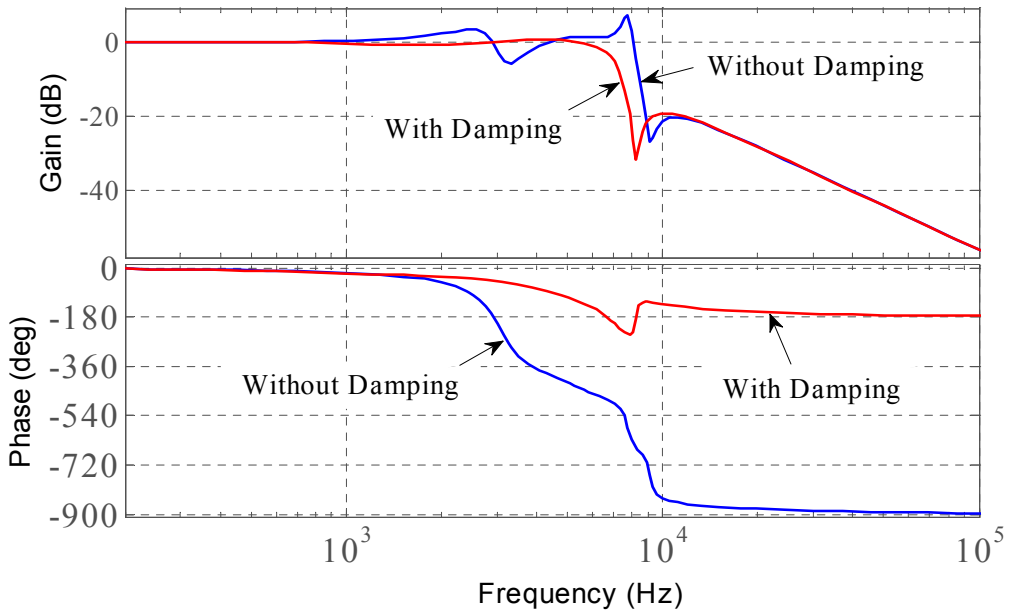

Fig. 3.31. Effect of a well-damped input filter on the bode plot of cascade buck converters. (Parameter values: $C_1 = C_2 = 1\mu$F, $C_F = 0.47\mu$F, $L_F = 4m$H, $L_1 = L_2 = 0.8m$H, $f_s = 100$kHz, $R = 33\Omega$, $D = 0.5$, $k = 10$ and $R_d = 35\Omega$)

It can be observed from Fig. 3.31 that a well-damped input filter has not only removed the -360° phase shift due to filter dynamics but it has also alleviated the interactions due to converter-converter interface. Thus it seems that the input-filter damping alone is sufficient in this case to eliminate the interaction between the two converter stages as well[1]. However, this result is somewhat misleading and cannot be generalized to all the cases because stability conditions (3.47) are functions of the converter parameters. Hence in a given application this objective may or may not be achievable by damping only the filter circuit because region of stability varies with the converter parameters. So, it is fairly possible that in some particular case (i.e. for a given set of converter parameters) such a stable zone does not exist or it requires exceptionally large values of R_d or k to be used in the filter circuit. In that case, to avoid over sizing of the input-filter damping, some resistance can be added to the output filter of the first stage, and its exact value can be determined by following the same procedure as described in this chapter. However, the oscillations due to the filter-converter interface can still be damped by adding resistance to the input filter circuit.

3.9.3.3 Experimental Validation

An experimental prototype of 2-stage cascade buck converter with an input filter as shown in Fig. 3.32 was developed in order to validate stability conditions (3.47). An image of this prototype is shown in Fig. 3.33. The converter was designed for v_{in} = 48V, v_o = 12V (d_1=d_2=0.5) and f_s = 112kHz, and it contained nominal circuit parasitics (see Fig. 3.32). The rest of the circuit parameters are the same as used for simulation in Fig. 3.29. For these parameter values and k = 10 the design equations (3.47) give the minimum damping resistance R_d = 28.7Ω that must be added in a lossless converter (this value of R_d can also be found directly from Fig. 3.30 for k = 10). However in our test circuit, approximately measured[2] parasitic resistances were r_{LF} = 0.75Ω, r_{CF} = 0.05Ω and C_d = 4.7μF with ESR = 2.25Ω. Thus a total of 3.05Ω is naturally contributed to R_d by the parasitic resistances of our test circuit; hence only 25.6Ω (i.e. approx. 28.7-3.05) is actually required to be inserted externally.

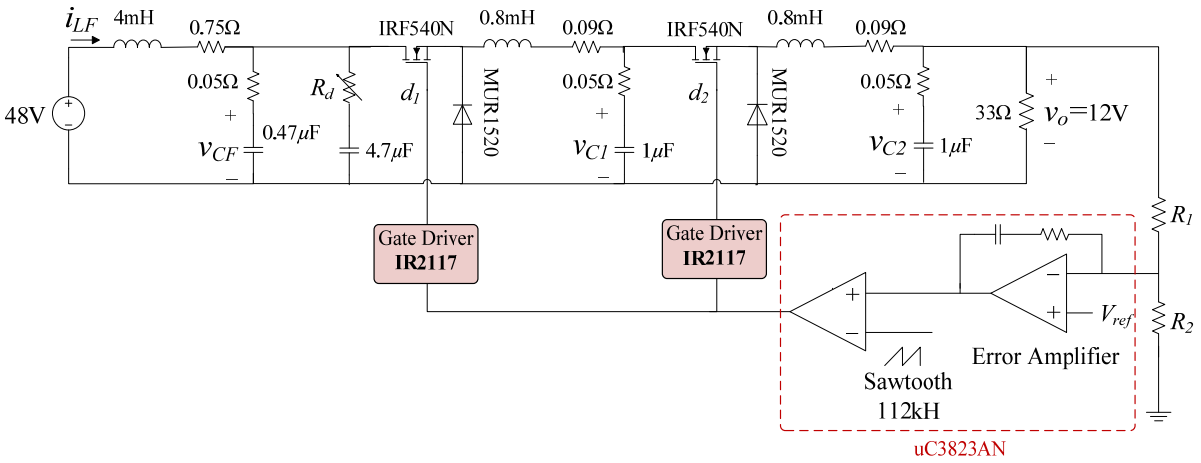

Fig. 3.32. Cascade converter schematic used for experimental measurements.

[1] This observation is in agreement with the conclusions of [min08], which states that the presence of a well-damped input-filter can sometimes increase the stability region of a stand-alone buck converter.
[2] These parasitics were measured at switching frequency using an impedance analyzer

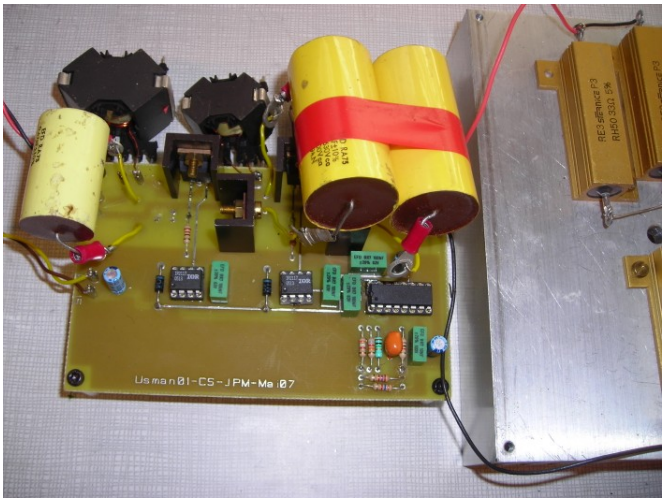

Fig. 3.33. Image of the cascade converter prototype used for experimental measurements.

Two capacitor voltages v_{CF} and v_{C1} are measured for different values of externally added R_d (Fig. 3.34). First there is only 2Ω inserted in the circuit and it is observed that the circuit is unstable because v_{CF} and v_{C1} are oscillating at the frequencies equal to the resonant frequencies of the input filter and the first converter stage, respectively. This oscillation is observable in all converter stages including the output stage. Moreover we can even hear a significant audible noise because these frequencies lie in the audible frequency range. Next we increased the resistance to 25.6Ω and beyond in small increments. However, we note that as soon as 25.5Ω is inserted in the circuit, both measured voltages become stable and equal to 48V and 24V respectively, eliminating the audible noise as well. Fig. 3.34(a) and (b) show the transition of voltages v_{CF} and v_{C1} respectively, when the resistance is switched from 2Ω to 25.5Ω. It can be noticed that there is a small difference between theoretically calculated value of required resistance and the actual value of R_d that practically stabilizes the system. This is because theoretical value is calculated for the worst case (i.e. ideal lossless converter); therefore it would always result in a value slightly greater than the actual required value of R_d in the real circuits. Other reasons for this small difference can be the measurement error, component tolerances or the wiring and connection losses which are not easy to take into account.

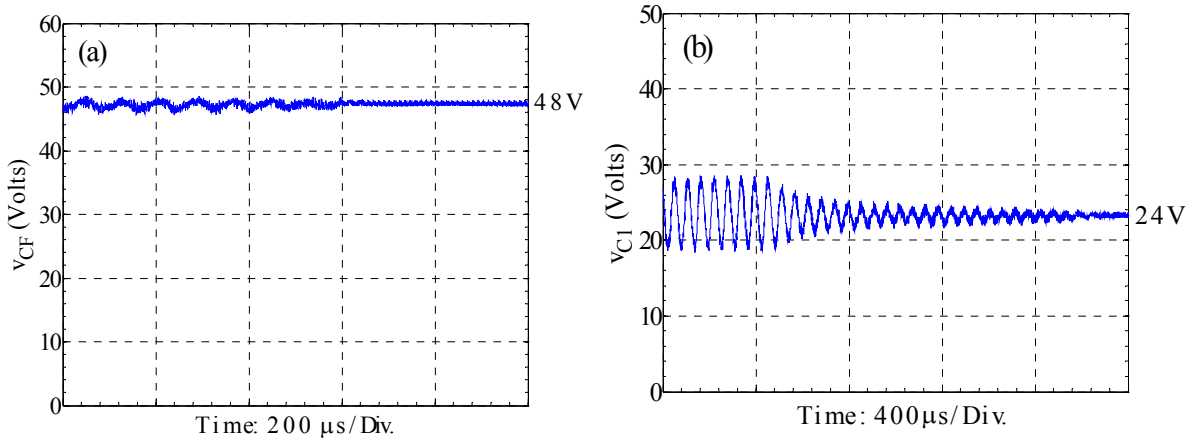

Fig. 3.34. Measured voltages when R_d is switched from 2 to 25.5Ω; (a): voltage across C_F, (b): voltage across C_1.

3.10 SUMMARY

An undamped or lightly damped filter connected to the input port of dc-dc converter tends to lead to instability. In this chapter, these input-filter interactions are explained using small-signal averaged models and the instability problem is treated using a passive damping solution. The dimensioning of this passive solution is elaborated using control-to-output transfer function. A methodology for stability analysis of dc-dc converter with input filter is presented and a design procedure for parallel R_d-C_d damping of input filter is suggested using the open-loop transfer function. Based on the damping circuit parameters, conditions of stability are derived for basic converter topologies (i.e. buck, boost and buck-boost). Thus a region of stable operation is subsequently identified for each of them which provide minimum and maximum limits on the damping resistance that must be added if the natural parasitic resistance of the input filter is not sufficient. Results have been validated experimentally. Design considerations for the optimum damping are also discussed.

A complete analysis of input filter interactions is also presented for the cascaded dc-dc converters based on their small-signal averaged model. Four conditions of stability are derived for the particular example of cascaded buck converters including the determination of the boundary between the stable and unstable operation. It is shown that all the right hand side zeros can be moved to the left hand side by adding adequate damping only to the input filter. A design procedure is proposed which gives the value of this damping resistance that must be added externally. This method is also applicable to other basic converter topologies connected in cascade (boost and buck-boost).

Chapter 4

INFLUENCE OF PASSIVE DAMPING ON THE CONVERTER EFFICIENCY: A CRITICAL ANALYSIS

In this chapter, power-losses in the damping circuit (which is discussed in the previous chapter) are quantified. Effects of damping losses on the conversion efficiency are investigated qualitatively under varying operating conditions. Thus various criticisms raised in the literature are discussed. Theoretical and experimental results are compared.

4.1 INTRODUCTION

Low-pass input filters have traditionally been employed to attenuate power-converter switching ripples to acceptable levels. However, dc-dc converters exhibit negative dynamic resistance characteristics at their inputs that can provoke oscillations when an input filter is inserted [mid76, usm06, usm07]. As illustrated in the previous chapter, addition of a second-order filter at the converter input introduces two complex conjugate zeros in the right-half *s*-plane of the open-loop control-to-output transfer function. These zeros are the cause of instability in closed-loop. The usual method to remedy this problem is to move these zeros to the left-half *s*-plane by adding some damping to the filter, thus avoiding the unstable behavior in the closed-loop. In some applications, however, parasitic resistances of the filter components can be sufficient to provide the required amount of damping but if this is not the case then external dampers need to be added in the filter circuit. A systematic procedure for the dimensioning of these damping resistors is described in the preceding chapter. For dc-dc converter applications such a damping circuit usually consists of an R_d-C_d network connected in parallel with the filter capacitor C_F as shown in Fig. 4.1.

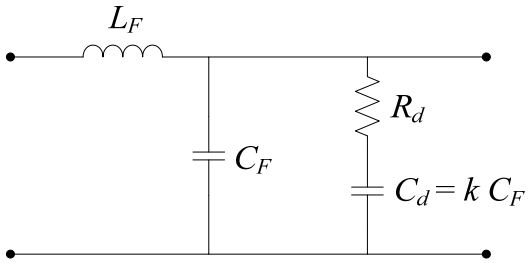

Fig. 4.1. A practical method used for damping the input filter, including damping resistance R_d and a dc blocking capacitor C_d.

One major drawback of adding R_d-C_d branch to the filter circuit is the degradation of efficiency due to power dissipation in damping resistor R_d. Passive damping of input filters in dc-dc converter applications has suffered enormous criticism due to presumably high conduction losses in the damping resistors. However an accurate quantitative assessment of their adverse impact on efficiency is still lacking. Similarly, not enough attention has been paid to the severity and extent to which they can effectively deteriorate a converter-efficiency under varying operating conditions. Since a large dc blocking capacitor is placed in series with the damping resistance, so ideally no dc current can flow through R_d thus its dc power loss is virtually eliminated. However this is not necessarily true in the reality. It has been a subject of discussion that by using such damping circuits the efficiency of the converters has often to be sacrificed while on the other hand absence of sufficient damping resistance imposes more demands on the control systems eventually making them more robust but more complex at the same time. More complex control systems offer other design and implementation issues (some of which will be discussed in the next chapter). Considering an unsatisfactory situation in the use of damping resistors, an effort was undertaken during this thesis to analyze this damping network in detail, so that its impact on the efficiency can be predicted quantitatively, making the choice easier during design process. This chapter is a compilation of the major results evolved from that effort.

In order to quantify damping losses a generalized power-loss analysis is presented in this chapter that helps in estimating the harmful effect of damping resistors on overall filter-converter system efficiency. Although the proposed approach is straightforward, it provides an improved and accurate understanding of those detrimental effects associated with the use of damping resistors which have usually been ignored in the literature. A practical damping approach using a shunt R_d-C_d network (see Fig. 4.1), which is most commonly suggested in dc-dc converter applications, is investigated theoretically as well as experimentally. Hence those operating conditions are identified under which damping losses can actually increase to an unacceptable level. For instance, results show that converter efficiency is susceptible to severe degradation, especially at high loads as well as at smaller damping resistor values. Furthermore, it is shown that these losses are considerably higher in buck-type converters than in boost-type converters. In addition, it is found that these losses are also a function of the converter operating point. As a consequent of these results, it is to be emphasized that a careful consideration of power economy is necessary while optimizing such a damping network. If damping losses are intolerable or a power-efficient optimal damping solution cannot be feasible, then employing an active solution to assure stability becomes indispensable. The final choice is, however, up to the designer of a given application. Usually a trade-off has to be made between the complexity of the control system that one can afford and the efficiency that one can sacrifice in a given application.

This chapter is devoted to the efficiency investigation of dc-dc converters with passively damped input filters and is organized as follows:

- Overview of various approaches to input filter damping design and its non-dissipative alternatives from the literature
- A comprehensive power-loss analysis of R_d-C_d damping network for buck-type and boost-type converters, as representatives of basic topologies, demonstrating its quantitative influence on the efficiency of these converters
- Experimental validation of the theoretical predictions made in this chapter.

4.2 REVIEW OF THE PREVIOUS WORK

Several criteria have been proposed for the dimensioning of the R_d-C_d network. A systematic design procedure was first presented in [mid78] based on a strategy to minimize the output impedance of the filter thus avoiding its interaction with the negative differential input impedance of the converter. Finally a criterion was derived to achieve optimum damping for a given input impedance characteristic of a dc-dc converter. Ref. [eri99] outlines a similar optimization procedure for three types of single resistor damping networks and extends this study further to multiple-section cascaded filters with damping. An other technique is proposed in [cal02] for input filter damping design using zero dynamics analysis which yielded equivalent results to those obtained using classical approach of [mid78]. However the application of this new method was extendable to other converters with an intermediate capacitor but without input filter (e.g. buck and boost with two inductors and dual SEPIC). Similarly, [sad04] and [usm07] proposed design procedures solely based on the open-loop control-to-output transfer function and determined lower and upper limits on R_d for which all of the transfer function zeros remain on the left-hand side of the *s*-plane. These limits are obtained by application of Routh-Hurwitz criterion to the numerator polynomial of the transfer function. Thus a stability region was defined in the damping-circuit parameters space. Instabilities in power converters with input filters are also discussed by [tsu01] for railway vehicle applications. Three different methods are analyzed for damping the input filter dynamics. At the end authors urge for further study on damping networks given the increasing demands on efficient power use. [kim05] stated that the impedance constraints for a minimal input filter interaction are significantly easier to meet in the current-mode controlled converters rather than in voltage-mode controlled converters. However they focus more on the analysis and shed little light on the design of damping circuits. Numerous references like [cho95, liz96, mit99] have also focused on the power-line filter design intended for distributed power applications. The design procedures realize an input filter that also includes the damping branch and meets the impedance compatibility and EMI requirements simultaneously.

Almost all of the above referred methods have suggested shunt type R_d-C_d damping network for dc-dc converters; however none of them takes into account the damping resistor power dissipation in their design of optimal damping. Although using external damping resistors may be unavoidable for stability reasons in some applications, ignoring completely their effects on conversion efficiency can be harmful under certain operating conditions, as will be shown later in this chapter.

In parallel, many efforts have been made to find an alternative way to assure the closed-loop stability of the filter-converter system by avoiding the use of dissipative damping but at a cost of making the control systems more complex (see [dah02, nic95, raj02] and [vla96]). In [dah02] a control method was proposed in order to damp transient oscillations in the input LC-filter of ac-dc PWM converters. This method was based on the implementation of a virtual resistor in the control algorithm thus having no negative influence on efficiency. However this method needs an additional current or voltage sensor and the design is usually difficult. A sliding-mode control scheme for dc-dc converters with input filter was reported in [nic95] in which the sliding surface was obtained from Lyapunov function approach. Although this control scheme assured stability in the steady-state but it still needed damping resistors to improve transient response of the converter. Ref. [vla96] suggested new passive and active damping methods that guarantee optimal damping of the filter pole, while nearly eliminating damping resistor power dissipation. But these damping methods are suitable only for ac power converter filters, and their utility for dc-dc converters is not demonstrated. Another effort

towards the replacement of large passive components in power filter circuits was reported by [mur04] which explored an active ripple-filtering technique for common-mode EMI filters in automotive applications. This method employs active op-amp control circuitry that makes use of smaller passive components. Likewise [bar02] suggested another method to avoid dissipative damping by deteriorating the problematic property of dc-dc converters as constant-power loads, hence eliminating the risk of instability. By treating the example of a sliding-mode controlled chopper, authors have demonstrated that it is possible to stabilize the system without adding excessive passive damping.

4.3 POWER-LOSS ANALYSIS

4.3.1 General Framework

Switching converters typically have fast current variations at their inputs. Flyback and buck topologies are particularly notorious for discontinuous input currents, since a semiconductor switch is directly in series with the input power line. In contrast, other topologies such as boost and Cuk converters inherently produce lesser input noise. Since nature of the input current is converter topology-dependent, we have investigated buck and the boost converters as two representatives of the basic converter topologies. In order to assess the efficiency, we first need to evaluate the current flowing through R_d-C_d branch. For this purpose, let's reconsider the damped input filter circuit as shown in Fig. 4.2.

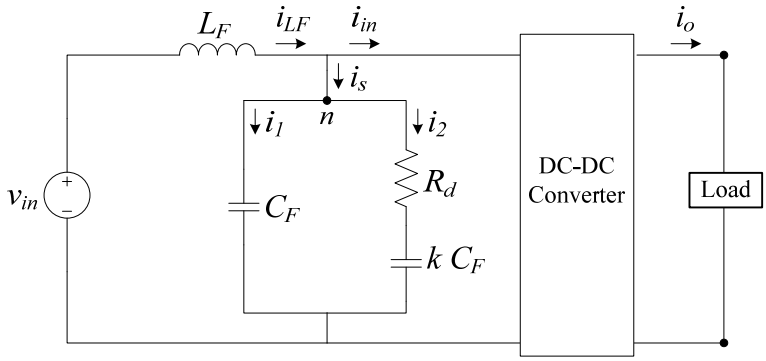

Fig. 4.2. Flow of current in the input filter and damping branch.

Assuming that in steady state the current drawn from the source $i_{LF}(t)$ is maintained constant and can be represented as $I_{LF} = f(d, I_o)$. Here d is the duty cycle of the switch and I_o is the steady-state output current which is given as $I_o = V_o / R$. Where V_o is the steady-state output voltage and R is load resistance. Moreover, the total current entering into shunt branch $i_s(t)$ can always be found as:

$$i_s(t) = i_{LF}(t) - i_{in}(t) \tag{4.1}$$

Since $i_s(t)$ is known in a given converter, $i_2(t)$ can be determined by writing the KCL equation at node n (see Fig. 4.2), thereby giving the following first order non-homogenous linear differential equation:

$$\frac{di_2(t)}{dt} + a \cdot i_2(t) = b(t) \tag{4.2}$$

where

$$a = \frac{1+1/k}{R_d C_F}$$
$$b(t) = \frac{i_s(t)}{R_d C_F} \tag{4.3}$$

The solution of equation (4.2) is the instantaneous value of the desired current $i_2(t)$ that depends on the converter topology.

4.3.2 Analysis of Buck Converter

In case of an ideal buck converters, three current waveforms, i.e. the input current $i_{in}(t)$, the source current $i_{LF}(t)$ and the shunt branch current $i_s(t)$ can be drawn as in Fig. 4.3.

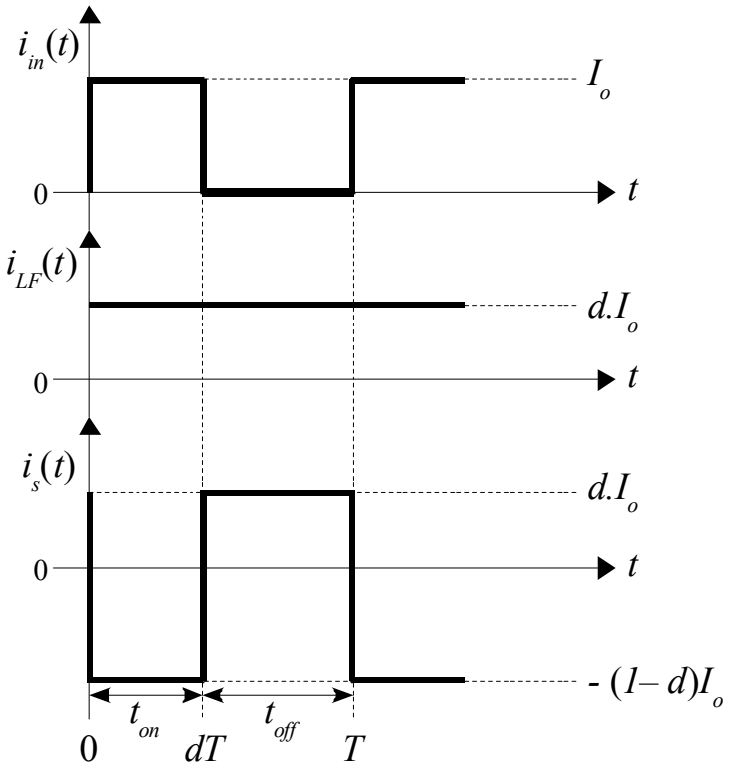

Fig. 4.3. Idealized current waveforms for a buck converter.

Using these waveforms, a piece-wise solution of equation (4.2) can be obtained in two subintervals of the switching cycle as follows:

Interval t_{on} : $0 < t < dT$

$$i_{2(on)}(t) = A + \lambda_1 \cdot e^{-at} \tag{4.4a}$$

Interval t_{off} : $0 < t < (1-d)T$

$$i_{2(off)}(t) = B + \lambda_2 \cdot e^{-at} \tag{4.4b}$$

where

$$A = -\frac{(1-d)I_o}{aR_dC_F}\ , \quad B = \frac{dI_o}{aR_dC_F}$$
$$\lambda_1 = \frac{I_o}{aR_dC_F}\left(1 - \frac{(e^{-adT}-1)}{(e^{-aT}-1)}\cdot e^{-a(1-d)T}\right) \tag{4.5}$$
$$\lambda_2 = -\frac{I_o}{aR_dC_F}\cdot\frac{(e^{-adT}-1)}{(e^{-aT}-1)}$$

Note that λ_1 and λ_2 are integration constants whose values are determined by imposing following boundary conditions:

$$i_{2(on)}(0) = i_{2(off)}\left((1-d)T\right)$$
$$i_{2(off)}(0) = i_{2(on)}(dT) \tag{4.6}$$

The RMS value of $i_2(t)$ can now be calculated using the following relation:

$$I_{2RMS} = \sqrt{\frac{1}{T}\left(\int_0^{dt} i_{2(on)}^2(t)\cdot dt + \int_0^{(1-d)T} i_{2(off)}^2(t)\cdot dt\right)} \tag{4.7}$$

The instantaneous current given by (4.4) and its RMS value I_{2RMS} are now simulated in Fig. 4.4(a) along with the total current $i_s(t)$ entering into shunt branch. Once the current is known, instantaneous and average power losses can then be calculated using $i_2^2(t)R_d$ and $I_{2RMS}^2 R_d$ respectively and are simulated in Fig. 4.4(b) for a buck converter. The parameters used for these simulations are: $C_F = 0.47\mu\text{F}$, $k = 10$, $R_d = 10\Omega$, $d = 0.5$, $f_s = 112\text{kHz}$ and $I_o = 0.8\text{A}$.

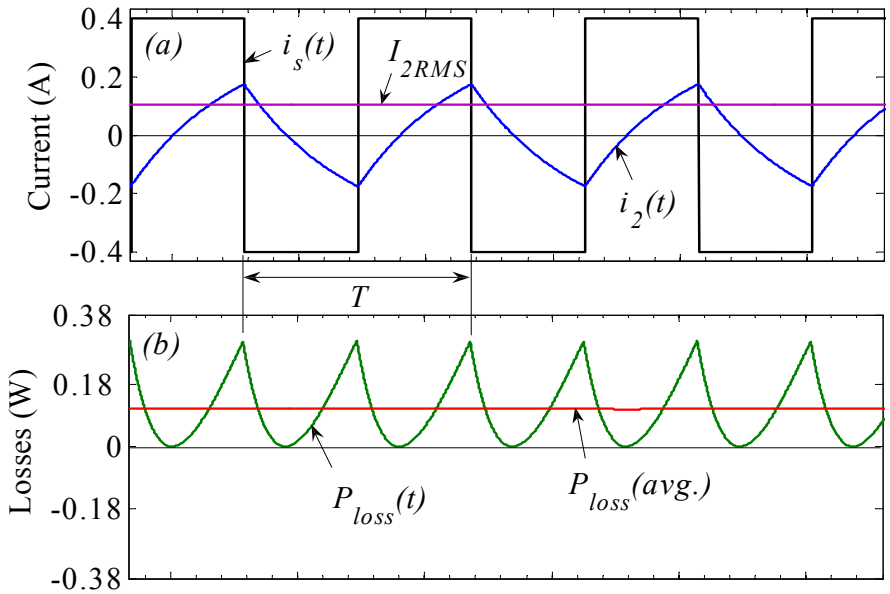

Fig. 4.4. *(a)*: Simulated RMS and instantaneous waveforms of i_2 and i_s for buck converter; *(b)*: Simulated instantaneous and average power losses in R_d.
(Parameter values: $C_F = 0.47\mu\text{F}$, $k = 10$, $R_d = 10\Omega$, $d = 0.5$, $f_s = 112\text{kHz}$ and $I_o = 0.8\text{A}$)

Following the same procedure average power loss can be calculated for varying values of R_d keeping load current constant and vice versa. Fig. 4.5 shows the variation of this average power loss for a 10W buck converter as a function of damping resistance R_d and the load current I_o.

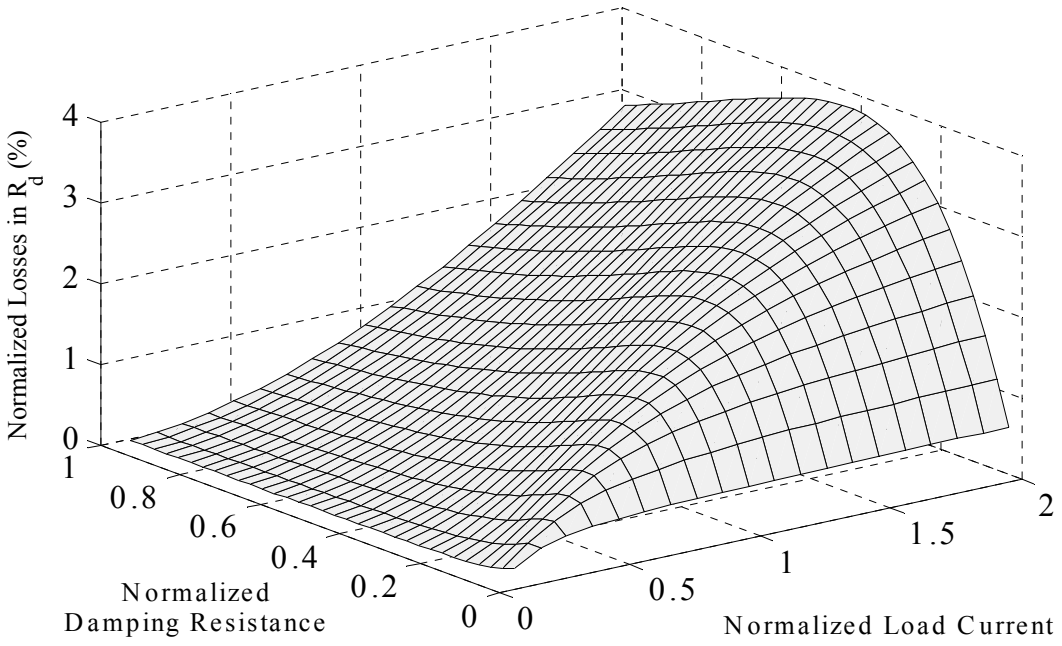

Fig. 4.5. Buck converter simulated variation of average power loss in R_d-C_d branch as a function of load current and R_d.

In Fig. 4.5, the power losses, damping resistance and output current are normalized with respect to input power, load resistance and the nominal output current, respectively. Thus it may serve as a measure of efficiency reduction as a function of R_d and output current. This effect is more clearly depicted from the corresponding efficiency plot in Fig. 4.6. Here R_d is varied from 3% to 99% of the load resistance and I_o is varied from 10% to 200% of its nominal value. It can be noticed that at very small values of R_d the effect of parallel R_d-C_d damping on overall conversion efficiency first tends to increase with R_d, reaches its maximum, and then starts decreasing again for higher values of R_d. For a given converter design parameters, the value of R_d that corresponds to the maximum loss can easily be found by differentiating $R_d I_{2RMS}^2$ expression and equating it to zero. For the optimum damping design this value of R_d must be avoided, while still fulfilling the stability requirements. It is also notable that the efficiency tends to decrease significantly as the output current increases. For example, efficiency can reduce up to about 4% when the converter operates at twice its nominal load current (see Fig. 4.6).

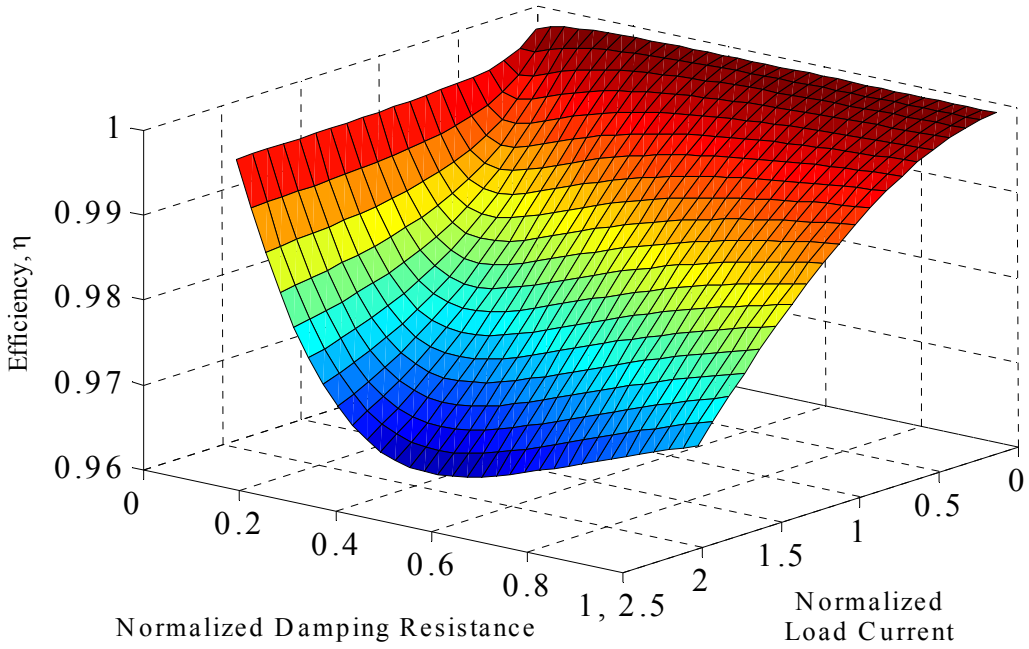

Fig. 4.6. Buck converter efficiency as a function of load current and R_d.

It is noteworthy that simulations in Fig. 4.5 and Fig. 4.6 correspond to a fixed duty ratio that is 50%. Consequently, trying to deduce a conclusion solely based on them might be misleading. Moreover, in many contemporary applications power converters are being fed by highly unregulated renewable energy sources (e.g. solar panels, fuel-cell stacks etc.) with vast voltage variations which can subsequently cause the duty cycle to deviate largely from its nominal value in the downstream converters. So it may be useful to study the effect of d on damping power losses. To gain some insights, we have plotted normalized power losses as a function of d and R_d in Fig. 4.7 for the same 10W buck converter with nominal output current of 0.8A and for a variation of d from 0.2 to 0.8. Fig. 4.7 implies that efficiency of the converter would tend to degrade progressively as d approaches 0.5, while maximum losses occur at $d = 0.5$. Furthermore, it is also evident that the plot in Fig. 4.7 is symmetrical with respect to the curve corresponding to $d = 0.5$. Thus it appears that a particular damping resistance designed to work pretty good at one operating point may severely worsen the situation at others. The severity and extent of this deterioration though strongly depend on the values of both d and R_d.

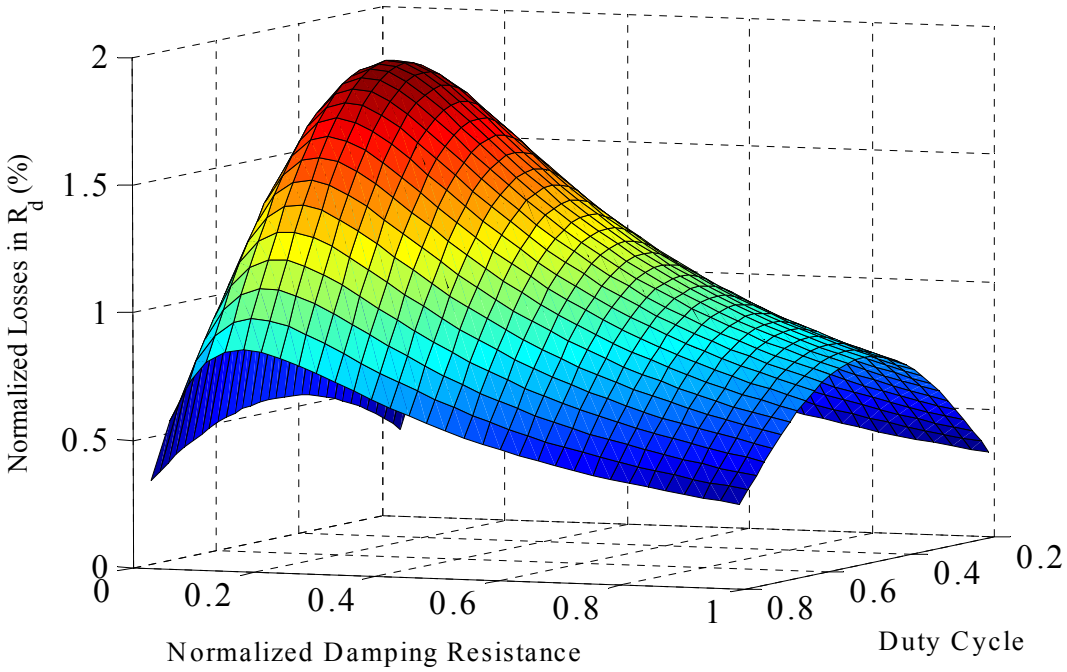

Fig. 4.7. Buck converter damping power-loss as a function of d and R_d.

4.3.3 Analysis of Boost Converter

For a boost converter, the current waveforms $i_{LF}(t)$, $i_{in}(t)$ and $i_s(t)$ are shown in Fig. 4.8.

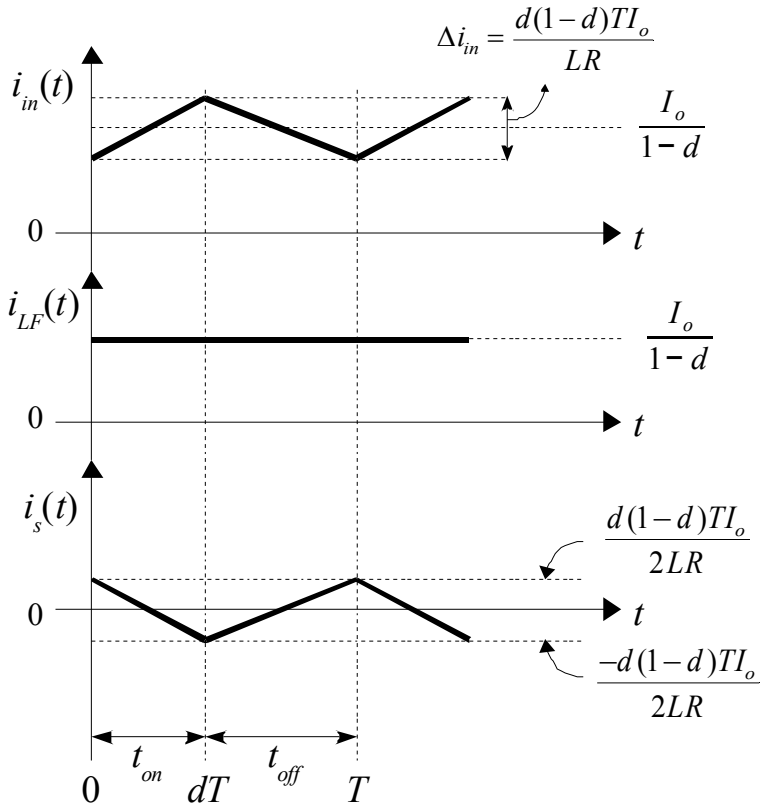

Fig. 4.8. Idealized current waveforms for a boost converter.

Using these waveforms a piece-wise solution of equation (4.2) can be obtained for a boost converter as follows:

Interval t_{on} : $0 < t < dT$

$$i_{2(on)}(t) = A(t) + \lambda_1 \cdot e^{-at} \tag{4.8a}$$

Interval t_{off} : $0 < t < (1-d)T$

$$i_{2(off)}(t) = B(t) + \lambda_2 \cdot e^{-at} \tag{4.8b}$$

where

$$\begin{aligned} A(t) &= \frac{(1-d)(2-2at+adT)I_o}{2a^2LRR_dC_F} \\ B(t) &= -\frac{d(2-2at+a(1-d)T)I_o}{2a^2LRR_dC_F} \\ \lambda_1 &= -\frac{I_o}{a^2LRR_dC_F} \cdot \frac{(e^{-a(1-d)T}-1)}{(e^{-aT}-1)} \\ \lambda_2 &= \frac{I_o}{a^2LRR_dC_F} \cdot \left(1 - \frac{(e^{-a(1-d)T}-1)}{(e^{-aT}-1)} \cdot e^{-adT}\right) \end{aligned} \tag{4.9}$$

Same boundary conditions as given by (4.6) are applied to evaluate the integration constants λ_1 and λ_2 in this case. The analytical solution (4.8), its RMS value and the corresponding instantaneous and average losses are simulated in Fig. 4.9(a) and (b) respectively. The boost converter parameters for this simulation are the same as used in Fig. 4.4 except $L = 100\mu$H and $R = 15\Omega$.

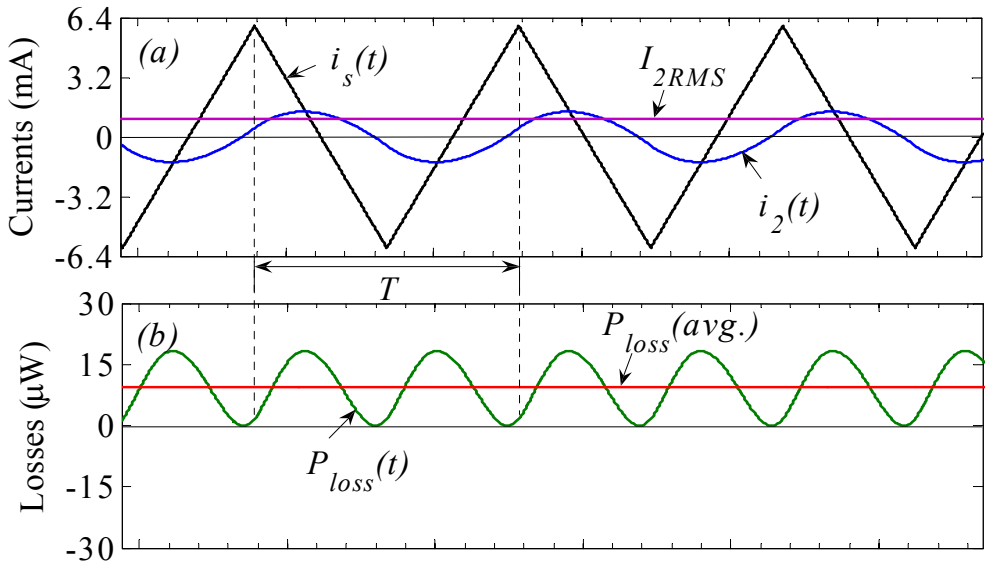

Fig. 4.9. *(a):* Simulated RMS and instantaneous waveforms of i_2 and i_s for boost converter; *(b)*: Simulated instantaneous and average power losses in R_d. (Parameter values: $L = 100\mu$H, $C_F = 0.47\mu$F, $k = 10$, $R_d = 10\Omega$, $d = 0.5$, $f_s = 112$kHz, $R = 15\Omega$ and $I_o = 0.8$A)

The normalized power losses, its influence on efficiency and the effect of *d* in a 10W boost converter are shown in Fig. 4.10, Fig. 4.11 and Fig. 4.12 respectively.

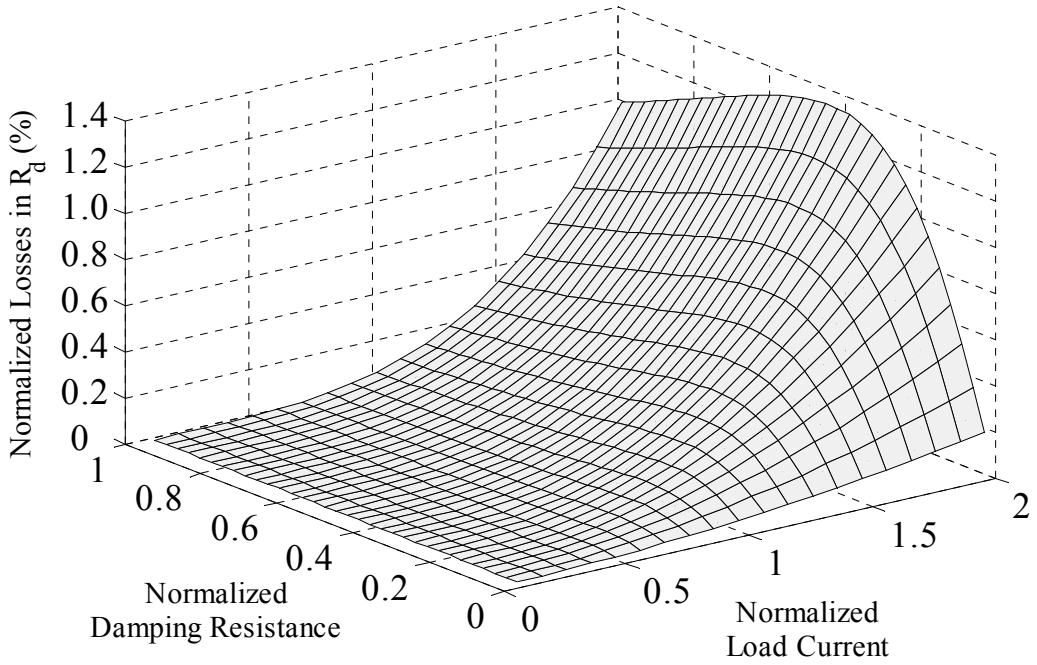

Fig. 4.10. Boost converter simulated variation of average power-loss in R_d-C_d branch as a function of load current and R_d.

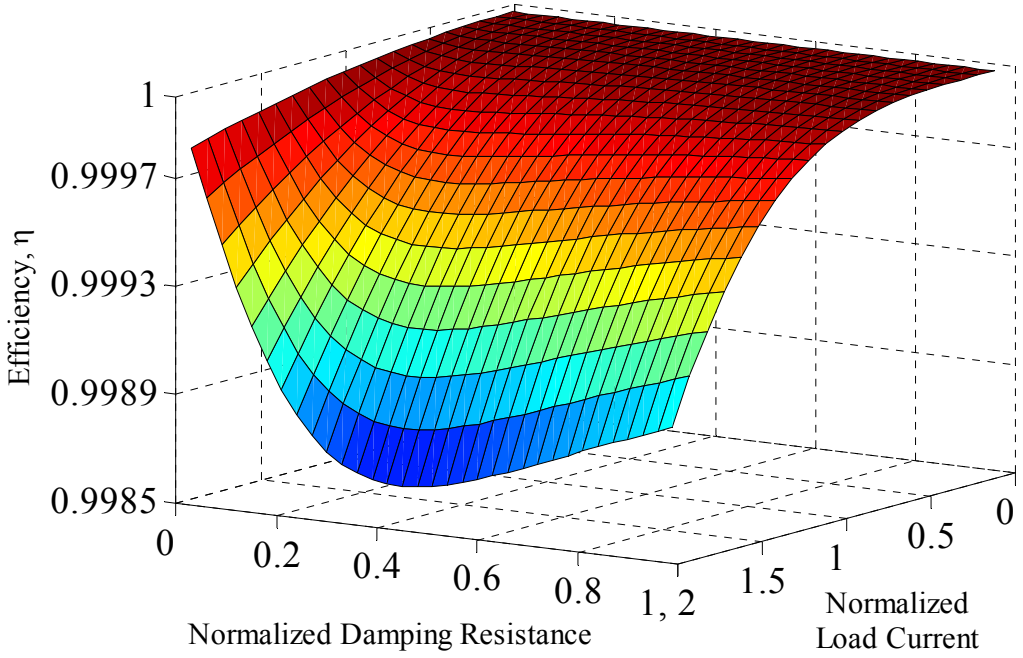

Fig. 4.11. Boost converter efficiency as a function of load current and R_d.

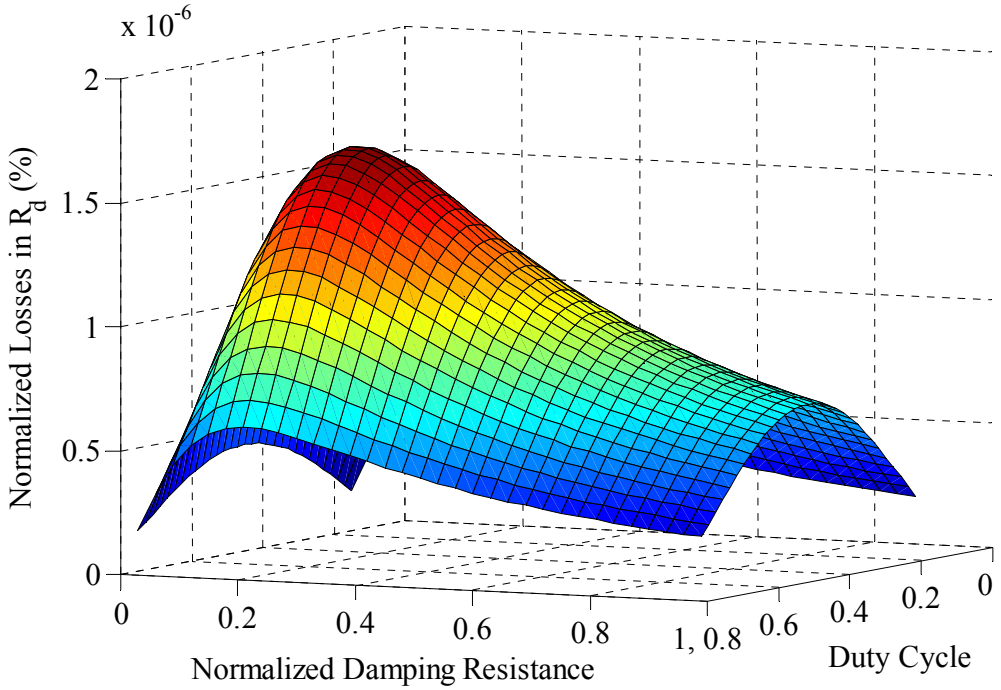

Fig. 4.12. Boost converter damping power-loss as a function of d and R_d.

Through a fine examination of these results and by a comparison with their counterparts in the previous subsection it can be inferred that the variation tendency of damping power losses in boost converters is consistent with that in the buck converters. However the magnitude of this effect is substantially large in case of buck-type converters, whereas it is quite small and negligible in boost-type converters. For instance, when the load current is doubled its nominal value, the maximum power-loss in buck and boost converters can go up to 4% and 1.3% respectively. This significant difference in losses can be attributed to the discontinuous nature of the input current in buck converters and their derivatives.

4.3.4 Effect of C_F on Damping Power-Loss

In this subsection, the role of filter capacitor C_F on damping losses is addressed. An increasing value of C_F causes a subsequent decrease of RMS voltage across the damping branch, hence some reduction in damping losses. In order to have a better idea of this effect, damping power losses are plotted for different values of C_F in Fig. 4.13(a) and (b) for buck and boost converters respectively. For all of these plots C_d is fixed at 4.7μF (hence k is varying).

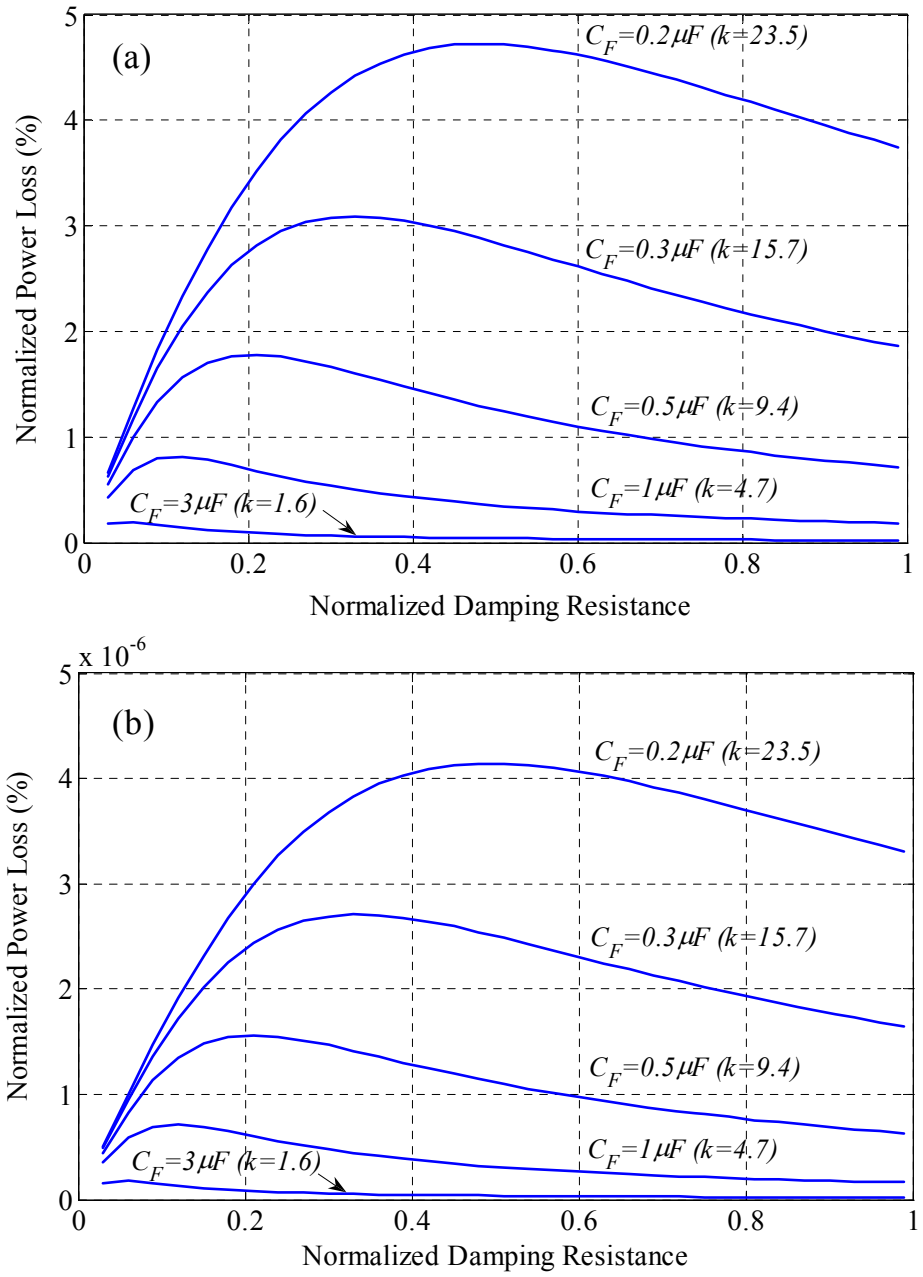

Fig. 4.13. Effect of filter capacitor C_F on damping power-loss; (a): Buck converter, (b): Boost converter.

At first glance, it seems obvious that choosing a sufficiently large value of capacitor C_F can easily render these losses negligible even in case of buck-type converters. However, it is important to be considered that the input filter is usually dimensioned to meet EMI/EMC requirements. One of the critical factors involved in designing a second-order filter is the attenuation characteristic at its corner frequency. The detailed design of the input filter is not the subject of this chapter; however, various design methods are widely discussed in the literature [eri01, mit99, oze00]. Consequently, such EMI-filter design constraints may not leave us with an open choice of C_F that is also optimal from an efficiency viewpoint. Moreover, a greater value of C_F will also shift the input-filter resonance towards a lower frequency. This will further make the control-loop design a more challenging task. An oversized input filter unnecessarily adds cost and volume to the design and compromises system performance. Hence in order to minimize damping losses an arbitrarily large value of

C_F cannot be selected without compromising the attenuation characteristics of the filter. However a careful trade-off can possibly be adopted to design an optimal filter capacitor.

4.4 DESIGN CONSIDERATIONS FROM EFFICIENCY VIEWPOINT

The power-loss analysis presented in the previous section shows that there are certain values of R_d for which maximum power is dissipated in the damping branch, hence leading to maximum degradation of efficiency. If possible, this value of damping resistance must be avoided in the design of input filter. As mentioned previously, the value of R_d that corresponds to the peak power loss, for a given k, can easily be found by differentiating $R_d I_{2RMS}^2$ expression and then equating to zero. We denote this value of damping resistance by R_d'. If R_d' is calculated for varying values of k then a contour can be plotted in the (R_d, k) plane by joining all the (R_d', k) points for a given load. Now it is interesting to see where this contour actually lies with reference to the stability region determined in the preceding chapter. In order to visualize this we have superimposed two such contours on their respective stability regions for two different values of load resistance in Fig. 4.14.

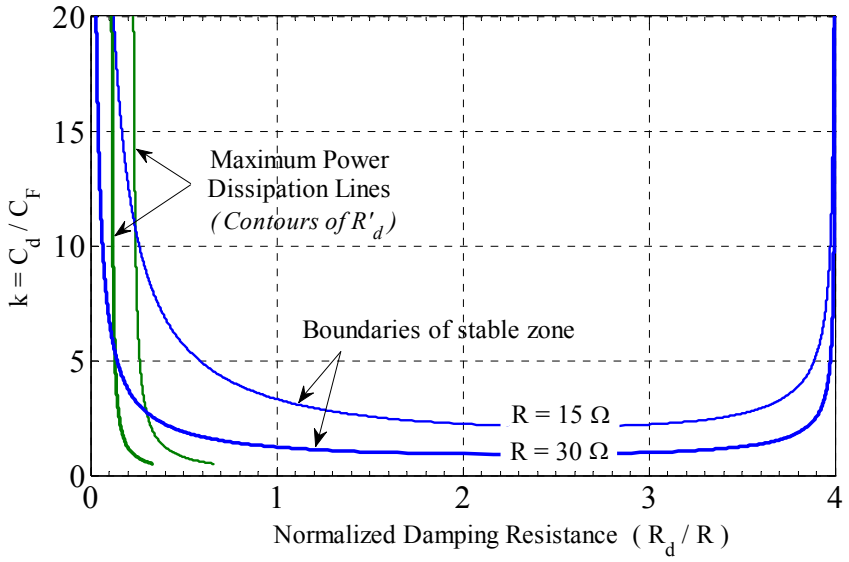

Fig. 4.14. Plot of maximum power dissipation lines on the stability regions of buck converter for two different loads; *Solid Lines*: R = 30Ω, *Thin Lines*: R = 15Ω.

The thick solid lines in Fig. 4.14 correspond to R = 30Ω, whereas thin lines are plotted for R = 15Ω. First of all it is necessary to notice that contours of R_d', for any load resistance, represent an almost straight line in the (R_d, k) plane, except for very small values of k (usually below k = 4). Hence it can be inferred that R_d' is mainly a function of load and can be considered almost independent of k. Moreover, with increasing load currents (i.e. decreasing values of R) the value of R_d' also increases. This observation is also true for boost and buck-boost converters. Next observation is that this R_d' contour intersects the lower boundary of the stable zone at a certain value of capacitor-ratio k. More the load resistance R is smaller; more this intersecting value of k is larger. Above this intersection point the stability region is divided into two parts by this contour, one on the left side of R_d' and the other on its right side. From efficiency viewpoint, it's better to select an R_d value which is greater than the R_d'

(i.e. from the right-hand side of R_d' contour). Because otherwise it will be too close to the lower boundary of the stable zone (i.e. R_{dmin}), and it will also exclude the choices of k from the range below the intersection point. These design guidelines are also valid for other types of converters such as boost and buck-boost.

4.5 EXPERIMENTAL RESULTS

An experimental prototype of a 4.3W buck converter with an input filter was developed in order to validate theoretical predictions. The converter was designed for the nominal conditions of: $V_o = 24$V, $I_o = 0.18$A and $f_s = 112k$Hz. For these parameter values and $C_d = 10C_F$ (with ESR=1Ω) the RMS value of the current flowing through R_d-C_d branch was measured for various values of R_d. For instance, the measured current $i_2(t)$ is shown in Fig. 4.15 for R_d =10Ω. Then two sets of measurements were taken by operating the closed-loop converter with d first having a value of 0.5 and then 0.7, respectively. The corresponding losses were calculated, while regulating the output voltage constant in both cases via a conventional voltage-mode control. However, in order to operate the closed-loop converter at two different duty cycles, the input voltage was varied accordingly. In Fig. 4.16 measured losses are compared with the predicted losses (i.e. corresponding simulated curves for d = 0.5 and 0.7). The damping losses for $d = 0.3$ were also measured and found to be coinciding with those corresponding to $d = 0.7$. A good agreement can be seen between experimental measurements and the theoretical predictions of this chapter.

It is worth mentioning here that the equivalent series resistance (ESR) of C_d also contributes positively to the damping of input-filter oscillations. Since a resistor is to be placed in series with this capacitor anyways, so C_d can be realized using capacitor types having substantial ESR, such as electrolytic and tantalum types. Moreover, if desired, its power dissipation can also be determined using the same current i_2 in the R_d-C_d branch. In the measurements shown in Fig. 4.16, this parasitic loss is included in the total damping losses.

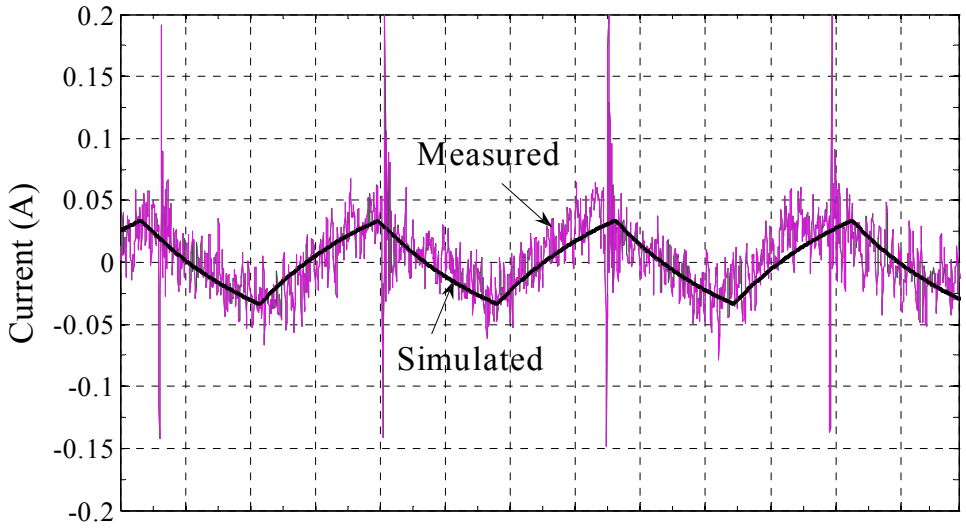

Fig. 4.15. Measured and simulated current $i_2(t)$ in R_d-C_d branch for R_d=10Ω. (Parameter values: $L_F = 4m$H , $C_F = 0.47\mu$F , $L = 0.8m$H , $C = 1\mu$F , $k = 10$, $d = 0.5$, $f_s = 112k$Hz , $V_o = 24$V and $I_o = 0.18$A)

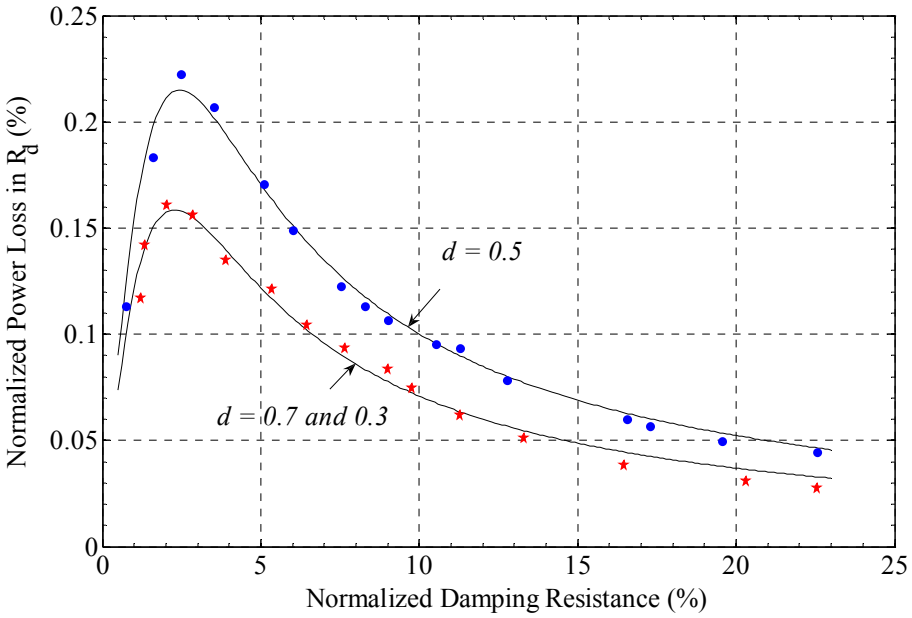

Fig. 4.16. Comparison of measured and predicted power losses in R_d-C_d branch as a function of R_d; *Lines*: Simulations, *Dotes*: Measurements. (Parameter values: $L_F = 4m\text{H}$, $C_F = 0.47\mu\text{F}$, $L = 0.8m\text{H}$, $C = 1\mu\text{F}$, $k = 10$, $d = 0.5$, $f_s = 112k\text{Hz}$, $V_o = 24\text{V}$ and $I_o = 0.18\text{A}$)

4.6 SUMMARY

A generalized analysis of efficiency for dc-dc converters with passively damped input filters is presented in this chapter. Simulated and experimental results reveal that the use of damping networks needs careful considerations in the design of dc-dc converters because it can significantly deteriorate the converter efficiency especially at overload conditions. Usually a compromise has to be made between the complexity of the control system that we can afford and the efficiency that we can sacrifice. Since in most converters even a few percent efficiency is actually quite important, so this negative impact of damping resistors may not always be negligible. However as a result of the investigation carried out in this work, it is shown that this effect, which is mainly a function of the nature of input current, is more pronounced in buck-type converters than in boost-type converters of the same ratings. Moreover, from the analysis it appears that the maximum power dissipation in R_d and subsequent efficiency degradation occurs when d = 0.5 and it varies in a direct proportion to the load currents while in an inverse proportion to the value of R_d itself (except for very small values of R_d). Hence this loss can reasonably be expected tolerable in such applications where relatively large values of R_d can be employed for the sake of having a simple control system (e.g. a conventional PI controller). Nevertheless, in other applications the use of these resistors still remains questionable. However prior to any decision, a systematic analysis as proposed in this chapter may help predetermine the efficiency.

Chapter 5

CONTROL OF DC-DC CONVERTERS WITH INPUT FILTER: AN ACTIVE SOLUTION FOR STABILITY

This chapter addresses the stabilization problem of filter-converter system using control solutions. For this purpose, a full state-feedback control with pole-placement is proposed and its dynamic performance is evaluated. A sliding-mode control scheme is also studied from the literature in order to make a comparative analysis of both control schemes.

5.1 INTRODUCTION

In most of the contemporary applications, very robust performance in stability, dynamic response and accuracy is required for switched-mode power supplies especially in the fields of telecommunications, aeronautics and space. However, as explained in Chapter 3, when an input filter is combined with a closed-loop converter, it can provoke instability in the system if the filter is not sufficiently damped [mid76]. In many dc-dc converter applications an easy and commonly employed method to damp the filter oscillations is to use external resistors in the input-filter circuit to assure stability [mid78, usm07]. These passive damping methods are discussed in detail in Chapter 3. Although such type of passive dampers can stabilize the system, excessive conduction losses are undesirable in the circuit since it can severely degrade the system efficiency (as discussed in detail in Chapter 4). Moreover, it is found that input-filter oscillations are function of the regulator performances. The use of fast regulators increases the risk of system instability. It is difficult to find a control law which overcomes this issue because of the nonlinear behavior and resonance problem of an underdamped input filter. Moreover, although input-filter interactions have been studied quite extensively in various publications and some control solutions have also been reported for diverse applications, however their direct extension to our application of dc-dc converters with input filters (without using external resistors) is not so evident.

In this chapter we discuss some active solutions as alternatives to the dissipative damping of the input filter. A state-feedback controller combined with a PI-control loop is proposed for the stability of dc-dc converters in the presence of input filter. The resonance due to input filter makes it highly difficult to control such kind of systems. However the proposed control algorithm assures stability of the system without using any passive components in the filter circuit and thus avoiding any undesirable losses. The control law is based on a full state-

feedback as shown in Fig. 5.1. To adjust system response, the computation of feedback gains is carried out by a closed-loop pole placement. So, an adequate level of small-signal dynamic performance is guaranteed, and then a varying gain state-feedback strategy is performed to extend local performances to global ones. Although a thorough analysis of robustness of this method still lacks in this work, however simulation studies are successfully carried out to confirm the effectiveness of the suggested control strategy under large load and line perturbations. In order to cancel the steady-state errors in the response, an integral of the error between reference and the output voltage is also added to this state-feedback. Computation of the feedback gains is adapted to varying operating points by a continuous evolution of the gain vector. This is achieved by using lookup tables indexed by the input voltage and output load.

Then in the second step, a sliding-mode control based on the Lyapunov function approach [nic95] is discussed. This approach is already presented in [nic95], but we have selected this method only for the purpose of comparison with our proposed state-feedback control. The outline of this chapter is as follows:

- In section 5.2, a literature survey is presented and some already existing control techniques are recalled while citing their relevant references.
- In section 5.3, the control problem is defined and the challenges faced due to filter-converter interactions are discussed.
- A small-signal augmented averaged model is presented in section 5.4 which is used for the subsequent state-feedback control design proposed in the same section. Then, performance of the proposed control is also analyzed. The analysis is based on simulated dynamic response of a closed-loop buck converter with input filter, wherein switched model of the converter is used.
- In section 5.5, a sliding-mode control scheme chosen from the literature is described and is compared with the proposed state-feedback scheme in section 5.6. Finally conclusions of this work are discussed.

5.2 STATE OF THE ART

It's been more than a decade since researchers are looking for some active solution to damp input filter oscillations. Various control techniques have been applied to stabilize the closed-loop system by avoiding the use of passive damping. For instance, a control method was proposed in [dah02] to damp transient oscillations in the input LC filter of ac-dc PWM converters. This method was based on the implementation of a virtual resistor in the control algorithm and thus having no negative influence on efficiency. However this method needs an additional current or voltage sensor and also its design is usually difficult. Moreover its application is demonstrated only for the ac-dc converters and is not evident for the dc-dc converter case. Similarly, a sliding-mode control scheme for dc-dc converters with input filter was reported in [nic95] mainly for high power applications. This method is a nonlinear control in which the sliding surface is obtained from Lyapunov function approach and the switching frequency is variable. Although this control scheme assured stability in the steady-state, it still needed damping resistors to improve transient response of the converter, and its dynamic performance varies depending upon the operating point. Besides, it has some other disadvantages which will be discussed in more detail later in this chapter.

The techniques of state-feedback and the theory of linear quadratic optimal regulator (LQR) have also been presented in the literature for the control design of various types of switching converters (but usually without considering input filter). For instance, for the switching converters having RHP zeros in their open-loop transfer functions, linear state-feedback controllers were proposed in [fra91] and [gar94]. The control design was treated as a general linear quadratic regulator (LQR) problem. In [cza95], the robustness and stability of state-feedback controlled PWM dc-dc push-pull converter was analyzed under variations in circuit parameters. A state-feedback control had also been proposed for current-type PWM ac-dc converters to suppress the transient oscillations of the ac side current due to LC filter resonance [sat93]. Authors of [ley01] suggested linear state-feedback controller for large-signal stability of boost converter. Likewise a complete state-feedback digital control algorithm was developed for current-mode and voltage-mode synchronous buck converter in [oli05], wherein authors designed the feedback gains of the controller by pole-placement in the state-space. However in most of the above cited references, no EMI filter was considered at the converter input.

5.3 PROBLEM DEFINITION

Insertion of LC filters at the input of dc-dc converter adds complex conjugate RHP zeros in the open-loop control-to-output transfer function. These RHP zeros are the cause of instability in the closed-loop if the regulator bandwidth is greater than the filter resonant frequency. Our objective is to find some control solution for this instability with adequate transient response to external disturbances. As far as control is concerned, switching converters are generally regarded as highly nonlinear systems. Nonlinearities are mainly due to two reasons: 1) nonlinear characteristics of electronic switching (fast dynamics), 2) nonlinear system parameter variations because of external disturbances (slow dynamics). In order to deal with these nonlinearities, one of following two approaches can be adopted [fra91]:

1. Use an approximate linearized model to average out the effect of fast dynamics. Such a linearized model is usually quite accurate in the bandwidth of interest (i.e. below 1/2 of switching frequency). However owing to the nonlinearities mentioned above, it has to be assumed that the regulator is working at one operating point and the disturbances in line voltage and load current are small enough to lie within the sensitivity tolerance of the controller.
2. The second approach could be to design a high-quality adaptive controller that is capable of adapting significant nonlinearities and multioperating point conditions.

Comparing the above two approaches, the application of approach 1 is obviously simple but more restrictive due to the constraints imposed by the assumptions made in it. However the approach 2, on the other hand, is more general but the design and implementation of such a controller is complex and requires a more advanced control theory. Nevertheless approach 1 is found to be sufficiently good in many practical cases. In this thesis, we used the first approach to design a full state-feedback controller to stabilize a dc-dc converter with input filter. However the feedback parameters can be adapted to the changing operating point using lookup tables.

In this approach, a linearized ac small-signal model has to be considered. Based on the linearized small-signal model, the controller is to be designed to stabilize the output in presence of input filter with sufficiently good transient response. Moreover the controller has

to be robust enough to handle modest variations in the line voltage, reference voltage and load current.

5.4 STATE-FEEDBACK CONTROL

The circuit diagram of a buck converter with an undamped input filter is shown in Fig. 5.1. This schematic will be used as an example to introduce the state-feedback controller in this section.

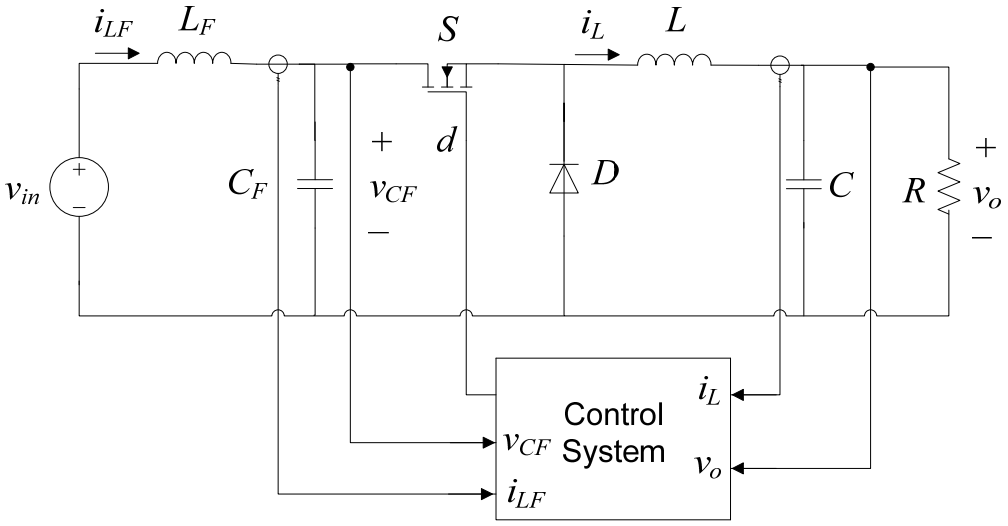

Fig. 5.1. Buck converter with input filter: example used to introduce state-feedback controller.

5.4.1 Model of Converter for Control Design

In general, a switching dc-dc converter can readily be represented by a linearized small-signal state-space model as given below:

$$\dot{\tilde{x}} = A\tilde{x} + B\tilde{d} + G\tilde{v}_{in} \tag{5.1a}$$

$$\tilde{v}_o = C\tilde{x} \tag{5.1b}$$

where $\tilde{x}$ is state vector of the linearized system containing all inductor currents and capacitor voltages. For a converter such as one shown in Fig. 5.1, this state vector can be defined as $\tilde{x} = \begin{bmatrix} \tilde{i}_{LF} & \tilde{i}_L & \tilde{v}_{CF} & \tilde{v}_o \end{bmatrix}^T$. The sign "~" above x denotes small variations in the corresponding signals. Moreover, $\tilde{d}$, $\tilde{v}_o$ and $\tilde{v}_{in}$ are the scalar quantities that represent small-signal variations in the duty cycle, output voltage and input voltage, respectively.

In order to reject small disturbances, an integral of the difference between output and reference voltage can be included in the feedback path so that the closed-loop steady-state error is zero. To implement this integral feedback, state-space system represented by (5.1a) and (5.1b) has to be augmented and the controller is then to be designed for the augmented system. The new system thus obtained is given below:

$$\dot{\tilde{x}}_a = A'\tilde{x}_a + B'\tilde{d} + G'\tilde{v}_{in} + H'\tilde{v}_{ref} \tag{5.2a}$$

$$\tilde{v}_o = C'\tilde{x}_a \tag{5.2b}$$

where $\tilde{x}_a$ represent the augmented state vector which includes integral term as an additional state variable. Hence the new system state becomes: $\tilde{x}_a = \begin{bmatrix} \tilde{i}_{LF} & \tilde{i}_L & \tilde{v}_{CF} & \tilde{v}_o & \tilde{e} \end{bmatrix}^T$, where $\tilde{e}$ is defined as:

$$\tilde{e} = \int_0^t (\tilde{v}_{ref} - \tilde{v}_o)\, dt \tag{5.3}$$

This model (5.2) will be used in the next section for the synthesis of state-feedback controller.

5.4.2 Controller Design

The objective of the controller is to guarantee the regulation of the output voltage to a constant reference and assure system stability in presence of input filter. It should also be robust to reject modest disturbances in the line voltage, load current and dc reference, while adapting to the changing operating point.

5.4.2.1 Stabilization with State-Feedback

Using the linear state-feedback technique, a control law can be defined as:

$$\tilde{d} = -k \cdot \tilde{x}_a \tag{5.4}$$

where $k = \begin{bmatrix} k_1 & k_2 & \cdots & k_5 \end{bmatrix}$ is the feedback gain vector which is to be determined. The state equations of the closed-loop system can now be written as:

$$\dot{\tilde{x}}_a = (A' - B'k)\tilde{x}_a + G'\tilde{v}_{in} + H'\tilde{v}_{ref} \tag{5.5a}$$

$$\tilde{v}_o = C'\tilde{x}_a \tag{5.5b}$$

Assuming that (A', B') is controllable, the dynamics of the closed-loop system can then be stabilized by an appropriate choice of eigenvalues of $(A' - B'k)$.

5.4.2.2 Pole-Placement

To evaluate feedback gains k_i, the eigenvalues of $(A' - B'k)$ can be assigned by a closed-loop pole-placement. One simple approach to do this is to calculate the characteristic polynomial of $(A' - B'k)$ and identify its coefficients using another polynomial that has the desired dominant poles p_i as its roots:

$$\det\left(sI - (A' - B'k)\right) = \prod_{i=1}^{n} (s - p_i) \tag{5.6}$$

where n is the number of poles to be placed. For any system with all zeros on the LHP of the s-plane, the eigenvalues can possibly be assigned such that the dominant poles are close to the zeros of the system. However, when the zeros are in the RHP (as in our case of filter-converter system), the dominant poles cannot be chosen close to the "unstable" zeros of the system [fra91]. In this case, for any RHP zero $z_i = \sigma_i + j\omega_i$ in the s-plane, the corresponding dominant pole can be located near the position $p_i = -\sigma_i + j\omega_i$. Nevertheless, if necessary the location of dominant poles can be modified to make it sufficiently far from the stability boundary.

5.4.2.3 Feedback Gain Adaptation to Load and Line Variations

Computation of the feedback gains can be adapted to varying operating points by a continuous evolution of the gain vector. This can be achieved by using 2D lookup tables indexed by input voltage and load resistance, as shown in Fig. 5.2. The lookup method used for the points between and beyond the stored values is interpolation and extrapolation. The value of load resistance can be estimated by measuring the load current. However, for this purpose an additional current sensor may be required.

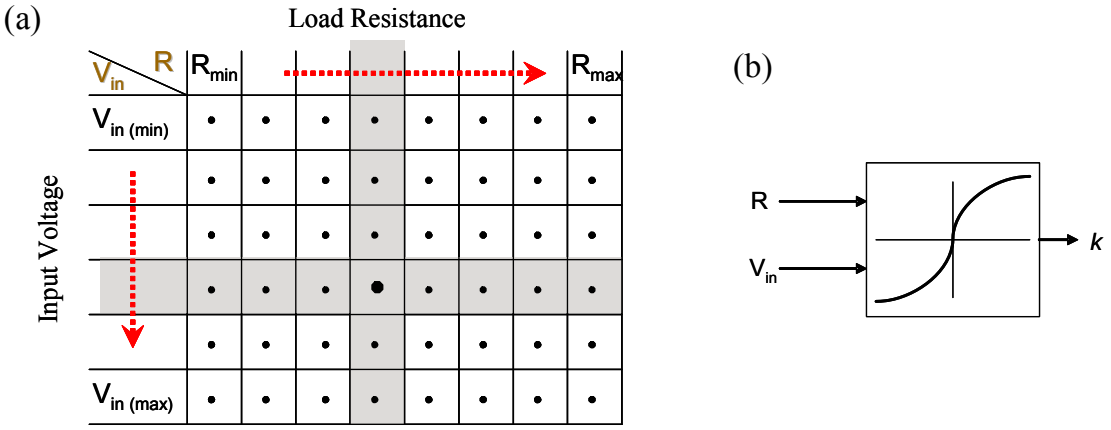

Fig. 5.2. (a): 2D-lookup table indexed by load resistance and input voltage; (b): Block symbol of a 2D lookup table.

5.4.3 Application Example: Buck Converter with Input Filter

A buck converter operating in CCM and having an input filter (see Fig. 5.1) is chosen as a plant to illustrate the control design and performance evaluation. For this converter, the matrix A' and vectors B', C', G' and H' of its augmented state-space model (as given by (5.2)) are presented hereafter:

$$
\begin{aligned}
A' &= \begin{bmatrix} 0 & 0 & -\frac{1}{L_F} & 0 & 0 \\ 0 & 0 & \frac{D}{L} & -\frac{1}{L} & 0 \\ \frac{1}{C_F} & -\frac{D}{C_F} & 0 & 0 & 0 \\ 0 & \frac{1}{C} & 0 & -\frac{1}{RC} & 0 \\ 0 & 0 & 0 & -1 & 0 \end{bmatrix} \\
B' &= \begin{bmatrix} 0 & \frac{V_{CF}}{L} & -\frac{I_L}{C_F} & 0 & 0 \end{bmatrix}^T \\
G' &= \begin{bmatrix} \frac{1}{L_F} & 0 & 0 & 0 & 0 \end{bmatrix}^T \\
H' &= \begin{bmatrix} 0 & 0 & 0 & 0 & 1 \end{bmatrix}^T \\
C' &= \begin{bmatrix} 0 & 0 & 0 & 1 & 0 \end{bmatrix}
\end{aligned}
\tag{5.7}
$$

In this representation, D, V_{CF} and I_L are the steady-state values of d, v_{CF} and i_L, respectively. The circuit parameters of the converter and nominal conditions are taken as: $L_F = L = 1mH$, $C_F = 4.7\mu F$, $C = 2\mu F$, $R = 10\Omega$, $f_s = 100kHz$, $V_{in} = 48V$ and $V_o = 24V$ ($D = 0.5$). The

simulated magnitude and phase response of its open-loop control-to-output transfer function is shown in Fig. 5.3. It can be noticed that the input filter resonance produces two complex zeros in the RHP and thus an additional phase lag of 360°. So it is evident that this system would exhibit instability if conventional controllers (e.g. PI regulators) are used and loop bandwidth is kept greater than filter resonant frequency.

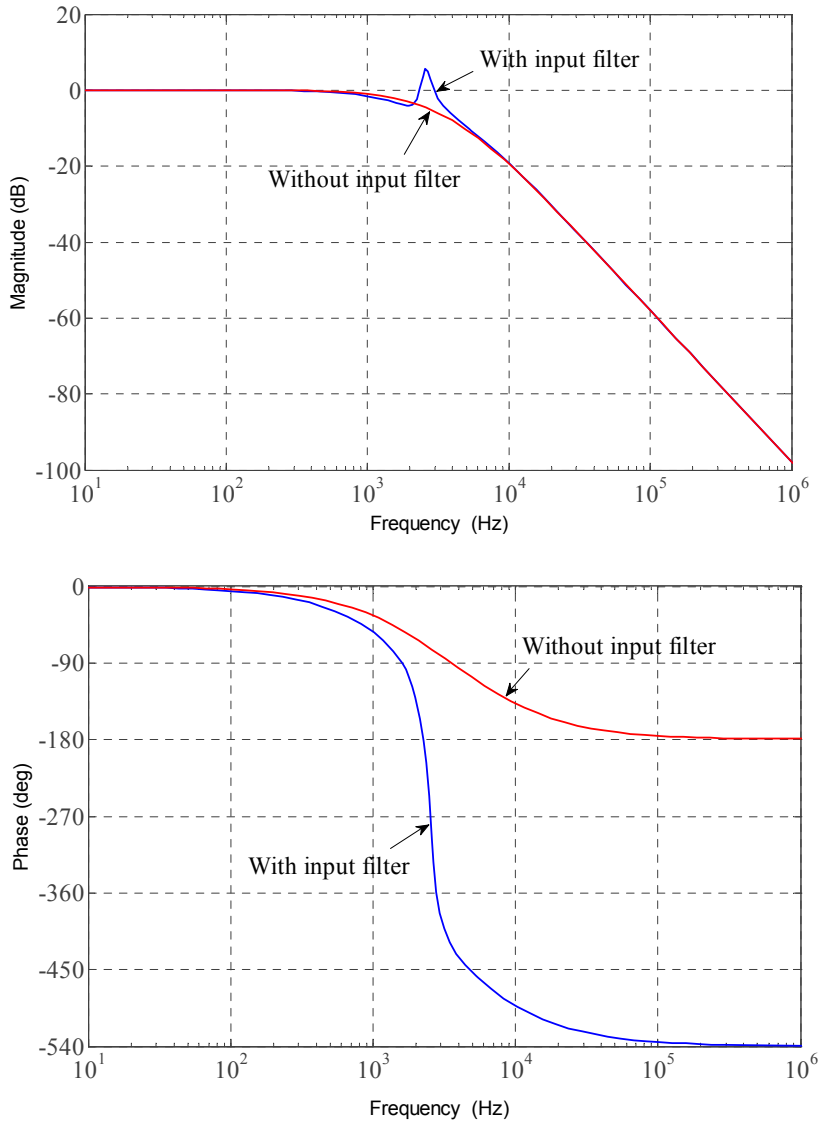

Fig. 5.3. Bode diagram of the open-loop control-to-output transfer function of the buck converter with and without input filter. (Parameter values: L_F=L=1mH, C_F=4.7μF, C=2μF, R=10Ω, f_s=100kHz, V_{in}=48V and V_o=24V, D = 0.5)

In order to achieve desired dynamic response, the poles of the closed-loop system are located at -0.5×10^4, $-2(1 \pm i)\times10^4$ and $-3(1 \pm i)\times10^4$. These pole locations correspond to 795Hz, 4.5kHz and 6.75kHz, respectively. Here it is worth mentioning that the linearized averaged models are generally valid up to about 1/3 of the switching frequency [dav06b] (f_s=100kHz in our case). Therefore, the dominant poles of the system are placed within this frequency range. The state-feedback and integral feedback-loop gains are calculated using (5.6). These gains are allowed to vary in order to adapt changes in the operating point. This is realized by using a 2D lookup table for each element of the gain vector, which is indexed by input voltage and load resistance.

5.4.3.1 Control Implementation

In order to investigate the performance of this control on a switching converter, the closed-loop system is simulated in the MATLAB/Simulink® environment using a switched model of the converter. The block diagram of this control system is depicted in Fig. 5.4, wherein complete switched model of a buck converter with input filter is represented by a single block. Such a control of this system is robust, i.e. $v_o - v_{ref} = 0$, for the steady-state operation as long as the system remains stable under its parameter variations. The controller mainly consists of two feedback loops: an integral loop and a state-feedback loop. The outputs of both loops are summed up before applying to the input of PWM generator, which controls the switch via gate-drive circuitry. The hardware implementation of the whole control scheme using state measuring sensors and moderate performance digital signal processor is feasible and should be studied in the future work.

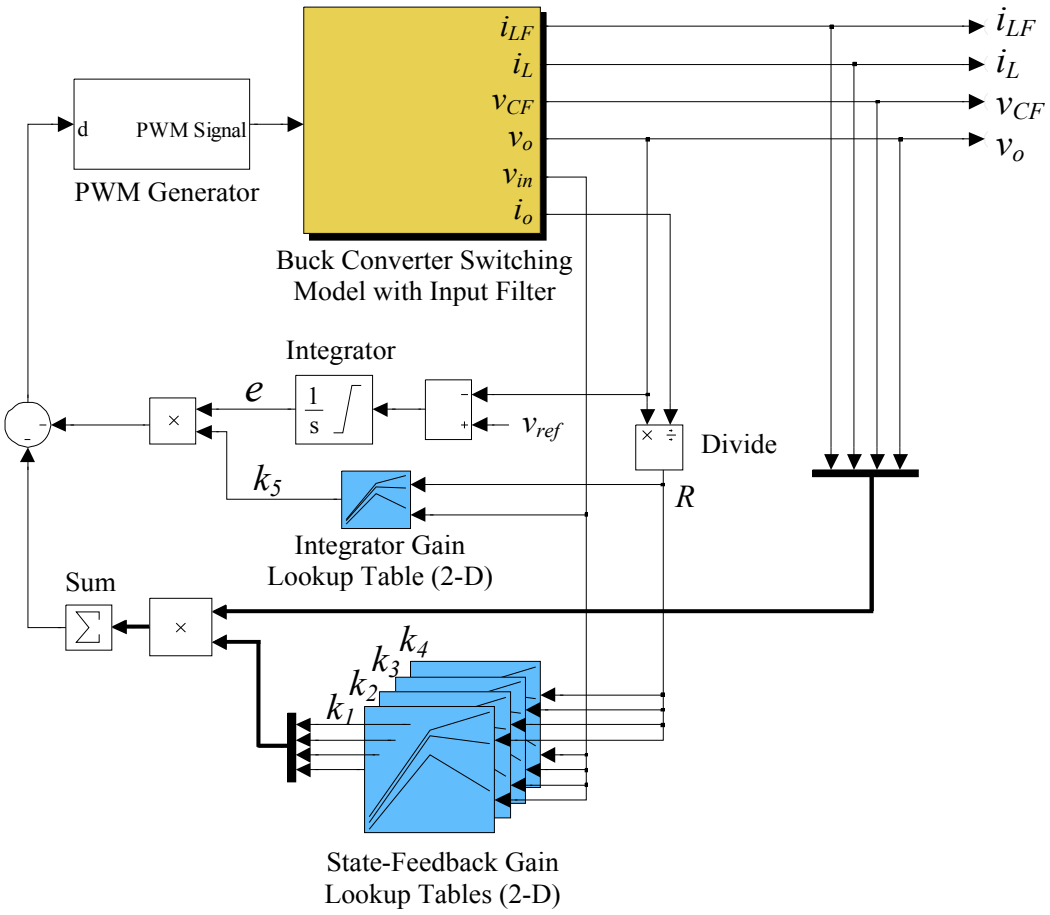

Fig. 5.4. Block diagram of a buck converter with state-feedback control.

5.4.3.2 Dynamic Response

The closed-loop system responses to the step changes in the input voltage, load current and dc voltage reference are shown in Fig. 5.5, Fig. 5.6 and Fig. 5.7 respectively. The corresponding variations in the control signal *d* are depicted in Fig. 5.8. The system is simulated for a buck converter with an input filter (without external damping) using the same nominal circuit parameters as used for simulation in Fig. 5.3. The results reveal that the proposed control is

advantageous in providing zero steady-state errors and guaranteed stable system even in presence of an undamped input filter. No passive components have been used in the filter circuit. It can also be seen that the responses are satisfactory in terms of overshoot, settling time, and fall time.

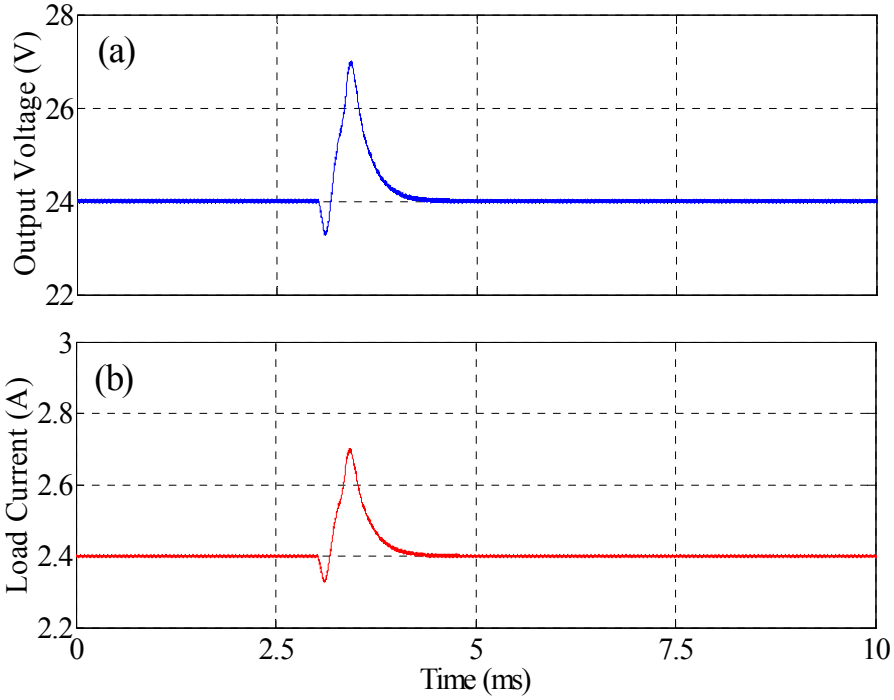

Fig. 5.5. Response to step increase in the input voltage (step size = 10V in 30μs); (a): Output Voltage, (b): Load Current. (Parameter values: $L_F = L = 1m$H, $C_F = 4.7\mu$F, $C = 2\mu$F, $R = 10\Omega$, $f_s = 100k$Hz, $D = 0.5$)

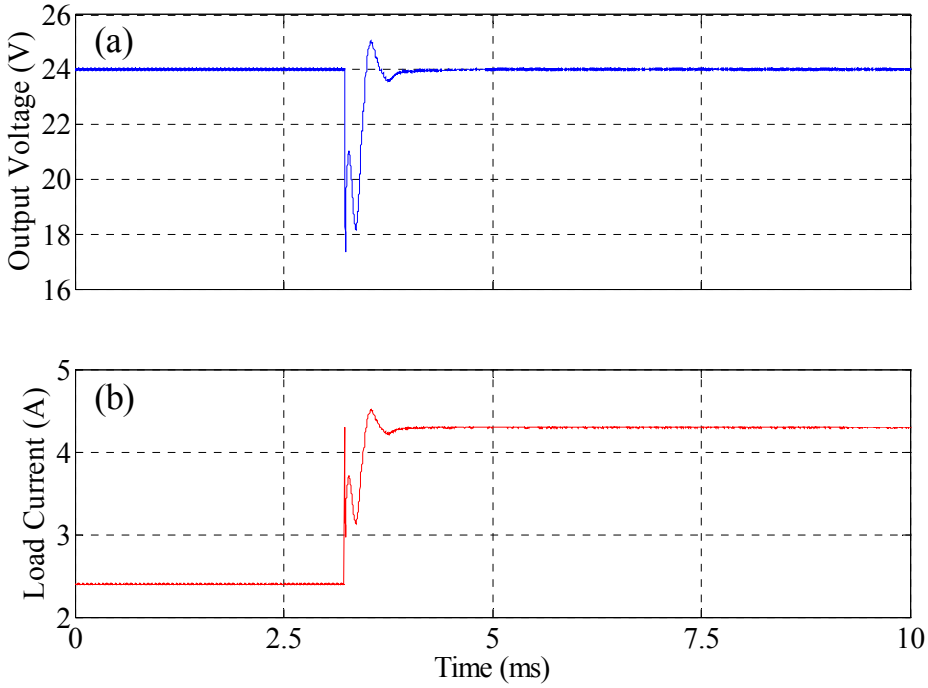

Fig. 5.6. Response to step increase in the load current (load is doubled its nominal value in 0s); (a): Output Voltage, (b): Load Current. (Parameter values: $L_F = L = 1m$H, $C_F = 4.7\mu$F, $C = 2\mu$F, $R_{nom} = 10\Omega$, $f_s = 100k$Hz, $D = 0.5$)

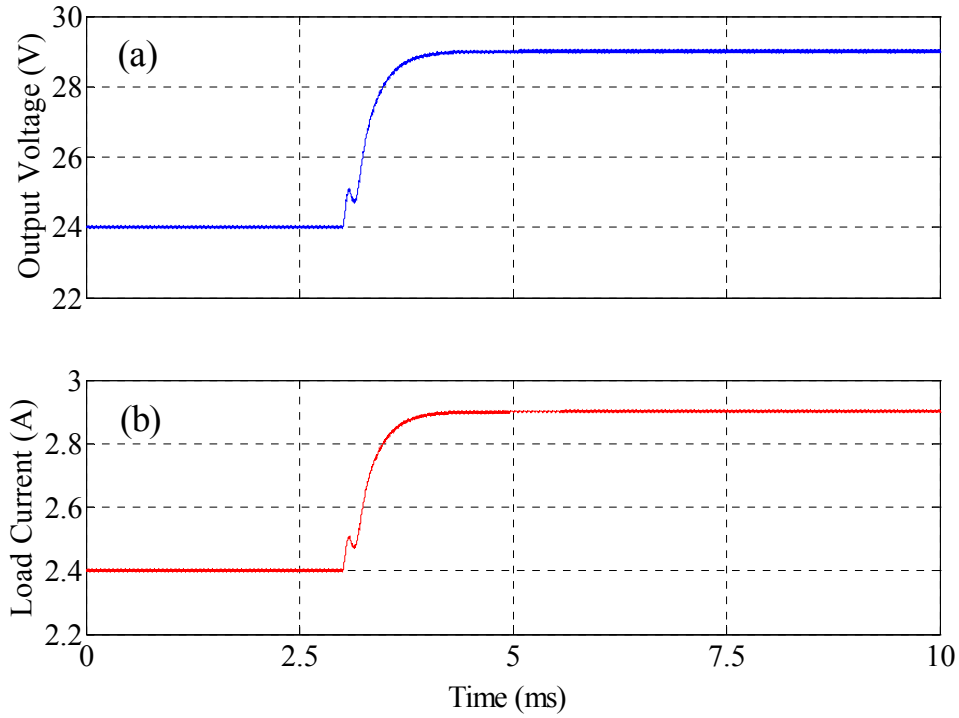

Fig. 5.7. Response to step increase in the dc reference voltage (step size = 5V in 0s); (a): Output Voltage, (b): Load Current. (Parameter values: $L_F = L = 1m\text{H}$, $C_F = 4.7\mu\text{F}$, $C = 2\mu\text{F}$, $R = 10\Omega$, $f_s = 100k\text{Hz}$)

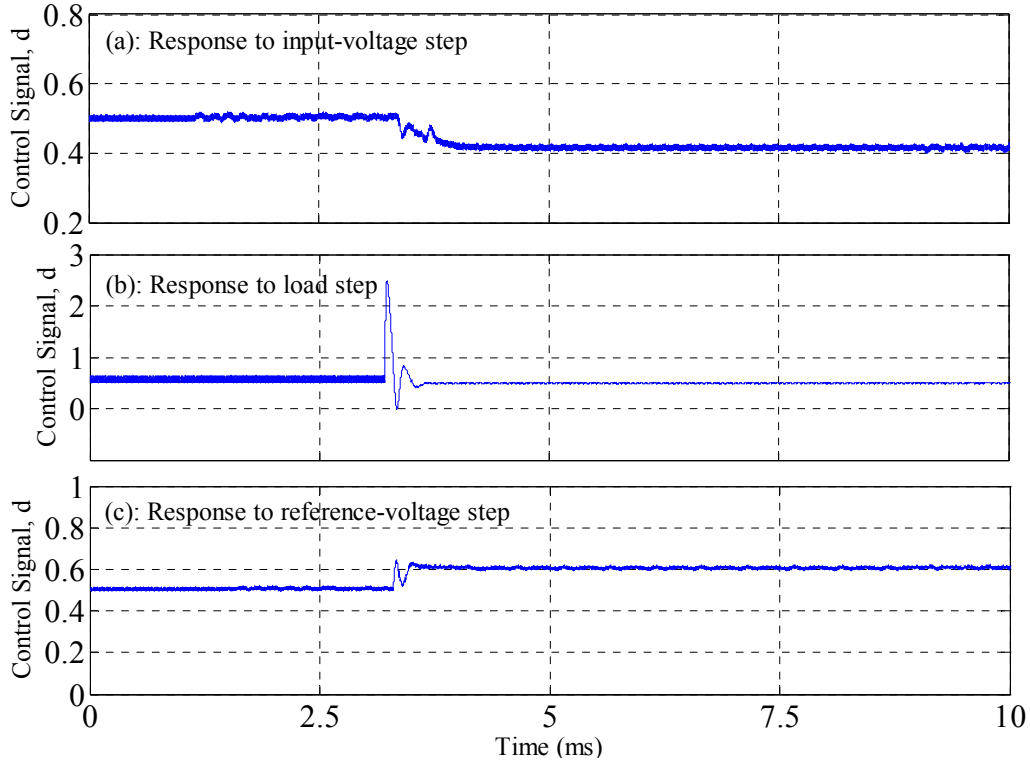

Fig. 5.8. Variations in duty cycle d; (a): Response to 10V step increase in the input voltage; (b): Response to $R_{nom}/2$ step decrease in the load resistance; (c): Response to 5V step increase in the reference voltage. (Parameter values: $L_F = L = 1m\text{H}$, $C_F = 4.7\mu\text{F}$, $C = 2\mu\text{F}$, $f_s = 100k\text{Hz}$, $v_o = 24\text{V}$, $v_{in\,(nom)} = 48\text{V}$, $R_{nom} = 10\Omega$)

5.4.3.3 Effect of Adaptive State-Feedback

The controller adapts efficiently to the line and load variations using lookup tables. A comparison between the varying gain state-feedback and a fixed gain state-feedback is depicted in Fig. 5.9 and Fig. 5.10. The corresponding evolution of feedback gains is shown in Fig. 5.11. It is noteworthy that the transient response is significantly improved by adapting feedback gains to the changing operating points. A faster response with smaller overshoots is observed under large load and line variations, as evident from Fig. 5.9 and Fig. 5.10, respectively. The lookup tables in the feedback path can be realized by storing only a few points and then implementing interpolation and extrapolation. The controller has simple structure and formal design procedure.

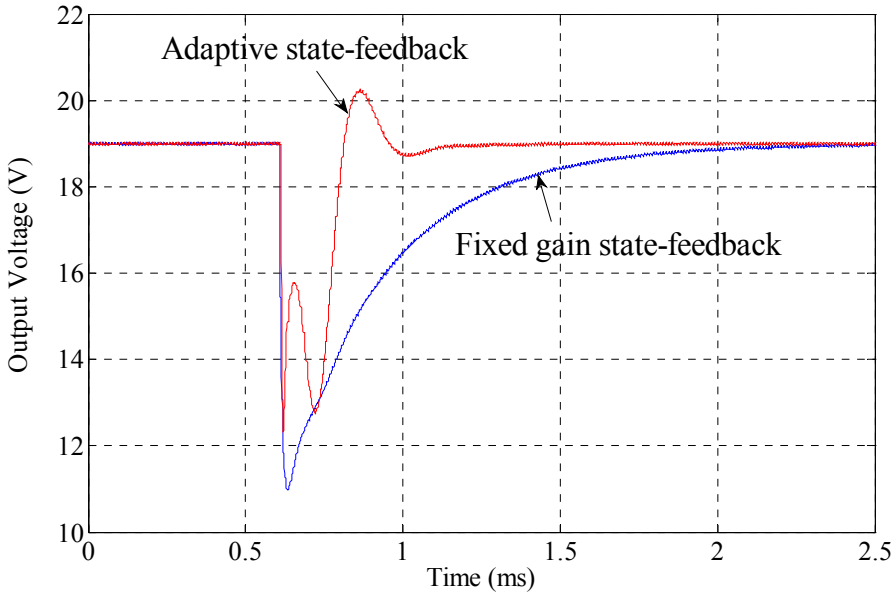

Fig. 5.9. Load to output step response for step size in $R = R/2$. (Parameter values: $L_F = L = 1m\text{H}$, $C_F = 4.7\mu\text{F}$, $C = 2\mu\text{F}$, $f_s = 100k\text{Hz}$, $v_{in} = 48\text{V}$, $v_{ref} = 19\text{V}$, $R_{nom} = 10\Omega$)

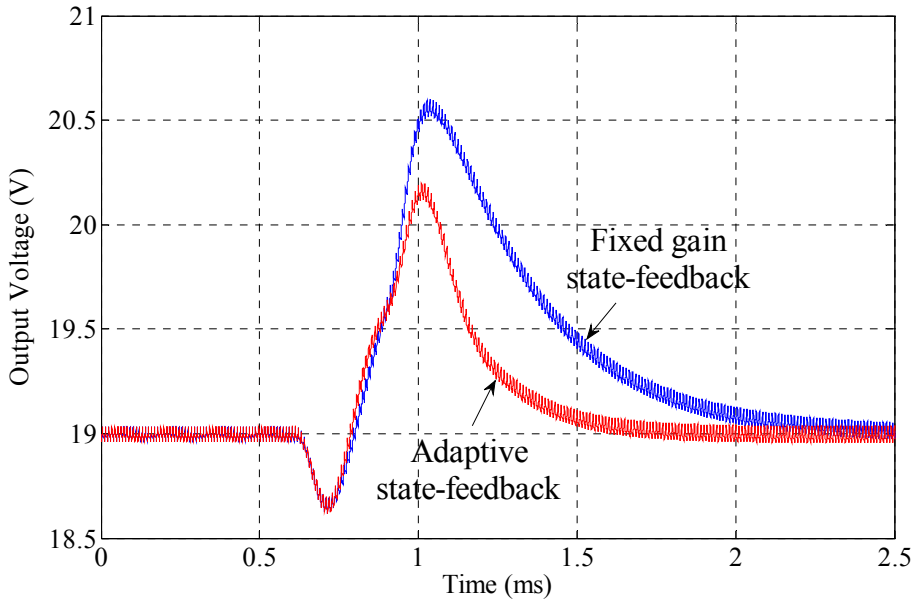

Fig. 5.10. Line to output step response for step size in $v_{in} = 10\text{V}$. (Parameter values: $L_F = L = 1m\text{H}$, $C_F = 4.7\mu\text{F}$, $C = 2\mu\text{F}$, $f_s = 100k\text{Hz}$, $R = 10\Omega$, $v_{ref} = 19\text{V}$)

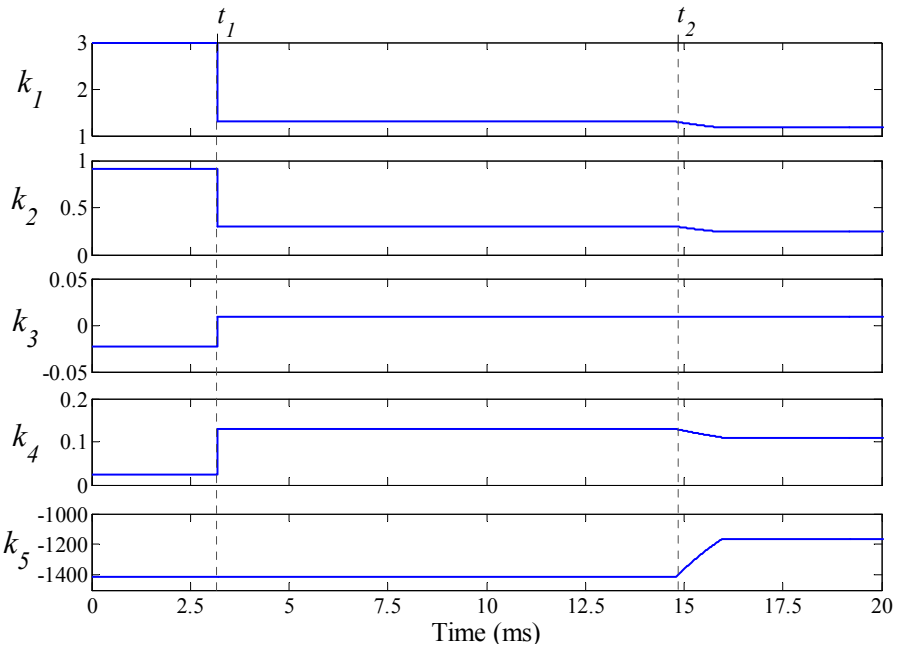

Fig. 5.11. Evolution of the gain vector with load and line changes; t_1: step in load, t_2: step in input voltage.

5.5 SLIDING-MODE CONTROL

5.5.1 Variable Structure Control of Nonlinear Systems

Previously we have based our control law on state-space linearized averaged model [usm08c]. The derivation of these models relies on the assumptions that the switching frequency is much greater than the natural frequency of the system and state variable ripples are small. However, modeling inaccuracies can have strong adverse effects on nonlinear control systems. One of the important approaches to deal with model uncertainty is to have a robust control system. In this context, Sliding-Mode approach for Variable Structure Systems (VSS) offers an alternate way to implement a control action which exploits inherent variable structure nature of dc-dc converters [hun93, spi97]. In particular, the converter switches are driven as a function of the instantaneous values of the state variables in such a way so as to force the system trajectory to stay on a suitable selected surface in the state-space. This surface is called "sliding surface" (or "switching surface"). The most remarkable feature of sliding-mode approach is its ability to result in very robust control systems. Furthermore, sliding-mode control design provides a systematic approach to deal with the problem of maintaining stability and a consistent performance in the face of modeling imprecision. The theory of Sliding-Mode Control (SMC) has been widely discussed in the literature for various applications [ahm03, hun93, mat97, utk93]. This control is also shown to be an efficient approach for the control of switch-mode power supplies and its application to basic converter structures is investigated in a number of publications [ahm03, bay03, nic95, ven85]. Therefore, without going into much detail, we outline only a brief introduction of sliding-mode control before presenting its application to the filter-converter system.

Consider a single-input nonlinear system represented by the following state equation:

$$\dot{x} = f(x) + g(x) \cdot u \ , \qquad u = \{0, 1\} \tag{5.8}$$

where x is the state of the system of order n, and $f(x)$, $g(x)$ are vector fields of dimension n. This equation describes the dynamic behavior of switched power converter with reversible

switches. The control input u defines the switch position of commutation cell. The two switches must be in opposite state at a given time.

A variable structure control law results in stable large-signal behavior of nonlinear systems described by (5.8). During sliding mode, the state trajectory tends asymptotically to the equilibrium point with a dynamic behavior imposed by the location of the switching surface in the state-space. The control design consists of choosing a sliding surface $s(x)$ associated with a commutation law on which a sliding motion with the desired dynamic performance can be created. Ideally, once intercepted, the control law maintains the state trajectory on the surface for all subsequent times and the state trajectory slides along this surface. The most important task is to design a switched control that will drive the system state to the switching surface and maintain it on the surface upon interception. A Lyapunov approach is usually used to characterize this task.

An ideal sliding mode exists only when the state trajectory $x(t)$ of the controlled plant agrees with the desired trajectory at every time. This may require infinitely fast switching as shown in Fig. 5.12a. However, in real systems a switched controller has imperfections which limit the switching to a finite frequency. The representative point then oscillates within a neighbourhood of the switching surface. This oscillation, called "chattering", is illustrated in Fig. 5.12b.

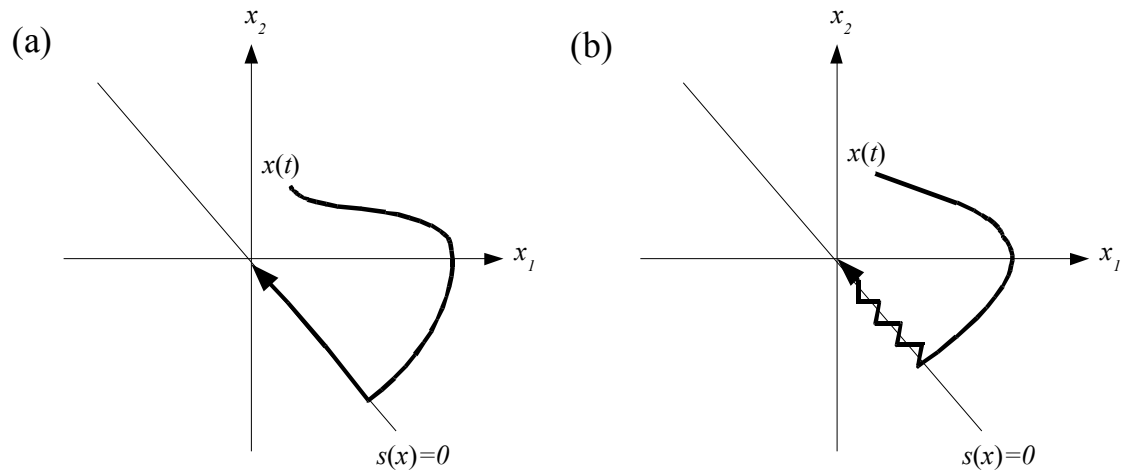

Fig. 5.12. (a): Ideal switching surface with infinite switching frequency, (b): Switching surface with hysteresis having finite switching frequency.

5.5.2 Control Design Based on Lyapunov Function Approach

Several methods have been proposed for the design of switching surface $s(x)$ [hun93, nic95, san92]. In this thesis, we have chosen a Lyapunov-Function approach which is presented in [nic95] for a buck converter with input filter. The only reason of choosing [nic95] from the literature is to discuss the performance of state-feedback scheme presented in this chapter in comparison to that of a sliding-mode controller. The design of sliding surface of [nic95] is outlined here for the ease of understanding[1]. In this approach, by choosing a positive defined Lyapunov function $V(x)$, which represents an energy quantity, a global condition of reachability can be given by:

$$\dot{V}(x) < 0 \qquad \text{when} \quad s(x) \neq 0 \tag{5.9}$$

[1] The reader is referred to [nic95] for further detail on this sliding-mode control design.

A linear transformation is necessary in order to describe the dynamic behavior of system (5.8) in terms of deviation from nominal values:

$$\begin{aligned} x &= X + \Delta x \\ u &= U_{eq} + \Delta u = \{0,1\} \end{aligned} \tag{5.10}$$

where U_{eq} represents the equivalent control which in case of infinitely fast switching action (i.e. ideal case) keeps the system stable on equilibrium point X. Note that the control input Δu remains a discontinuous value. The system description now reduces to:

$$\begin{aligned} \dot{x} = \Delta\dot{x} &= f(x) + g(x)U_{eq} + g(x)\Delta u \\ \Delta u &= \{-U_{eq}, 1 - U_{eq}\} \end{aligned} \tag{5.11}$$

The total stored energy in the reactive elements of the converter is given by:

$$W(t) = \frac{1}{2} x^T Q x \,, \qquad Q = Q^T > 0 \tag{5.12}$$

where Q is a symmetric positive definite matrix. Equivalently (5.12) can be written as (using (5.10) into (5.12)):

$$W(t) = \frac{1}{2} X^T Q X + \frac{1}{2} \Delta x^T Q \Delta x + \Delta x^T Q X \tag{5.13}$$

The second term $V(\Delta x) = ½\ \Delta x^T Q \Delta x$ is a positive defined quadratic function which can be chosen as a Lyapunov function [nic95, san92]. According to Lyapunov's theorem, nonlinear system (5.8) will be asymptotically stable if the total time derivative of V is negative. Differentiating V along the system trajectories and making use of (5.11), we obtain:

$$\dot{V}(\Delta x) = \Delta x^T Q f(x) + \Delta x^T Q g(x) U_{eq} + \Delta x^T Q g(x) \Delta u \tag{5.14}$$

Assuming that in ideal case the system (5.8), composed of ideal switches and linear passive and reactive elements, is stable in open loop with a constant control input (i.e. $\Delta u = 0$). Then it is evident that under these conditions the following will be true:

$$\Delta x^T Q f(x) + \Delta x^T Q g(x) U_{eq} \le 0 \tag{5.15}$$

A stabilizing control scheme for the regulated converter can then be obtained by choosing the control input Δu according to the value of $\Delta x^T Q\ g(x)$ such that the resulting expression (5.14) is always negative. Hence the feedback control law takes the form:

$$\begin{aligned} \Delta u &= \begin{cases} 0 - U_{eq} & \Delta x^T Q g(x) > 0 \\ 1 - U_{eq} & \Delta x^T Q g(x) < 0 \end{cases} \\ 0 &< U_{eq} < 1 \end{aligned} \tag{5.16}$$

or, equivalently we can write it as:

$$\begin{aligned} u &= \begin{cases} 1 & \mathrm{s}(x) > 0 \\ 0 & s(x) < 0 \end{cases} \\ \text{with} \quad s(x) &= -\Delta x^T Q g(x) \end{aligned} \tag{5.17}$$

The position of semiconductor switches is now defined as a function of the sign of $s(x)$. In case of infinitely high switching frequency, this commutation law induces a sliding motion on the switching surface $s(x) = 0$.

5.5.3 Application Example: Buck Converter with Input Filter

The dynamic behavior of a buck converter with an LC input filter (Fig. 5.1) is governed by the following state equation:

$$\dot{x} = f(x) + g(x) \cdot u \tag{5.18}$$

where:

$$\begin{aligned} x &= \begin{bmatrix} i_{LF} & i_L & v_{CF} & v_C \end{bmatrix}^T \\ f(x) &= \begin{bmatrix} \frac{v_{in} - v_{CF}}{L_F} & -\frac{v_C}{L} & \frac{i_{LF}}{C_F} & \frac{1}{C}\left(i_L - \frac{v_C}{R}\right) \end{bmatrix}^T \\ g(x) &= \begin{bmatrix} 0 & \frac{v_{CF}}{L} & -\frac{i_L}{C_F} & 0 \end{bmatrix}^T \\ u &= \{0,1\} \end{aligned} \tag{5.19}$$

The Lyapunov function V represents an energy quantity with the matrix Q chosen as:

$$Q = I \cdot \begin{bmatrix} L_F & L & C_F & C \end{bmatrix} \tag{5.20}$$

where I denotes the identity matrix of order $n = 4$ in this case.

5.5.3.1 Control Implementation

The control strategy developed in the previous section results in a commutation law of the form of (5.17). In [nic95], a sliding surface is obtained by imposing a reference current I_{ref} on the value of inductor current i_L. Hence, the application of (5.17) to this example of buck converter with input-filter would induce a sliding motion on the following surface:

$$s(x) = I_{ref} \frac{v_{CF}}{v_{in}} - i_L \tag{5.21}$$

However, this solution presents a disadvantage that the output voltage regulation is performed by imposing a reference current $I_{ref} = V_{ref}/R$. The dependency of sliding surface on i_L can be eliminated by modifying (5.21). Thus replacing i_L by $(i_C + v_C/R)$ yields:

$$s = \frac{1}{R}\left(V_{ref} \frac{v_{CF}}{v_{in}} - v_C\right) - i_C \tag{5.22}$$

where i_C is the current passing through the output capacitor C. The load resistance R now determines the dynamic behavior of the closed-loop system instead of a fixed reference current I_{ref}. Therefore, this control scheme presents another drawback that the dynamic performance depends upon the operating point. However, in [nic95] this parameter R is replaced by a constant value c_1 in order to impose the dynamic performance for a given nominal load R_N as follows:

$$\begin{aligned} s &= c_1 C\left(V_{ref} \frac{v_{CF}}{v_{in}} - v_C\right) - i_C \\ \text{with} \quad c_1 &= \frac{1}{R_N C} \end{aligned} \tag{5.23}$$

Reachability of sliding surface (5.23) is now accomplished by the control law (5.17) for the specific value of the load resistance $R = R_N$. Consequently, the closed-loop system will be stable even if the input filter presents no damping at all. Since stability is also ensured for the load resistance greater than R_N, R_N must be chosen as the nominal load resistance dissipating maximum output power.

A hysteresis-band control provides a simple way of realizing this control law resulting in operation at variable switching frequency. The control law (5.17) is based on the assumption of infinitely high switching frequency. In practical relay control systems, chattering appears during sliding-mode resulting in oscillations of the state trajectory around the sliding surface. Fig. 5.13 shows the schematic diagram of this sliding-mode controller for the buck converter with input filter. We have simulated the response of this controller using a switching model of the buck converter with undamped input filter (with nominal output power of about 60W). An experimental system was implemented in [nic95] to verify the effectiveness of this control method in which the controller was realized with simple analog-logic circuits[1]. Moreover, in [nic95] a damping resistance of $R_d = 39\Omega$ was still placed across the input inductance in order to improve the dynamic behavior of the regulator (this resistor is not used in our simulations). Nevertheless, the stability was ensured by the control law, rather than by the damping resistance.

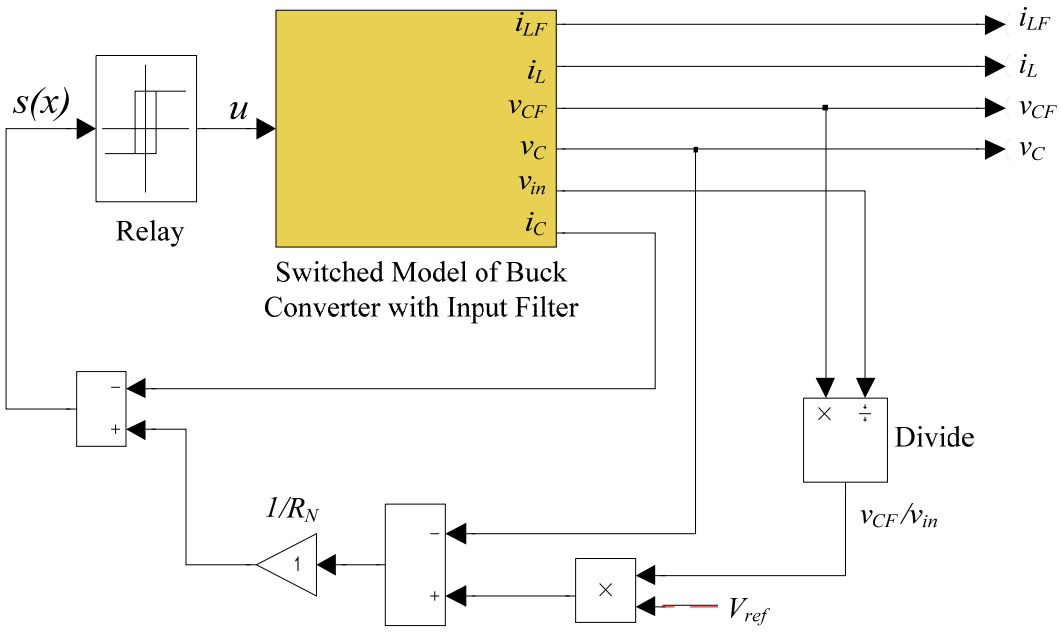

Fig. 5.13. Block diagram of a sliding-mode controller [**nic95**] for buck converter with input filter.

5.5.3.2 Dynamic Response

The transient response of the closed-loop buck converter (with undamped input filter) using sliding-mode control of Fig. 5.13 is shown in Fig. 5.14, Fig. 5.15 and Fig. 5.16. First of all, response to a step input is simulated in Fig. 5.14 for a 10V step change in the input voltage. Then, Fig. 5.15 shows the dynamic response for a step change in the load current, wherein the output power is doubled from 58W to 116W. Similarly, response to the step change in

[1] In [nic95], the control performance was evaluated for a buck converter with input filter having maximum output power of 5*k*W and maximum switching frequency of 20*k*Hz.

reference voltage is simulated in Fig. 5.16 for a 5V step size. In order to have a consistent comparison with the performance of full state-feedback control scheme, we have used the same circuit parameter values for the simulations in both cases. It is observable that the sliding-mode control can also give a performance robust enough to cope with the load, line and reference voltage variations. However, its detailed comparison with the proposed state-feedback controller is discussed in the next section.

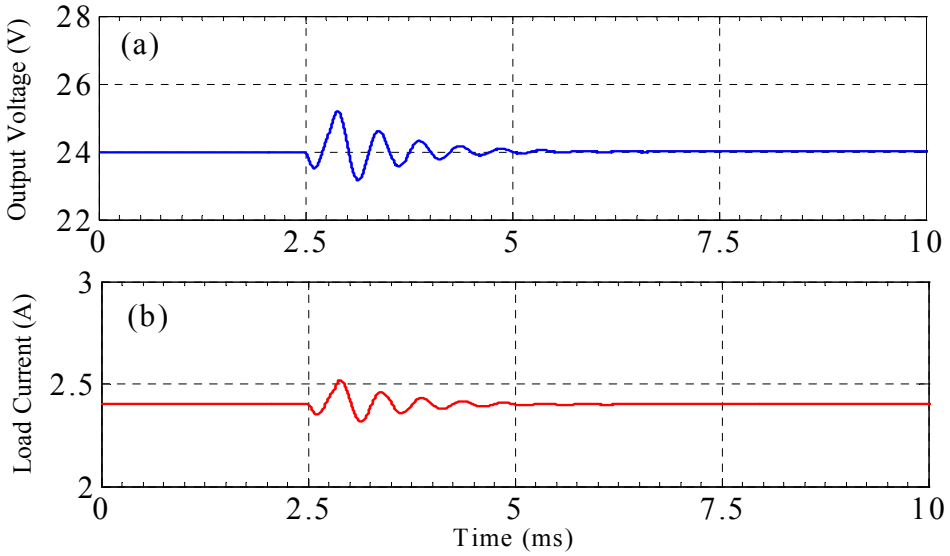

Fig. 5.14. Response to step increase in the input voltage (step size = 10V in 30μs); (a): Output Voltage, (b): Load Current. (Parameter values: $L_F = L = 1m$H, $C_F = 4.7\mu$F, $C = 2\mu$F, $R = 10\Omega$)

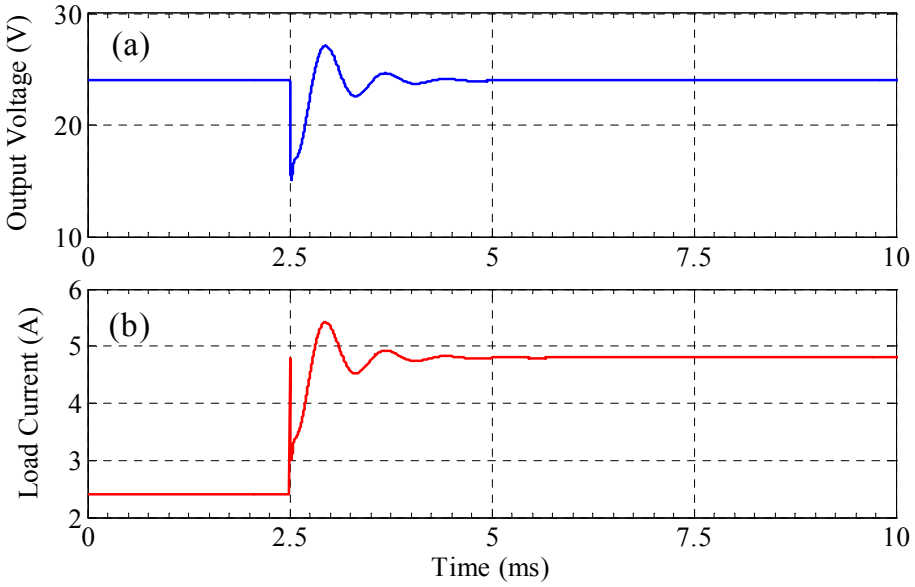

Fig. 5.15. Response to step increase in the load current (load is doubled its nominal value in 0s); (a): Output Voltage, (b): Load Current. (Parameter values: $L_F = L = 1m$H, $C_F = 4.7\mu$F, $C = 2\mu$F, $R_{nom} = 10\Omega$)

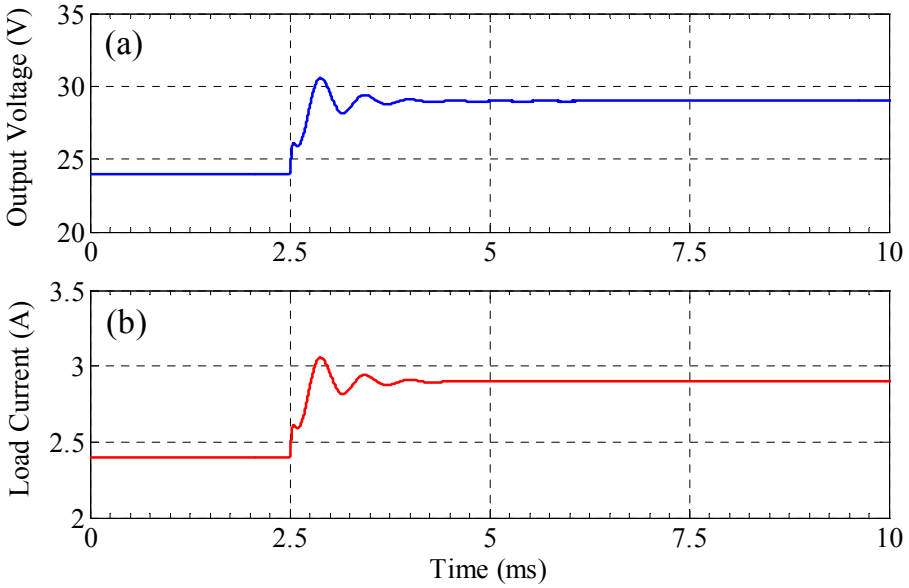

Fig. 5.16. Response to step increase in the dc reference voltage (step size = 5V in 0s); (a): Output Voltage, (b): Load Current. (Parameter values: $L_F = L = 1mH$, $C_F = 4.7\mu F$, $C = 2\mu F$, $R = 10\Omega$)

5.6 COMPARISON OF CONTROL SCHEMES

In order to carry out a comparative analysis of both control strategies presented in this chapter, the transient responses of both controllers are superimposed in Fig. 5.17. From this figure, it can be noticed that the dynamic performance of the proposed full state-feedback controller seems much better than that of sliding-mode controller (especially in terms of damping and settling time), except for its response to the line voltage variations (for which sliding-mode control has a better response). However, since a proper tool to analyse this inconsistency is not available, therefore its exact reason could not be clearly identified. Nevertheless, sliding-mode controller has some other disadvantages which are to be discussed in this section. As far as comparison of both control strategies is concerned, following important points are to be drawn:

1. First of all, sliding-mode control is a variable frequency control. Although robust sliding-mode controller is an efficient way to deal with the modeling inaccuracies of nonlinear systems, but variable switching frequencies are undesirable in many applications due to the problem of handling EMI/EMC. On the other hand, full state-feedback scheme proposed in this chapter uses a conventional PWM method with fixed switching frequency.
2. One of the underlying assumptions in the design of sliding-mode scheme is that the control law is discontinuous across sliding surface and can be switched from one value to another at infinitely high frequency. In practical systems, however, it is impossible to achieve such a high switching control that is necessary to most SMC designs. Since it is impractical to switch the control at infinite rate, a phenomenon called “chattering” occurs in the sliding-mode controlled system (see Fig. 5.12b). In the steady state, chattering appears as a high-frequency oscillation around the desired equilibrium point. Chattering is almost always objectionable since it involves high control activity and may excite high frequency dynamics which are neglected in the course of modeling.

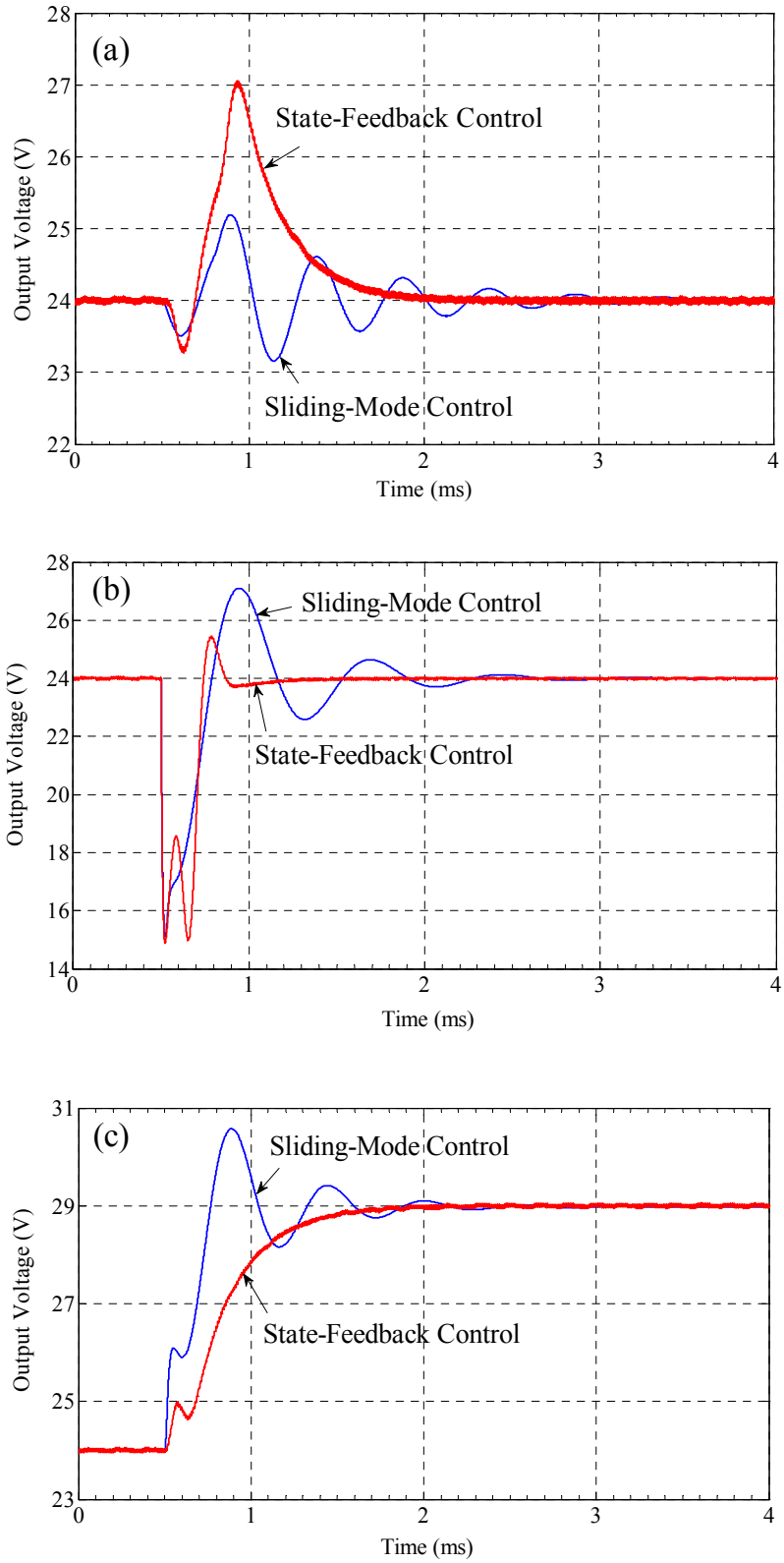

Fig. 5.17. Comparison between transient responses of sliding-mode control [**nic95**] and full state-feedback control [**usm08c**]; (a): Voltage response to step change in input voltage (step=10V), (b): Voltage response to step change in load (step=$R/2$), (c): Voltage response to step change in reference voltage (step=5V). (Parameter values: $L_F = L = 1m\text{H}$, $C_F = 4.7\mu\text{F}$, $C = 2\mu\text{F}$, $R = 10\Omega$)

3. The sliding mode control solution based on Lyapunov function approach (as presented in [nic95]) has another disadvantage. This is because the output voltage regulation in this scheme is performed by imposing a reference current $I_{ref} = V_{ref}/R$. Moreover, in order to make the sliding surface independent of the inductor current i_L, the output capacitor current i_C is introduced into the surface expression. This involves measurement of an additional current (which is not a state variable) and thus requires an extra current sensor. Whereas in state-feedback approach, the output voltage regulation is attained by directly imposing a reference voltage V_{ref}, so it inherently avoids these problems.
4. Moreover, the dynamic performance of the sliding-mode control method [nic95] depends upon the operating point. However this problem is solved in case of full state-feedback control, because its response can be adapted to the load and line variations using lookup tables in the feedback path.
5. Another drawback of sliding-mode control of [nic95] is that a transient output error can be observed due to the modification of the reference value by a factor of v_{CF}/v_{in}. Moreover, practically it still uses some damping resistance in the input-filter circuit to improve its transient response (though stability is ensured even without this extra damping resistance). On the other hand, the proposed state-feedback scheme does not have this problem because it is combined with an integral action in the feedback path to ensure a zero steady-state error.
6. However, one drawback of the proposed state-feedback solution is that its implementation in the present form requires measurement of the system state. Nevertheless, for the future work it is suggested to study the feasibility of using an observer for estimating the state variables of the system, thus reducing the number of required sensors in the circuit.

5.7 SUMMARY

In this chapter, at first place, a full state-feedback approach for stabilizing PWM dc-dc converters with input filters is presented. With this control algorithm, the overall system stability is retained and the transient dynamics remain satisfactory while no passive components are required in the filter circuit. The feedback gains are calculated using closed-loop pole-placement and an integral loop is also included in the feedback path to eliminate the steady-state error in the output. The controller adapts to the changing operating point conditions. This is accomplished by a continuous evolution of the feedback-gain vector using 2D-lookup tables which shows a great improvement over fixed gain state-feedback. This improvement is mainly reflected in a faster system response, especially under large disturbances. This control strategy assures stability without requiring any damping resistor in the filter circuit, so it can be considered a potential alternative to the passive damping solution. However, as an extension to this work, we suggest that inherent system parameter variations should be given special attention, since they can cause a shift in the system zeros. Moreover, the feasibility and performance of this controller should be evaluated with a state-estimating observer and its practical performance should be assessed using an experimental setup.

In the second place, the proposed state-feedback scheme is compared with a sliding-mode scheme which has already been reported in the literature for the same application (i.e. for buck converter with input filter). The pros and cons of both control methods are discussed and the comparison is based on the dynamic performance of both controllers as well as the underlying

assumptions in their design procedures. Although there are still problems to be investigated in sliding-mode controllers, SMC is naturally attractive to control engineers because its basic concepts are rather easy to understand and has given satisfactory performance in many practical areas of industrial electronics. More importantly, SMC is applicable to many control systems where no other design methods are well-developed.

Chapter 6

GENERAL CONCLUSIONS AND FUTURE PERSPECTIVES

6.1 MAJOR CONTRIBUTIONS OF THE THESIS

The major contributions of this thesis are listed below:

- First of all, a detailed state-of-the-art study of averaged modeling of dc-dc converters is carried out in this thesis, with special attention to the DCM operation. This comprehensive study covers almost all types of averaged models that have been proposed from the very beginning of this research field to the most recent developments. Thus it depicts an overall picture of the evolution of averaged modeling from reduced-order models to full-order models and then to corrected full-order models. Each type of averaged model (be it a state-space model or an equivalent-circuit model) can be categorized into one of these groups and salient characteristics of each of these groups are reviewed in this thesis.
- Averaging methodology is reviewed during this thesis in detail for its application to the DCM. Models of different orders are studied and their state-space equations are reformulated by including circuit parasitics. A frequency-domain comparison is then carried out between these models for both ideal and non-ideal cases. Accuracies of these models are investigated using an experimental prototype. As a result, the range of validity of each type of models is clearly defined in terms of frequency. Effects of some significant circuit parasitics on frequency-domain characteristics and high-frequency pole location are also studied. Predictions of different types of models in this regard are compared and discussed.
- A simple experimental methodology is proposed for a systematic validation of average models in frequency domain. This technique is based on the injection of small-signal perturbations in the control signal and subsequent measurements of the phase and gain variations. The experimental effectiveness of this method is successfully tested and demonstrated in the frequency range of interest (up to about 1/3 of switching frequency).
- Input-filter interaction problem is treated using small-signal averaged models. The instability problem originating from the interactions of input filter with converter control-loop is explained. A comprehensive literature survey is also carried out while discussing various works already reported in this field. As a first step, a conventional "passive" damping solution is discussed in detail for the treatment of this problem of instability. However, a new approach is proposed for the dimensioning of this damping circuit, which is based on the application of Routh-Hurwitz criterion to the numerator polynomial of open-loop transfer function. As a result, stability conditions are determined for each of the basic converter topologies. These conditions are also validated experimentally. Boundaries

between stable and unstable operations are clearly defined in terms of damping circuit parameters.

- Analysis of input-filter interactions is further extended to cascade converters. A case study of 2-stage cascade buck converter with an input filter is treated in detail. The damping-circuit design procedure as proposed for standalone converters is shown to be equally applicable to this specific case of cascade converters. However, new stability conditions are derived for this case and subsequently validated using an experimental prototype.
- Effect of damping losses on the converter efficiency are analyzed quantitatively in order to answer the criticism often faced by such type of passive solution. Power dissipation in the damping resistors is quantified under varying operating point condition and its influence on efficiency is shown as a function of damping resistance, load current and duty cycle. These results may greatly help a designer while making tradeoffs between efficiency-loss and the complexity of feedback control systems during design process.
- As one step forward to avoid the efficiency-loss due to passive damping, a control solution is proposed in this thesis. This active solution consists of a full state-feedback controller with pole-placement. The design of this control is based on an augmented state-space averaged model, whereas its dynamic performance is evaluated using a switched converter model. This control scheme is also robust and well-adapted to the load and line variations and has shown promising response to the large-signal perturbations. For comparison purposes, a variable structure control scheme based on sliding-mode and Lyapunov function approach is chosen from the literature. This scheme is also illustrated in this thesis and its transient behavior is simulated using a switched converter model. Finally the pros and cons of both control strategies are discussed for comparison.

6.2 SUGGESTIONS FOR FUTURE RESEARCH

Research is an on-going process and it's never evident to arrive at an ultimate solution of any problem. The research carried out in this thesis has contributed to answer some of the long-existed questions regarding modeling, input-filter interactions, damping losses, stability and control of converters. Progress is also made towards improvement of some already existing solutions, techniques and methodologies. However, more work is still needed in certain domains. Throughout the course of this PhD, several ideas and unresolved issues have been appearing into mind through research as well as through brainstorming. Based on those thoughts, some suggestions for the future areas of research are given as follows:

- Throughout this work, we have assumed a purely resistive load which is not always the case in practice. It can be interesting to study input-filter interactions with an active load in the future work.
- The formulation established in this thesis for input-filter interactions can also be extended to dc power distribution networks in which there are several converters connected in cascade and parallel combinations, with an LC filter present in-between two converters. However, significant research work on the stability analysis of such power distribution systems is already being done from various perspectives and different authors are using different approaches.
- Although damping power losses have been quantified in the R_d-C_d damping network in this thesis, however no optimum criterion could be proposed for the design of damping resistance to achieve the least efficiency degradation while still meeting stability conditions. The research must be continued on the passive damping circuits so that we

might come to propose a criterion for the optimal damping design from the efficiency viewpoint. However, as discussed in this thesis, several tradeoffs are involved in this issue of optimum damping design. So, apparently it is quite difficult to define a criterion which will be optimum from every point of view (i.e. size/weight, attenuation characteristics, stability, efficiency etc…)

- The state-feedback technique, as presented in this work, relies on the measurement of system state. However, in future, its feasibility should also be studied using a state-estimating observer in order to reduce number of sensors in the circuit and to deal with the issues related to measurement delays. The performance of such a state-feedback controller should also be evaluated on a hardware prototype.
- The idea of varying feedback gains presented in this thesis using lookup tables is quite preliminary and needs further investigation. Several questions such as: how the pole-placement can be optimized and how this variable-gain scheme can be refined and implemented in practice still need to be discussed thoroughly. One of the possible ways to realize this scheme can be to store some pre-determined gains corresponding to only a few operating points and then using interpolation and extrapolation. However, this approach can lead to significant errors if the variation in real gains is quite large. Another method for its realization can be to approximate each feedback gain with its corresponding polynomial function and then implement that polynomial function in the feedback path. Whether we use the first method or the second one or a combination of both, it is indispensable to develop appropriate methods for its systematic analysis, design and supervision.
- Proper tools for the analysis of robustness of the proposed state-feedback control need to be developed. Its robustness under different operating conditions, which are less frequent but fairly possible, should be studied. For example, how the controller will behave to the situation if the converter enters from CCM to the DCM or vice versa. The adaptability of the controller to the transitions from one conduction mode to the other need to be addressed in detail.
- Practical implementation of this controller should be given special attention in the future work. Feasibility of its digital implementation should be studied using any one of the available devices (i.e. DSP, Microcontroller, DSpic, FPGA…) depending upon its complexity, cost and other design related issues. Moreover, as it has been shown in this thesis that the output capacitor ESR has a significant influence on the converter dynamics, so it can be useful to incorporate this parasitic effect in the control design for the future work.
- The performance of the sliding-mode control essentially depends on the choice of switching surface. By introducing weighted derivative terms and taking account of the uncertainties associated with operating point and system parameters it is possible to improve its performance. Another possible solution for this problem is the passive control with its adaptive variant which would eliminate the problem of parametric uncertainties and would provide a self-convergence towards the operating point, thus damping the oscillations induced by the filter.
- A significant part of this thesis is dedicated to the accuracy investigation of averaged models and defining their limitations and constraints. Since it is proven now that linearized averaged models are not accurate at frequencies higher than about 1/2 of switching frequency, nonlinear or bilinear models should be considered if we need to predict converter behavior more accurately at higher frequencies (up to switching

frequency). Discrete-time models seem to be a suitable choice in this regard and their application for high-frequency control design is an interesting field for future research.

Appendices

APPENDIX A

Transfer Function Coefficients of Cascade Buck Converter Example

A.1 Coefficients of Transfer Function (3.44):

The coefficients A_k and B_k of the open-loop transfer function $G(s)$ given by (3.44) are listed below:

$$A_0 = 2D\left(r_2 + R'R - D^4(r_0 - 2r_{CF})\right)R'$$

$$A_1 = DR'\Big(D^2(C_1((r_2 + R'R)(r_0 - 2r_{CF}) + (r_1 - r_{C1})r_{C1} - L_1)) + (r_2 + R'R)(2C_2r_{C2} + 2C_Fr_0 + C_1(r_1 + r_{C1})) + D^4(2(C_Fr_{CF}^2 - L_F) - (r_0 - 2r_{CF})(2C_2r_{C2} + C_1r_{C1}))\Big)$$

$$A_2 = DR'\Big(-D^2C_2r_{C2}(2D^2L_F + L_1) + C_1(-D^4r_{C1}(C_2r_{C2}(r_0 - 2r_{CF}) + L_F) + (r_2 + R'R)(C_2r_{C2}(r_1 + r_{C1}) + L_1) + D^2(C_2((r_2 + R'R)(r_0 - 2r_{CF}) + (r_1 - r_{C1})r_{C1})r_{C2} + L_F(r_2 + R'R))) + C_F(-D^2(C_1(r_2 + R'R)r_{CF}^2 + r_0(L_1 - C_1r_{C1}(r_1 - r_{C1}))) + D^4r_{CF}^2(2C_2r_{C2} + C_1r_{C1}) + (r_2 + R'R)(2C_2r_{C2}r_0 + 2L_F + C_1r_0(r_1 + r_{C1})))\Big)$$

$$A_3 = DR'\Big(C_1C_2((D^2L_F + L_1)(r_2 + R'R) - D^4L_Fr_{C1})r_{C2} + C_F(C_1C_2D^4r_{CF}^2r_{C1}r_{C2} - D^2(C_2(C_1(r_2 + R'R)r_{CF}^2 + r_0(L_1 - C_1r_{C1}(r_1 - r_{C1})))r_{C2} + L_F(L_1 - C_1r_{C1}(r_1 - r_{C1}))) + (r_2 + R'R)(2C_2L_Fr_{C2} + C_1(L_1r_0 + (r_1 + r_{C1})(C_2r_0r_{C2} + L_F))))\Big)$$

$$A_4 = DR'C_F\left(C_1L_1L_FR'^2(r_2 + R'R) + (C_1L_FL_1R'(r_2 + R'R) + C_2(-D^2L_F(L_1 - C_1r_{C1}(r_1 - r_{C1})) + C_1(r_2 + R'R)(L_1r_0 + L_F(r_1 + r_{C1}))))r_{C2}\right)$$

$$A_5 = DC_FC_1C_2L_FL_1R'(r_2 + R'R)r_{C2}$$

$$B_0 = m$$

$$B_1 = \tfrac{1}{R'}\Big(C_2R(r_2 + D^4(r_0 - 2r_{CF}) + D^2(r_1 - 2r_{C1})) + R'(L_2 + (C_Fr_0 + C_1r_1)(r_2 + R'R) + D^4(L_F - C_Fr_{CF}^2) + D^2(L_1 + C_Fr_0(r_1 - 2r_{C1}) + C_1(r_0r_2 + R'Rr_0 - 2r_2r_{C0} - 2R'Rr_{CF} - r_{C1}^2)))\Big)$$

$$B_2 = \tfrac{1}{R'}\Big(C_2R(L_2 + C_Fr_0r_2 + C_1r_1r_2 + D^4(L_F - C_Fr_{CF}^2) + D^2(L_1 + C_Fr_0(r_1 - 2r_{C1}) + C_1(r_0r_2 - 2r_2r_{CF} - r_{C1}^2))) + R'(C_1(L_2r_1 + L_1(r_2 + R'R) + D^2(L_F(r_2 + R'R) + L_2(r_0 - 2r_{CF}))) + C_F(L_2r_0 + (L_F + C_1r_0r_1)(r_2 + R'R) + D^2(L_1r_0 + L_F(r_1 - 2r_{C1}) - C_1(r_2r_{CF}^2 + R'Rr_{CF}^2 + r_0r_{C1}^2))))\Big)$$

$$B_3 = \tfrac{1}{R'}\Big(C_1((D^2L_F + L_1)L_2R' + C_2R(L_2r_1 + L_1r_2 + D^2(L_2r_0 + L_Fr_2 - 2L_2r_{CF}))) + C_F(R'(C_1r_0(L_2r_1 + L_1(r_2 + R'R)) + L_F(L_2 + C_1r_1(r_2 + R'R) + D^2(-C_1L_2r_{CF}^2 + L_F(L_1 - C_1r_{C1}^2))) + C_2R(L_2r_0 + L_Fr_2 + C_1r_0r_1r_2 + D^2(L_1r_0 + L_F(r_1 - 2r_{C1}) - C_1(r_2r_{CF}^2 + r_0r_{C1}^2)))))\Big)$$

$$B_4 = \tfrac{1}{R'}\Big(C_1C_2(D^2L_F + L_1)L_2R + C_F(C_1R'(L_FL_2r_1 + L_1(L_2r_0 + L_Fr_2 + L_FR'R)) + C_2R(L_FL_2 + C_1L_2r_0r_1 + C_1L_1r_0r_2 + C_1L_0r_1r_2 + D^2(L_FL_1 - C_1L_2r_{CF}^2 - C_1L_Fr_{C1}^2)))\Big)$$

$$B_5 = \tfrac{1}{R'}\big(C_FC_1(C_2R(L_1L_2r_0 + L_FL_2r_1 + L_FL_1r_2) + L_FL_1L_2R'\big)$$

$$B_6 = C_FC_1C_2L_FL_1L_2(R + r_{C2})$$

A.2 Coefficients of Stability Conditions (3.47):

The coefficients a_k, b_k, c_k and d_k of stability inequalities given by (3.47) are all constant functions of circuit parameters (L_k, C_k, D, R and k), and are listed below:

$$a_0 = C_FL_FC_1L_1DR(1+k)$$

$$a_1 = -C_F^2L_FL_1D^3k$$

$$b_0 = -C_F^2L_F^2C_1L_1^2D^4(1+k)^2R$$

$$b_1 = C_F^2L_FL_1D^2k(C_FL_FL_1D^4(1+k) + C_1^2(L_1 + D^2L_F)kR^2)$$

$$b_2 = C_F^3L_F^2L_1D^4k^2R(C_1D^2 - 2C_F)$$

$$c_0 = C_F^2L_F^3C_1L_1^2D^5(1+k)^2(C_1D^2 - 2C_F(1+k))R^2$$

$$c_1 = C_F^2L_FL_1D^3kR(2C_F^2L_F^2L_1D^4(1+k)^2 - C_1^3(L_1 + D^2L_F)^2kR^2 + C_FL_FC_1D^2(1+k)(D^2L_1^2k + D^4L_1L_F(2k-1) + 2C_1L_FkR^2))$$

$$c_2 = -C_F^3L_FL_1D^5k^2(4C_F^2L_F^2(1+k)R^2 + C_1^2(L_1 + D^2L_F)(kL_1 + D^2L_F(2k-1)R^2 + C_FL_Fk(D^4L_1^2 + 2D^6L_1L_F - 4C_1L_1R^2 - 2C_1D^2L_FR^2))$$

$$c_3 = C_F^4L_F^2D^9L_1(4C_FL_F - C_1(L_1 + 2D^2L_F))k^3R$$

$$d_0 = -C_F^3L_F^4C_1^2L_1^3D^{11}(1+k)^3(C_1(L_1 + 2D^2L_F) - 4C_FL_F(1+k))R^3$$

$$d_1 = -C_F^3L_F^2C_1L_1^2D^7k(1+k)R^2(8C_F^2L_F^3D^6L_1(1+k)^2 + C_1^3(L_1 + D^2L_F)^2(L_1 + 2D^2L_F)kR^2 - 4C_1^2C_FL_F(L_1^2 + D^2L_1L_F - D^4L_F^2)k(1+k)R^2 + C_FL_FC_1L_1(1+k)(4D^8L_F^2(k-1) + D^4L_1^2k + 2D^6L_1L_F(2k-1) + 4C_FL_Fk(1+k)R^2)) + D^4L_1^2k + 2D^6L_1L_F(2k-1) + 4C_FL_Fk(1+k)R^2))$$

$$d_2 = C_F^4L_F^2L_1^2D^7k^2R(4C_F^2L_F^3L_1D^8(1+k)^2 + 2C_FL_FC_1^2L_1D^2(1+k)(L_1(k-4)k + D^2L_F(1-6k+2k^2))R^2 + C_FL_FC_1D^2(1+k)(2D^4L_1^3k + 2D^8L_F^2L_1(4k-1)D^6L_FL_1^2(8k-1) + 8C_FL_F^2D^2(1+k)R^2 + 8C_FL_FL_1k(1+k)R^2) + C_1^3R^2(D^2L_1^3k(2+k) + 2D^8L_F^3(2k^2 + 2k - 1) + D^4L_FL_1^2(5k^2 + 8k - 1) + D^6L_F^2L_1(8k^2 + 10k - 3) + 4C_FL_F^2k^2(1+k)R^2))$$

$$d_3 = -C_F^5 L_F^2 L_1^2 D^7 k^3 (4C_F^2 L_F^2 (1+k) R^2 (2D^6 L_F + D^4 L_1 k + + C_1 k R^2) + C_1^2 (L_1 + 2D^2 L_F) R^2 (-3D^8 L_F^2 + 2D^6 L_1 L_F (k-1) + D^4 L_1^2 k + 2L_1 C_1 k (1+k) R^2 + 2C_1 D^2 L_F k (1+k) R^2) + C_F L_F (4D^{10} L_F L_1^2 k + 4D^{12} L_1 L_F^2 k + 2C_1 D^4 L_1^2 k (2k-1) R^2 + 2C_1 L_1 D^6 L_F (3+4k^2) R^2 - 4C_1^2 D^2 L_F k R^4 - 8C_1^2 L_1 k (1+k) R^4 + D^8 (L_1^3 k + 4C_1 L_F^2 (2+k) R^2)))$$

$$d_4 = C_F^6 L_F^2 L_1^2 D^9 k^4 R (2C_1^2 (L_1 + 2D^2 L_F)(kL_1 - D^2 L_F) R^2 + 2C_F L_F (4D^8 L_F^2 + D^8 L_1^2 k + 2D^6 L_1 L_F (1+k) + 4C_F L_F k R^2) - C_1 L_F (D^6 L_1^2 + 4D^8 L_1 L_F + 4D^{10} L_F^2 + 8C_F L_1 k R^2 - 4C_F L_F D^2 (2+k) R^2))$$

$$d_5 = 2C_F^7 L_F^3 D^{13} L_1^2 (-4C_F L_F + C_1 (L_1 + 2D^2 L_F)) k^5 R^2$$

APPENDIX B

Mathematica® Codes for the Derivation of Transfer Functions

A computational software package, Mathematica® (versions 5.2 and 6.0), is exploited throughout this thesis for the symbolic computation of the transfer function expressions of complex and higher order systems. At many instances this package has also been used for the verification of the manually derived formulations, which greatly helped in double-checking the theoretical results of this thesis and avoiding possible human errors. A complete help and user guide for Mathematica® can be found in [ste03], which also includes a comprehenssive list of the Mathematica® functions. This guide is suitable for beginners as well as for expert users.

Only two Mathematica® scripts are listed in this Appendix for reference. These codes were originally written by the author of this thesis and were then reused frequently (with relevant modifications wherever necessary) during most part of this PhD.

B.1 Transfer Functions for CCM:

Following Mathematica® program code was generally used in this thesis for the derivation of small-signal transfer functions in CCM. Wherever it was necessary, appropriate modifications and extensions to this code were made for the specific cases. This example code is shown here for the case of an ideal buck converter with input filter[1].

*** Derivation of the small-signal transfer function of a lossless buck converter with input-fitler using its state matrices***

Remarks related to the notations used:
x is the state vector
y is the output voltage vo
u is the input voltage vin
d is the duty cycle of the switch
Lower case letters denote small-signal values, whereas upper case letters correspond to steady-state
A1, B1, C1 and D1 are the state-space matrices for the circuit when the switch is closed
A2, B2, C2 and D2 are the state-space matrices for the circuit when the switch is open
A, B, Cav and Dav are the state-space matrices averaged over a complete switching period T

[1] For other cases, only the elements of state-space matrices have to be modified accordingly, whereas rest of the code remains almost unchanged.

1st phase : Switch closed (During the periode dT)

In[1]:=
```
Clear[A1,B1,C1,D1,A2,B2,C2,D2,A,B,Cav,Dav];
```

$$A1 = \begin{pmatrix} 0 & -\frac{1}{LF} & 0 & 0 \\ \frac{1}{CF} & 0 & -\frac{1}{CF} & 0 \\ 0 & \frac{1}{L} & 0 & -\frac{1}{L} \\ 0 & 0 & \frac{1}{C} & -\frac{1}{RC} \end{pmatrix};$$

In[3]:=
$$B1 = \begin{pmatrix} \frac{1}{LF} \\ 0 \\ 0 \\ 0 \end{pmatrix};$$

$$C1 = (0\ 0\ 0\ 1);$$

$$D1 = (0);$$

$$x = \begin{pmatrix} iLF \\ vCF \\ iL \\ vC \end{pmatrix};$$

$$u = vin;$$

$$y = vo;$$

2nd phase : Switch open (During the period (1-d)T)

In[9]:=
$$A2 = \begin{pmatrix} 0 & -\frac{1}{LF} & 0 & 0 \\ \frac{1}{CF} & 0 & 0 & 0 \\ 0 & 0 & 0 & -\frac{1}{L} \\ 0 & 0 & \frac{1}{C} & -\frac{1}{RC} \end{pmatrix};$$

$$B2 = \begin{pmatrix} \frac{1}{LF} \\ 0 \\ 0 \\ 0 \end{pmatrix};$$

$$C2 = (0\ 0\ 0\ 1);$$

$$D2 = (0);$$

In[13]:=
```
(A = Simplify[d A1+(1-d) A2]) // MatrixForm
(B = Simplify[d B1+(1-d) B2]) // MatrixForm
(Cav = Simplify[d C1+(1-d) C2]) // MatrixForm
(Dav = Simplify[d D1+(1-d) D2]) // MatrixForm
```

Out[13]//MatrixForm=
$$\begin{pmatrix} 0 & -\frac{1}{LF} & 0 & 0 \\ \frac{1}{CF} & 0 & -\frac{d}{CF} & 0 \\ 0 & \frac{d}{L} & 0 & -\frac{1}{L} \\ 0 & 0 & \frac{1}{C} & -\frac{1}{CR} \end{pmatrix}$$

Out[14]//MatrixForm=
$$\begin{pmatrix} \frac{1}{LF} \\ 0 \\ 0 \\ 0 \end{pmatrix}$$

Out[15]//MatrixForm=
$$(0\ 0\ 0\ 1)$$

Out[16]//MatrixForm=
$$(0)$$

Calculation of Operating Point (Steady-state values)

In[17]:=
```
(Id = IdentityMatrix[4]) // MatrixForm;
(Ainv = Simplify[Inverse[A]]) // MatrixForm;
(U = (Vin)) // MatrixForm;
(X = Simplify[-Ainv.B.U]) // MatrixForm;
(Y = Simplify[Cav.X + Dav.U]) // MatrixForm;
```

Calculation of Transfer Function (small-signal)

* Input-to-output transfer function: vo / vin = Tyu
* Control-to-output transfer function: vo / d = Tyd (or element (1, 4) of vector Txd)

In[22]:=
```
(Txu = Simplify[Inverse[s Id - A].B]) // MatrixForm;
(Txd = Simplify[Inverse[s Id - A].((A1 - A2).X + (B1 - B2).U)]) // MatrixForm;
(Tyu = Simplify[Cav.Txu + Dav]) // MatrixForm;
(Tyd = Simplify[Cav.Txd + (C1 - C2).X + (D1 - D2).U]) // MatrixForm;
```

Literal Expressions of Transfer Functions

- **1) Gvovin: Transfer Function between output voltage vo and input voltage vin**

In[26]:=
```
Gvovin = FullSimplify[Tyu];
NumGvovin = Numerator[Gvovin];
DenGvovin = Denominator[Gvovin];
NumGvovinS = Collect[Expand[NumGvovin], s, Simplify];
DenGvovinS = Collect[Expand[DenGvovin], s, Simplify];
GvovinS = NumGvovinS / DenGvovinS
```

Out[31]=
$$\left\{\left\{\frac{d\,R}{R + (L + d^2\,LF)\,s + (CF\,LF + C\,(L + d^2\,LF))\,R\,s^2 + CF\,L\,LF\,s^3 + C\,CF\,L\,LF\,R\,s^4}\right\}\right\}$$

- **2) Gvod: Transfer Function between output voltage vo and duty cycle d**

In[32]:=
```
Gvod = FullSimplify[Tyd];
NumGvod = Numerator[Gvod];
DenGvod = Denominator[Gvod];
NumGvodS = Collect[Expand[NumGvod], s, Simplify];
DenGvodS = Collect[Expand[DenGvod], s, Simplify];
GvodS = NumGvodS / DenGvodS
```

Out[37]=
$$\left\{\left\{\frac{R\,Vin - d^2\,LF\,s\,Vin + CF\,LF\,R\,s^2\,Vin}{R + (L + d^2\,LF)\,s + (CF\,LF + C\,(L + d^2\,LF))\,R\,s^2 + CF\,L\,LF\,s^3 + C\,CF\,L\,LF\,R\,s^4}\right\}\right\}$$

B.2 Transfer Functions for DCM:

Following Mathematica® program code was generally used in this thesis for the derivation of small-signal models in DCM. This example code is shown here for the reduced-order model of a buck converter without input filter[1].

*** Derivation of the small-signal model of buck converter in DCM ***

1st Interval : Switch closed (During the period d*T)

```
In[1]:= Clear[A,A1,B1,C1,D1,A2,B2,C2,D2,A3,B3,C3,D3,A,B,Aav,Bav,Cav,Dav];
        A1 = {{0, -1/L}, {1/C, -1/(RC)}};
        B1 = {{1/L}, {0}};
        C1 = (0 1);
        D1 = (0);
        x = {{iL}, {vC}};
        u = (vin);
        y = (vo);
```

2nd Interval : Switch open (During the period d2*T)

```
In[9]:= A2 = {{0, -1/L}, {1/C, -1/(RC)}};
        B2 = {{0}, {0}};
        C2 = (0 1);
        D2 = (0);
```

3rd Interval: Switch and diode open (During the period (1-d-d2)*T)

```
        A3 = {{0, 0}, {0, -1/(RC)}};
        B3 = {{0}, {0}};
        C3 = (0 1);
        D3 = (0);
```

[1] For full-order and corrected full-order models, their respective duty-ratio constraints are to be used in place of d_2. Moreover, for corrected full-order models the correction matrix **M** has to be incorporated into the state-space equations, as explained in chapter 2.

In[17]:=
```
(Aav = Simplify[(d A1 + d2 A2 + (1-d-d2) A3)]) //MatrixForm
(Bav = Simplify[d B1 + d2 B2 + (1-d-d2) B3]) //MatrixForm
(Cav = Simplify[d C1 + d2 C2 + (1-d-d2) C3]) //MatrixForm
(Dav = Simplify[d D1 + d2 D2 + (1-d-d2) D3]) //MatrixForm
```

Out[17]//MatrixForm=

$$\begin{pmatrix} 0 & -\frac{d+d2}{L} \\ \frac{d+d2}{C} & -\frac{1}{CR} \end{pmatrix}$$

Out[18]//MatrixForm=

$$\begin{pmatrix} \frac{d}{L} \\ 0 \end{pmatrix}$$

Out[19]//MatrixForm=

$$\begin{pmatrix} 0 & 1 \end{pmatrix}$$

Out[20]//MatrixForm=

$$\begin{pmatrix} 0 \end{pmatrix}$$

Calculation of Operating Point (Steady-state values)

In[21]:=
```
(Id = IdentityMatrix[2]);
(Ainv = Simplify[Inverse[Aav]]) // MatrixForm;
(U = (Vin)) // MatrixForm;
(X = Simplify[-Ainv.Bav.U]) // MatrixForm;
(Y = Simplify[Cav.X + Dav.U]) // MatrixForm;
```

Calculation of Small-Signal State-Space Matrices

In[26]:=
```
StateEquations = Aav.x + Bav.u /. {d2 → d (vin - vC) / vC, iL → d T (vin - vC) / 2 L} // FullSimplify
```

Out[26]=

$$\left\{\{0\}, \left\{\frac{-2 L vC^2 + d^2 R T vin (-vC + vin)}{2 C L R vC}\right\}\right\}$$

In[27]:=
```
StateEq1[iL_, vC_, d_, vin_] = 0;
```

In[28]:=
```
coefEq1[iL_, vo_, d_, vin_] = D[StateEq1[iL, vC, d, vin], {{iL, vC, d, vin}}] // Simplify
```

Out[28]= {0, 0, 0, 0}

In[29]:=
```
StateEq2[iL_, vC_, d_, vin_] = (-2 L vC^2 + d^2 R T vin (-vC + vin)) / (2 C L R vC);
```

In[30]:=
```
coefEq2[iL_, vC_, d_, vin_] = D[StateEq2[iL, vC, d, vin], {{iL, vC, d, vin}}] // Simplify
```

Out[30]=

$$\left\{0, -\frac{\frac{2}{R} + \frac{d^2 T vin^2}{L vC^2}}{2 C}, \frac{d T vin (-vC + vin)}{C L vC}, -\frac{d^2 T (vC - 2 vin)}{2 C L vC}\right\}$$

In[31]:=
```
coef1IL = coefEq1[IL, VC, D, Vin][[1]] // Simplify;
```

In[32]:=
```
coef1VC = coefEq1[IL, VC, D, Vin][[2]] // Simplify;
```

In[33]:=
```
coef1d = coefEq1[IL, VC, D, Vin][[3]] // Simplify;
```

In[34]:=
```
coef2IL = coefEq2[IL, VC, D, Vin][[1]] // Simplify;
```

In[35]:=
```
coef2VC = coefEq2[IL, VC, D, Vin][[2]] // Simplify;
```

In[36]:=
```
coef2d = coefEq2[IL, VC, D, Vin][[3]] // Simplify;
```

```
In[37]:= A = {{coef1IL, coef1VC}, {coef2IL, coef2VC}} /. {IL → d Vin / R, VC → M Vin, D → M Sqrt[2 L / (R T (1 - M))]} // Simplify;

In[38]:= B = {{coef1d}, {coef2d}} /. {IL → d Vin / R, VC → M Vin, D → M Sqrt[2 L / (R T (1 - M))]} // Simplify;
```

Calculation of Small-Signal Transfer Functions

```
In[39]:= matrix = Id * s - A;

In[40]:= solution = LinearSolve[matrix, B] // Simplify;

In[41]:= Gvod = solution[[2]] // Simplify;

In[42]:= GvodS = Collect[Expand[Numerator[Gvod]], s, Simplify] /
          Collect[Expand[Denominator[Gvod]], s, Simplify]

Out[42]= {-(Sqrt[2] (-1 + M)^2 R T Sqrt[L / (RT - MRT)] Vin / (L (-2 + M) + C L (-1 + M) R s))}
```

APPENDIX C

MATLAB® Codes Used for Filtering the Measured Signals and their Phase-Shift Calculation

In Chapter 2, for the experimental acquisition of transfer function, output and control signals were differentially captured using a multi-channel oscilloscope and then treated in the MATLAB/Simulink® environment. In order to filter out unwanted noise from the measured signals and subsequently calculate the desired phase-shift, following MATLAB® code was written. This code further invokes a MATLAB® function named *peakdet.m* which is also given later in this Appendix.

```
% ================== Filename: TF_Measurement.m ====================
% MATLAB Code for Filtering Noise from the Measured Signals and then
% Calculating their Phase-Shift (Used in the Measurement of Transfer
% Function in Chapter 2)
% ==================================================================

output = csvread('TEK00000.csv'); % Reading the data file for output signal
control = csvread('TEK00001.csv');% Reading the data file for control signal

time = control(:,1);
c = control(:,2);
s = output(:,2);
couple = horzcat(c,s);
plot(time, couple)
hold on; grid on;

windowSize = 400;
x = filtfilt(ones(1,windowSize)/windowSize,1,c);
y = filtfilt(ones(1,windowSize)/windowSize,1,s);
plot(time, y, 'r', time, x, 'm')

% ============ Filtering is complete here ==================

Fs = 10e6;                  % Sampling frequency
T = 1/Fs;                   % Sample time
L = 10000;                  % No. of points in signals
t = (0:L-1)*T;              % Total duration of the signals

[maxtabx mintabx] = peakdet(x, 0.1);    % Detecting all peaks of signal x
[maxtaby mintaby] = peakdet(y, 0.05);   % Detecting all peaks of signal y
peaks1 = t(maxtabx(:,1));               % Time location of first peak of x
peaks2 = t(maxtaby(:,1));               % Time location of first peak of y

   Time = zeros(length(peaks1)-1,1);
   for i=1:length(peaks1)-1
```

```
      Time(i)=abs(peaks1(i)-peaks1(i+1));
   end
   Time = mean(Time)    % Average duration of one complete period (control)

firstPeakindex = 1;
timeDifference = zeros(length(peaks1)-(firstPeakindex+1),1);
j = 1;

% Finding Phase shift and converting it into degrees
% deltaT = mean(timeDifference)
% phaseShift = (360*deltaT)/Time

for k = firstPeakindex:length(peaks1)
   timeDifference(k) = abs(peaks1(k)-peaks2(k));
   phaseShift(j) = (360*timeDifference(k))/Time
   j = j+1;
end

averagephaseshift = mean(phaseShift)

figure
plot(x); hold on;

plot(mintab(:,1), mintab(:,2), 'g*');
plot(maxtab(:,1), maxtab(:,2), 'r*');

plot(y,'k');
plot(mintab1(:,1), mintab1(:,2), 'g*');
plot(maxtab1(:,1), maxtab1(:,2), 'r*');

% ================== End of file TF_Measurement.m ================


% ======================== Filename: peakdet.m ====================
function [maxtab, mintab]=peakdet(v, delta)
%PEAKDET Detects peaks in a vector
%        [MAXTAB, MINTAB] = PEAKDET(V, DELTA) finds the local
%        maxima and minima ("peaks") in the vector V.
%        A point is considered a maximum peak if it has the maximal
%        value, and was preceded (to the left) by a value lower by
%        DELTA. MAXTAB and MINTAB consists of two columns. Column 1
%        contains indices in V, and column 2 the found values.

maxtab = [];
mintab = [];
v = v(:); % Just in case this wasn't a proper vector

if (length(delta(:)))>1
  error('Input argument DELTA must be a scalar');
end

if delta <= 0
  error('Input argument DELTA must be positive');
end

mn = Inf; mx = -Inf;
mnpos = NaN; mxpos = NaN;
lookformax = 1;
```

```
for i=1:length(v)
  this = v(i);
  if this > mx, mx = this; mxpos = i; end
  if this < mn, mn = this; mnpos = i; end

  if lookformax
    if this < mx-delta
      maxtab = [maxtab ; mxpos mx];
      mn = this; mnpos = i;
      lookformax = 0;
    end
  else
    if this > mn+delta
      mintab = [mintab ; mnpos mn];
      mx = this; mxpos = i;
      lookformax = 1;
    end
  end
end

% ==================== End of file peakdet.m ===============
```

Bibliography

BIBLIOGRAPHY

[ahm03] M. Ahmed, M. Kuisma, K. Tolsa, and P. Silventoinen, "Implementing sliding mode control for buck converter," in *34th IEEE Power Electronics Specialist Conf. (PESC'03)*, volume 2, pp. 634–637, Jun. 2003.

[alf99] M. Alfayyoumi, A. H. Nayfeh, and D. Borojevic, "Input filter interactions in dc-dc switching regulators," in *IEEE Power Electronics Specialists Conf. (PESC'99)*, volume 2, pp. 926–932, Jun. 1999.

[alm04] S. Almer, U. Jonsson, Chung-Yao Kao, and J. Mari, "Global stability analysis of dc-dc converters using sampled-data modeling," in *Proc. of the American Control Conference*, volume 5, pp. 4549–4554, Jun-Jul. 2004.

[alt04] A. Altowati, K. Zenger, and T. Suntio, "Dynamic analysis of a buck converter with input filter via polynomial representation approach," in *Nordic Workshop on Power and Industrial Electronics (NORPIE'04)*, pp. 1-7, Jun. 2004.

[art01] F. Arteche, B. Allongue, F. Szoncso, and C. Rivetta, "EMI filter design and stability assessment of dc voltage distribution based on switching converters," in *Proc. of 7th Workshop on Electronics for LHC Experiments*, pp. 353–357, Stockholm, Sep. 2001.

[asm02] PC Krause and Associates Inc., *Automated State Model Generator*, 2002, Version 2, Available Online: http://www.pcka.com.

[bar02] P. Barrade, C. Turpin, and H. Piquet, "Stabilisation d'un ensemble convertisseur-filtre," *Revue Internationale de Génie Électrique (France)*, 5/3-4: pp. 557–577, 2002. ISSN: 1295-490X.

[bar96] P. Barrade, H. Piquet, and Y. Chéron, "Méthode d'étude de la stabilité des ensembles convertisseurs-filtres," *Journal de Physique III, France*, 6(1): pp. 91–104, Jan. 1996.

[bay03] E. H. E. Bayoumi, "A simplified method for controlling dc-dc converters using sliding mode control," in *22nd IASTED International Conference on Modeling, Identification and Control (MIC'03)*, pp. 1–6, Feb. 2003.

[ben94] S. Ben-Yaakov, D. Wulich, and W. M. Polivka, "Resolution of an averaging paradox in the analysis of switched-mode dc–dc converters," *IEEE Trans. on Aerospace and Electronic Systems*, 30: pp. 626–632, Apr. 1994.

[bie71] Y. Yu and J. J. Biess, "Some design aspects concerning input filters for dc-dc converters," in *IEEE Power Conditioning Specialists Conf.*, pp. 66–76, Record 1971.

[byu99] C. Byungcho, B. H. Cho, and H. Sung-Soo, "Dynamics and control of dc-to-dc converters driving other converters downstream," *IEEE Trans. on Circuits and Systems I: Fundamental Theory and Applications*, 46(10): pp. 1240–1248, Oct. 1999.

[cal02] J. Calvente, L. M. Salamero, P. Garces, and A. Romero, "Input filter damping design using zero dynamics analysis," in *6th European Space Power Conference*, pp. 6–10, May 2002.

[che01] J. Chen, R. Erickson, and D. Maksimovic, "Averaged switch modeling of boundary conduction mode dc-to-dc converters," in *27th IEEE IECON*, pp. 844–849, 2001.

[che81] P. R. K. Chetty, "Current injected equivalent circuit approach (CIECA) to modeling of switching dc-dc converters in continuous inductor conduction mode," *IEEE Trans. on Aerospace and Electronic Systems*, AES-17(6): pp. 802–808, Nov. 1981.

[che82] P. R. K. Chetty, "Current injected equivalent circuit approach (CIECA) to modeling of switching dc-dc converters in discontinuous inductor conduction mode," *IEEE Trans. on Ind. Electron.*, IE-29(3): pp. 230–234, Aug. 1982.

[cho91] B. H. Cho and B. Choi, "Analysis and design of multi-stage distributed power systems," in *IEEE International Telecommunication Energy Conf. (INTELEC)*, pp. 220–226, Nov. 1991.

[cho95] B. Choi and B. H. Cho, "Intermediate line filter design to meet both impedance compatibility and EMI specifications," *IEEE Trans. on Power Electronics*, 10(5): pp. 583–588, 1995.

[chu75] L. O. Chua and P. M. Lin, *Computer-Aided Analysis of Electronic Circuits, Algorithms and Computational Techniques*. Englewood Cliffs, NJ: Prentice-Hall, 1975.

[chu99] Chung-Chieh Fang and E. H. Abed, "Sampled-data modeling and analysis of closed-loop PWM dc-dc converters," in *IEEE International Symposium on Circuits and Systems*, volume 5, pp. 110–115, 1999.

[cuk77] S. Cuk and R. D. Middlebrook, "A general unified approach to modeling switching dc-to-dc converters in discontinuous conduction mode," in *IEEE Power Electron. Spec. Conf.*, pp. 36–57, Jun. 1977.

[cza95] D. Czarkowski, L. R. Pujara, and Marian K. Kazimierczuk, "Robust stability of state-feedback control of PWM dc-dc push-pull converter," *IEEE Trans. on Industrial Electronics*, 42(1): pp. 108–111, Feb. 1995.

[dah02] P. A. Dahono, "A control method to damp oscillation in the input LC filter of ac-dc PWM converters," in *IEEE Power Electronics Specialists Conf. (PESC)*, volume 4, pp. 1630-1635, 2002.

[dav06a] A. Davoudi and J. Jatskevich, "Realization of parasitics in state-space average-value modeling of PWM dc-dc converters," *IEEE Trans. on Power Electron.*, 21(4): pp. 1142–1147, Jul. 2006.

[dav06b] A. Davoudi, J. Jatskevich, and T. De Rybel, "Numerical state-space average-value modeling of PWM dc/dc converters operating in DCM and CCM," *IEEE Trans. on Power Electron.*, 21(4): pp. 1003–1012, Jul. 2006.

[eri01] R. W. Erickson and D. Maksimovic, *Fundamentals of Power Electronics*. Norwell, MA: Kluwer, 2nd edition, 2001.

[eri92] S. Y. Erich and W. M. Polivka, "Input filter design criteria for current-programmed regulators," *IEEE Trans. on Power Electronics*, 7(1): pp. 143–151, Jan. 1992.

[eri99] R. W. Erickson, "Optimal single-resistor damping of input filters," in *IEEE Applied Power Electronics Conf.*, pp. 1073–1079, Mar. 1999.

[fra91] Frank H. F. Leung, Peter K. S . Tam, and C. K. Li, "The control of switching dc-dc converters – a general LQR problem," *IEEE Trans. on Industrial Electronics*, 38(1): pp. 65–71, Feb. 1991.

[gar94] F. Garofalo, P. Marino, S. Scala, and F. Vasca, "Control of dc-dc converters with linear optimal feedback and nonlinear feedforward," *IEEE Trans. on Power Electronics*, 9(6): pp. 607–615, Nov. 1994.

[gho96] E. W. Gholdston, K. Karimi, F. C. Lee, J. Rajagopalan, Y. Panov, and B. Manners, "Stability of large dc power systems using switching converters with application to the international space station," in *31st IEEE Intersociety Energy Conversion Engineering Conf. (IECEC)*, volume 1, pp. 166–171, Aug. 1996.

[han06a] M. Hankaniemi, M. Karppanen, and T. Suntio, "EMI-filter interactions in a buck converter," in *12th EPE-PEMC'06*, pp. 54–59, Aug. 2006.

[han06b] M. Hankaniemi, T. Suntio, and M. Karppanen, "Load and supply interactions in VMC-buck converter operating in CCM and DCM," in *IEEE Power Electronics Specialists Conf. (PESC'06)*, pp. 1–6, 2006.

[hul89] F. Huliehel and S. Ben-Yaakov, "Low-frequency sampled-data models of switched mode dc-dc converters," in *20th IEEE Power Electronics Specialists Conf.*, pp. 492–499, Jun. 1989.

[hun93] J. Y. Hung, W. Gao, and J. C. Hung, "Variable structure control: a survey," *IEEE Trans. on Industrial Electronics*, 40(1): pp. 2–22, 1993.

[jan92] Y. Jang and R. W. Erickson, "Physical origins of input filter oscillations in current programmed converters," *IEEE Transactions on Power Electronics*, 7(4): pp. 725–733, Oct. 1992.

[jat00] J. Jatskevich, O. Wasynczuk, E. A. Walters, and C. E. Lucas, "Continuous state-space modeling of switched electric networks," in *Proc. IEEE International Conference on Control Applications*, pp. 902–907, 2000.

[jat04] J. Jatskevich and T. Aboul-Seoud, "Automated state-variable formulation for power electronic circuits and systems," in *Proc. IEEE Int. Symposium on Circuits and Systems (ISCAS'04)*, volume 5, pp. 952–955, 2004.

[jos98] M. Joshi and V. Agarwal, "Generation and propagation of EMI waves in power electronic circuits," in *IEEE Power Electronics Specialists Conf. (PESC'98)*, volume 2, pp. 1165–1171, May 1998.

[kar03] C. Karimi, D. Sadarnac, and C. Prévot, "On the interaction of the input filter and the converter regulation," in *EPE-Toulouse*, pp. 163–168, Sep. 2003.

[kel82] S. S. Kelkar and F. C. Lee, "A novel input filter compensation scheme for switching regulators," in *IEEE Power Electronics Specialists Conf. (PESC'82)*, pp. 260–271, Rec. 1982.

[kel83] S. S. Kelkar and F. C. Lee, "A novel feedforward compensation canceling input filter-regulator interaction," *IEEE Trans. on Aerospace and Electronic Systems*, 19: pp. 258–268, Mar. 1983.

[kel84a] S. S. Kelkar and F. C. Lee, "Adaptive input filter compensation for switching regulators," *IEEE Trans. on Aerospace and Electronic Sys.*, AES-20(1): pp. 57–66, Jan. 1984.

[kel84b] S. S. Kelkar and F. C. Lee, "Stability analysis of a buck regulator employing input filter compensation," *IEEE Trans. on Aerospace and Electronic Systems*, AES-20(1): pp. 67–77, Jan. 1984.

[kim05] D. Kim, B. Choi, D. Lee, and J. Sun, "Analysis of input filter interactions in switching power converters," in *IEEE Applied Power Electronics Conf. (APEC)*, volume 1, pp. 191–198, March 2005.

[kis94] A. Kislovski, R. Redl, and N. Sokal, *Analysis of Switching-Mode DC-DC Converters*. New York: Van Nostrand Reinhold, 1994.

[koh92] C. R. Kohut, "Input filter design criteria for switching regulators using current-mode programming," *IEEE Trans. on Power Electronics*, 7(3): pp. 469–479, Jul. 1992.

[kre90] P. T. Krein, J. Bentsman, R. M. Bass, and B. C. Lesieutre, "On the use of averaging for the analysis of power electronic systems," *IEEE Trans. on Power Electron.*, 5(2): pp. 182–190, Apr. 1990.

[lac08] T. Laczynski, T. Werner, and A. Mertens, "Active damping of LC-filters for high power drives using synchronous optimal pulsewidth modulation," in *IEEE Power Electronics Specialists Conf. (PESC'08)*, pp. 1033–1040, Jun. 2008.

[lee79] F. C. Lee and Yuan Yu, "Input filter design for switching regulators," *IEEE Trans. on Aerospace and Electronic Sys.*, AES-15(5): pp. 627–634, Sep. 1979.

[lee85] Y. S. Lee, "A systematic and unified approach to modeling switches in switch-mode power supplies," *IEEE Trans. on Ind. Electron.*, IE-32: pp. 445–448, Nov. 1985.

[leh96] B. Lehman and R. M. Bass, "Switching frequency dependent averaged models for PWM dc–dc converters," *IEEE Trans. on Power Electron.*, 11(1): pp. 89–98, Jan. 1996.

[lew89] L. R. Lewis, B. H. Cho, F. C. Lee, and B. A. Carpenter, "Modeling, analysis and design of distributed power systems," in *IEEE Power Electronics Specialists Conf. (PESC)*, volume 1, pp. 152–159, 1989.

[ley01] R. Leyva, L. Martinez-Salamero, H. Valderrama-Blavi, J. Maixé, R. Giral, and F. Guinjoan, "Linear state-feedback control of a boost converter for large-signal stability," *IEEE Trans. on Circuits and Systems-I: Fundamental Theory and Applications*, 48(4): pp. 418–424, Apr. 2001.

[liz96] F. Lizarraga, M. Witulski, and F. Arthur, "Input filter design for multiple-module dc power systems," *IEEE Trans. on Power Electronics*, 11(3): pp. 472–479, 1996.

[mah97] J. Mahdavi, A. Emaadi, M.D. Bellar, and M. Ehsani, "Analysis of power electronic converters using the generalized state-space averaging approach," *IEEE Trans. on Circuits and Systems I: Fundamental Theory and Applications*, 44(8): pp. 767–770, Aug. 1997.

[mak00] D. Maksimovic, “Computer-aided small-signal analysis based on impulse response of dc/dc switching power converters,” *IEEE Trans. on Power Electron.*, 15(6): pp. 1183–1191, Nov. 2000.

[mak01] D. Maksimovic, A. M. Stankovic, V. J. Thottuvelil, and G. C. Verghese, “Modeling and simulation of power electronic converters,” *Proceedings of The IEEE*, 89(6): pp. 898–912, Jun. 2001.

[mak91] D. Maksimovic and S. Cuk, “A unified analysis of PWM converters in discontinuous mode,” *IEEE Trans. on Power Electron.*, 6(4): pp. 476–490, Jul. 1991.

[mat76] H. Matsuo and K. Harada, “The cascade connection of switching regulators,” *IEEE Trans. on Industry Applications*, IA-12(2): pp. 192–198, Mar/Apr. 1976.

[mat97] P. Mattavelli, L. Rossetto, and G. Spiazzi, “Small-signal analysis of dc-dc converters with sliding mode control,” *IEEE Trans. on Power Electronics*, 12(1): pp. 96–102, Jan. 1997.

[maz01] S. K. Mazumder, A. H. Nayfeh, and D. Boroyevich, “Theoretical and experimental investigation of the fast- and slow-scale instabilities of a dc-dc converter,” *IEEE Trans. on Power Electron.*, 16(2): pp. 201–216, Mar. 2001.

[mer08] A. Merdassi, L. Gerbaud, and S. Bacha, “A new automatic average modeling tool for power electronics systems,” in *Proc. IEEE Power Electronics Specialists Conf.*, pp. 3425–3431, 2008.

[mid73] G. W. Wester and R. D. Middlebrook, “Low frequency characterization of switched dc-dc converters,” *IEEE Trans. on Aerospace and Electronic Systems*, AES-9: pp. 376–385, May 1973.

[mid76] R. D. Middlebrook, “Input filter considerations in design and application of switching regulators,” in *IAS'76 Annual Meeting*, pp. 366–382, Oct. 1976.

[mid77a] R. D. Middlebrook and S. Cuk, “A general unified approach to modeling switching-converter power stages,” *International Journal of Electronics*, 42(6): pp. 521–550, Jun. 1977.

[mid77b] R. D. Middlebrook and S. Cuk, “Modeling and analysis methods for dc-to-dc switching converters,” in *IEEE Int. Semiconductor Power Converter Conf.*, pp. 90–111, Mar. 1977 Record.

[mid78] R. D. Middlebrook, “Design techniques for preventing input-filter oscillations in switched-mode regulators,” in *Proc. of Powercon 5*, pp. A3–1–A3–16, May 1978.

[mid88] R. D. Middlebrook, “Transformerless dc-to-dc converters with large conversion ratios,” *IEEE Trans. on Power Electronics*, 3(4): pp. 484–488, Oct. 1988.

[mid89] R. D. Middlebrook, “Null double injection and the extra element theorem,” *IEEE Trans. on Education*, 32(3): pp. 167–180, Aug. 1989.

[mid98] R. D. Middlebrook, V. Vorperian, and J. Lindal, “The N extra element theorem,” *IEEE Trans. on Circuits and Systems I: Fundamental Theory and Applications*, 45(9): pp. 919–935, Sep. 1998.

[mil86] MIL-STD-461, Electromagnetic emissions and susceptibility requirements for the control of electromagnetic interference, *US Department of Defence Military Standard*, 20 Aug. 1986, Version C, 183 Pages, Online: https://acc.dau.mil/.

[min08] Ming Li, Dong Dai, and Xikui Ma, “Effects of the input filter on the stability of a voltage-mode controlled buck converter,” *International Journal of Circuit Theory and Applications*, 36(3): pp. 367–373, 2008.

[mit88] D. M. Mitchell, *DC-DC Switching Regulator Analysis*. New York: McGraw-Hill, 1988.

[mit99] D. M. Mitchell, “Power line filter design considerations for dc-dc converters,” *IEEE Industry Application Magazine*, 5(6): pp. 16–26, Nov/Dec 1999.

[mor02] J. A. Morales-Saldana, E.E.C. Gutierrez, and J. Leyva-Ranos, “Modeling of switch-mode dc-dc cascade converters,” *IEEE Trans. on Aerospace and Electronic Systems*, 38(1): pp. 295–299, Jan. 2002.

[mur04] P. C-Murphy, T. C. Neugebauer, C. Brasca, and D. J. Perreault, “An active ripple filtering technique for improving common-mode inductor performance,” *IEEE Power Electronics Letters*, 2(2): pp. 45–50, 2004.

[nic95] B. Nicolas, M. Fadel, and Y. Chéron, “Sliding mode control of dc-to-dc converters with input filter based on Lyapunov-function approach,” in *Proc. of EPE-PEMC*, pp. 1.338–1.343, 1995.

[nir01] G. Nirgude, R. Tirumala, and N. Mohan, “A new, large signal average model for single-switch dc-dc converters operating in both CCM and DCM,” in *IEEE Power Electron. Spec. Conf.*, volume 3, pp. 1736–1741, 2001.

[oli05] A. Oliva and H. Chiacchiarini and G. Bortolotto, “Development of a state-feedback controller for the synchronous buck converter,” *Latin American Applied Research*, 35(2): pp. 83–88, 2005.

[ora03] M. Orabi and T. Ninomiya, “Stability investigation of the cascade two-stage PFC converter,” in *IEEE International Telecommunication Energy Conf.*, pp. 565–572, Oct. 2003.

[oze00] R. L. Ozenbaugh, *EMI Filter Design: Second Edition Revised and Expanded*, Marcel Dekker, 2000.

[pej95] P. Pejovic and D. Maksimovic, “Determination of network state in switching power converters,” in *Proc. IEEE Power Electronics Specialists Conf.*, volume 2, pp. 816–822, 1995.

[phe79] T. Phelps and W. Tate, “Optimizing passive input filter design,” in *Proc. of Powercon 6*, pp. G1.1–G1.10, May 1979.

[raj02] V. Rajasekaran and B. S. Heck, “On stability enhancing control methods in power electronic converters,” in *IEEE Power Electronics Specialists Conf. (PESC)*, volume 4, pp. 1593–1598, 2002.

[sad04] D. Sadarnac, C. Karimi, and K. Louati, “Input filter influence on control stability of dc-dc converters,” in *IEEE International Symposium on Industrial Electronics*, pp. 1165–1171, May 2004.

[san91a] S. R. Sanders and G. C. Verghese, “Synthesis of averaged circuit models for switched power converters, *IEEE Trans. on Circuits and Systems*, 38: pp. 905–915, Aug. 1991.

[san91b] S. R. Sanders, J. M. Noworolski, X. Z. Liu, and G. C. Verghese, “Generalized averaging method for power conversion circuits,” *IEEE Trans. on Power Electron.*, 6(2): pp. 251–259, Apr. 1991.

[san92] S. R. Sanders and G. C. Verghese, "Lyapunov-based control for switched power converters," *IEEE Trans. on Power Electronics*, 7(1): pp. 17–24, Jan. 1992.

[sat93] Y. Sato and T. Kataoka, "State-feedback control of current-type PWM ac-to-dc converters," *IEEE Trans. on Industry Applications*, 29(6): pp. 1090–1097, Nov/Dec. 1993.

[sch90] S. Schulz, B. H. Cho, and F. C. Lee, "Design considerations for a distributed power system," in *IEEE Power Electronics Specialists Conf. (PESC)*, pp. 611–617, Jun. 1990.

[spi97] G. Spiazzi, P. Mattavelli, and L. Rossetto, "Sliding mode control of dc-dc converters," in *4th Congresso Brasileiro de Elettronica de Potencia (COBEP)*, pp. 59–68, BeloHorizonte, Dec. 1997.

[ste03] Stephen Wolfram. *The Mathematica Book*. Wolfram Media, Inc., 5th edition, 2003, Pages: 1488, Online: http://www.wolfram.com/.

[sun00] J. Sun, "Unified averaged switch models for stability analysis of large distributed power systems," in *IEEE Applied Power Electronics Conf. (APEC)*, volume 1, pp. 249–255, 2000.

[sun01] J. Sun, D. M. Mitchell, M. F. Greuel, P. T. Krein, and R. M. Bass, "Averaged modeling of PWM converters operating in discontinuous conduction mode," *IEEE Trans. on Power Electron.*, 16(4): pp. 482–492, Jul. 2001.

[sun02a] T. Suntio and I. Gadoura, "Use of unterminated two-port modeling technique in analysis of input filter interactions in telecom DPS systems," in *IEEE International Telecommunication Energy Conf. (INTELEC)*, pp. 560–565, 2002.

[sun02b] T. Suntio, I. Gadoura, and K. Zenger, "Input filter interactions in peak-current-mode-controlled buck converter operating in CICM," *IEEE Transactions on Industrial Electronics*, 49(1): pp. 76–86, Feb. 2002.

[sun02c] T. Suntio, I. Gadoura, and K. Zenger, "Input filter interactions in current-mode controlled converters – a unified analysis approach," in *IEEE 28th Annual Conference of Industrial Electronics Society (IECON)*, volume 2, pp. 1179–1184, Nov. 2002.

[sun03] T. Suntio, "Input invariance as a method to reduce EMI filter interactions in telecom DPS systems," in *IEEE International Telecommunication Energy Conf. (INTELEC)*, pp. 592–597, Oct. 2003.

[sun04] T. Suntio and A. M. Altowati, "Design of EMI filter for stability and performance in switched-mode converters," in *IEEE Power Electronics Specialist Conf. (PESC)*, volume 4, pp. 3077–3083, 2004.

[sun92] J. Sun and H. Grotstollen, "Averaged modeling of switching power converters: Reformulation and theoretical basis," in *Proc. IEEE Power Electronics Specialists Conf.*, volume 2, pp. 1166–1172, 1992.

[sun97] J. Sun and H. Grotstollen, "Symbolic analysis methods for averaged modeling of switching power converters," *IEEE Trans. on Power Electron.*, 12(3): pp. 537–546, May 1997.

[sun98] J. Sun, D. M. Mitchell, M. F. Greuel, P. T. Krein, and R. M. Bass, "Modeling of PWM converters in discontinuous conduction mode – a reexamination," in *IEEE Power Electron. Spec. Conf. (PESC)*, volume 1, pp. 615–622, May 1998.

[tab92] W. A. Tabisz, M. M. Jovanovic, and F. C. Lee, "Present and future of distributed power systems," in *IEEE Applied Power Electronics Conf. and Expo. (APEC)*, pp. 11–18, Feb. 1992.

[tsa92] H. Tsafrin and S. Ben-Yaakov, "The dynamic response of PWM dc-dc converters with input filters," in *IEEE Applied Power Electronics Conf. (APEC)*, pp. 764–771, Feb. 1992.

[tsu01] K. Tsubol, M. Tsuji, and E. Yamada, "Instability of a chopper system with input LC filter and its solution," *Electrical Engineering in Japan*, 137(4): pp. 49–63, Sep. 2001.

[tym86] R. Tymerski and V. Vorperian, "Generation, classification and analysis of switched-mode dc-to-dc converters by the use of switching cell," in *Intl. Telecommunications Energy Conf. (INTELEC)*, pp. 181–195, 1986.

[usm06] M. Usman Iftikhar, D. Sadarnac, and C. Karimi, "Conducted EMI suppression and stability issues in switch-mode dc-dc converters," in *IEEE International Multitopic Conference (INMIC'06)*, pp. 389–394, Dec. 2006.

[usm07] M. Usman Iftikhar, D. Sadarnac, and C. Karimi, "Input filter damping design for control loop stability of dc-dc converters," in *IEEE International Symposium on Industrial Electronics (ISIE'07)*, pp. 353–358, Jun. 2007.

[usm08a] M. Usman Iftikhar, A. Bilal, D. Sadarnac, P. Lefranc, and C. Karimi, "Analysis of input filter interactions in cascade buck converters," in *IEEE International Conference on Industrial Technology (ICIT'08)*, pp. 1–6, Apr. 2008.

[usm08b] M. Usman Iftikhar, P. Lefranc, D. Sadarnac, and C. Karimi, "Theoretical and experimental investigation of averaged modeling of non-ideal PWM dc-dc converters operating in DCM," in *Proc. IEEE Power Electronics Specialists Conf. (PESC'08)*, pp. 2257–2263, Jun. 2008.

[usm08c] M. Usman Iftikhar, E. Godoy, P. Lefranc, D. Sadarnac, and C. Karimi, "A control strategy to stabilize PWM dc-dc converters with input filters using state-feedback and pole-placement," in *Proc. IEEE International Telecommunications Energy Conf. (INTELEC'08)*, pp. 1–5, Sep. 2008.

[utk93] V. I. Utkin, "Sliding mode control design principles and applications to electric drives," *IEEE Trans. on Industrial Electronics*, 40(1): pp. 23–36, 1993.

[vee03] M. Veerachary, "V^2 control of cascade buck converters," in *IEEE International Telecommunications Energy Conf. (INTELEC)*, pp. 470–472, 2003.

[ven85] R. Venkataramanan, A. Sabonovic, and S. Cuk, "Sliding mode control of dc-to-dc converters," in *IEEE International Conference on Industrial Electronics, Control and Instrumentation (IECON'85)*, pp. 251–258, 1985.

[ver81] G. Verghese and U. Mukherji, "Extended averaging and control procedures," in *IEEE Power Electronics Specialists Conf.*, pp. 329–336, Rec. 1981.

[vla96] V. Vlatkovic, D. Borojevic, and F. C. Lee, "Input filter design for power factor correction circuits," *IEEE Trans. on Power Electronics*, 11(1): pp. 199–205, 1996.

[vor89] V. Vorperian, R. Tymerski, and F. C. Lee, "Equivalent circuit models for resonant and PWM switches," *IEEE Trans. on Power Electron.*, 4(2): pp. 205–214, Apr. 1989.

[vor90] V. Vorperian, "Simplified analysis of PWM converters using the model of the PWM switch, part II: Discontinuous conduction mode," *IEEE Trans. on Aerosp. Electron. Syst.*, 26(3): pp. 497–505, May 1990.

[wan03] X. Wang, R. Yao, and F. Rao, "Three-step impedance criterion for small-signal stability analysis in two-stage dc distributed power systems," *IEEE Power Electronics Letters*, 1(3): pp. 83–87, Sep. 2003.

[wil98] P. R. Willcock, J. A. Ferreir, and J. D. Van Wyk, "An experimental approach to investigate the generation and propagation of conducted EMI in converters," in *IEEE Power Electronics Specialists Conf. (PESC)*, volume 2, pp. 1140–1145, May 1998.

[wu92] T. F. Wu, K. Siri, and C. Q. Lee, "A systematic method in designing line filters for switching regulators," in *IEEE Applied Power Electronics Conf. (APEC)*, pp. 179–185, Feb. 1992.

VITA

M. Usman Iftikhar was born in Lahore, Pakistan, in 1980. He received his B.S. degree in Electrical Engineering from University of Engineering and Technology, Lahore, Pakistan in 2003. In March 2003 he joined Pakistan Space & Upper Atmosphere Research Commission (SUPARCO) where he worked with the Satellite Power Subsystems Design group. In July 2004, he came to France for higher studies and received M.S. degree in Electrical Engineering in 2005 from Institut National Polytechnique de Grenoble (INP-G) France. He was awarded a doctoral scholarship in 2005 from the French Ministry of Research to pursue his PhD. Since November 2005 he is working towards his Ph.D. degree at Department of Energy and Power Systems of Ecole Supérieure d'Electricité (Supélec), France. His general areas of interest include dc-dc converter modeling and control, power electronics, renewable energy sources and systems.